REMOTE SENSING APPROACH FOR ESTIMATING AGROFORESTRY AREA, SUITABILITY MAPPING AND CARBON SEQUESTRATION POTENTIAL OF AGROFORESTRY SYSTEMS IN SOLAN DISTRICT OF HIMACHAL PRADESH

Thesis

by

DIVYA KHATRI
(F-2020-09-D)

submitted to

Dr. YASHWANT SINGH PARMAR UNIVERSITY
OF HORTICULTURE AND FORESTRY
SOLAN (NAUNI) HP – 173 230 INDIA

in

partial fulfilment of the requirements for the degree

of

DOCTOR OF PHILOSOPHY
(FORESTRY)
AGROFORESTRY

DEPARTMENT OF SILVICULTURE AND AGROFORESTRY
COLLEGE OF FORESTRY

2024

Department of Silviculture and Agroforestry College of forestry Dr. Y.S. Parmar University of Horticulture and Forestry, Nauni, Solan (HP)173230 India

Dr. DR Bhardwaj
Major Advisor
Prof. and Head
(M): 082193 27754
Email:bhardwaj_uhf@rediffmail.com

CERTIFICATE-I

This is to certify that the thesis titled, **"Remote sensing approach for estimating agroforestry area, suitability mapping and carbon sequestration potential of agroforestry systems in Solan district of Himachal Pradesh"** submitted in partial fulfilment for the award of the degree of **DOCTOR OF PHILOSOPHY (FORESTRY) AGROFORESTRY** to Dr. Yashwant Singh Parmar University of Horticulture and Forestry. Nauni, Solan (HP) 173230 is a bonafide research work carried out by **Ms. DIVYA KHATRI (F-2020-09-D)** d/o Sh. Virendra Singh Khatri under my supervision and no part of this thesis has been submitted for any other degree or diploma.

The assistance and help received during the course of investigations have been fully acknowledged.

Place: Nauni, Solan
Date:

Chairperson
Advisory Committee

CERTIFICATE - II

This is to certify that the thesis titled **"Remote sensing approach for estimating agroforestry area, suitability mapping and carbon sequestration potential of agroforestry systems in Solan district of Himachal Pradesh"** submitted by **Ms. Divya Khatri (F-2020-09-D)** D/o Sh. Virendra Singh Khatri to Dr. Yashwant Singh Parmar University of Horticulture and Forestry, Nauni, Solan (HP) - 173 230 in partial fulfilment of the requirements for the award of degree of **Doctor of Philosophy** in the discipline of **Forestry (Silvicultrure and Agroforestry)** has been approved by the Advisory Committee after oral examination of the same in collaboration with the external examiner.

Dr. DR Bhardwaj
(Prof. and Head)
Chairman, Advisory Committee

9/4/24
Dr. D P Sharma
External Examiner

Members of the Advisory Committee

9.4.24
Dr CL Thakur
(Dean College of Forestry)

Dr. RK Gupta
(Professor)
Department of Basic Sciences

Dr Rajeev Aggarwal
(Professor)
Department of Environmental Science

Mr. Shreshtha Nand
(DFO)

Professor and Head
Department of Silviculture and Agroforestry

Countersigned

Dean
College of Forestry
Dr. Yashwant Singh Parmar University of Horticulture and Forestry, Nauni, Solan (HP) - 173 230

ACKNOWLEDGEMENT

I take great joy in expressing my sincere gratitude to those who have been instrumental in the successful completion of this work, driven not by convention but by a profound conviction. Firstly, I extend my heartfelt thanks to the ***Almighty, Lord Golu Devta, the God of Justice in the Kumaon region of Uttarakhand****, for His protection and guidance throughout this journey, which still continues with numerous destinations ahead.*

I am privileged to acknowledge and express my deep appreciation to my Major Advisor, ***Dr. D.R. Bhardwaj****, Professor and Head of the Department of Silviculture and Agroforestry. His invaluable guidance, timely suggestions, close counsel, critical evaluation, everlasting patience, and constant encouragement have played a pivotal role at every step of my thesis research work, fostering my research ability and aptitude.*

*I am equally grateful to the esteemed members of my advisory committee—****Dr. C.L. Thakur, Dr. RK Gupta, Dr. Rajeev Aggarwal and Mr. Shreshtha Nand****—for their consistent suggestions and cooperation throughout my degree program. I extend my thanks to other respected teachers, namely Dr. Rohit Bishist, Dr. Prem Prakash Sharma, Dr. Praveen Kumar, Dr. Prashant Sharma, Dr. Dhirendra Kumar, and Dr. Rajeev Dhiman, for their ideological contributions and valuable suggestions.*

Special appreciation is extended to Sh. Jeet Ram, Sh. Joginder, Sh. Madan Lal, and the entire staff of the Department of Silviculture and Agroforestry for their unwavering help and cooperation.

My gratitude also extends to my parents, ***Smt. Ranjeeta Khatri*** *and* ***Sh. Virendra Singh Khatri****, and grandparents* ***Smt. Janki Khatri*** *and* ***Late Sh. Maan Singh Khatri****, whose love, dedication, and inspiration motivated me to pursue higher studies. Their sacrifices and firm faith have transformed this documentation into a humble tribute to translate our collective dreams into reality.*

I am indebted to my loving elder sister, ***Mrs. Bhumika Bisht****, brother-in-law* ***Squadron Leader. Gaurav Bisht****, brother* ***Harshvardhan Singh Khatri****, and dearest person* ***Abhishek Aswal*** *for their invaluable support and love. Gratitude is also extended to friends who stood by me during moments of despondency—Shilpa, Pooja, Vaishali, Ruchi, Midhun, Alok, Jatin, Avinash and Saakshi—for their cooperation and support. Special thanks are reserved for my seniors and juniors for their unwavering support throughout my study.*

I appreciate the technical support from DPT Computers Nauni and express my thanks to Satyanand Stokes Library of Dr. YS. Parmar University of Horticulture and Forestry Nauni, Solan, for providing necessary information. Acknowledging the countless individuals who may have slipped my mind, I conclude with endless thanks to the friendly and helpful people who contributed to this journey.

Place: Nauni-Solan (HP)
Date: **Divya Khatri**

CONTENTS

ABBREVIATIONS USED

$	:	Dollar
%	:	Per cent
°C	:	Degree Celsius
ACZ	:	Agro-Climatic Zones
AFS	:	Agroforestry Systems
AGR	:	Agriculture
AHP	:	Analytic Hierarchy Process
amsl	:	Above means sea level
B	:	Boron
BD	:	Bulk density
BL	:	Barren land
C	:	Carbon
CEC	:	Cation Exchange Capacity
CO_2	:	Carbon dioxide
CSP	:	Carbon Sequestration Potential
C ha^{-1}	:	Carbon per hectare
DES	:	District Economic Survey
E	:	East
e.g.	:	For Example
et al.	:	Co-workers
etc.	:	Etcetera
FAO	:	Food and Agriculture Organization
FSI	:	Forest Survey Of India
GIS	:	Geographic Information System
GL	:	Grassland
Gt	:	Gigaton
ha	:	Hectare (10000 m^2)
i.e.	:	That is
InVEST model		Integrated Valuation of Ecosystem Services model
IPCC	:	Intergovernmental Panel on Climate Change

IRS	:	Indian Remote Sensing
K	:	Potassium
kg	:	Kilogram
LISS	:	Linear Imaging Self-Scanning Sensor
LULC	:	Land-use and land cover
m	:	Meter
MCDM	:	Multi-criteria decision making
Mg	:	Magnesium
Mg C ha^{-1}	:	Mega gram Carbon per hectare
mm		millimetre
N	:	Nitrogen
NDVI	:	Normalized Difference Vegetation Index
NPV		Net Present Value
OA	:	Overall Accuracy
OC	:	Organic Carbon
P	:	Phosphorus
P	:	Pages
PA	:	Producer's Accuracy
pH	:	Puissance d' Hydrogen
q ha^{-1}	:	Quintal per hectare
RS	:	Remote sensing
SDGs	:	Sustainable Development Goals
SE	:	Standard error
spp.	:	Species
sq. km	:	Square kilometre
TOF	:	Tree outside forest
t C ha^{-1}	:	Tonne Carbon per hectare
UA	:	User's Accuracy
vis-a-vis	:	in relation to
viz	:	namely or in particular

LIST OF TABLES

LIST OF FIGURES

Chapter-1

INTRODUCTION

Agroforestry is a sustainable approach to land management that combines agriculture and forestry activities within a single land area. This practice involves strategically incorporating trees or shrubs alongside crops or livestock, creating a more diverse and resilient agricultural system (Bishaw et al. 2022). Agroforestry systems are increasingly being adopted due to their ability to enhance biodiversity, improve soil quality, increase crop productivity, and mitigate climate change (Reppin et al. 2020). Agroforestry has been a part of human history for centuries, with diverse practices developed across different regions, cultures, and ecosystems. India has a long and rich tradition of agroforestry dating back to ancient times (Nair et al. 2021). The country boasts an estimated natural forest cover of 713,789 sq. km, which is 21.71% of its total land area. Additionally, an estimated 95,748 sq. km of land where trees coexist with other land uses, as observed in agroforestry practices, accounts for 2.91% of the nation's total land area (FSI 2020).

Agroforestry practices have been extensively studied at both global and regional levels, and the results consistently show that they provide numerous benefits across various domains, including environmental, social, cultural, and economic. These benefits are particularly significant when agroforestry practices are implemented across landscapes. Therefore, agroforestry plays a critical role in promoting the transition towards perennial agriculture by emphasizing the establishment of long-lasting vegetative cover to safeguard and enhance ecosystems (Rosenstock et al. 2019 and Torralba et al. 2016).

Trees outside forests (TOF) refers to discrete trees and small groups of trees in non-forest settings considered valuable resources worldwide (Meneguzzo et al. 2013). TOF is crucial in conserving biodiversity, controlling erosion, and providing essential resources such as fuel, wood, and fodder. However, due to their small and isolated nature, comprehensive mapping of these resources is challenging (FSI 2020). Nevertheless, these resources still need to be studied more on a large-scale basis due to their small and isolated nature, which poses challenges for comprehensive mapping (Pujar et al. 2016). The spatial resolution, often called the scale or pixel size, of satellite sensors plays a crucial role when utilizing satellite remote sensing data to map such resources. As noted by Chabra et al. (2004), the choice of spatial

resolution is a critical factor that impacts the accuracy and effectiveness of remote sensing applications in mapping these dispersed TOF resources. Apart from mapping, knowledge of local beneficiaries on TOF is vital for collecting relevant information about ecosystem services provided by TOF (FSI 2020) as they have knowledge and experience about the types of trees and their benefits provided to them, especially in the provisioning services such as wood, food, and fruits (Hein et al. 2006). They provide insight into which services are provided to them because they are regarded as the managers, beneficiaries, and stakeholders of the TOF. This can help develop a better understanding of the relationship between tree-based ecosystems and as a source of valuing ecosystem services (Tassew 2017). Furthermore, accurate mapping and estimation of the extent of agroforestry area in the country is of utmost importance for planners and policymakers. For this purpose, geo-spatial technologies like GIS, GPS and satellite remote sensing have a crucial role (Rizvi et al. 2020b).

Geographic Information System (GIS) is a powerful tool that contains detailed maps and location references for a range of themes, including natural resource management, biodiversity assessment, watershed planning, disaster management, forest cover mapping, crop acreage estimation and accurate determination of the species, soil, land cover, topography and hydrology of the area (Rizvi et al. 2016a). Satellite images identify the type of vegetation present in an area. At the same time, the GIS component is used to categorize and locate its position on the Earth's surface, providing a complete site record. Integrating satellite remote sensing data into GIS has significantly contributed to various fields. It has proven an effective tool for mapping and monitoring agriculture, forestry and other earth features (Rizvi et al. 2017b).

In 2007, the ICAR-Central Agroforestry Research Institute (CAFRI) in India began using geospatial technologies to estimate agroforestry areas. They developed various methodologies for medium-resolution (>10 m spatial resolution) and high-resolution (<10 m spatial resolution) remote sensing satellite data. For mapping and estimating areas under agroforestry using medium-resolution remote sensing data, a methodology has been proposed (Rizvi et al. 2016a). High-resolution satellite imagery can detect individual trees and estimate the extent of Trees Outside the Forest at the local scale. However, these images can be expensive and may require more spatial coverage for assessments of agroforestry at regional to national scales. Mapping agroforestry is challenging because it is not enough to detect

trees; integrated methods are needed to capture both the trees and the land-use systems (Rizvi et al. 2020b).

According to the Design and Diagnostic Survey, agroforestry practices are prevalent in various regions of the country. However, it is still challenging to obtain accurate and reliable data on the extent of agroforestry areas (Rizvi et al. 2020b). Estimating the size of agroforestry is a significant challenge due to the need for more suitable and reliable methods for defining the area affected by trees within mixed stands of trees and crops. The problem is further complicated in the case of simultaneous agroforestry, where the tree and crop components grow concurrently and closely enough for mutual interactions. In the case of multi-strata systems such as home gardens, shaded perennial methods, and intensive tree intercropping situations, the entire area occupied can be listed as agroforestry (Rizvi et al. 2014). However, it is more difficult to estimate the area for practices such as windbreaks and boundary planting, where trees are planted at a vast distance between rows or around agricultural fields. In such cases, the influence of trees extends over a larger area than is easily perceivable (Nair et al. 2009). Therefore, it is essential to collect more systematic ground reference information for the development of predictive models for the extent of agroforestry area and the validation of these estimates (Rizvi et al. 2016b).

In 1976, the Food and Agriculture Organization (FAO) introduced methods for assessing land suitability. Land evaluation involves studying the performance and capability of land used for a specific purpose, incorporating surveys and analysis of various factors, including landforms, soils, vegetation, climate, and other characteristics, to determine the suitability of the land for specific objectives (Ahmad and Goparaju, 2017a). This concept is particularly pertinent today, given the increasing pressure on finite land resources. Agroforestry suitability mapping is critical to land suitability, especially in regions like India, where land resources are under tremendous pressure (Ahmad et al. 2017b).

Mapping agroforestry suitability in different agroecological zones of India can open up new opportunities for agroforestry ventures. Using ancillary data within the GIS domain holds immense potential for mapping land, particularly for rural communities down to the village level. Several researchers and scientists have explored land suitability for agroforestry applications using remote sensing and GIS techniques. Land Suitability Analysis (LSA) is a scientific method aimed at assessing the degree of fitness of land for specific purposes,

identifying the most appropriate spatial patterns for future land uses (Singha and Swain, 2016, Ahmad et al. 2019a). A broader evaluation of LSA for agroforestry at the country level has been carried out for India, considering parameters like climatic conditions, soil quality, topography, and ecological criteria. The assessment classifies approximately 33% of the country's land as highly suitable for agroforestry, with 40% falling into the moderately appropriate category and 12% being marginally relevant. However, this country-level approach must be more precise and suitable for local planning (Nath et al. 2021).

Climate change and global warming have become crucial issues in the global environmental scenario. Even minor temperature increases have severe consequences. The Intergovernmental Panel on Climate Change (IPCC) recommends implementing mitigation policies to reduce greenhouse gas (GHG) emissions. GHG emissions are primarily due to carbon dioxide (CO_2) emissions from fossil fuel combustion and industrial processes, accounting for 75% of the total GHG emissions. From 1850 to 2019, the cumulative net CO_2 emissions have reached 2400 ± 240 Gt CO_2, with a significant portion remaining in the atmosphere (IPCC 2022). One practical approach to mitigating climate change is sequestering atmospheric carbon in trees and soils through plant respiration (Albrecht and Kandji 2003). However, primary forests are shrinking due to deforestation caused by the increasing human population and the resulting pressure on land resources. Combining tree cultivation with crop farming through agroforestry offers a valuable solution for carbon sequestration. Agroforestry is a climate-friendly practice with numerous environmental and socioeconomic co-benefits (Albrecht and Kandji 2003) and lower costs than other CO_2 mitigation options (Feliciano et al. 2018).

Carbon sequestration in agroforestry systems also presents an effective strategy for reducing greenhouse gas emissions and offers multiple co-benefits (Panwar et al. 2022). Furthermore, farmers can sell in carbon stocks accumulated from agroforestry as CO_2 emission in carbon offset markets (Luedeling et al. 2011). New approaches have become essential to quantify Land Use and Land Cover (LULC) changes, as anthropogenic land cover changes have significantly altered the carbon balance. Over the past century, one-third of anthropogenic CO_2 emissions have been attributed to land cover change. Quantifying LULC dynamics is increasingly necessary to address these challenges and imbalances in the global carbon budget (Houghton, 2003). There is a growing need to characterize and quantify changes in LULC at various scales, from local to global, to understand their impact on

terrestrial ecosystem processes that govern the carbon cycle (Gupta et al. 2017). Quantifying land-use/land cover (LULC) dynamics is essential to address global carbon imbalances and improve our understanding of their effects on the carbon cycle (Gupta et al. 2017).

The Solan district, with elevations ranging from 650 m to 1800 m above mean sea level, is the focus of the present study. It is a region with diverse landforms that have experienced significant changes in land use patterns over the past 30 years. These changes are attributed to shifts in agricultural practices, urbanization, industrialization, and tourism and are identified as contributing factors to the observed impacts of climate change. A study conducted by Vaidya et al. (2017) in the mid-hills of Solan district reports notable changes, including a 430 ha increase in the built-up area and a 1771 ha expansion in agricultural land, alongside a decline of 572 ha in forest areas. However, detailed comprehensive information about the estimation of the agroforestry area, agroforestry suitability, and the carbon sequestration potential of the Solan district. This study aims to fill these gaps by utilizing remote sensing and GIS techniques to comprehensively determine the extent of different agroforestry practices and other landforms. This information is urgently required for climate change adaptation, mitigation, and achieving Sustainable Development Goals (SDGs). The objectives of the present study are:

i) To determine the area under different agroforestry practices and other land use systems using geospatial techniques;
ii) To prepare the agroforestry suitability map of the Solan district;
iii) To estimate biomass carbon stock and carbon sequestration potential of agroforestry systems and other land use systems.

Chapter-2

REVIEW OF LITERATURE

Trees Outside Forest (TOF) are present in a wide range of settings within both rural and urban landscapes throughout the country. They manifest in various configurations, including small woodlots, block plantations, trees along linear features such as roads, canals, bunds, and scattered trees on farmlands, agricultural lands, homesteads, community lands, and urban areas. The landscape also encompasses diverse forms of agroforestry systems, such as agri-silviculture, agri-horticulture, and the establishment of block plantations on agricultural fields (FSI 2020). To accurately depict and analyse these agroforestry systems, the mapping process involves the utilization of remote sensing imagery, which necessitates the application of classification techniques, both hard and soft, within software platforms like QGIS and ArcGIS. The utilization of geospatial technologies in agroforestry systems has evolved significantly, encompassing tasks such as delineating the spatial extent of agroforestry, evaluating land suitability for agroforestry practices, and estimating the potential for carbon sequestration. The prevalence of these applications has exhibited a consistent upward trend over the past two decades, with a notable acceleration in the generation of literature observed in the last decade. Within this chapter, an analysis of the coherence in research representation in the form of literature has been conducted with regard to the ongoing investigation titled "Remote sensing approach for estimating agroforestry area, suitability mapping, and carbon sequestration potential of agroforestry systems in Solan district of Himachal Pradesh." This examination falls under the specified headings:

2.1. Agroforestry area and other land-use systems mapping

2.2. Agroforestry suitability mapping

2.3. Biomass carbon stock and Carbon sequestration potential of agroforestry systems

2.1 AGROFORESTRY AREA AND OTHER LAND-USE SYSTEMS MAPPING

Trees Outside Forest (TOF), are found in diverse formations in the rural and urban landscapes in the country like small woodlots, block plantations, trees along linear features such as roads, canals, bunds, etc and scattered trees on farmlands, agricultural lands, homesteads, community lands and urban areas. Several forms of agroforestry systems exist

such as agri-silviculture, agri-horticulture, block and others plantations on agricultural fields. Mapping of these agroforestry systems requires processing of remote sensing images using some hard or soft classifier in software like ERDAS and ArcGIS.

Chhabra (2004) examined Trees Outside Forests (TOF) in a Dehradun suburb through assessing different data sets and classification accuracy. IKONOS MSS achieved the highest overall accuracy at 73%, followed by 8m simulated data at 68%. Fused data sets, IKONOS (MSS & PAN), and IRS (LISSIII & PAN) showed reasonable accuracy and precise area estimation. Spatial resolution impacts accuracy, with higher resolution sensors offering better results. Reference point selection influenced overall accuracy; when chosen from IKONOS PAN, 8m resolution performed best. Fused IKONOS and IRS were suitable for small-scale TOF mapping, while ETM at 30m resolution provided medium-scale accuracy. Different factors, including sensor characteristics, affect accuracy and area statistics.

Rizvi et al. (2009) estimated the agroforestry area in Yamunanagar district for the year 2007 using remote sensing satellite data from Resourcesat-1 with a spatial resolution of 23.5 meters. Two classification approaches, unsupervised and supervised, were applied for this purpose, and spectral analysis to identify and delineate agroforestry areas was performed with the assistance of Arc Info 9.3 and IDRISI Andes software. In the case of supervised classification, the maximum likelihood classifier was utilized to predict the agroforestry area, resulting in an estimated coverage of 32,485.12 hectares, accounting for 18.76% of the district's total land area. On the other hand, the NDVI (Normalized Difference Vegetation Index) image was subjected to classification using the Minimum Distance to Mean classifier. According to this analysis, the agroforestry area in the district was estimated to be 32,475.87 hectares, constituting 20.81% of the total land area. When considering major vegetation covers, the agroforestry area was estimated to be 28,660.3 hectares, representing 16.55% of the district's land. It's worth noting that the NDVI values within the agroforestry systems fell within the range of 0.37036 to 0.51073, providing a specific spectral signature for the identification of these areas.

Ekadinata and Vincent (2011) conducted a study in the Bungo district of Jambi, Sumatra, Indonesia, covering an area of 4,550 sq. km. Over the years, significant land cover changes have occurred in this region, primarily driven by the conversion of extensive forested areas into rubber plantations, oil palm plantations, and other forms of agricultural land use.

The research relied on Landsat satellite images captured between 1973 and 2005 to assess the trends in land cover transformation systematically. The forest cover substantially decreased from over 75% to around 30% during this period. Concurrently, monoculture plantations expanded from a mere 3% to over 40%. In contrast, the extent of rubber agroforests declined from 15% to 11%. Notably, a significant portion of the rubber agroforests in 2005 were absent in 1973, while most of the rubber agroforests present in 1973 had been replaced by more intensive agricultural systems by 2005. Rubber agroforests emerged as a critical repository of the original lowland forest biodiversity since the natural forest had nearly disappeared from the peneplain. However, these rubber agroforests faced increasing pressures and experienced an accelerated conversion to more intensive agricultural systems from 2002 to 2005.

Meneguzzo et al. (2013) conducted a study in Steele County, located in southern Minnesota, USA. They used digital aerial imagery from the US Department of Agriculture's Farm Service Agency National Agriculture Imagery Program (NAIP) to complete the research. The Object-Based Image Analysis (OBIA) and Image Classification Analysis (ICA) approaches required data layers derived from the NAIP imagery or obtained directly from it. The accuracy of the maps generated by both classification approaches was assessed at the specific study site. The results showed that both methods effectively distinguished between areas with and without tree cover, with high overall accuracy. The ICA output achieved an accuracy of 88%, while the OBIA output demonstrated an even higher accuracy of 95%. Both the producer's and user's accuracies for the classification output in the OBIA approach exceeded 90% for both classes, confirming the reliability of the results. However, the accuracy assessment results for the ICA approach displayed more variability. The user's 'tree' class accuracy was commendable at 100%, but the producer's accuracy was 76%. As for the 'no-tree' class, the user's accuracy reached 81%, while the producer's accuracy achieved 100%.

Rizvi et al. (2013) conducted a study to estimate the agroforestry area in the Ludhiana district using remote sensing data. They used medium-resolution (LISS III) and high-resolution (LISS IV) data and a pixel-based classification method. The results showed significant differences in the estimated agroforestry area between the two data types. With LISS IV data, the agroforestry area was estimated to be 14.87% of the total area. On the other hand, using LISS III data resulted in a lower estimate of only 5.56% of the district's land. The

researchers also applied a sub-pixel classifier to LISS III data and compared the results. In this case, the agroforestry area was estimated to be 14.91%, close to the result obtained using LISS IV data. This finding suggests that the sub-pixel classification method can improve the accuracy of agroforestry area assessment in the Ludhiana district and provide estimates similar to those obtained with higher-resolution data.

Das and Das (2014) conducted a study in the Barak Valley region of Assam, located in the north-east of India. The research focused on identifying and mapping rural home gardens, considered a part of the Trees Outside Forests (TOF) category within the broader landscape. The study covered three districts: Cachar, Hailakandi, and Karimganj. The researchers used high-resolution satellite data from the IRS-P6 LISS-IV to identify and map these home gardens. The data was analyzed using an on-screen visual interpretation technique within a GIS environment. This analysis identified two major TOF classes from the satellite data, with home gardens being the prominent TOF class. They covered the highest percentage of the total geographical area across the three districts. The study demonstrated the usefulness of high-resolution satellite data from IRS-P6 LISS-IV in classifying and mapping various land use and land cover categories, including home gardens. The overall classification accuracy of this analysis was an impressive 91%.

Kumar et al. (2014) conducted a study in the Kalesar Block of Yamunanagar district, Haryana, India, encompassing the geographical coordinates of 29°50' N to 30°30' N latitude and 77°13' E to 77°36' E longitudes. The total land area examined in this study amounted to 7,525.1 hectares. For this research, digital data from Cartosat-I (Panchromatic) in October 2009 and IRS LISS – IV were employed. Software tools such as ERDAS IMAGINE 9.3 and ARC/MAP 9.2 were used for analysis. The satellite data analysis revealed the presence of Trees Outside Forests (TOF) covering an area of 785.9 hectares, which accounted for approximately 10.4% of Kalesar Block's total land area. Furthermore, the study computed 66 points for large trees, 148 points for small trees, and 11 points for cluster trees. In terms of linear features, the analysis identified a total length of 30,582.8 meters. Additionally, polygon or block plantations occupied a significant portion of the TOF, covering an area of 233.2 hectares within the study area.

Wani et al. (2014) used geospatial technology to map the agroforestry resources in the southern region of the Kashmir Himalayas. Through visual interpretation, they classified

Landsat datasets from 1980, 1992, 2001, and 2009 into 12 Land Use/Land Cover (LULC) categories. These categories included various land types such as evergreen closed forest, evergreen open forest, forest scrub, grassland, horticulture plantation, agricultural plantation, double-crop, wasteland, built-up areas, and snow. Accuracy of the mapping was ensured by using approximately 450 ground truth points for accuracy assessment. The overall accuracy for the 2009 map was 90.04%, with a Kappa Coefficient of 0.84. The overall accuracy for LULC in other years was as follows: 89.06% for 2001, 88.28% for 1992, and 79.42% for 1980, corresponding to Kappa values of 0.84, 0.83, and 0.79, respectively.

Rizvi et al. (2015) conducted a study using satellite imagery from IRS-P6/LISS IV to evaluate the extent of agroforestry systems across four different districts: Sultanpur, Vaishali, Ludhiana, and North Dinajpur spread over different parts of the country. The process involved using an unsupervised classification method to classify the satellite images within the ERDAS IMAGINE software, followed by a supervised classification method. The results showed that the agroforestry area varied across the districts. Sultanpur district covered 7,977.58 hectares, making up approximately 3.43% of the total area. In Vaishali district, the agroforestry area extended to 22,926.0 hectares, accounting for 11.26% of the district's land. Ludhiana district had an agroforestry area of 54,821.7 hectares, representing 14.87% of the total area. In North Dinajpur district, the agroforestry area was measured at 13,543.07 hectares, equivalent to 4.41% of the district's land. The study also found that mixed plantations comprised about 44.2% of the total agroforestry area. The classification accuracy of this approach was estimated to be around 87%.

Ahmad et al. (2016) conducted an extensive study on agroforestry systems in the Ludhiana district, Punjab, using high-resolution satellite data obtained from LISS IV. The study used unsupervised and supervised classification methods with ERDAS IMAGINE software to create a comprehensive district land use/land cover map. The study found that the unsupervised classification approach identified 41,692.85 hectares of agroforestry area, equivalent to 11.32% of the total area. In contrast, the supervised classification method, specifically the maximum likelihood classification, yielded a lower estimate of agroforestry area, amounting to 6,043.50 hectares, or 1.64% of the district's land. Moreover, the study revealed that Populus, Eucalyptus, and Melia-based agroforestry covered 4,543, 1,426, and 74 hectares, respectively. The classification accuracy of this study was notably high, at 94.28%, with a Kappa Coefficient of 0.93, indicating a substantial agreement between the

classified land uses/land covers and the actual conditions, underscoring the reliability of the results.

Pujar et al. (2016) conducted a study in the Telangana region using high-resolution imagery from Indian Remote Sensing (IRS) satellites. Specifically, PAN (Panchromatic) data from Cartosat 1 and 2 and multispectral data from IRS LISS IV were utilized to extract information related to Trees Outside Forests (TOF). The satellite images provided a detailed resolution of up to 2.5 meters and were analysed using ArcGIS 9.1 software. The study assessed 4,005 grids, each containing approximately 73-84,000 trees, resulting in an average of 73.7 trees per sq. km in the study area. The assessment of TOF quantity within each grid revealed a remarkable 73.5% correspondence with the actual ground content, confirming the reliability and accuracy of the findings.

Rizvi et al. (2016a) conducted a study to evaluate the agroforestry areas in Bathinda and Patiala districts. They used medium-resolution LISS III data and applied pixel and sub-pixel classifiers. The images were sourced from the National Remote Sensing Centre in Hyderabad. The pixel-based classification method estimated the agroforestry area to be 7.09% in Bathinda district and 4.95% in Patiala district. However, the sub-pixel-based classification approach showed a significant increase in the agroforestry areas, with 14.76% in Bathinda district and 13.25% in Patiala district. The accuracy assessment of the classification process revealed an overall accuracy of 83.3% with a Kappa Coefficient of 0.81 for Bathinda district. In Patiala district, the overall accuracy was 82.3%, with a Kappa Coefficient of 0.80. These findings demonstrate the reliability and accuracy of the analysis conducted in both districts.

Rizvi et al. (2016b) conducted a study to evaluate the extent of agroforestry areas in different districts of Gujarat. The assessment employed a sub-pixel classifier using medium-resolution remote sensing data from RS-2/LISS III. The Dahod district had the highest agroforestry area, accounting for 12.48% of its total land area, while Junagarh district had an agroforestry area of 10.95%. The average agroforestry coverage across all districts was estimated to be 9.12%. Additionally, in Junagarh district, a specific mapping of sapota-based agroforestry was undertaken, which revealed an area of 1.13% dedicated to this type of agroforestry. The accuracy assessment of this sub-pixel classifier for delineating sapota-based

agroforestry in the district achieved an accuracy rate of 87.2%. These findings offer valuable insights into the agroforestry landscape in the districts of Gujarat.

Mahato et al. (2016) conducted a study in the Garhwal Himalaya region, focusing on identifying the areas used for agroforestry. The researchers used data from Google Earth Pro in 2011 to delineate the agroforestry zones. To refine the analysis, information on slope and elevation was derived from the Advanced Spaceborne Thermal Emission and Reflection Radiometer (ASTER) Global Digital Elevation Model (GDEM) data in 2011. The geographical information system (GIS) and image processing software used in this study were ArcGIS 9.1 and ERDAS IMAGINE 9.3. The results of the analysis showed varying extents of agroforestry land in the four districts, with Tehri having the highest coverage at 2.13%, followed by Pauri at 1.05%, Chamoli at 0.75%, and Rudraprayag at 0.62%. These findings provide valuable insights into the distribution of agroforestry in the Garhwal Himalaya region.

Den Herder et al. (2017) systematically mapped agroforestry areas in Europe 27 using LUCAS (Land Use and Land Cover) data. This mapping process involved the identification of specific combinations of primary and secondary land cover and land management practices, enabling the pinpointing and categorization of agroforestry points within three distinct systems. Based on the estimations using the LUCAS database, the total agroforestry area in Europe 27 was determined to be approximately 15.4 million hectares. This equates to roughly 3.6% of the total territorial area and accounts for 8.8% of the utilised agricultural land within the region. Among the three studied agroforestry systems, livestock agroforestry was found to be the most extensive, covering approximately 15.1 million hectares, signifying its significant presence in the European landscape.

Newaj et al. (2017) conducted a study where they meticulously mapped agroforestry areas in the ten agro-climatic regions of India. The mapping process relied on LISS III satellite data and utilized a sub-pixel classifier. To ensure a representative sample, 20% of the total districts from each region were selected for analysis. The study revealed that agroforestry covered approximately 16.599 million hectares across these ten regions, accounting for 7.98% of the total land area. The Upper Gangetic Plains region had the highest agroforestry coverage at 15.47%, followed by the West Coast Plains and Hill region at 14.18% and the Gujarat Plains and Hill regions at 13.56%. On the other hand, the Western

dry areas had the lowest agroforestry coverage at 2.41% among the regions studied. These results provide valuable insights into the distribution of agroforestry across diverse agro-climatic regions of India.

Rizvi et al. (2017a) assessed agroforestry areas in four districts of Maharashtra using Resourcesat-2/LISS III remote sensing imagery with a spatial resolution of 23.5 meters. The study focused on the years 2011-12 and employed ERDAS IMAGINE 2015 and ArcGIS 9.3 software for land use and land cover (LULC) classification through visual and digital interpretation. A sub-pixel classifier was utilized to classify agroforestry coverage in Latur, Nashik, Wardha, and Thane districts. The results showed that the Latur district had the highest agroforestry coverage, accounting for 5.17% of the area assessed. Nashik came in second with 4.69%, while Wardha exhibited 4.62% agroforestry coverage. Thane district recorded the lowest agroforestry area at 2.84%. The accuracy of the agroforestry classification in these selected districts ranged from 82.5% to 83.3%, highlighting the reliability and precision of the analysis.

Rizvi et al. (2017b) studied agroforestry and grassland resources in the Uttarakhand state in two districts, namely Rudraprayag and Uttarkashi. Medium-resolution remote sensing data from LISS III was employed for this study, utilizing both pixel and sub-pixel classifiers to estimate the extent of agroforestry and grassland areas. The assessment results indicated that the agroforestry areas in Rudraprayag and Uttarkashi districts were estimated at 2,286.31 hectares (1.15%) and 5,147.45 hectares (0.64%), respectively. Additionally, the grassland areas encompass 18.87% of the Rudraprayag district and 10.88% of the Uttarkashi district. The classification process demonstrated high accuracy, with Rudraprayag district achieving 84.4% accuracy and a Kappa Coefficient of 0.829. In Uttarkashi district, the classification accuracy reached 83.8%, accompanied by a Kappa Coefficient of 0.822.

Tassew (2017) executed a study in the croplands surrounding Nkasiem village within the Goaso district, located in the Brong Ahafo region of Ghana, West Africa. The research covered a total area of 621 hectares with a perimeter spanning 10.3 km. Within this study area, a specific inventory of Trees Outside Forests (TOF) was carried out, focusing on 147 hectares of croplands. The identification of cropland locations in the study area was achieved through visual assessment of satellite images obtained from Google Earth. This assessment was primarily based on tree cover to discern cropland areas. Google Earth imagery from the

date 4/2/2015, provided by CNES/Astrium in 2016, was utilized, featuring a resolution of 2.6 x 2.6 meters. The acquired image from Google Earth was downloaded and processed into rectified images. Subsequently, manual digitization of cropland boundaries was improved in ArcMap 10.4.1 based on field observations and the TOF inventory, resulting in the development of the final cropland map. In the 147 hectares of croplands within the study area, a total of 786 individual TOF observations and 50 different TOF species were identified and documented. On average, there were approximately 5 TOF trees per hectare.

Vikrant et al. (2018) researched in the agroforestry area in Tehri district, situated in the North Western Himalaya region of Uttarakhand, using remote sensing data from Resourcesat-2, specifically LISS IV imagery. This imagery provided a spatial resolution of 5.8 meters and encompassed three spectral bands, including Green (0.52–0.59 μm), Red (0.62–0.68 μm), and NIR (0.77–0.86 μm). For the analysis, ERDAS IMAGINE Professional 2011 software was employed. Through the application of both unsupervised and supervised classification methods, the area under agroforestry was estimated. The unsupervised classification method yielded an estimation of 5,572.26 hectares, equivalent to 1.53% of the total area. In contrast, the supervised classification method produced a slightly higher estimate of 7,029.06 hectares, accounting for 1.93% of the total land area. The classification process exhibited an accuracy rate of 86.5% for the agroforestry class. The distribution of agroforestry was further analyzed with the highest area, 3,707.36 hectares, found in elevations ranging from 1,200 to 2,000 meters, followed by 2,231.26 hectares in elevations spanning 288 to 1,200 meters. Moreover, the estimated area under *Grewia oppositifolia, Celtis australis, and Quercus leucotrichophora*-based agroforestry systems was determined to be 2,330.82, 1,456.80, and 1,129.10 hectares, respectively.

Rizvi et al. (2019a) estimated agroforestry area in Koraput district of Odisha was accomplished through the utilization of multispectral remote sensing images from RS-2A, specifically LISS IV (with a resolution of 5.8 meters) for mapping purposes. This study employed both supervised classification and Object-Based Image Analysis (OBIA) methods. The processing, analysis, and spatial data integration were carried out using ERDAS 2015 and ArcGIS software version 10.4. Under the maximum likelihood classifier (MLC) approach, the agroforestry area was determined to be 31,795.28 hectares, constituting 3.80% of the total area. The overall accuracy of the Land Use and Land Cover (LULC) classification reached 80.81%, accompanied by a Kappa Coefficient of 0.783 using MLC. Alternatively,

when employing the OBIA method, the agroforestry area was estimated to be 42,978.55 hectares, equivalent to 5.14% of the total land area. This method achieved very high accuracy, with an accuracy rate of 91.2%.

Rizvi et al. (2019b) analysed seven districts, namely Dausa, Guna, Hamirpur, Hoshangabad, Lalitpur, Pali, and Panna, all belonging to agro-climatic zone-8. This analysis harnessed Resourcesat-2/LISS III multispectral remote sensing data featuring a spatial resolution of 23.5 meters. The data was subjected to both visual and digital interpretation using ERDAS IMAGINE 11.0 software. Thematic maps for land use and land cover, including agroforestry, were meticulously prepared through the utilization of ArcGIS 10.0 software. The findings of this assessment revealed that the estimated area under agroforestry was most prominent in Pali district, encompassing 6.71% of the total land area. Dausa district followed closely with 6.54%, while Lalitpur district exhibited 6.53%. On average, the selected districts recorded an agroforestry area of approximately 5.18%. These results provide valuable insights into the prevalence of agroforestry in these districts and represent a past research endeavour.

Hassanin et al. (2020) studied Bandipora district of Jammu and Kashmir, and used Sentinel-2A satellite bands with varying spatial resolutions of 10 meters and 20 meters. The study area was around 178.63 sq. km, and a segmentation approach was used to delineate the area from the satellite image. The study employed a finer segmentation resolution to capture Trees Outside Forest (TOF) objects and coarser segmentation for non-forest areas. The results showed that the water bodies covered an area of about 36.807 sq. km, while agricultural, wasteland and wetland categories occupied an area of 239.38 sq. km. Settlements covered a substantial area of 36.40 sq. km. The study primarily focused on Trees Outside the Forest, and the space under this category was identified as 178.63 sq. km. This area mainly consisted of tree species such as willow, poplar, apple, walnut etc. The Bandipora district is affluent in Trees Outside the Forest resources, which can support industries like bat, wicker willow, and horticulture. Additionally, these areas serve as valuable CO_2 sinks, contributing to environmental sustainability. The study achieved an impressive overall accuracy rate of 93.57%, with a Kappa Coefficient 0.91.

Rizvi et al. (2020a) mapped agroforestry areas across six districts in Karnataka, India. The districts included were Bagalkot, Bellary, Gulbarga, Mysore, Shimoga, and Tumkur. The

researchers used multi-spectral remote sensing images taken from RS-2/LISS III to assess the areas' land uses and land covers (LULC). The spatial resolution of these images was 23.5 meters. The study found that Tumkur district had the highest area under agroforestry, accounting for 22.05% of the total area. The agroforestry systems in this district were primarily based on coconut (*Cocos nucifera*) and supari (*Areca catechu*). Shimoga district also had a substantial area under agroforestry, with approximately 80,255.64 hectares, equivalent to 9.47% of its total land area. On the other hand, Bellary district had the lowest area under agroforestry, at only 3.0%. This was mainly due to the low tree density within the district, which averaged only 2.38 trees per hectare. Across all six districts, the estimated area under agroforestry was around 0.47 million hectares, which accounted for 9.21% of the total land area. The LULC classification of these districts achieved an accuracy rate ranging from 83% to 85%.

Zahoor et al. (2020) analysed the Land Use/Land Cover (LULC) classes in the Ganderbal district, located in the Kashmir Himalaya region. They used Landsat-8 (OLI) imagery captured in 2018. They employed image processing software (ERDAS IMAGINE) and mapping software (ArcGIS) to assist with their analysis. The team identified ten distinct LULC classes in the study area, which included forest, forest scrub, grassland, snow, wasteland, agriculture, Trees Outside Forest (TOF), built-up areas, water bodies, and wetlands. Forests were the most dominant class, covering 33.96% of the total area, while wetlands were the smallest at 1.35%. To validate the accuracy of the LULC map, the team used ground truth points, which resulted in an overall classification accuracy of 90.14%, with a Kappa Coefficient of 0.8897. These findings offer valuable insights into the distribution of LULC in the Ganderbal district, which can be used to support land management and environmental planning efforts.

Ganz et al. (2020) used aerial images and Sentinel-2 data to create a comprehensive forest map. The process was highly automated, making it suitable for assessing forest coverage on a large scale. The results showed that approximately 37.12% of the state's land area was covered with forests. This finding agrees with the National Forest Inventory (NFI) report, which reported a forest cover of 37.26% with a margin of error of ± 0.44%. The study demonstrated that forest cover mapping can be effectively done using aerial images and Sentinel-2 data, even under various data acquisition conditions and settings. The forest cover map created was compared to the 34,429 NFI plots, and the results showed a remarkable

spatial agreement of 95.21%. These findings confirm the reliability and usefulness of the forest mapping approach and highlight the factors that may contribute to any differences with existing datasets.

Kumar et al. (2021) conducted a study in Haryana State, India, to estimate the extent of Trees outside the Forest (TOF) using very high-resolution data from CARTOSAT-1 and LISS-IV on Indian Remote Sensing (IRS) satellites. The study identified different formations of ToF, such as linear and block configurations, which covered a total area of 128.83 sq. km and 20.51 sq. km, respectively. These formations accounted for about 3.38% of the state's geographical area. The researchers mapped point formations with a scale of 1:10,000 and achieved an impressive overall accuracy of 94.5%, with a Kappa Coefficient 0.91. Linear formations were similarly mapped with high accuracy, at 93.5% (Kappa of 0.93), while polygon formations displayed the highest overall accuracy of 95% (Kappa of 0.94).

Rizvi et al. (2021) conducted a comprehensive study on agroforestry in nine districts of the Western Himalayan Region. They used high-resolution (LISS-IV) remote sensing data and an object-oriented classification methodology to map the area. The districts included Kangra, Kullu, and Sirmour in Himachal Pradesh, Champawat and Pauri Garhwal in Uttarakhand, and Badgam, Kulgam, Pulwama, and Udhampur in Jammu & Kashmir. The research showed that the total agroforestry area across these nine districts was approximately 332,127.55 hectares, equivalent to 12.4% of the total land area. *Salix alba*, a popular agroforestry species, comprised around 12% of the total agroforestry area in three districts in the Kashmir valley. Pulwama district had the most extensive agroforestry coverage, with approximately 20.7% of its total land area covered. Udhampur district followed closely with agroforestry coverage of 19.8%.

Malkoc et al. (2021) addressed the issue of gaps in spatial data related to Tree Outside Forest (TOF) resources across the country. They used an automated mapping approach based on the UNFAO-FRA definition. The study utilized various datasets within the ArcGIS framework, which included a Vegetation Height Model (VHM), a Topographic Landscape Model (TLM Regio), a land cover map, and a Forest Mask. The results were validated against data from the Swiss National Forest Inventory (NFI), achieving an overall accuracy of 95%, with 55% for the producer's accuracy and 75% for the user's accuracy. Regional variations in accuracy were observed, with the Central Plateau showing the highest accuracy and the Alps

exhibiting relatively lower accuracy levels. The study demonstrates the effectiveness of automated mapping approaches to improve the completeness and precision of TOF resource mapping at the national level.

Nandasena et al. (2022) demonstrated the ability to classify land cover with high accuracy and detail using Sentinel-2A satellite images, elevation data, and the Google Earth Engine platform. Their focus was mainly on forestry classes in Sri Lanka. The methodology involved extracting ten spectral, 16 textural, and three topographical features from the input datasets. Using a random forest classification model, the researchers were able to distinguish between various vegetation types such as forests, forest plantations, shrubs, grassland, home gardens, and cultivation. The results were impressive, with an overall accuracy of 94% and a high Kappa value of 0.91. The study also highlights the importance of the elevation feature in discriminating between forest and agroforestry classes.

Liu et al. (2023) collected data from Planet Scope-based maps of tree cover and height and used specific criteria to classify land areas into forests and trees outside forests. According to their study, forests are areas with woody vegetation with a canopy cover of more than 10% for trees taller than 5 meters. They are not categorized as urban or agricultural land use. Forests covered about 377 million hectares, which accounts for 28% of the total land area. On the other hand, trees outside forests have a lower canopy cover of tall trees and occupy about 16.1 million hectares or 1% of the total land area and 4% of the tree cover. The study also pointed out differences in the forest and trees outside forests categories across various European countries, with northern European countries having significant forest cover and limited areas classified as trees outside forests.

2.2 AGROFORESTRY SUITABILITY MAPPING

Agroforestry suitability refers to land suitability to various agroforestry crops. Remote sensing and GIS based themes help to integrate information on GIS platform. Multicriteria analysis using weighted means are being applied for spatial modeling, which is one of the widely acceptable methods for the suitability analysis (Ayehu and Besufekad 2015). The geospatial modeling is executed to obtain agroforestry suitability analysis using weighted overlay technique. Agroforestry suitability surface obtained by integrating the various factor used and based on their surface values they are classified into three agroforestry suitability class (high, medium and low). Soil nitrogen (N), phosphorus (P), potassium (K), organic

carbon (C), pH and soil sulphur (S) used for producing nutrient availability map, they are important parameters which manifest soil fertility and can ensure food security. The factors which contribute potentially towards agroforestry are nutrient availability, slope, wetness, rainfall and elevation whose weights are scientifically chosen. These parameters have the potential for delineating intensive suitable area for various crops (Goparaju et al. 2017)

Ahmad and Goparaju (2016) conducted a study to identify suitable locations for development within open spaces in Firayalal Chowk, Ranchi. They used Landsat OLI satellite data with a 30-meter resolution from 2015 and covered a 30 km radius of the city centre. The researchers integrated additional data sources, such as ASTER DEM, wetness maps, slope data, soil carbon content, drainage information, and urban buffer data, into a GIS environment. They created thematic maps, such as slope and drainage maps, using ArcGIS Software and ERDAS IMAGINE spatial analyst tools. The land use/land cover classification achieved an impressive overall accuracy rate of 92% with a Kappa Coefficient value of 0.87. The suitability map categorized potential areas into three classes: highly suitable (27%), moderately suitable (38%), and least suitable (35%) within existing open spaces.

Ahmad et al. (2017) assessed agroforestry suitability in the Chakardharpur subdivision, part of India's West Singhbhum district. They acquired satellite data with 11 spectral bands from the United States Geological Survey (USGS) portal. Analysis was conducted using ERDAS IMAGINE (Version 9.1) and ArcGIS Spatial Analyst (Version 10.1). Parameters like nutrient availability, slope, wetness, rainfall, and elevation were considered. Through spatial analysis, the study generated an agroforestry suitability map for the region. Results classified the study area into different suitability classes: approximately 21.6% was highly suitable, 12.5% moderately suitable, and 8.3% had low suitability for agroforestry practices.

Ahmad and Goparaju (2017a) studied nutrient availability and agroforestry suitability map in open area in the Palamu district of Jharkhand, India. The Landsat-8 satellite data having spatial resolution 30 m with projection was used which was downloaded from the website of United States Geological Survey (USGS). Agroforestry suitability surface was generated using the layers *viz*., nutrient availability, slope, wetness, rainfall and elevation through GIS integration in the ArcGIS 10.1 platform. A total of 3334 open-area grids were identified, 62% of which were found to be highly suitable for agroforestry.

Ahmad and Goparaju (2017b) evaluated various spatial (soil and environmental) datasets in Dumka district of Jharkhand using remote sensing and GIS technology to achieve a nutrient availability and agroforestry suitability map. The satellite data used for the study was Landsat-8 OLI having spatial resolution 30 m with projection system (UTM- Zone 45). The agroforestry suitability map was generated utilizing the layers *viz*., nutrient availability, slope, wetness, rainfall and elevation by GIS integration/modelling in ArcGIS 10.1 software. The study shows that the total open area land grids were 3421 out of which 50% of grid was found to be highly suitable towards agroforestry. The study reveals high agroforestry suitability land grid proximity towards high poverty grid was approximately more than 70%, whereas the proximity to the drainage pattern was roughly 60%. One of the completed watersheds in the part of the study area evaluation reveals approximately 50% of the watershed area grid has the proximity of high agroforestry suitable land grid.

Ahmad and Goparaju (2017c) attempted to study the upper watershed part of Subarnarekha basin in Jharkhand state of India. The satellite data used for the analysis was Landsat 8 having a spatial resolution of 30 meter (OLI bands) and 100 meters (TIRS bands). The image processing software used are ERDAS IMAGINE (version 9.0) and Arc GIS spatial analyst (version 10.0). ASTER DEM with resolution of 30 meter was downloaded from the portal of USGS and used to generate different thematic layers such as watershed, slope and drainage. Several thematic layers like slope, drainage and rainfall were integrated to achieve a priority area map using spatial multicriteria decision making. The bands used for the analysis are NIR (5), Red (4), and Green (3). The high priority area was 16.63% of the total study area.

Ahmad et al. (2018a) identified Samastipur, Bihar, India, a suitable land for agroforestry using GIS modeling. The research integrated various data sources, including soil fertility and satellite data (Sentinel, Landsat-8, and ASTER DEM), and employed software like ERDAS IMAGINE and ARC/GIS to achieve its objectives. Agroforestry suitability maps were generated for the Samastipur district, classifying 48.22% of the land as very highly suitable, 22.83% as highly suitable, 23.32% as moderately suitable, and 5.63% as low suitable. The cross-evaluation of agroforestry suitability with land use/land cover categories revealed that 86.4% (agriculture) and 30.2% (open areas) of the land were classified as very highly suitable for agroforestry.

Ahmad et al. (2018b) investigated the suitability of land use/land cover of Lohardaga district of state of Jharkhand, India for agroforestry use based on FAO land suitability criteria utilizing Landsat-8 images (NDVI/wetness), ASTER DEM (elevation/slope/ drainage and watershed), ancillary data source (rainfall/ organic carbon/pH and nutrient status). The analysis of the study for agroforestry suitability reveals that 50.5% area as highly suitable (S1), 28.2% area as moderately suitable (S2), 20% area as marginally suitable (S3) and 1.3% area as not suitable (NS). Only 2.9% of the total land area is dominated by two season crops.

Kahsay et al. (2018) aimed to assess the suitability of land for sorghum (Sorghum bicolour L. Moench) cultivation, employing Geographic Information System (GIS), fuzzy set models, and the Analytical Hierarchy Process (AHP). The evaluation considered soil, climate, and topographic characteristics. The results categorized the study area as follows: 30.54% (29,534 ha) were moderately suitable, 36.17% (34,984.74 ha) were marginally suitable, 18.05% (17,455 ha) were currently unsuitable, and 15.24% (14,744.61 ha) were permanently unsuitable for sorghum production. Key limiting factors included slope gradient, altitude, temperature, length of the growing period, available water capacity, mean weight diameter, total nitrogen, available phosphorus, and soil organic carbon content.

Ahmad et al. (2019a) evaluated the land potentiality in India for agroforestry based on FAO land suitability criteria utilizing various land, soil, climate, and topographic themes. This was achieved in GIS Domain by integrating various thematic layers scientifically. Used Arc/GIS and ERDAS IMAGINE software to execute the objectives. Used SPOT4 satellite-based vegetation cover (VEGA 2000 dataset) having 1-km spatial resolution for this study. The analysis of land potentiality in India for agroforestry suitability reveals 32.8% as highly suitable (S1), 40.4% moderately suitable (S2), 11.7% marginally suitable (S3), and 9.1% not suitable (NS). About 52% of land of India is under the cropland category. In addition, it revealed that the 46% of these cropland areas fall into high agroforestry suitable category.

Ahmad et al. (2019b) conducted a study to evaluate nutrient availability and develop agroforestry suitability maps for the Bundu, Namkum, and Rahe blocks in the Ranchi district. The study employed geospatial technology using primary Landsat OLI satellite imagery data to generate maps at a 30-meter spatial resolution. The suitability maps were developed using Food and Agriculture Organization (FAO) criteria for land suitability and integrating several geospatial layers, including Land Use and Land Cover (LULC), Normalized Difference

Vegetation Index (NDVI), wetness factor, elevation, slope percentage, drainage patterns, watershed delineation, rainfall data, organic carbon content, pH levels, and nutrient status. The findings showed that only 6% of the study area was used for pure agricultural cultivation, while 32.8% showed agroforestry suitability. The Rahe block had the highest percentage of highly suitable land at 79.1%, followed by Bundu with 56.5%, and Namkum with only 1.1% highly suitable land for agroforestry.

Ahmad et al. (2020a) executed an assessment of agroforestry suitability mapping in Gumla district, Jharkhand, using the FAO-based land suitability criteria. They integrated various layers, including Land Use and Land Cover (LULC), NDVI, wetness, elevation, slope, rainfall, organic carbon, pH, and nutrient status. The agroforestry suitability map revealed that 28% of the area was highly suitable, 38% moderately suitable, 25% marginally suitable, and 9% not suitable at all for agroforestry practices.

Ahmad et al. (2020b) conducted a study to quantify the land potential for scaling agroforestry in South Asia using geospatial techniques and FAO's land suitability criteria, which encompassed eleven parameters including vegetation/NDVI, rooting condition, oxygen availability to roots, nutrient availability and retention capacity, excess salts, toxicity, aridity, precipitation, temperature, and slope. The findings of the study revealed that 56.34% of the area was highly suitable for agroforestry, 27.46% moderately suitable, 9.11% low suitable, and 7.09% not suitable for agroforestry practices.

Rahmawaty et al. (2020a) carried out research to assess the suitability of land for cultivating Rambutan (*Nephelium lappaceum*) in community agroforestry areas located in Gunung Ambat village and Simpang Kuta Buluh village. The evaluation incorporated multiple factors, including temperature, water availability, rainfall, oxygen availability, drainage, root zone medium, texture, soil depth, nutrient retention, cation exchange capacity, pli, organic carbon, erosion hazard, slope, flood hazard, and inundation, using geographic information system (GIS). The results revealed that in Gunung Ambat village, Rambutan cultivation was found to be moderately suitable, covering 97.56% of the area. In Simpang Kuta Buluh Village, it was also rated as moderately suitable, encompassing 52.92% of the land.

Rahmawaty et al. (2020b) conducted a land suitability assessment for the cultivation of *Lansium domesticum* on agroforestry land in Sei Bingai Sub-district, Langkat District,

North Sumatra, Indonesia. The study employed a matching method and geographic information system (GIS) to consider various criteria, including temperature, water availability, rainfall, oxygen availability, drainage, root zone medium, texture, soil depth, nutrient retention, cation exchange capacity, pH, organic carbon, erosion hazard, slope, flood hazard, and duration of waterlogging. The findings indicated that approximately 88.95% of the assessed land was moderately suitable, while the remaining 11.05% was marginally suitable for Lansium domesticum cultivation in agroforestry systems.

Ahmad et al. (2021) analyzed Nepal's agricultural landscape and ecological zones, employing topographical and vegetation data, such as Digital Elevation Models for slope maps and MODIS Normalized Difference Vegetation Index (NDVI) data for NDVI maps. Geospatial datasets on land, soil, climate, and topography were used for modeling and mapping suitable areas for trees in Nepal. The study revealed that 18.9%, 12.8%, and 68.3% of the total land area were categorized as low (<30%), medium (30–60%), and high (≥60%) suitability for trees, respectively. Notably, 68.6% of the Tarai region exhibited over 80% tree suitability, with 40.2% tree cover (>10%). Similarly, 67.7% of hilly land with more than 70% tree suitability displayed 49.2% tree cover (>10%). In the mountain regions, which experience extended snow cover and feature undulating terrain, approximately 28.1% of the land demonstrated over 60% tree suitability, with 22.9% tree cover (>10%).

Kumar et al. (2021) analysed Parasai-Sindh Watershed which is located in Babina block of Jhansi district by using LISS–III (spatial resolution- 23.5m) and LANDSAT (spatial resolution- 30m) data for pre- and post-watershed intervention periods (2008, 2011 and 2016). Soil maps were generated using geostatistical interpolation tools of ArcGIS software. A total of 56 soil samples were collected and analyzed for soil quality assessment. Results revealed that more than 50% watershed area had soil quality in good or very good category.

Chuma et al. (2021) conducted a suitability assessment for agroforestry in the vicinity of Itombwe Natural Reserve, Eastern DR Congo, using the Analytic Hierarchy Process (AHP) approach within a geographic information system (GIS) framework. The study considered eight parameters: climate, soil, land use land cover, distance from roads, aspect, slope, distance from villages, and distance from rivers, which were weighted and overlaid. The AHP technique was employed to calculate the weight of each parameter. The findings indicated that approximately 29% of the area was highly suitable for agroforestry practices,

22% had a high suitability, 34% exhibited moderate suitability, and 14% was deemed unsuitable for agroforestry.

Nath et al. (2021) evaluated the land suitability of the Eastern Indian Himalayan region (Arunachal Pradesh, Assam, Meghalaya, Nagaland, Manipur, Mizoram, Tripura, Sikkim, Assam, and hill regions of West Bengal) for agroforestry through multi-criteria evaluation modelling through GIS. Several variables related to climate, soil, topography, ecology, and socioeconomic criteria having high relevance for agroforestry were analysed and integrated to generate an agroforestry suitability map. The model output reveals that 60,523 sq. km (~77%) of the region's arable land has very good to good suitability for agroforestry, while 21,281 sq. km (~27%) area has very good suitability.

Ngwijabagabo et al. (2021) carried out a spatial suitability analysis and mapping of agroforestry areas in Rwanda's Musanze district, located in the Northern province. This analysis utilized the Analytical Hierarchy Process (AHP) and GIS modeling, incorporating five criteria: rainfall, temperature, soil pH, altitude, and land use/land cover. The results of this study revealed that 24.3% of the study area was very suitable for agroforestry, 56.4% was highly suitable, 17.8% was moderately suitable, and 0.5% was not suitable for agroforestry plantation.

Zhang et al. (2021) assessed coffee farming areas in China's Yunnan Province, categorizing them into four suitability grades: "most suitable," "suitable," "less suitable," and "not suitable." The study found that suitability for coffee cultivation was strongly influenced by factors like the lowest average temperature during the coldest month and altitude. For *Coffea arabica*, the distribution was divided into four grades, accounting for 16.28%, 23.19%, 28.71%, and 31.82% of the total area. Regions in Baoshan, Dehong, Puer, Lincang, Yuxi, Xishuangbanna, Honghe, and Wenshan were identified as the "most suitable" and "suitable" areas for *Coffea arabica*. Similarly, Coffea canephora was also classified into four grades, with respective proportions of 2.21%, 21.70%, 36.79%, and 39.30% of the total area. The "most suitable" and "suitable" areas for *Coffea canephora* were primarily located in regions such as Xishuangbanna, Honghe, Puer, Dehong, Lincang, and Wenshan. These findings have practical implications for spatial planning and risk management in Yunnan Province's coffee production sector.

Babu et al. (2022) conducted research in Haryana's Panchkula district, India, using on-screen digitization techniques on 2019 LISS-IV satellite imagery. They employed ERDAS-2011 and ARC-MAP software to identify and map potential agroforestry sites in the district, specifically targeting scrub lands, fallow lands, and piedmont areas for future agroforestry practices. Their analysis revealed 4,023.45 hectares of wastelands (comprising scrub lands, fallow lands, and piedmont areas) in Panchkula district suitable for agroforestry. These areas, considered in conjunction with factors like soil type, groundwater quality, and rainfall patterns, were recommended for agroforestry development. The study also investigated the driving forces behind agroforestry changes using GPS-based Ground Truth verification alongside 2019 satellite data. This comprehensive analysis aids in the identification and utilization of potential agroforestry sites in Panchkula district, contributing to sustainable land management practices and the expansion of agroforestry in the region.

Mushtaq et al. (2023) delves into the Anantnag district in the Kashmir valley, exploring its potential suitability for mulberry agroforestry. Identifying appropriate sites for mulberry-based agroforestry has become pivotal in sustainable land use planning and agriculture, with a focus on preserving ecological balance. This assessment encompassed factors like slope, temperature, rainfall, land use and land cover (LULC), and soil physical and chemical properties. Scores for these criteria were assigned using the analytic hierarchy process (AHP) technique. This map revealed that 16.59% of the land is highly suitable, 28.16% moderately suitable, 40.29% marginally suitable, and 14.96% unsuitable. Satellite images, Sentinel-2b LULC mapping, and GPS-enabled field surveys were employed to validate the results for accuracy.

2.3 BIOMASS CARBON STOCK AND CARBON SEQUESTRATION POTENTIAL OF AGROFORESTRY SYSTEMS

Carbon sequestration is a phenomenon for the storage of CO2 or other forms of carbon to mitigate global warming. Agroforestry is a land use where trees are integrated with crops and/or animals on farmlands. With adequate management of trees on farmlands, a significant fraction of atmospheric CO2 could be captured and stored in plant biomass and in the soils.

Gupta et al. (2017) generated LULC map for the Bidhalna MWS watershed in Dehradun district of Uttarakhand in India by employing supervised classification of Landsat TM data for

the years 1990 and 2013. The classification resulted in the identification of seven distinct LULC classes, namely Sal, Open scrub, Pine, Degraded Forest, Scrub, Settlement, Agriculture, Plantation, and Riverbed. The InVEST model, version 3.2.0, was utilized to estimate the economic value associated with carbon sequestration. For 2013, the highest total carbon value was observed in pine plantations, amounting to 58.29 Mg of carbon, while the lowest value was attributed to river and riverbed areas, which lack vegetation and are classified as non-forest regions. In the overall landscape, the total carbon was estimated at 697,593.65 Mg. However, in the future scenario (*i.e*., the year 2030), the total carbon value was found to be 573,905.87 Mg.

Paquit et al. (2017) modelled the spatial distribution of carbon stock within Central Mindanao University (CMU) campus. In the study area, a total of 33 distinct land use/land cover (LULC) categories were identified. The quantification of carbon stored in each LULC type was determined by utilizing pertinent secondary information obtained from local and international research sources. The process of mapping carbon distribution across CMU's landscape was carried out using the InVEST tool and ArcMap version 10.1. The study results revealed variations in carbon storage across different LULC types. Considering CMU's land area of 3,080.82 hectares, it currently holds an estimated 234,380 metric tonnes of carbon. LULC types characterized by rich vegetation exhibited higher carbon content per hectare. The natural forest stood out with the highest carbon storage, totalling 41,455.10 metric tonnes (equivalent to 209 tonnes of carbon per hectare), constituting 17.69% of the total carbon stock in the area. As a result, it was identified as a potential area for initiatives such as the Reduction of Emission from Deforestation and Degradation Program (REDD+) and other related activities.

Zhao et al. (2017) evaluated the effects of ecological engineering on carbon storage in the upper reaches of the Heihe River Basin in semi-arid northwestern China by linking the CA-Markov and InVEST models. The 16-day 1000 m MODIS NDIV data for 2001, 2008 and 2015 were used to classify land cover types in the upper reaches of the Heihe River Basin. The InVEST model was adopted to assess changes in carbon storage due to LUCC. The results showed that ecological engineering could increase carbon storage by 10.27 Tg from 2015 to 2029 by increasing the proportion of land cover types with higher carbon storage capacity. The relative error of the linked model was 0.22%, indicating that the linked model

was highly applicable in assessments of the effects of ecological engineering on carbon storage in the study area.

Pechanec et al. (2018) conducted a research based on the Czech Republic comes from Corine Land Cover (CLC) database inventory mapped in 1990, 2000, 2006, and 2012. The concept of model InVEST 3 - Carbon was applied to determine the existing carbon stocks and its future development using four carbon pools (aboveground biomass, underground biomass, dead organic matter and soil carbon). The current total carbon stock in the Czech Republic is 950,393,943 t. The largest contribution to the stock comes from carbon stored in the soil (57.6%), followed by the aboveground biomass (31.4%), the underground biomass (7.7%), and the lowest amount of carbon is deposited in the dead mass (3.3%).

KVG and Barik (2018) conducted a study in Visakhapatnam district, Andhra Pradesh, analysing land cover changes over four years. They used Landsat 5 Thematic Mapper data for 2014 and Landsat 8 Operational Land Imager (OLI) data for 2014, 2015, and 2016. The research focused on assessing carbon stored in different pools and estimating potential carbon sequestration or loss. In 2014, aboveground biomass values were 224.73, 721.79, and 3796.74 metric tonnes for sparse, moderate, and dense vegetation. In 2015, these values decreased to 116.95, 630.55, and 3456.04 metric tonnes, respectively. Belowground biomass values in 2014 were 52.81, 169.62, and 1106.32 metric tonnes for sparse, moderate, and dense vegetation, decreasing to 43.65, 140.65, and 956.19 metric tonnes in 2015. Soil organic matter values in 2014 were 210.30, 209.86, and 123.06 metric tonnes and decreased to 187.79, 191.56, and 100.44 metric tonnes in 2015 for sparse, moderate, and dense vegetation. Dead organic matter had values of 1170.88, 5204.46, and 6885.49 metric tonnes in 2014, which decreased to 1045.57, 5982.57, and 7379.06 metric tonnes in 2015 for sparse, moderate, and dense vegetation. The InVEST model estimated a loss of 1,392,299,789.91 Mg of carbon from 2011 to 2014, a loss of 423,909,045.87 Mg of carbon from 2014 to 2015, and a sequestration of 1,512,332,394.91 Mg of carbon from 2015 to 2016 in Visakhapatnam district.

Zhang et al. (2020) investigated the correlation between carbon sequestration and land use changes in Shanghai city. They used Landsat images from 1990 to 2015 and the InVEST model for a detailed assessment of carbon sequestration changes in response to urban expansion. Their study revealed a decrease of 73.19 × 105 metric tons in total carbon stocks

from 1990 to 2015, equivalent to an annual decline of 0.48%. The process of urbanization and associated land use changes had a significant negative impact on carbon sequestration in the urban ecosystem. The findings suggest potential policy measures to mitigate carbon losses and promote sustainable development in the region in alignment with Sustainable Development Goals (SDGs).

Lahiji et al. (2020) conducted a scenario-based land allocation analysis in northern Iran to evaluate the influence of diverse land use policies on carbon storage within a landscape featuring a blend of agriculture and forest. Landsat imagery from 2016 was used to track changes in land use and land cover (LULC) categories over time. Suitability maps for agriculture, forest, urban, and rangeland were created based on ecological and socio-economic criteria. A Multi-Objective Land Allocation procedure was applied to allocate land to each LULC class under five different scenarios, resulting in varying LULC distribution patterns. The Integrated Valuation of Ecosystem Services and Trade-offs (InVEST) model estimated carbon storage potential, with significant variations observed across scenarios. Carbon storage ranged from 1.29 tons per hectare per year in an agriculture-dominated scenario (76% of the area) to 5.40 tons per hectare per year in a forest-dominated scenario (77% of the area). While extreme scenarios, these findings facilitate stakeholder dialogue and provide insights into potential ecosystem service trends associated with expanding agricultural land.

Babbar et al. (2021) evaluated carbon sequestration by analysing changes in total carbon under two scenarios, utilizing the Markov chain and InVEST model, for the years 2000, 2018, and a predictive assessment for 2035. The findings indicated that 1.351 Tg of carbon had been lost between 2000 and 2018 in the forest area of Sariska Tiger Reserve, with an additional expected loss of 0.107 Tg of carbon in the future when comparing the land use and land cover of 2035 to the present scenario. The lower carbon release anticipated in 2035, in comparison to 2018, was attributed to forest management practices, such as plantations carried out in areas like Tehla-Talabberi, Sariska-Ganeshpura, Alwar buffer-Shoydanpura, Talvriksh-Manavaas, Akbarpur-Kalikhol, and Ajabgarh-Jatwana. The study revealed that the economic value of carbon lost from 2000 to 2018 amounted to $214.57 million. In contrast, the economic value of carbon sequestration for the predicted year 2035 was estimated at $17.19 million.

Sarathchandra et al. (2021) researched in Xishuangbanna region of South China, rubber cultivation is expanding rapidly, creating an urgent need to comprehend and monitor changes in land use and land cover (LULC) and how their spatial variations impact carbon storage (CS). This knowledge is crucial for the development and implementation of improved land use management practices. Our study focused on analysing LULC changes over a 22-year period, with a particular emphasis on how these changes have influenced CS. We used remote sensing methods to quantify LULC changes between 1988 and 2010 and employed the InVEST model to calculate CS changes. The findings revealed that between 1988 and 2010, the rate of deforestation accelerated to 203.2 sq. km per year, leading to the loss of approximately 23% of the forest cover. Notably, the conversion of natural forest into rubber plantations was responsible for 78% of this deforestation. The expansion of rubber cultivation occurred at a rate of 153.4 sq. km per year. These changes in LULC drove a temporal reduction in CS, equating to 0.223 tera-grams of carbon per sq. km.

Imran et al. (2021) focused on evaluating the current state and spatial variations in the net carbon storage and its associated economic value within different land use/land cover (LULC) categories in Bagrote Valley, situated in Gilgit-Baltistan. To accomplish this, we applied the InVEST carbon and sequestration model, utilizing LULC classifications obtained through object-based analysis of Sentinel-2 satellite imagery. The findings reveal that carbon stocks are predominantly concentrated within six specific forest types out of a total of 14 LULC categories identified. The overall carbon stock in the valley amounted to 8114.10 metric tonnes in 2016, with dense conifer forests emerging as the primary contributors, accounting for 5409.16 metric tonnes of carbon. In terms of economic valuation, the storage of carbon in this region is estimated at approximately 74728 US dollars per hectare.

Islam et al. (2022) examined the spatio-temporal changes in Tree-Over-Forest (TOF) in the eastern coastal zone of Bangladesh from 1988 to 2018 using Landsat Land Use Land Cover (LULC) maps and the InVEST carbon model. The research revealed dynamic shifts in land use, with TOF, mangrove forests, built-up areas, and salt-aquaculture land expanding at the expense of agricultural land, mudflats, water bodies, and hill vegetation. While TOF saw the most significant increase, contributing to a 9.01 Tg C rise in carbon storage, agricultural land and hill vegetation diminished, resulting in reduced carbon storage. Effective management of land erosion and accretion is crucial for balancing food and environmental security in the region.

Li et al. (2021) researched in Huining County in China's Loess Plateau region, the land use and land cover changes (LUCC) following the GGP were quantified, and their effects on carbon storage between 2000 and 2016 were evaluated using the InVEST model. The results showed that, a total area of about 3996.13 km2 underwent changes following the GGP in Huining County during the study period, accounting roughly for 74% of the county. The total carbon storage increased from 6470.72 Gg in 2000 to 7335.07 Gg in 2016. Spatially, carbon density in the south of this county was greater than the northern part. Directly induced by the GGP (conversions of farmlands to forests and grasslands), the carbon storage increased by 786.84 Gg in total, with a rate of 46.28 Gg per year, the majority of which occurred during the first stage of the study period (from 2000 to 2008).

Kaur et al. (2022) used the InVEST model to assess carbon sequestration in Delhi for the years 2000 and 2020. The study revealed a consistent increase in Forest and Tree Cover during this period, resulting in the sequestration of 6.9 × 105 Megagrams (Mg) of carbon. This rise was attributed to improved forest management and government-led afforestation and reforestation initiatives. Economically, the increased carbon sequestration represents a potential value of approximately 106.27 million dollars, highlighting the economic significance of these positive changes in Delhi's forest and tree cover.

Li et al. (2022) conducted research in Changchun City, northeastern China, using the FLUS model to simulate land use changes from 2010 to 2020. The simulation achieved high accuracy, with 91.07% overall accuracy and a 77.43 Kappa Coefficient, indicating reliability. The findings showed a significant decrease in cultivated land, an increase in construction land and water bodies, reflecting urban expansion. This transformation resulted in a carbon storage loss of 5.81 × 106 Megagrams (Mg), primarily driven by the conversion of cultivated land into construction land. Land use transfers frequently involved the conversion of cultivated land into other types due to urban expansion, leading to a carbon storage loss of 5.99 × 106 Mg. Forests were often transformed into grassland, and water bodies expanded.

Zheng and Zheng (2023) used the Integrated Valuation of Ecosystem Services and Trade-offs (InVEST) and the Patch-generating Land Use Simulation (PLUS) model to study the relationship between land use and carbon storage in Shandong Province over the past 20 years. Cropland decreased by 9.41%, while built-up land increased by 7.66%, with fewer changes in forest, grassland, wetland, water, and bare land. Cropland, a dominant land type,

served as a significant carbon pool with moderate storage. High carbon storage areas were mainly in mountainous regions with grassland and forest, as well as the Yellow River Delta wetland. Urban built-up areas had low carbon storage. The study revealed a loss of 47.96×106 Mg of carbon storage due to land changes. Implementing ecological protection measures could increase regional carbon storage by 6.64×106 Mg, focusing on reducing land conversions into built-up areas, especially in cropland, forest, grassland, wetland, and water, to enhance carbon storage.

Kafy et al. (2023) used remote sensing and the Google Earth Engine (GEE) to analyse spatiotemporal changes in carbon stocks (CS) in the Chittagong Hill Tracts (CHT) from 1996 to 2021. They employed the Integrated Valuation of Ecosystem Services and Trade-offs (InVEST) model. The study found a substantial loss of 21.65 × 106 metric tons of CS in the CHT, mainly due to a 21% reduction in vegetation cover (equivalent to 2862.85 km^2) over the study period. The central city area of Chittagong experienced the most significant CS loss (7.99 × 106 metric tons), while suburban areas like Khagrachari and Rangamati had lower losses. A multiple regression model highlighted the influence of elevation and vegetation on CS. The study underscores the need for policies and strategies to mitigate the impacts of land cover changes on CS and advocates for sustainable forest management practices that balance ecological, social, and economic factors.

He et al. (2023) assessed carbon storage in Guilin City, projecting 2035 scenarios based on Sustainable Development Goals. Four scenarios were analyzed: natural development, economic prioritization, ecological focus, and comprehensive sustainable development. Analysis involved FLUS, InVEST models, GeoDa 1.20, and ArcGIS. From 2005 to 2020, forest land dominated Guilin, with cropland and impervious areas expanding. By 2035, all scenarios showed significant forest land changes. During 2005-2020, northwestern Guilin had higher carbon storage, but carbon losses exceeded gains. Ecological emphasis projected the highest 2035 carbon storage at 874.76 × 106 tons, mainly in the northwest and northeast. Urban areas maintained lower carbon levels. Spatially, 2035 carbon distribution had more hot spots (high storage) than cold spots, concentrated in the northwest and east, while urban areas had lower carbon storage. These findings offer valuable insights for Guilin's sustainable development planning.

Mengist et al. (2023) assessed and mapped carbon storage and sequestration in a biosphere reserve over the years. Using the InVEST and CA Markov models, they estimated carbon stock changes from 1986 to 2019 and projected trends for 2034 and 2049. Field data collection involved 155 plots, including species identification, diameter, and tree heights. Carbon stock calculations used species-specific equations, while soil organic carbon was analyzed in the lab. Carbon storage varied among land use and cover types, with vegetated areas showing higher carbon stocks. The biosphere reserve stored 457.3 to 478.3 megatons of carbon from 1986 to 2019, releasing 4.4% of the 1986 carbon store. Emissions were recorded at about 0.33 (1986), 0.57 (1999), 0.46 (2009), and 0.21 (2019), highlighting the potential for substantial carbon emissions. These findings inform land-use planning, policy, and biodiversity conservation efforts.

Tao et al. (2023) employed a combination of the Patch-generating Land Use Simulation (PLUS) model and the Integrated Valuation of Ecosystem Services and Trade-offs (InVEST) model to simulate and evaluate the future Land Use and Land Cover (LULC) and ecosystem carbon storage in the Nanjing metropolitan circle for the year 2030. They considered four distinct scenarios: natural development (ND), economic development (ED), ecological protection (EP), and collaborative development (CD). The distribution of LULC and carbon storage exhibited spatial heterogeneity within the Nanjing metropolitan circle, with factors such as elevation, nighttime lights, and population serving as primary drivers of LULC changes. Under the ecological protection (EP) scenario, the Nanjing metropolitan circle was projected to experience a carbon increase of 0.50 Tg by 2030, while the other scenarios (ND, ED, and CD) would result in carbon losses of 1.74 Tg, 3.56 Tg, and 0.48 Tg, respectively.

Xu et al. (2023) conducted research in Guangzhou, China, from 2000 to 2020, revealing substantial changes in land use patterns. Woodland remained the largest category, followed by cropland, construction land, water areas, grassland, and unused land. Forest land covered 42.16% of the urban area by 2020. Cultivated land decreased from 35.89% in 2000 to 28.82% in 2020. Construction land expanded notably, from 11.16% to 20.40%. Water areas decreased slightly from 8.03% to 7.25%. Land use dynamics were most pronounced from 2000 to 2010, reflecting substantial urban expansion, especially in construction land. From 2010 to 2020, construction land continued to grow moderately, indicating balanced urban development. Carbon storage (CS) in Guangzhou declined by 4.11% from 2000 to 2020, with

the most significant decrease from 2000 to 2010 due to urban construction. Subsequent years saw reduced carbon loss, aligning with more sustainable land use practices in the city.

Houssoukpevi et al. (2023) assessed land use changes and carbon (C) stock distribution in Ferralsols from 2000 to 2018 using random forest models and the InVEST model. During this period, land use changes impacted 61% of the Ferralsols area, with forests and crop-plantation associations decreasing in extent and being replaced by tree plantations, adult palm groves, and built-up areas. This shift resulted in a decline of approximately -218 Gg C in C stocks, including -175 Gg C in soil pools and -125 Gg C in aboveground biomass. It is crucial to account for soil C stocks to avoid underestimating C stock changes in rural regions, highlighting the need for measures to control tree plantations and deforestation to maintain C stocks in tropical areas.

Chapter-3

MATERIALS AND METHODS

The present investigations entitled "**Remote sensing approach for estimating agroforestry area, suitability mapping and carbon sequestration potential of agroforestry systems in Solan district of Himachal Pradesh"** were carried out in Solan district of Himachal Pradesh in the year 2021-2023. The details of the studies, techniques used and methodologies adopted in undertaking these studies are given hereunder the major heads and subheads:

3.1 SITE DESCRIPTION

3.1.1 Location

The present investigations were conducted in the Solan district of the state, which falls in Zone I and Zone II, which include low and mid-hill regions. The district is situated between 30°75′ to 31°37′ North latitude and 76°58′ to 77°24′ East longitude of Himachal Pradesh. The area of the district is 1936 sq.km with an altitude ranging from 650 to 1800 m above mean sea level with gentle to steep slopes ranging from 3 to more than 50 % in hilly terrain.

3.1.2 Climate and edaphic factors

The climate of district Solan is sub-tropical to sub-temperate. The temperature ranges from 0°C in winter to 40 °C in summer. The fine climate of this place around the year makes it an ideal destination for all seasons. The climate of all the blocks varies differently. Most of the area of Nalagarh, Kunihar and Dharampur blocks have a sub-tropical climate. The climate of Solan and Kandaghat blocks is sub-temperate and sub-humid. The district receives an average annual rainfall of 1420.40 mm, mostly during monsoon. Snowfall is not a regular feature and is received in some parts of the district during December-January. As the district has hilly to plain areas, the soils are mainly neutral to slightly acidic, and the soil texture varies from sandy loam to clay loam. The soil depth is generally shallow except in areas having vegetation coverage.

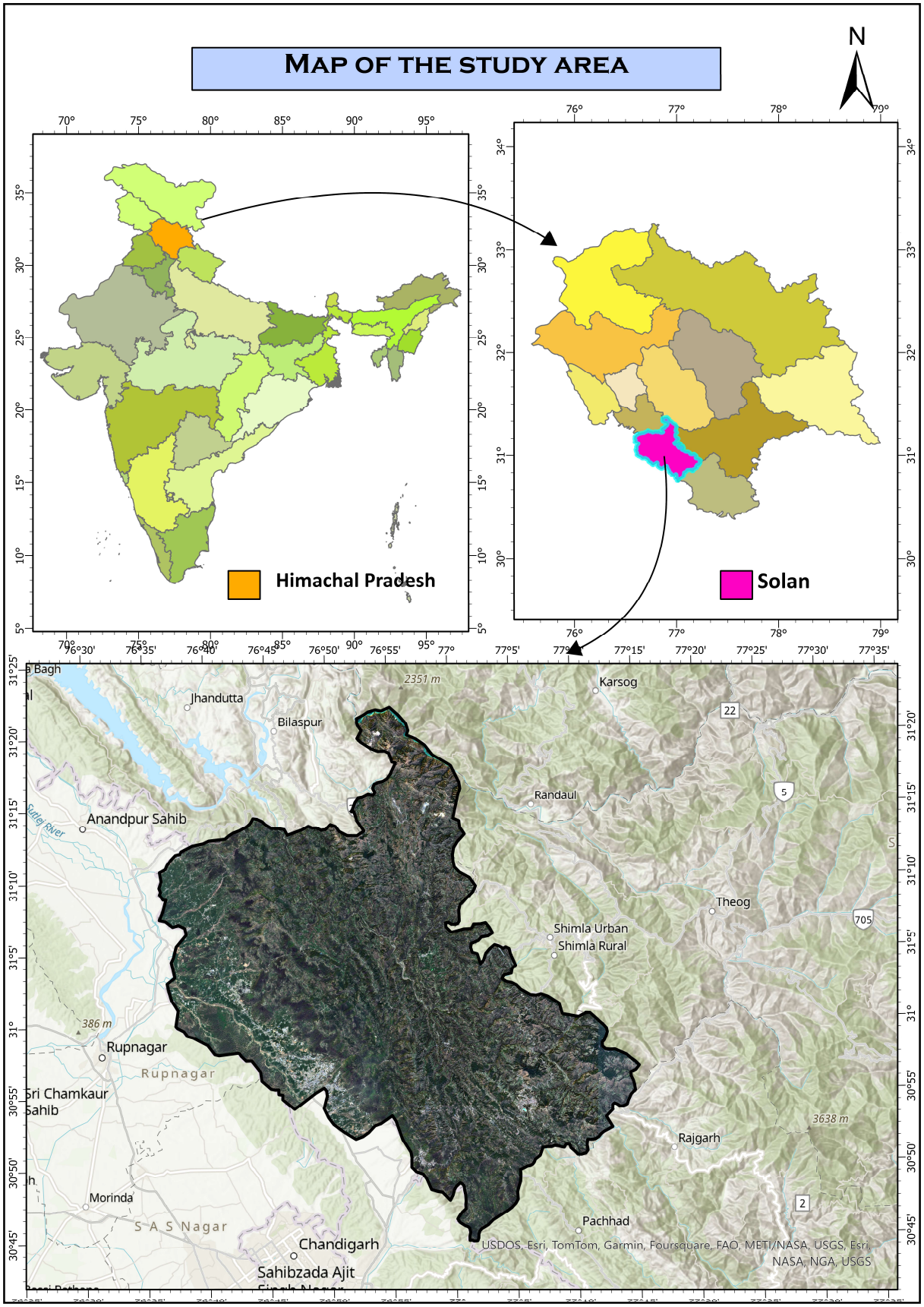

Figure 1. Map of the study area

3.1.3 Experimental details

Experiment I : To determine the area under different agroforestry practices and other land use systems using geospatial techniques;
Experiment II : To prepare the agroforestry suitability map of the Solan district;
Experiment III : To estimate biomass carbon stock and carbon sequestration potential of agroforestry systems and other land-use systems;

3.2. AGROFORESTRY AREA AND OTHER LAND-USE SYSTEMS MAPPING

3.2.1 Software used

ArcMap 10.8.2

QGIS Desktop 3.34.0

SNAP 8.0.9

3.2.2 Satellite used

Sentinel-2A and Sentinel-2B are Earth observation satellites that are part of the European Space Agency's (ESA) Copernicus program and were launched on June 23, 2015, and March 7, 2017, respectively. Sentinel-2A datasets were acquired from the Copernicus Open Access Hub in March 2022, with cloud cover of less than 10 per cent. Sentinel-2A is designed to provide comprehensive and precise data about the Earth's surface, and its observations are instrumental in various domains, including agriculture, forestry, environmental management, disaster response, and urban planning. Sentinel-2A has a Multi-Spectral Instrument (MSI), a cutting-edge imaging system. Its advanced imaging technology, frequent revisit times, and open data policy have made it an indispensable resource, supporting various applications and enhancing our understanding of Earth's dynamic processes. This satellite continues to be a cornerstone in decision-making processes across multiple sectors. Sentinel-2 has 13 spectral bands that range from the visible and near-infrared to the short-wave infrared, with four bands at 10 meters resolution, six bands at 20 meters, and three at 60 meters spatial resolution (Table 1).

3.2.3 Pre- processing

3.2.3.1 Atmospheric correction and ortho-rectification

The datasets procured were L1C level, thus have to be ortho-rectified and atmospheric corrected. The L1C datasets were processed using the Sensor 255 processor in

the SNAP 8.0.9 software for the atmospheric and geometric correction to make the final datasets L2A.

Table 1. Characteristics of Sentinel-2 bands used in the current study (adopted from ESA Sentinel-2 technical report)

Sentinel-2 bands	Band type	Central wavelength µm	Resolution (m)
Band 1*	Coastal aerosol	0.443	60
Band 2	Blue	0.490	10
Band 3	Green	0.560	10
Band 4	Red	0.665	10
Band 5	Vegetation red edge	0.705	20
Band 6	Vegetation red edge	0.740	20
Band 7	Vegetation red edge	0.783	20
Band 8	Near Infrared (NIR)	0.842	10
Band 8a	NIR Narrow	0.865	20
Band 9*	Water vapour	0.945	60
Band 10*	SWIR-Cirrius	1.375	60
Band 11	SWIR	1.610	20
Band 12	SWIR	2.190	20

*Bands not used in present study

3.2.3.2 Resampling

The L2A product was resampled to 10 m using the nearest neighbour resampling technique in SNAP 8.0.9 software. Band 1, 9, and 10 (having 60 m) resolution were removed from the analysis, as they are commonly used for atmospheric correction.

3.2.3.3 Mosaicking

A mosaic is the fusion or merging of two or more tiles. The georeferenced pictures were combined to represent the research region comprehensively. Two tiles were selected to cover the whole Solan district (Table 2).

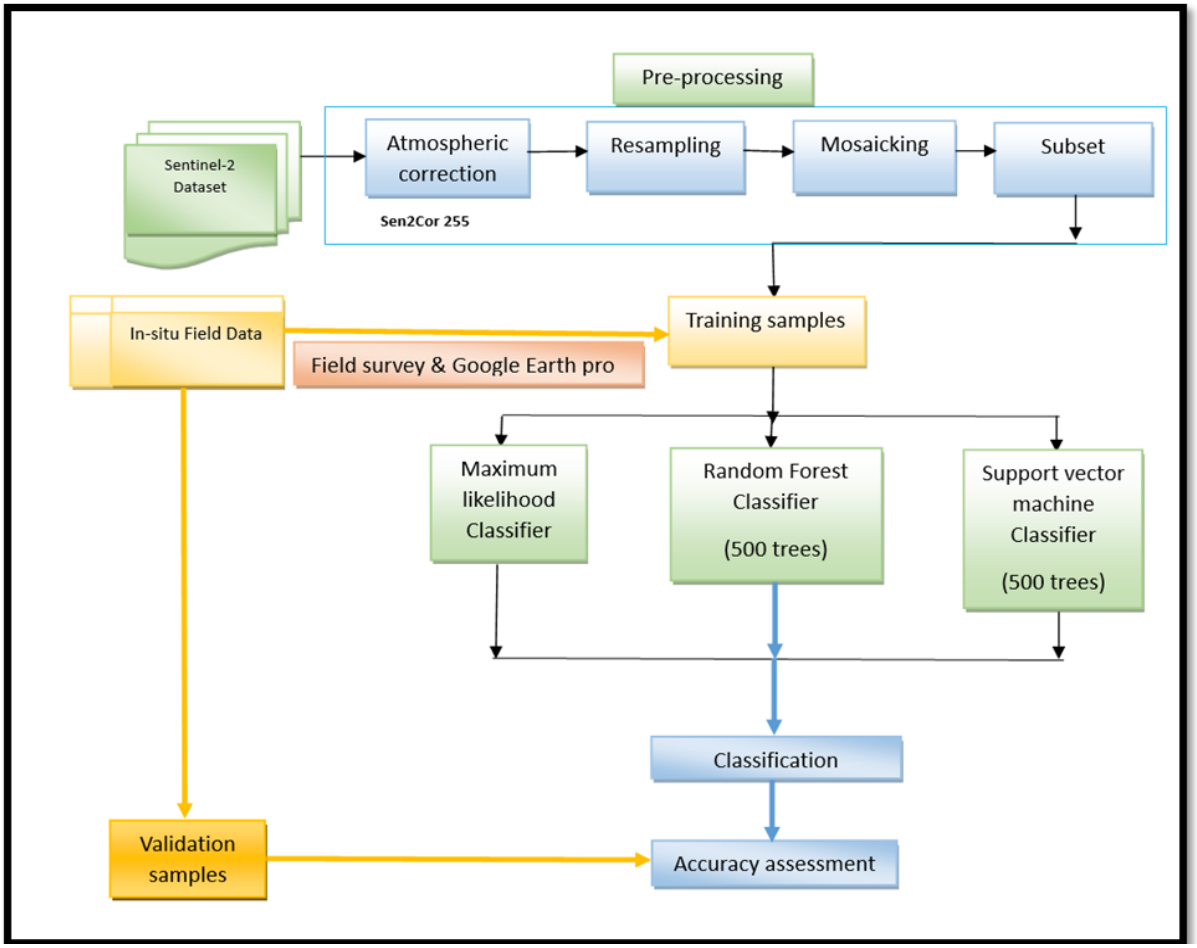

Figure 2. Flowchart of methodology followed for the estimation of area under agroforestry and other land use systems

Table 2. Details of the satellite product used for the mapping of the agroforestry and other major land-use classes.

Platform	ID	Acquisition date	Tile number
Sentinel-2A	L1C_T43RFQ_A035137_20220315T053616	15-03-2022	T43RFQ
Sentinel-2A	L1C_T43RGQ_A035137_20220315T053616	15-03-2022	T43RGQ

3.2.3.4 Bands composite

A band composite is an image that combines multiple spectral bands from a remote-sensing satellite or sensor into a single image. Each band corresponds to a specific range of wavelengths within the electromagnetic spectrum. By combining these bands, a band composite can provide valuable information about various features and phenomena on Earth's surface. In the present study, a band composite image was developed by merging ten bands of Sentinel-2A.

3.2.4 Machine learning algorithms

Machine learning algorithms are computational models that enable computers to learn from data and make decisions or predictions. These algorithms detect patterns, relationships, and insights within datasets. Supervised learning is a method where algorithms are trained on labelled data. The input data is paired with target outcomes or labels, and the algorithm learns to associate input data with the correct labels. Once trained, the algorithm can make predictions on new and unlabelled data.

3.2.4.1 Maximum likelihood Classification

Maximum Likelihood Classification (MLC) is a supervised image classification technique used to assign pixels in a raster dataset to specific classes by calculating the probability of a pixel belonging to a particular class. In MLC, each pixel is assigned to a class based on its probability of belonging to that class, determined by modeling the mean and covariance of the class as forming a normal distribution in multispectral feature space. The algorithm assumes that the statistics for each class in each spectral band are normally distributed. The classification process involves assigning each cell in the input raster to the class with the highest probability of containing it. This assignment is done by considering the

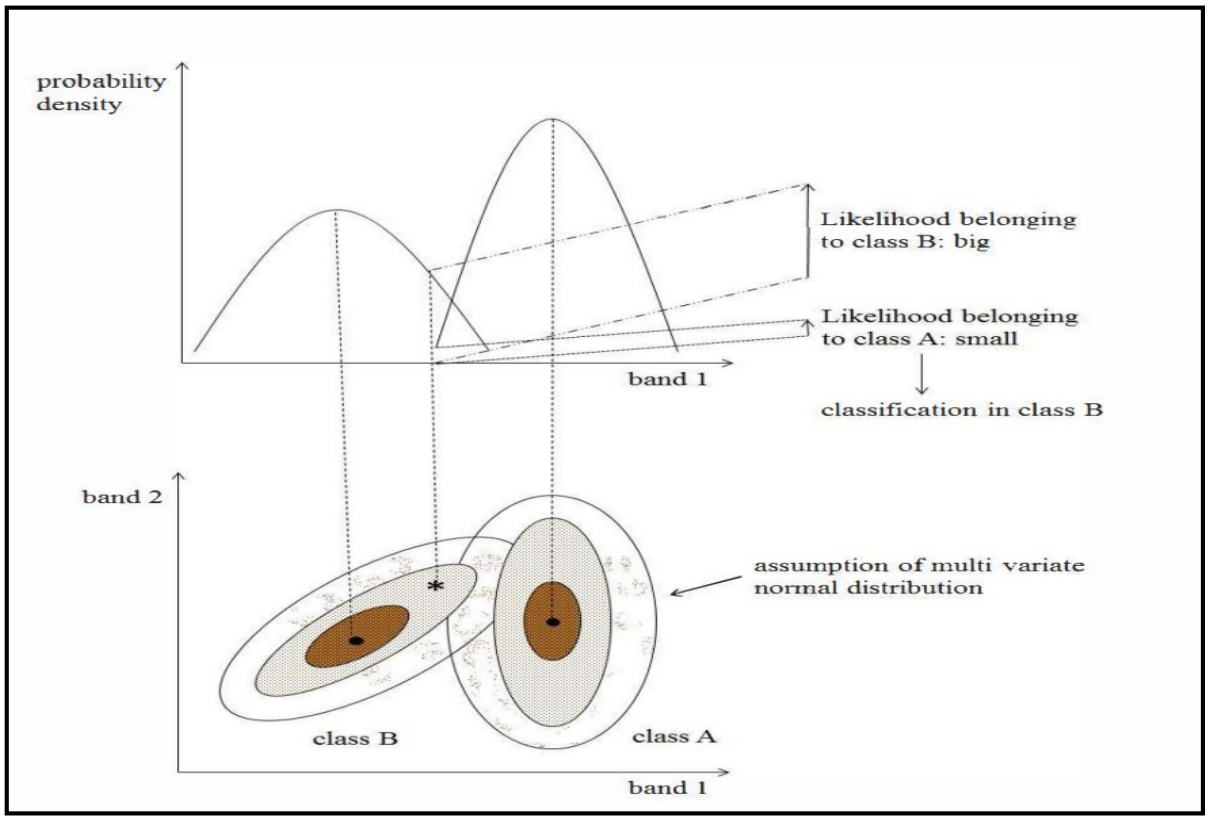

Figure. 3 Maximum likelihood Classifier model

mean and covariance of the class signatures, with the mean vector and covariance matrix uniquely characterizing each class. To determine the membership of cells to a particular class, the statistical likelihood is computed for each class by comparing the characteristics (mean and covariance) for each cell value. The tool then assigns each cell to the class with the highest likelihood.

Additionally, the MLC tool can generate an optional output known as a confidence raster. This raster provides information about the levels of confidence associated with each classification. The confidence raster is useful in understanding the reliability of the assigned classes for individual cells in the output raster. Maximum Likelihood Classification uses the normal distribution assumption of class statistics in multispectral feature space to assign pixels to classes based on their probability of belonging to each class. The mean and covariance of class signatures play a crucial role in this process, and the optional confidence raster provides insights into the reliability of the classification results. (Sisodia et al. 2014).

3.2.4.2 Random Forest Classification

Random Trees is a collection of individual decision trees where each tree is generated from different samples and subsets of the training data. The idea behind calling these decision trees is that for every classified pixel, a number of decisions are made in rank order of importance. It looks like a branch when it is graphed out for a pixel. When it classifies the entire dataset, the branches form a tree. This method is called random trees because it classifies the dataset a number of times based on a random sub-selection of training pixels, thus resulting in many decision trees. To make a final decision, each tree has a vote. This process works to mitigate overfitting.

Random Forest is a supervised machine-learning classifier based on constructing many decision trees, choosing random subsets of variables for each tree, and using the most frequent tree output as the overall classification. Random Trees corrects for the decision trees' propensity for overfitting to their training sample data. In this method, a number of trees are grown by an analogy, a forest and variation among the trees is introduced by projecting the training data into a randomly chosen subspace before fitting each tree. A randomized procedure optimizes the decision at each node. (Vens and Costa 2011).

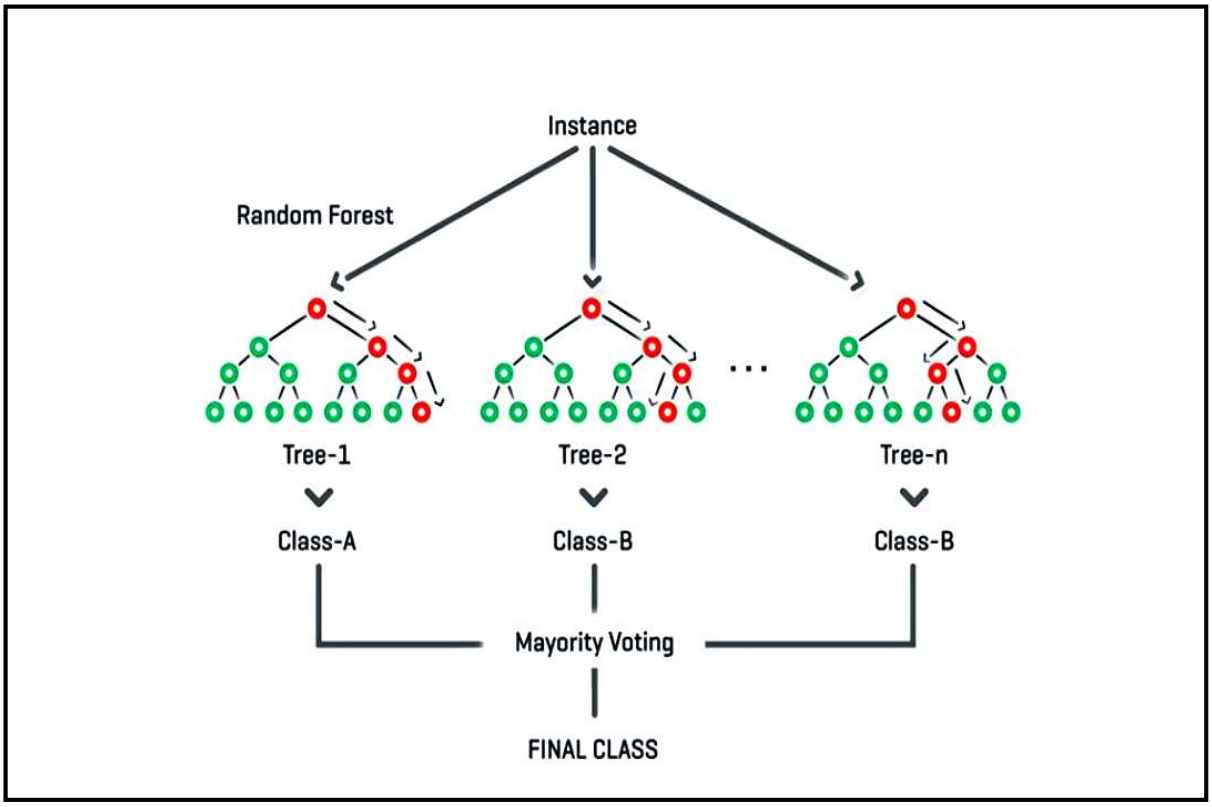

Figure. 4 Random Forest Classifier model

3.2.4.3 Support Vector Machine

Support Vector Machine (SVM) is a supervised machine learning algorithm known for classification and regression tasks. While SVM requires access to all training data during the training phase, it becomes sparse post-training, relying on a subset known as support vectors for predictions. These support vectors, crucial for defining hyperplane margins, are identified through an optimization process involving Lagrangian relaxation. SVM excels in multi-class scenarios, distinguishing between classes by maximizing hyperplane-based separation. The algorithm's efficiency depends on the number of support vectors, not the input space dimensionality. SVM's adaptability to non-linear data is achieved through the kernel trick, employing various kernels like linear, polynomial, RBF, and sigmoid. Additionally, SVM handles regression tasks, showcasing its versatility. The complexity of SVM is tied to the hypothesis space and empirical error, making it a powerful tool for diverse machine learning applications. (Awad and Khanna 2015).

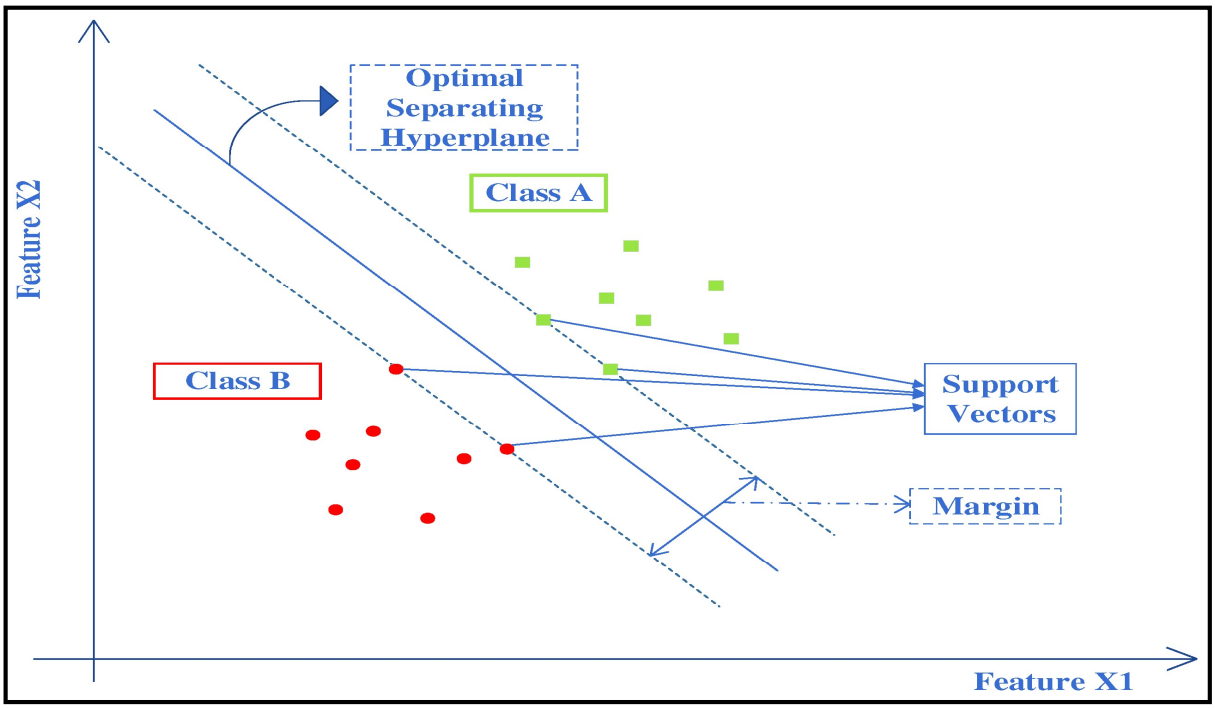

Figure 5. Support vector machine classifier model

3.2.5 Generation of training sample

In machine learning and remote sensing, training samples are critical as carefully chosen and labelled data points that represent distinct categories within a dataset. They are fundamental for instructing algorithms to effectively identify and differentiate between these categories. For instance, in the analysis of satellite images, training samples can be specific pixels or defined regions that have been marked to represent different land cover types, such as agriculture, agroforestry, barren land, built-up areas, grassland and water bodies (Table. 3). The quality and diversity of these training samples are of utmost importance as they greatly influence the accuracy of the models. By generalising from the provided examples, they ensure that algorithms can make precise predictions when applied to new, unlabelled data.

ArcGIS 10.8.2 offers robust tools for creating these training samples, which are indispensable for training classification algorithms. These labelled samples are the foundation for instructing machine learning algorithms to recognize and classify similar features across larger datasets. With the user-friendly interface and spatial analysis capabilities of ArcGIS, the process of generating training samples becomes more efficient and streamlined. This, in turn, enhances the accuracy and efficiency of various geospatial analyses, including land cover classification and object detection.

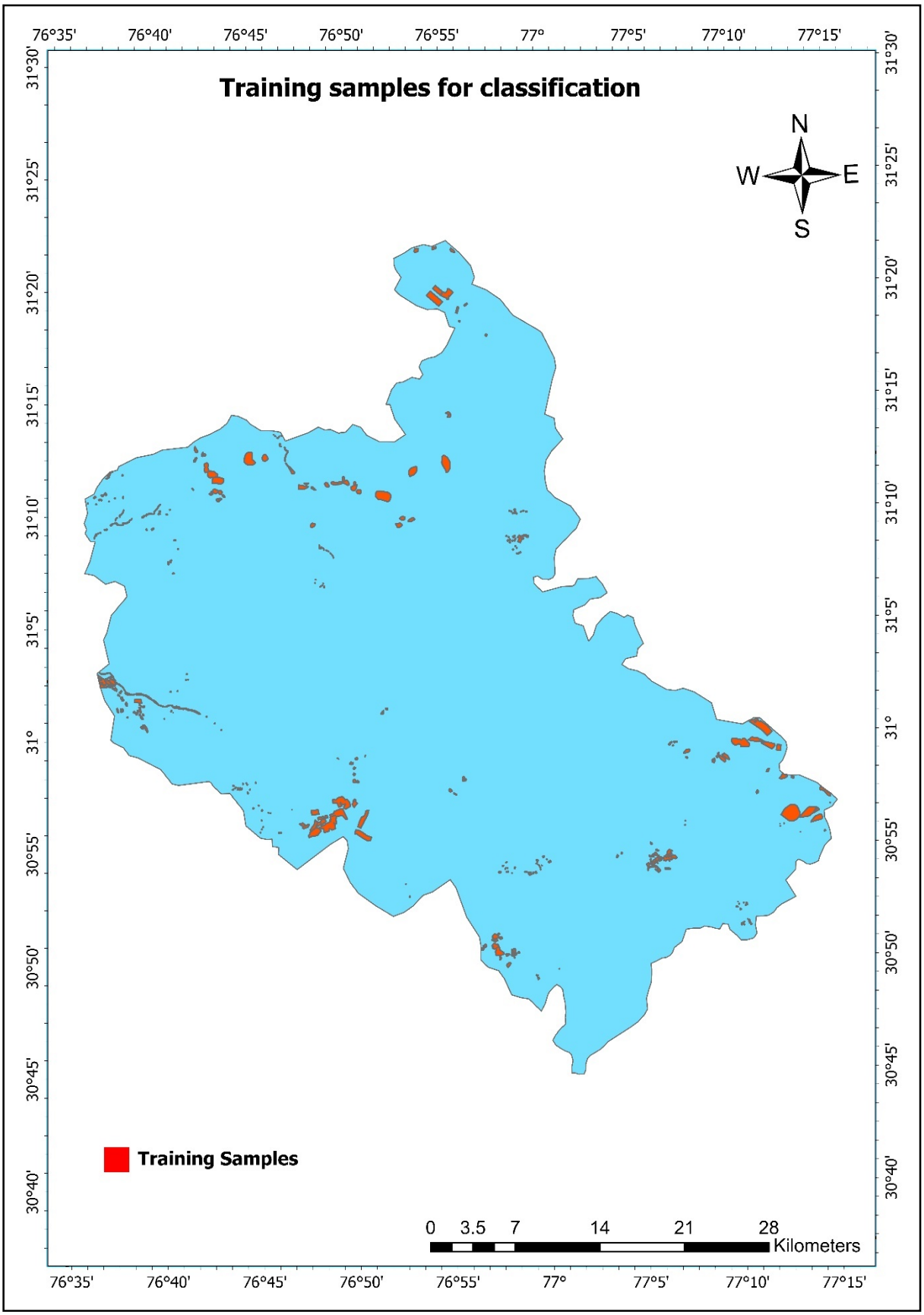

Figure 6. Samples for training the classifier in Solan district of (H.P)

Table. 3 Major land-use and land cover class used and their descriptions

Agricultural Land	Includes areas used for perennial and annual crops, irrigated areas, scattered rural settlements, commercial farms (sesame cultivations and sugarcane plantations).	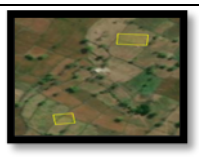
Agroforestry	Areas covered with trees along farms and in small patches up to 0.1 ha in area, roadside plantations, orchards, agroforestry plantations.	
Barren land	Areas covered with scrub land, gullied/ravenous land, barren rocky land.	
Built-up Area	Areas of commercial areas, urban and rural settlements, industrial areas.	
Forest Land	Areas covered with dense trees (deciduous forests, evergreen forests, mixed forests).	
Grassland	Areas covered by grasses are usually used for grazing and those remain for some months in a year.	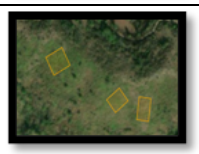
Water Body	Areas covered by rivers, streams, and reservoirs	

3.2.6 Validation data collection and Accuracy assessment

Accuracy assessment and validation are essential components of mapping projects. To effectively evaluate the accuracy of a classified image, it is imperative to consider factors such as the quantity, distribution, and precision of ground control points (GCP) and appropriate sampling techniques (Sharma 2022).

The sample size was determined using a stratified sampling technique for data validation across various land use categories. This approach was executed within ArcGIS 10.8.2 (Rwanga et al. 2017).

$$n = \left(\frac{\sum WiSi}{S(\hat{O})}\right)^2$$

Here n= number of samples required, $S(\hat{O})$ = standard error of estimated overall accuracy that would like to achieve, W_i = mapped proportion of the area of class I, and S*i*= standard deviation of the class.

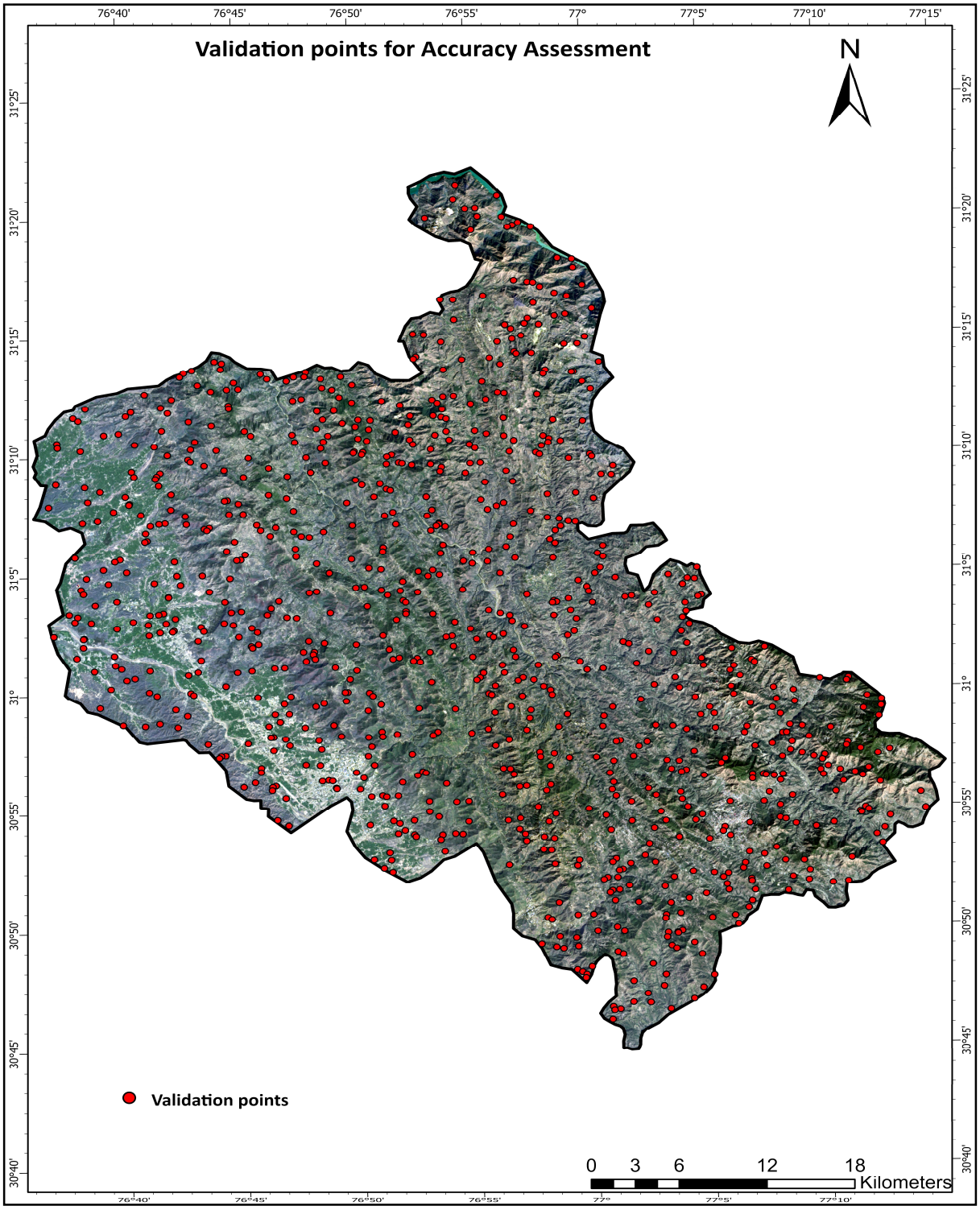

Figure 7. Validation points generated through the stratified random sampling

Table 4. Determination of sample size for validation as per the methodology of Olofsson et.al (2014)

Classes	Area Proportion (W*i*)	Standard deviation (S*i*)	Standard error ($S(\hat{O})$)	Validation points
Agriculture	0.09	0.1	0.01	98
Agroforestry	0.26	0.1	0.01	297
Barren land	0.06	0.1	0.01	61
Built-up	0.07	0.1	0.01	51
Forest	0.43	0.1	0.01	315
Grassland	0.07	0.1	0.01	52
Water body	0.01	0.1	0.01	26
Total	1	-	-	900

Once the sample size had been determined, the sample points were extracted and saved as a vector layer. These sample points were then imported into Google Earth Pro, where they were used for identifying the actual land use by referencing very high-resolution imagery. After identifying the land use at each sample point, a reference layer was created and subsequently imported into ArcMap 10.8.2. ArcMap determined the classified points by overlaying the reference layer with the classified image. This allowed for calculating various accuracy assessment parameters, including omission errors, commission errors, user accuracy, producer's accuracy, overall accuracy, and the Kappa Coefficient. These assessments were based on an error matrix that considered both points and area-based analysis, comprehensively evaluating the classification accuracy.

3.2.7 Accuracy assessment

3.2.7.1 Error Matrix

The error matrix is a table that compares the labels of the map and reference data. It helps to evaluate the accuracy of satellite data by comparing it to the ground truth data for selected references. The error matrix follows the standard procedure as established by Congalton (1988).

		***j*=Columns (Reference)**			**Row total**
		1	**2**	***k***	n_{i+}
	1	n_{11}	n_{12}	n_{1k}	n_{1+}
***i* = Rows**	**2**	n_{21}	n_{22}	n_{2k}	n_{2+}
(Classification)	***k***	n_{k1}	n_{k2}	n_{kk}	n_{k+}
Column total n_{+j}	n_{+1}	n_{+1}	n_{+2}	n_{+k}	n

Where *n* samples are distributed into k cells, each sample is assigned to one of the classes in the map (usually the rows) and, independently, to one of the same k classes in the reference data set (usually the columns).

nij denote the number of samples classified into class *i* (*i = 1, 2…. k*) in the map and class *j* (*j = 1, 2., k*) in the reference data set.

$$n_{i+} = \sum_{j=1}^{k} n_{ij}$$

n_{i+} be the number of samples classified into class *i* in the remotely sensed classification, and

$$n_{+j} = \sum_{j=1}^{k} n_{ij}$$

n_{+j} be the number of samples classified into class *j* in the reference data set. The plus sign in the notation here simply indicates all the values in that row or column.

So, if *i* = 1, then the total number of samples in class 1 is the sum of all the samples in row 1; if *i* = *k*, then the total number of samples in class *k* is the sum of all the samples in row *k*.

3.2.7.2 Commission error

Errors of commission refer to the portion of values expected to be assigned to a particular class but do not belong to that class. These errors are primarily used to quantify the number of false positives within a classification. In a confusion matrix, commission errors are depicted in the rows, except for the diagonal values. To compute commission errors, the process involves carefully examining classified sites to identify instances of incorrect classification. This is achieved by aggregating the inaccurately assigned classifications within each class's respective row and dividing this by the total count of classified sites within that class. This calculation helps in assessing the extent of misclassifications and false positive outcomes.

3.2.7.3 User's Accuracy

User's Accuracy (UA) pertains to the accuracy of a map as perceived by the map users rather than the map producers. It offers insights into how often a specific class depicted on the map corresponds to its presence on the actual ground, indicating its reliability. The

Commission Error complements the User's Accuracy and measures misclassifications and inaccuracies. In other words, the User's Accuracy can be calculated as 100 per cent minus the Commission Error. To derive the User's Accuracy, you divide the total count of correct classifications for a particular class by the total number of instances represented by that class in the rows of the confusion matrix. This calculation clearly shows how dependable and trustworthy the map is from the user's perspective.

$$UA = \frac{n_i}{n_{irow}}$$

Where, n_i= correctly identified pixels in the class and n_{irow} = row total for the considered class

3.2.7.4 Omission error

Errors of omission denote the proportion of values that should be categorized under a specific class but were erroneously assigned to another class. When a region is wrongly excluded from the class it genuinely belongs to, it is labelled as an omission error. Omission errors are a measure of false negatives. Similar to commission errors, omission errors are presented in the columns of a confusion matrix, excluding values along the main diagonal. To calculate omission errors, the process involves a thorough examination of reference sites to identify instances of inaccurate categorization. This is achieved by summing up the incorrect classifications for each class and subsequently dividing this sum by the total number of reference sites within each class. It's important to note that a distinct omission error is typically computed for each class, offering insights into the extent of misclassifications for various categories.

3.2.7.5 Producer's accuracy

Producer's Accuracy (PA) measures the map's accuracy as perceived by the map maker or producer. It reflects how often real-world features on the ground are accurately represented in the categorized map. In other words, it indicates the likelihood that a specific land cover category on the ground is correctly classified as such on the map. The Omission Error is the complementary metric to the Producer's Accuracy and the Producer's Accuracy can be calculated as 100 per cent minus the Omission Error. To compute the Producer's Accuracy, you divide the count of correctly classified reference sites for a specific class by the total number of reference sites within that class. This calculation provides valuable

insights into the accuracy of the map from the map maker's perspective, particularly regarding the precision of categorizing ground features.

$$PA = \frac{n_i}{n_{icol}}$$

Where, $n_{i=}$ correctly identified pixels in the class and n_{icol}= column total for the considered class.

3.2.7.6 Kappa Coefficient

The Kappa Coefficient is a statistical measure that assesses the overall agreement within an error matrix. It is widely regarded as a potent method for analysing a single error matrix and comparing the disparities among different error metrics. The Kappa Coefficient was determined using the formula given below:

$$K = \frac{N\sum_{i=1}^{n} Mii - \sum_{i=1}^{n}(GiCi)}{N^2 - \sum_{i=1}^{n}(GiCi)}$$

Where,

i is the class number

N is the total number of classified values compared to truth values

Mii is the number of values belonging to the truth class *i* that have also been classified as class *i* (*i.e.*, values found along the diagonal of the confusion matrix)

Ci is the total number of predicted values belonging to class *i*

Gi is the total number of truth value belonging to class *i*

The Kappa Coefficient falls within the range of -1 to 1, where its interpretation is as follows: A value of 0 indicates that the classification is no more accurate than random chance. A negative value implies that the classification is significantly worse than random chance. Conversely, a value approaching 1 indicates that the classification is considerably better than what would be achieved by chance alone.

3.2.7.7 Overall accuracy

The overall accuracy stands out as the most straightforward measure, providing a holistic assessment of the entire image's accuracy without delving into the accuracy of individual categories. It is commonly expressed as a percentage, where 100% accuracy signifies that all reference sites have been correctly categorized. Calculating the overall

accuracy is a relatively simple process, and it offers a basic and easily understandable evaluation of accuracy for both map users and producers. Essentially, the confusion matrix's diagonal elements represent the correctly classified areas. To determine the accuracy, one adds up the number of correctly classified points (those along the diagonal) and divides this sum by the total count of reference points. This calculation yields a straightforward indicator of the map's overall accuracy.

$$OA = \frac{1}{N}\sum_{i=1}^{r} n_i$$

Where, N-total number of pixels, r number of classes, n=correctly identified pixels in each class.

3.2.7.8 McNemar's test

A non-parametric test known as McNemar's test was conducted to assess the performance disparity between two classifiers. This test relies on the error matrices of the two classifiers and determines whether the differences between them are statistically significant (Foody 2004 and Leeuw et al. 2006). McNemar's test is based on the standardized normal test. It is expressed as:

$$Z = \frac{f12 - f21}{\sqrt{f12 - f21}}$$

Where, f 12 denotes the number of samples misclassified by the first classification algorithm but correctly classified by the second classification algorithm, and f 21 denotes the number of samples correctly classified by the first classification algorithm but misclassified by the second classification algorithm. A difference in accuracy between the confusion matrices of the classifiers is statistically significant ($p \leq 0.05$) if the Z value is more than 1.96.

3.3 AGROFORESTRY SUITABILITY MAPPING

3.3.1 Conceptual Framework

Geographic Information System (GIS) based Multi-Criteria Decision Making (MCDM) approaches were employed to assess land suitability for agroforestry. This entailed

the application of two distinct MCDM methodologies, namely the Analytic Hierarchy Process (AHP) and Fuzzy-AHP, as illustrated in (Figure 8). The initial step in the MCDM process involves carefully selecting pertinent evaluation parameters. These parameters are the basis for evaluating and determining land suitability for agroforestry.

3.3.2 Selection of evaluation parameters

Selecting criteria for identifying suitable areas for future agroforestry is crucial (Zhang et al. 2015). There is a multitude of factors that influence the quality of lands for various agricultural uses, each with varying degrees of importance. It's only feasible to consider some of these factors (Karlen et al. 2014).

Therefore, a comprehensive approach was adopted to determine the land characteristics that impact agroforestry systems, combining insights from a literature survey, analytical studies, and expert opinions. In total, eleven criteria were considered, encompassing a range of factors. These criteria included four topographical parameters (aspect, slope, elevation, and hillshade), three vegetation parameters (land use land cover (LULC), Normalized Difference Vegetation Index (NDVI), and Normalized Difference Moisture Index (NDMI)), one climate variable (precipitation), and one soil parameter (soil fertility). Two socio-economic parameters (distance from road and stream) were incorporated. For the determination of soil fertility criteria, a combination of soil nutrients (determined by overlaying seven parameters, such as available nitrogen, phosphorus, potassium, zinc, iron, boron, and magnesium) was integrated with soil characteristics (determined by overlaying seven parameters, including pH, organic matter, soil depth, particle size, soil drainage, available water capacity, and erosion susceptibility). Table 12 summarises the selected datasets and variables associated with these criteria, along with their type and sources, contributing to selecting suitable land for agroforestry.

3.3.3 Software used

ArcMap 10.8.2

3.3.4 Multi-Criteria Decision-Making Technique

3.3.4.1 Analytic Hierarchy Process (AHP)

The Analytic Hierarchy Process (AHP) is a crucial Multi-Criteria Decision Making (MCDM) technique that considers qualitative and quantitative information. AHP organises a

set of criteria or sub-criteria into a hierarchical structure, assigning each criterion a weight. This method serves as a framework for systematically quantifying the relative importance of design criteria and elements through a pairwise comparison process. In doing so, it simplifies the complexity of the decision-making process, as initially proposed by Saaty (1977). AHP derives the weights for individual criteria by utilising pairwise comparison matrices. These matrices are constructed by comparing factors to determine their relative preferences. The process involves finding the eigenvalue corresponding to the highest eigenvector of the completed matrix and normalising the total of the factors to unity, following the principles outlined by Saaty in 1980 and Pramanik et al. (2016). Saaty's scale of 1-9 (Table 5) is typically employed to facilitate these comparisons, allowing different criteria and sub-criteria to be assessed against one another. Pairwise comparison matrices are generated for all criteria within the hierarchical structure (available at https://bpmsg.com/ahp/ahp-calc.php). It's important to note that these matrices should exhibit reciprocity, which is mathematically represented as n (n-1)/2 for n components within the pairwise comparison matrix.

Table 5. The fundamental scale for pairwise comparison matrix according to Saaty (1980)

Intensity of importance	Definition	Explanation
1	Equal importance	Two criteria contributed equally to the objective criteria
3	Low importance one over another	Judgement and experience slightly favour one criterion over another
5	Strong or essential importance	Strongly favoured by judgements and experience
7	Judgements and experience strongly favour a criterion	A criterion is strongly favoured and its dominance established in practice
9	Absolute or high importance	The evidence favouring one criterion over another is of the highest probable order of affirmation
2,4,6,8	Intermediate values between the two adjacent importance or judgements	When adjustment is needed
Reciprocals	If criterion i has one of the above numbers designated to it when compared with criterion j, then j has the reciprocal value when compared with i	

Furthermore, the Analytic Hierarchy Process includes the analysis and calculation of inconsistencies introduced by decision makers during the process, helping ensure the

robustness and reliability of the outcomes. The efficiency criteria of analytic hierarchy process are estimated by consistency relationship (CR) as follow:

$$CR = \frac{CI}{RI}$$

Where CI indicates consistency index which can be calculated using the following formula:

$$CI = \frac{\lambda_{max} - n}{n - 1}$$

λmax is the principle or highest eigenvector of the computed matrix and n denotes the order of the matrix.

The Random Index (RI) represents the average consistency index value, which relies on the matrix order computed according to Saaty 1977 guidelines, as outlined in the provided Table 6. Additionally, the Consistency Ratio (CR) is a critical parameter. If CR falls below 0.1, it indicates that the matrix is consistent and reliable. However, if CR exceeds 0.1, adjustments are necessary to enhance consistency. This adjustment becomes necessary when discrepancies are observed in the weight values within the matrix. In such cases, the Analytic Hierarchy Process (AHP) may not yield a meaningful or practical result, as emphasized by Saaty (1980). Ensuring matrix consistency is vital for maintaining the integrity and validity of the decision-making process.

Table 6. Saaty's consistency indices of randomly generated reciprocal matric

Order of the matrix	**1**	**2**	**3**	**4**	**5**	**6**	**7**	**8**	**9**	**10**	**11**	**12**
RI value	0	0	.58	.90	.12	.24	.32	.41	.45	.49	.51	.48

3.3.4.1.1 Weighted Overlay

In addition to assigning weights to each criterion, ranks were assigned to the sub-criteria on a scale of 1 to 9. In this ranking system, 1 represents the lowest suitability for agroforestry, while 9 indicates the highest suitability. A Geographic Information System (GIS) was used to integrate all the thematic layers, and a weighted overlay technique was employed. This was accomplished using the Spatial Analyst tool within ArcMap 10.4.1. The following equation was used in this process to combine and synthesize the various thematic layers.

$$\text{Agroforestry suitability using AHP} = \sum_{i=1}^{n} WiXi$$

Where, *Wi* denotes the weight of the selected land suitability criterion, *Xi* indicates the assigned sub-criteria rank of *i* land suitability criteria, and denotes the total number of land capability criteria.

3.4.4.2 Fuzzy-AHP

While the Analytic Hierarchy Process (AHP) is commonly employed for Multi-Criteria Decision Making (MCDM) to address issues related to human uncertainty, it has limitations in handling the inherent uncertainty and imprecision associated with mapping decision makers' perceptions of real data (Rodcha et al. 2019). The fuzzy-AHP approach has been introduced to overcome this limitation, integrating the conventional AHP method with fuzzy logic, thereby enhancing the decision-making process (Ozkan et al. 2020). The current study utilised the method to calculate the weights of criteria and sub-criteria (Buckley 1985).

Buckley's method involves calculating the fuzzy weights of criteria through the geometric mean approach. The following steps were implemented in accordance with Buckley's method:

Step 1. Pairwise comparison matrices are created between all criteria in the hierarchical structure.

$$A=\begin{bmatrix} 1 & a_{12} & \dots & a_{1n} \\ a_{21} & 1 & \dots & a_{2n} \\ \vdots & \vdots & \ddots & \vdots \\ a_{n1} & a_{n2} & \dots & 1 \end{bmatrix}=\begin{bmatrix} 1 & a_{12} & \dots & a_{1n} \\ 1/a_{21} & 1 & \dots & a_{2n} \\ \vdots & \vdots & \ddots & \vdots \\ 1/a_{n1} & 1/a_{n2} & \dots & 1 \end{bmatrix}$$

Where,

$$a_{ij}=\begin{cases} 1,2,3,4,5,6,7,8,9(Criterion\ i\ is\ relative\ importance\ to\ criterion\ j) \\ 1(i=j) \\ 1^{-1},2^{-1},3^{-1},4^{-1},5^{-1},6^{-1},7^{-1},8^{-1},9^{-1}(Criterion\ i\ is\ relative\ less\ importance\ to\ criterion\ j) \end{cases}$$

Step 2. Simple intensity importance from the Saaty (1980) in pairwise comparison matrices are converted to triangular fuzzy numbers. The scale created by Gumus (2009) was used for the conversion of intensity importance into triangular fuzzy numbers (Table 7.)

Step 3. Buckley's (1985) geometric mean approach was used to obtain the fuzzy geometric mean and fuzzy weight of each criterion and sub-criterion.

$$\tilde{r}_i = (\tilde{a}_{i1} \otimes \tilde{a}_{i2} \otimes \ldots \otimes \tilde{a}_{in})^{1/n}$$

$$\tilde{w}_i = \tilde{r}_i \otimes (\tilde{r}_i \oplus \ldots \oplus \tilde{r}_n)^{-1}$$

$\tilde{a}_{in}$ a fuzzy pairwise comparison value of criteria *i* and criteria *n*. Accordingly, $\tilde{r}_i$ is the geometric mean of the fuzzy pairwise comparison value of criteria *i* with each criterion $\tilde{w}_i$ is fuzzy weight of criteria *i* and expressed as $w_i = (l_{wi}, m_{wi}, u_{wi})$. l_{wi}, m_{wi}, and u_{wi} represents the lower, middle and upper values of fuzzy weight of criteria *i*, respectively.

Step 4. The criteria weights obtained are represented as triangular fuzzy numbers. To convert these fuzzy numbers into precise numerical values, a clarification process is necessary. Among the various clarification techniques, the Centre of Area (COA) approach is frequently used due to its simplicity and practicality. The Best Non-Fuzzy Performance (BNP) value for a triangular fuzzy number 'w' is calculated using the following formula:

$$BNPi = lwi + \frac{(uwi - lwi) + (mwi - iwi)}{3}, \forall\, i$$

Step 5. All created thematic layers were integrated in GIS and overlay in ArcMap 10.4.1 using following equation:

Agroforestry suitability using Fuzzy-AHP = $\sum_{i=1}^{n} WiYi$

Where, *Wi* denotes the weight of the selected land suitability criterion, *Yi* indicates the weight of sub-criteria of *i* land suitability criteria, and *n* denotes the total number of land capability criteria.

Table 7. Triangular fuzzy conversion scale

Intensity of importance	Linguistic scales	Scale of triangular fuzzy number	Scale of triangular reciprocal fuzzy number
1	Equal	(1,1,1)	(1,1,1)
2	Weak advantage	(1,2,3)	(1/3,1/2,1)
3	Not bad	(2,3,4)	(1/4,1/3,1/2)
4	Preferable	(3,4,5)	(1/5,1/4,1/3)
5	Good	(4,5,6)	(1/6,1/5,1/4)
6	Fairly good	(5,6,7)	(1/7,1/6,1/5)
7	Very good	(6,7,8)	(1/8,1/7,1/6)
8	Absolute	(7,8,9)	(1/9,1/8,1/7)
9	Perfect	(8,9,10)	(1/10,1/9,1/8)

Table 8. List of criteria, datasets, and variables used for the agroforestry suitability analysis

Criterion		Name of dataset	Variables	Unit	Data type	Technique	Grid Size		Source
							Actual	Required	
	Ecology	ESRI	LULC	Meter	Raster	Extraction using GEE	10m	12.5	Karra et al. (2021)
		Sentinel-2	NDVI	Unitless	Raster	$NDVI = \frac{NIR - RED}{NIR + RED}$	10m	12.5	Extracted from sentinel-2 data (2022-01-01 to 2022-12-31) using GEE
	Soil properties	Block fertility Map	Nitrogen	kg ha^{-1}	Vector	Digitization	-	-	https://iiss.icar.gov.in/mapd_1.htm
			Phosphorus	kg ha^{-1}	Vector	Digitization	-	-	https://iiss.icar.gov.in/mapd_1.htm
			Potassium	kg ha^{-1}	Vector	Digitization	-	-	https://iiss.icar.gov.in/mapd_1.htm
			Magnesium	c mol kg^{-1}	Vector	Digitization	-	-	http://hillagric.ac.in/research/dr/BlockFertilityMap/index.html
			Boron	mg kg^{-1}	Vector	Digitization	-	-	https://iiss.icar.gov.in/mapd_1.htm
		Soil Characteristics	Soil texture	Unitless	Vector	Digitization	-	-	Harmonized World Soil Database (HWSD) V 1.2
			BD	kg dm^{-3}	Vector	Digitization	250m	30m	Soil Grids and WoSIS (isric.org)
			CEC	c mol kg^{-1}	Vector	Digitization	-	-	
			OC	g kg^{-1}	Vector	Digitization	-	-	https://iiss.icar.gov.in/mapd_1.htm
			pH	Unitless	Vector	Digitization	-	-	https://iiss.icar.gov.in/mapd_1.htm
	Climate	Climatic research unit	Rainfall	mm	Vector	Digitization	1 km	12.5	https://crudata.uea.ac.uk/
			Temperature	°C	Vector	Digitization	1 km	12.5	
	Topography	GTOPO30 Digital Elevation Model	Slope	Degree	degree	Digitization	-	12.5	https://earthexplorer.usgs.gov/
			Aspect	Direction	Meter	Digitization	-	12.5	
			Elevation	Meter	Direction	Digitization	-	12.5	
			Hill shade	Unitless	Unitless	Digitization	-	12.5	
			Stream distance	km	Vector	Digitization		12.5	
	SE	Open Street Map	Road distance	km	Vector	Digitization	-	-	https://www.openstreetmap.org/

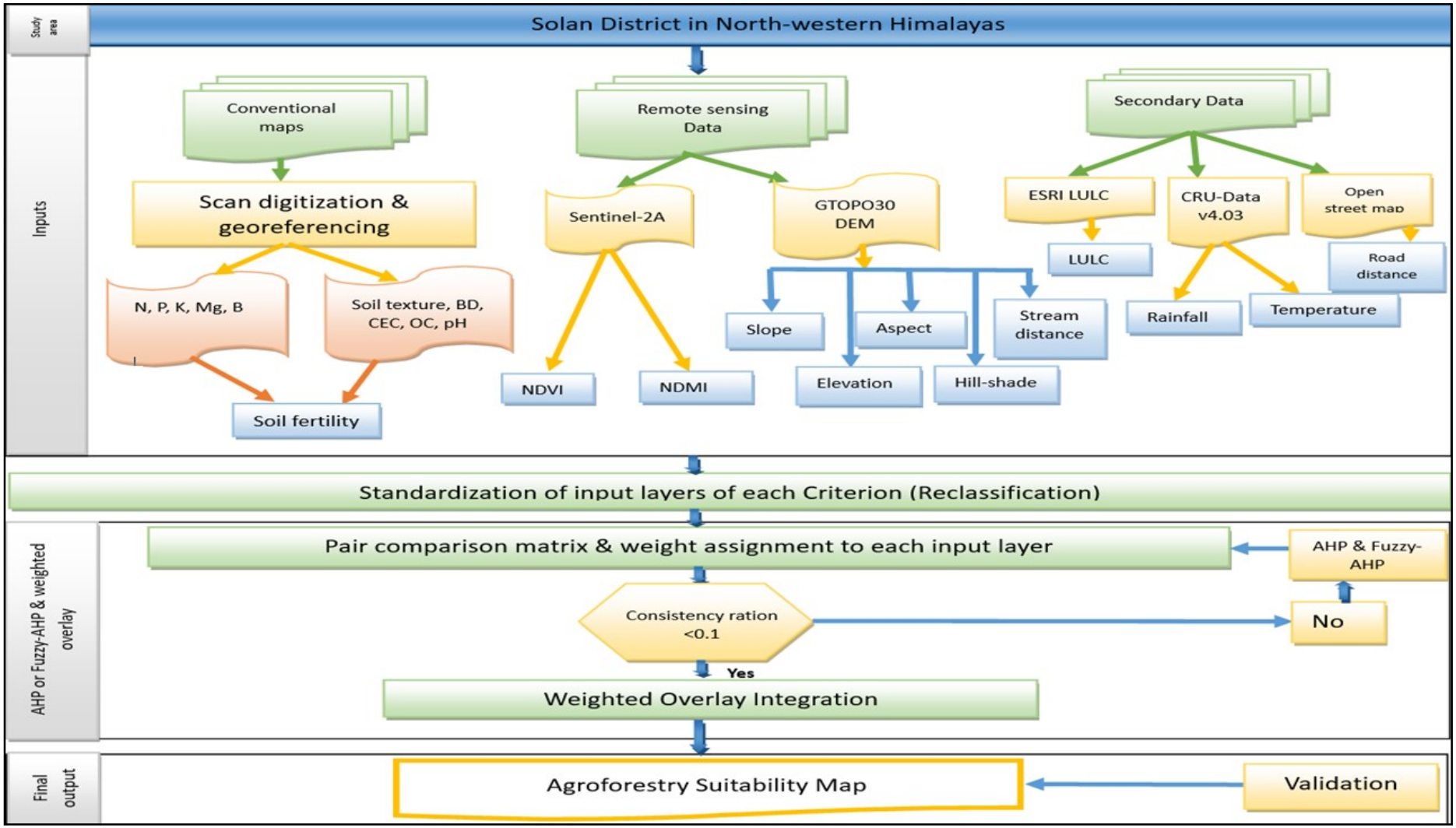

Figure 8. Schematic representation of the methodology for agroforestry suitability mapping in the study

Table 9. Suitability classification as per FAO guidelines

Suitability categories Class	Description
Highly suitable (S1)	Land having no limitations towards application of a given use, or only minor limitations that will not significantly reduce productivity and benefits and will not raise inputs above an acceptable level.
Moderately suitable (S2)	Land having limitations which in aggregate are moderately severe for sustained application of a given use, the limitations will reduce productivity or benefits and increase required inputs to the extent that the overall advantage to be gained from the use.
Marginally suitable (S3)	Land having limitations which in aggregate are severe for sustained application of a given use and will so reduce productivity and benefits, or increase required inputs, that this expenditure will be only marginally justified.
Not suitable (NS)	Land that cannot support the land use on a sustained basis, or land on which benefits do not justify necessary inputs

3.3.5 Validation of Agroforestry Suitability Analysis

The agroforestry suitability map was validated through a visual assessment process using high-resolution images from Google Earth Pro. Six polygons were randomly selected and drawn within the study area for this validation. The suitability maps for agroforestry generated using the AHP and Fuzzy-AHP methods were then compared to the high-resolution imagery in Google Earth Pro. This visual validation allowed for assessing the accuracy and alignment of the generated maps with real-world conditions.

3.4 BIOMASS CARBON STOCK AND CARBON SEQUESTRATION POTENTIAL OF AGROFORESTRY SYSTEMS

3.4.1 Software used

ArcGIS 10.8.2

InVEST model 3.13.0 Workbench

3.4.2 Land use land cover mapping

Land use and land cover mapping is a valuable technique for characterizing and understanding the distribution of different land cover types and their use in a specific geographic area. Landsat 7 ETM satellite imagery was used for mapping in 2003, and

Landsat 8 OLI/TIRS was used for mapping in 2013 and 2023. Preprocessing (bands merge, mosaicking and subset), training sample generation, random forest classification and accuracy assessment were done in ArcGIS 10.8.2 for 2003, 2013 and 2023.

3.4.2.1 Satellite data

Since 1972, the Landsat program, a collaborative effort between the United States Geological Survey (USGS) and NASA, has been pivotal in Earth observation. It facilitates various applications in agriculture, forestry, land use planning, environmental monitoring, and natural resource management. Landsat satellites utilize multispectral imaging, capturing data across visible light and infrared spectrums, offering insights into land cover and conditions. With global coverage and a revisit cycle of approximately 16 days, Landsat monitors temporal changes, including seasonal shifts, crop growth, and urban expansion. Users can access Landsat imagery at varying spatial resolutions, typically at 30 meters, 15 meters, or 10 meters, to suit their specific needs. Crucially, Landsat data is accessible to the public, promoting its extensive use in research, environmental monitoring, and commercial ventures. The comprehensive Landsat data archives, stretching back to the 1970s, provide a historical record of Earth's transformations. Landsat 7, launched in 1999, contributed to this dataset with the Enhanced Thematic Mapper Plus (ETM+) despite encountering data gaps due to a 2003 hardware anomaly. Landsat 8, part of the program since 2013, employs the Operational Land Imager (OLI) and Thermal Infrared Sensor (TIRS) instruments, delivering multispectral data at a 30-meter spatial resolution. This supports applications such as environmental assessments, agriculture, and land use planning, furthering the program's mission of long-term Earth observation.

Table 10. Characteristic of Landsat-07 ETM used in land-use/land cover mapping

Sensor	Band number	Band number	Wavelength (µm)	Resolution (m)
ETM+	1	Blue	0.45-0.52	30
ETM+	2	Green	0.52-0.60	30
ETM+	3	Red	0.63-0.69	30
ETM+	4	NIR	0.77-0.90	30
ETM+	5*	SWIR1	1.55-1.75	30
ETM+	6*	Thermal	10.40-12.50	60*(30)
ETM+	7*	SWIR2	2.09-2.35	30

* Bands not used in present study.

Table 11. Characteristic of Landsat-08 OLI/TIRS used in land-use/land cover mapping

Band number	Band number	Wavelength (µm)	Resolution (m)
1*	Coastal	0.43 – 0.45	30
2	Blue	0.45 – 0.51	30
3	Green	0.53 – 0.59	30
4	Red	0.64 – 0.67	30
5	NIR	0.85 – 0.88	30
6*	SWIR 1	1.57 – 1.65	30
7*	SWIR 2	2.11 – 2.29	30
8*	Cirrus	1.36 – 1.38	30
9*	TIRS 1	10.6 – 11.19	100
10*	TIRS 2	11.5 – 12.51	100

* Bands not used in present study.

Table 12. Details of satellite product used for the land-use/land cover mapping

Platform	ID	Acquisition date	Tile number
Landsat-07 ETM	LE71470382003041SGS00	10-02-2003	L2SP_147038
	LE71470392003041SGS00	10-02-2003	L2SP_147039
Landsat-8 OLI	LC81470382013108LGN02	18-04-2013	L2SP_147038
	LC81470392013108LGN02	18-04-2013	L2SP_147039
Landsat-8 OLI/TIRS	LC81470382023056LGN00	25-02-2023	L2SP_147038
	LC81470392023056LGN00	25-02-2023	L2SP_147039

Table 13. Major land-use land cover classes used and their descriptions

Agricultural Land	Includes areas used for perennial and annual crops, irrigated areas, scattered rural settlements, commercial farms [sesame cultivations and sugarcane plantations].	
Agroforestry	Areas covered with trees along farms and in small patches up to 0.1 ha in area, roadside plantations, orchards, agroforestry plantations.	
Barren land	Areas covered with scrub land, gullied/ravenous land, barren rocky land.	
Built-up Area	Areas of commercial areas, urban and rural settlements, mining, industrial areas.	

Dense Forest	All lands with tree canopy density of 70% and above.	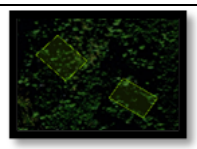
Moderate Forest	All lands with tree canopy density of 40% and more but less than 70%	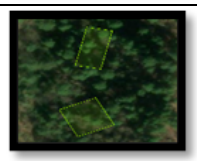
Open Forest	All lands with tree canopy density of 10 % and more but less than 40%	
Grassland	Areas covered by grasses are usually used for grazing and those remain for some months in a year.	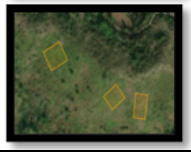
Water Body	Areas covered by rivers, streams, and reservoirs	

3.4.2.2 Land use land cover change detection

Detecting land use and land cover change involves comparing spatial data from different time periods to identify areas where significant changes have occurred. The following equation was used to calculate the degree of change (C) for each class:

$$Ci = Li - Bi$$

The change in class is divided with the covered area base year and again multiplied by 100, a straightforward computation was used to calculate the percentage change (C%). And it has been conducted in each land-use class.

$$Pi = \frac{Li - Bi}{Bi} \times 100$$

Where,

The number of classes in the image is indicated by 1

Ci indicates how much class 1 has changed.

Pi is the percentage change in class 1.

Li means "basic image" (2003).

The most current picture is Bi (2013).

3.4.3 InVEST model

InVEST 3.13.0 workbench, particularly its Carbon module, played a pivotal role in evaluating the current state of carbon stocks and forecasting future developments using four key carbon pools: aboveground, belowground, dead organic matter, and soil carbon (Kareiva et al. 2011). To enhance the assessment of land heterogeneity, this InVEST model was thoughtfully integrated into ArcGIS, a geospatial platform renowned for its robust analytical capabilities, the InVEST Carbon Storage and Sequestration model functions by aggregating carbon content within these distinct pools. InVEST, as a powerful geospatial tool, focuses on assessing how land-use changes impact ecosystem services, aligning with the works of Goldstein et al. (2012) and Qiu and Turner (2013). The model relies on input parameters encompassing land use maps for 2003, 2013, and 2023. For each specific land use category, it considers data on carbon stocks within the four carbon pools: living aboveground, belowground, litter and deadwood, and soil organic carbon within the 0-40 cm soil depth range. These input parameters are of paramount importance as they underpin the evaluation of carbon storage and enable a comprehensive analysis of changes in land use dynamics over time. The model's fundamental requirement for each land use and land cover (LULC) type is an estimate of carbon content, measured in megagrams per hectare (Mg ha^{-1}), across the four primary carbon pools (above ground, below ground, soil, and dead carbon). This model then applies these estimates to a LULC map to generate detailed carbon storage maps for each pool. To calculate net changes in carbon storage over time, the model compares the LULC maps from 2003 and 2023 on a pixel-by-pixel basis. The resulting output quantifies carbon storage in megagrams per pixel, and, if desired, it can be translated into a social value.

$$\mathbf{C_{total} = C_{above} + C_{below} + C_{soil} + C_{dead}}$$

Where,

C_{total} represents the total ecosystem carbon storage (Mg ha^{-1}),

C_{above} represents the carbon density in the above-ground biomass (Mg ha^{-1}),

C_{below} represents the carbon density in the belowground biomass (Mg ha^{-1}),

C_{soil} represents the carbon density of the soil (Mg ha^{-1}),

C_{dead} represents the carbon density of the dead matter (Mg ha^{-1}).

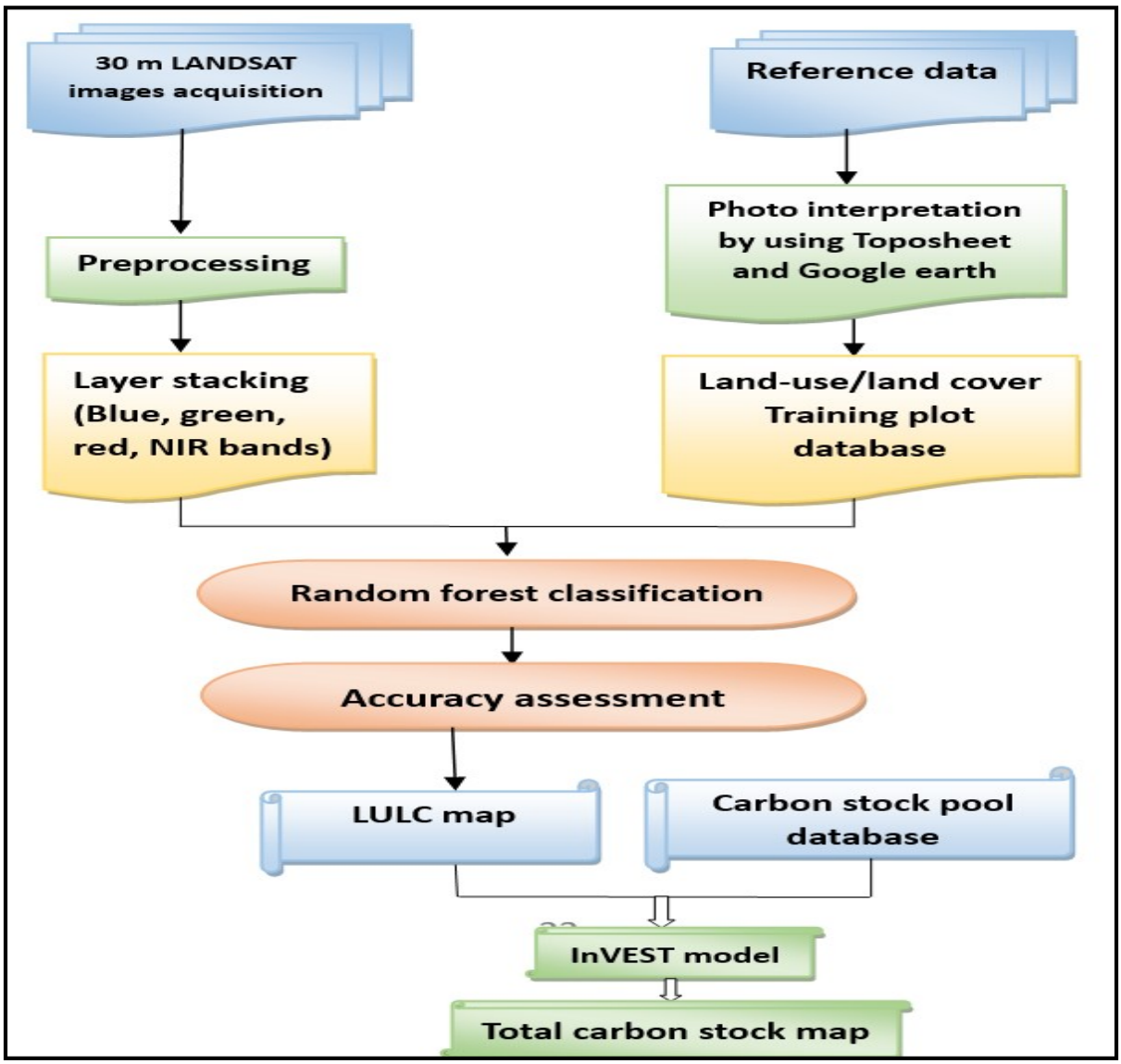

Figure 9. Flowchart for obtaining total Carbon stock map using InVEST model

The value of carbon sequestration over time for a given parcel *x* is:

$$Value\_seq_x = V\frac{S_x}{q-p}\sum_{t=0}^{q-p-1}\frac{1}{(1+\frac{r}{100})^t(1+\frac{c}{100})^t}$$

Where,

- V is the price per metric ton of carbon
- S_x is the amount of carbon, in metric tons, sequestered on parcel x
- q is the future year
- p is the current year
- r is the yearly market discount rate for the carbon price
- c is the yearly rate of change in the price of carbon

The valuation model assesses the financial worth of carbon sequestration, not just storage, and factors in the amount of carbon, the monetary value per unit of carbon, a monetary discount rate, and changes in the value of carbon sequestration over time. This allows for a comprehensive valuation to be applied to sequestration, not storage because market prices relate only to carbon sequestration. Discount rates are multipliers that typically reduce the value of carbon sequestration over time. The first type of discounting, the standard economic procedure of financial discounting, reflects that people value immediate benefits more than future benefits due to uncertainty and assumed monetary inflation over time. The second discount rate adjusts the social value of carbon sequestration over time. This value will change as the impact of carbon emissions on expected climate change-related damages changes.

Table 14. Value of carbon above, carbon below, carbon in soil and dead carbon (Mg C ha^{-1}) under different land use land cover classes

lucode	LULC name	C above	C below	C soil	C dead	Source
1	Agriculture	5.64	1.19	27.6	1.2	Sanneh 2007, Singh et al. 2015
2	Agroforestry	28.3	7.32	39.3	3.74	Singh et al. 2015
3	Barren land	10.9	5.82	21.3	1.36	LC Langlentombi PhD thesis
4	Built-up	2.45	1.2	11.78	1.9	Zheng and Zheng (2023)
5	Open forest	84.5	18.53	57.12	2.93	Bhardwaj et al. 2016
6	Moderate forest	98.77	22.68	76.12	5.74	
7	Dense forest	118.05	27.53	80.82	8.55	
8	Grassland	3.65	1.73	32.23	0.97	Sanneh 2007, Singh et al. 2015

3.4.4 Rate of change

The rate of change of carbon density of different land-use classes over a period of time is calculated assuming a linear change. Therefore, the rate of change in carbon stock a period of time is calculated as:

$$dC_{(L,t1,t2)} = \frac{C_{L1,t2} - C_{L1,t1}}{T}$$

Where,

$dC_{(L, t1, t2)}$: Rate of change in carbon stock in different land-use classes within project boundary during the period between a point of time in year t1 and a point of time in year t2

$C_{L1, t2}$: Carbon stock in particular land-use class within project boundary at appoint of time in year t2

$C_{L1, t1}$: Carbon stock in particular land-use class within project boundary at appoint of time in year t2

T: Time elapsed between two successive estimations (T=t2-t1); yr.

Chapter-4

RESULTS AND DISCUSSION

The results attained from the current investigations entitled "**Remote sensing approach for estimating agroforestry area, suitability mapping and carbon sequestration potential of agroforestry systems in Solan district of Himachal Pradesh"** are being presented and discussed in this chapter. The extent of area under agroforestry systems/ practices and other land use classes were delineated agro-climatic zones wise using different machine learning algorithms *viz.*, Maximum Likelihood, Random Forest and Support Vector Machine using ten bands of Sentinel-2 dataset. The two different MCDM techniques- AHP and Fuzzy-AHP were used for the assessment of land suitability for the agroforestry implementation and scaling up. For estimating Carbon storage and sequestration, InVEST model (Integrated Valuation of Ecosystem Services and Trade-offs) was used. Details of the current investigations' findings are being presented and discussed in this chapter under the following major heads and sub-heads:

4.1. Agroforestry area and other Land-use systems mapping

4.1.1. Area assessment

4.1.2. Accuracy assessment

4.2. Agroforestry suitability mapping

4.2.1. Criterion

4.2.2. Multi-criteria decision-making process

4.3. Biomass Carbon stock and carbon sequestration potential of agroforestry Systems

4.3.1. Land-use and land cover change in 20 years

4.3.2. The carbon stocks and carbon stock changes between 2003 and 2023

4.1. AGROFORESTRY AREA AND OTHER LAND-USE SYSTEMS MAPPING

4.1.1. Area assessment

The area assessment of the agroforestry vis-à-vis other land use carried out using three different machine learning algorithms *i.e.*, Maximum Likelihood, Random Forest and Support Vector Machine classification in ArcGIS 10.8.2 software.

4.1.1.1. Maximum Likelihood Classification

Solan district, encompassing an area of approximately 1936 sq. km, is divided into two Agro-Climatic Zones (ACZ): ACZ-I, characterized by a sub-tropical, sub-montane and low hills landscape with an altitude below 914 m a.m.s.l and ACZ-II, featuring a sub-temperate, sub-humid and mid-hills terrain at altitudes ranging from 914 to 1800 m a.m.s.l The land-use and land cover (LULC) statistics, obtained through maximum likelihood classification for Solan district is presented in Table 15 and Figure 10, shows that the majority of Solan district is covered by forest, spanning 871.41 sq. km (45.01%). Agroforestry and agriculture, account for 450.62 sq. km (23.28%) and 171.61 sq. km (8.86%) of the total area, respectively. The Solan district comprises three main types of land use: forest, agroforestry and agriculture. These three types of land use account for around 77.15 per cent of the district. Grassland covers 157.66 sq.km (8.14%) of the total area. Barren land spans 126.14 sq.km (6.52%) of the district. Built-up areas encompass 134.71 sq.km (6.96%) of the district's total area. Water bodies account for 23.85 sq.km (1.23%) of the district. These different types of land use show that the Solan district has a complex and varied land-use systems.

Table 15. Estimate of area (sq.km) under Agroforestry and other major land-use classes using Maximum likelihood classification in different agro-climatic zones of Solan District of (H.P)

Classes	ACZ-I (sq.km)	ACZ-II (sq.km)	Total Area (sq.km)	Area (%)
Agriculture	124.43	47.18	171.61	8.86
Agroforestry	259.33	191.29	450.62	23.28
Barren land	85.24	40.90	126.14	6.52
Built-up	85.01	49.70	134.71	6.96
Forest	358.58	512.83	871.41	45.01
Grassland	57.47	100.19	157.66	8.14
Water body	9.44	14.41	23.85	1.23
Total area (sq.km)	979.5	956.5	1936	100

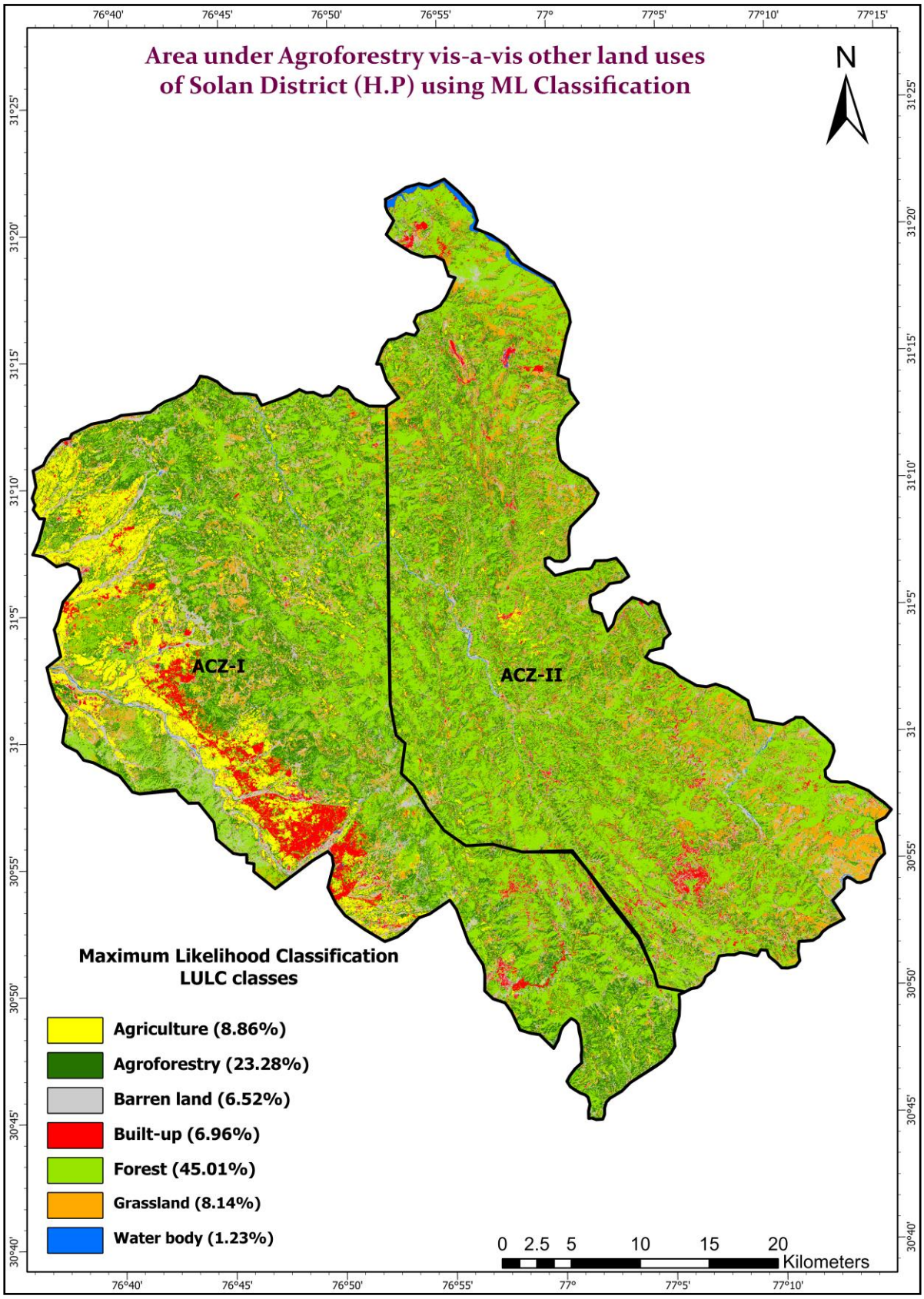

Figure 10. Map of the area (%) under major land-use classes using Maximum likelihood classification in Solan District (H.P)

The Solan district is divided into two agroclimatic zones - ACZ-I and ACZ-II. Each zone has distinct land-use patterns, as described in Table 15 and Figure 11. According to the maximum likelihood classifier, in ACZ-I, the forest is the predominant land cover, covering an area of 358.58 sq. km, which accounts for 36.61per cent of the total area. Agroforestry comes next, occupying 259.33 sq. km (26.48%), while agriculture covers 124.43 sq. km (12.70%). The built-up areas span 85.01 sq. km (8.68%), barren land comprises 85.01 sq. km (8.70%) and grassland and water bodies cover 57.47 sq. km (5.87%) and 9.44 sq. km (0.96%), respectively.

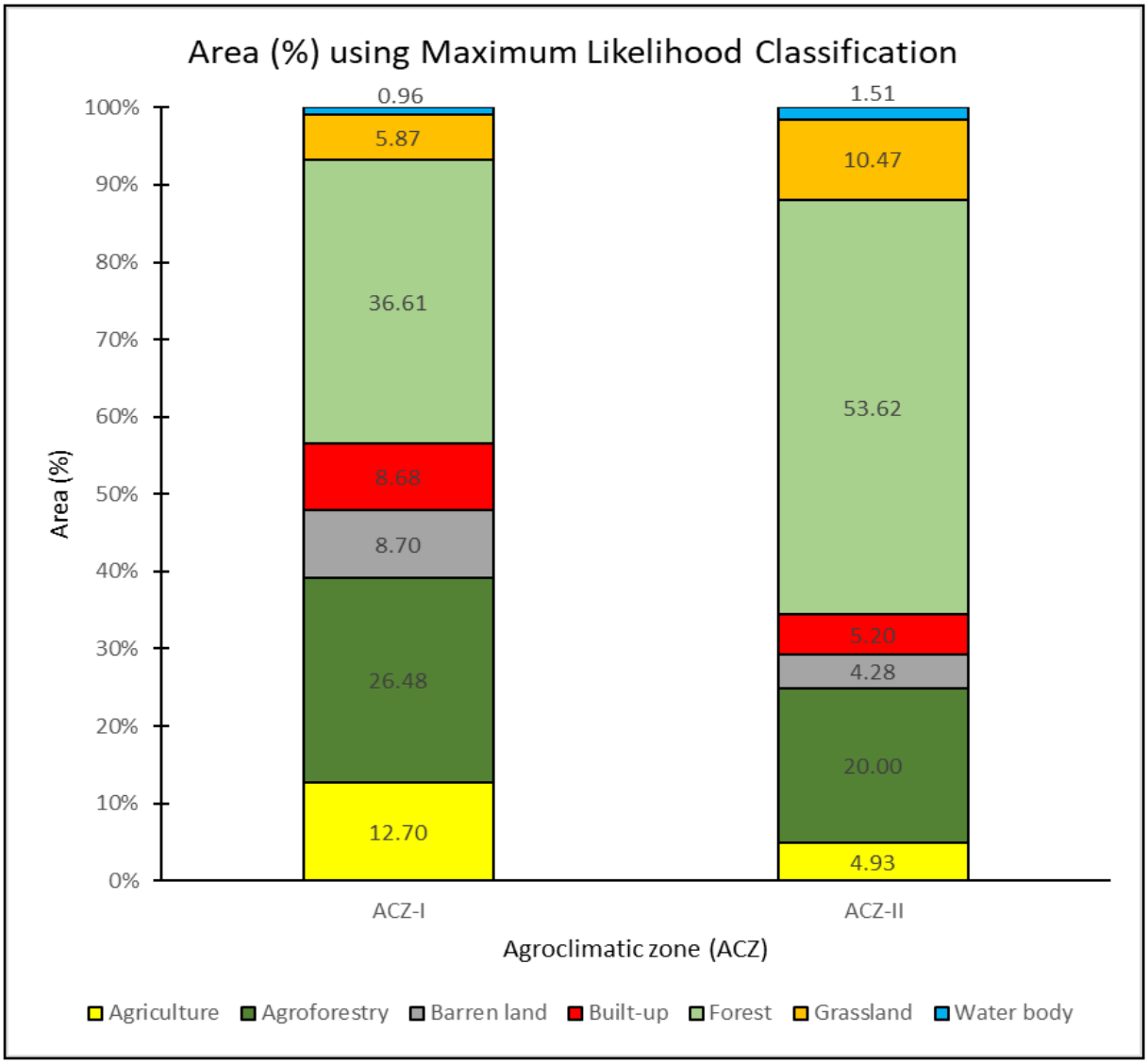

Figure 11. Area (%) under major land-use classes using Maximum Likelihood classification in different agroclimatic zones of Solan District (H.P)

In the ACZ-II region, the most extensive land use is forest, which covers 512.83 sq. km and makes up 53.62% of the total land. Agroforestry comes next with 191.29 sq. km

(20%). The remaining land is covered by grassland, built-up areas and agriculture, which occupy 100.19 sq. km (10.47%), 49.70 sq. km (5.20%) and 47.18 sq. km (4.93%), respectively. Barren land and water bodies comprise 40.90 sq. km (4.28%) and 14.41 sq. km (1.51%).

4.1.1.2. Random Forest Classification

The extensive Solan district, spanning a total area of 1936 sq. km, reveals its diverse landscape through comprehensive land-use and land cover (LULC) statistics derived from random forest classification (Table 16 and Figure 12). Solan district boasts a vast forest cover of 840.14 sq. km (43.40%) of the district's total area. The district is also committed to sustainable land management practices, as evidenced by the extensive expanse of agroforestry occupying 509.88 sq. km (26.34%). Agricultural activities are essential to the district's land use, with 174.87 sq. km (9.03%) dedicated to cultivation. The district also features 136.09 sq. km (7.03%) of grassland, highlighting its ecological diversity. The human footprint on the landscape is evident through the district's urban development, with 131.06 sq. km (6.77%) designated as built-up areas. Barren land covers 120.74 sq. km (6.24%), while water bodies occupy a relatively minor portion, amounting to 23.22 sq. km (1.20%).

Table 16. Estimate of area (sq.km) under Agroforestry and other major land-use classes using Random Forest classification in different agro-climatic zones of Solan District (H.P)

Classes	ACZ-I (sq.km)	ACZ-II (sq.km)	Total Area (sq.km)	Area (%)
Agriculture	121.07	53.80	174.87	9.03
Agroforestry	301.79	208.09	509.88	26.34
Barren land	57.90	62.84	120.74	6.24
Built-up	77.48	53.58	131.06	6.77
Forest	350.26	489.88	840.14	43.40
Grassland	62.12	73.97	136.09	7.03
Water body	8.88	14.34	23.22	1.20
Total area	979.5	956.5	1936	100.00

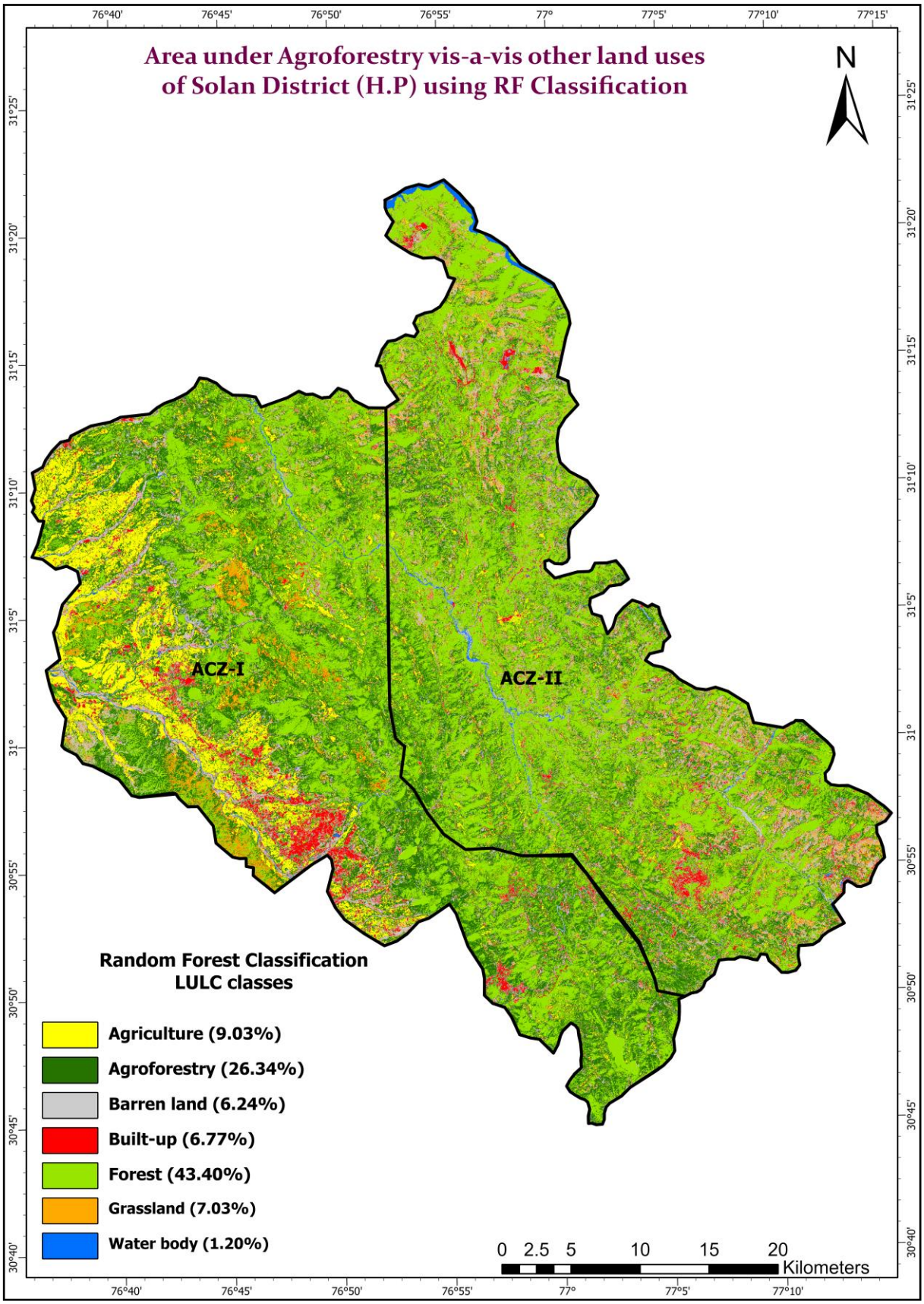

Figure 12. Map of the area (%) under major land-use classes using Random Forest Classification in Solan District (H.P)

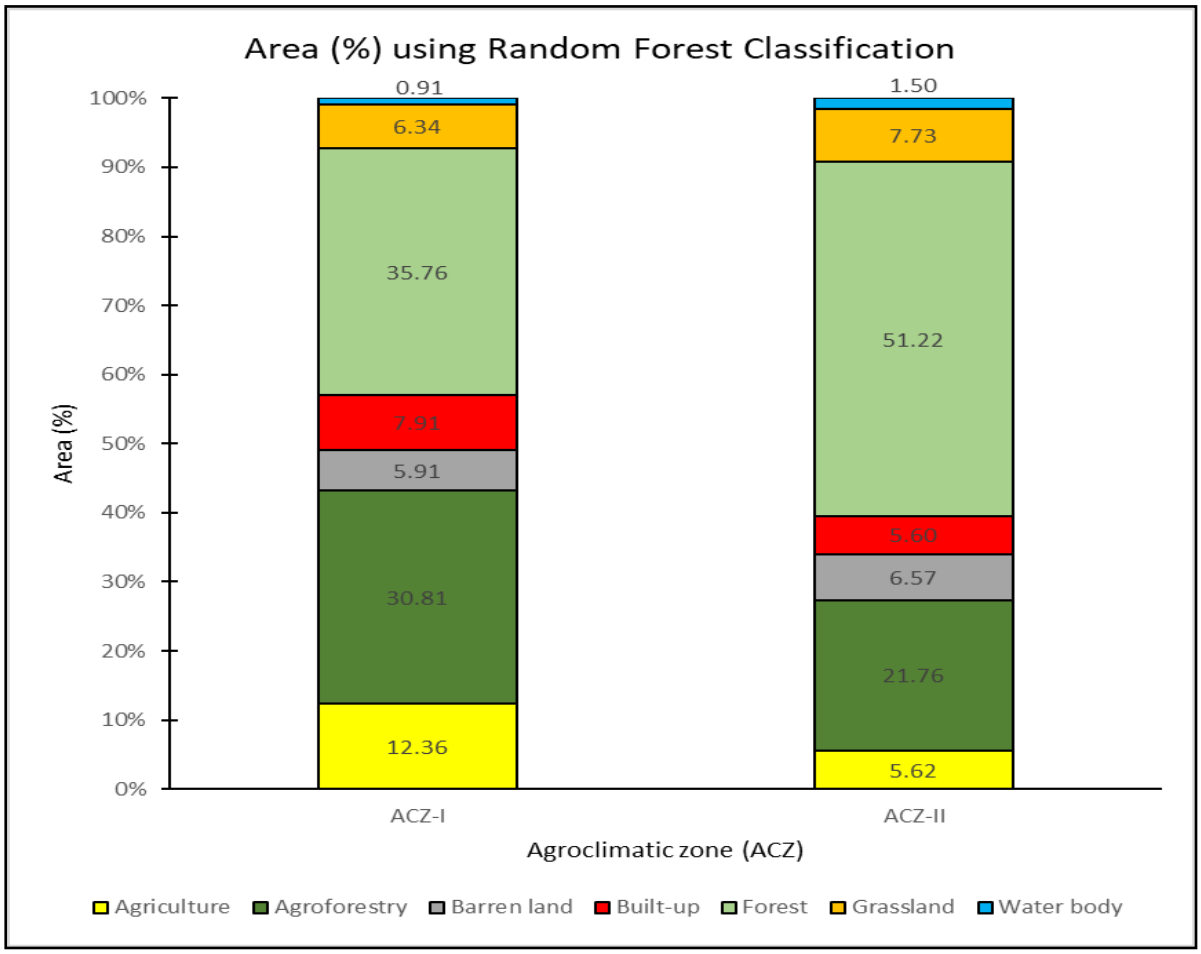

Figure 13. Area (%) estimated under different land classes using Random Forest classification in different agroclimatic zones of Solan District (H.P)

The Solan district is divided into two agroclimatic zones, ACZ-I and ACZ-II. Table 16 and Figure 13, created using a random forest classifier, show these differences. ACZ-I is mainly covered by forests, which span 350.26 sq. km (35.76%) of the total area. Agroforestry covers 301.79 sq. km (30.81%), indicating that ACZ-I promotes integrated land management practices. Agriculture is also significant, covering 121.07 sq. km (12.36%), followed by built-up areas 77.48 sq. km (7.91%), grassland 62.12 sq. km (6.34%), barren land 57.90 sq. km (5.91%) and water bodies 8.88 sq. km (0.91 %).

In ACZ-II, more than half of the total land area is covered by forested expanses, which amounts to 489.88 sq. km and constitutes 51.22% of the land. The region's commitment to sustainable land use practices is highlighted by agroforestry, which covers 208.09 sq. km (21.76%). The remaining land is distributed among different land covers, including grassland 73.97 sq. km (7.73%), barren land 62.84 sq. km (6.57%) and built-up areas 53.58 sq. km (5.60%). Agriculture and water bodies occupy 53.80 sq. km (5.62%) and

14.34 sq. km (1.50%), respectively, showcasing the interplay of natural and anthropogenic elements within ACZ-II.

4.1.1.3. Support vector Machine

This detailed overview of Solan district covers an extensive area of 1936 sq. km. It provides a nuanced understanding of its complex landscape by meticulously analysing land use and land cover (LULC) statistics. The statistics were derived through support vector machine classification and the results are presented in Table 17 and Figure 14. The defining feature of the district is its vast forest cover, which extends over 864.18 sq. km (44.64 %) of the total area. This extensive wooded region indicates the district's rich ecological diversity and underscores the importance of preserving natural habitats. The realm of agroforestry covers 484.52 sq. km (25.03%), demonstrating a notable commitment to sustainable land management practices. The district's landscape further unfolds with 169.72 sq. km (8.77%) devoted to cultivation, highlighting the coexistence of agriculture and human activity. The ecological balance within Solan is further underscored by 144.08 sq. km (7.44%) of grassland. Urban development has left its mark, with 140.37 sq. km (7.25%) designated as built-up areas, underscoring the evolving human footprint on the district's terrain. The district's environmental composition is completed by 108.96 sq. km (5.63%) of barren land and a relatively minor portion of 24.17 sq. km (1.25%) occupied by water bodies.

Table 17. Estimate of area (sq.km) under Agroforestry and other major land-use classes using Support vector machine classification in different agro-climatic zones of Solan District (H.P)

Classes	ACZ-I (sq.km)	ACZ-II (sq.km)	Total Area (sq.km)	Area (%)
Agriculture	127.43	42.29	169.72	8.77
Agroforestry	286.48	198.04	484.52	25.03
Barren land	59.08	49.88	108.96	5.63
Built-up	84.16	56.21	140.37	7.25
Forest	355.5	508.68	864.18	44.64
Grassland	57.48	86.60	144.08	7.44
Water body	9.37	14.80	24.17	1.25
Total area	979.5	956.5	1936	100.00

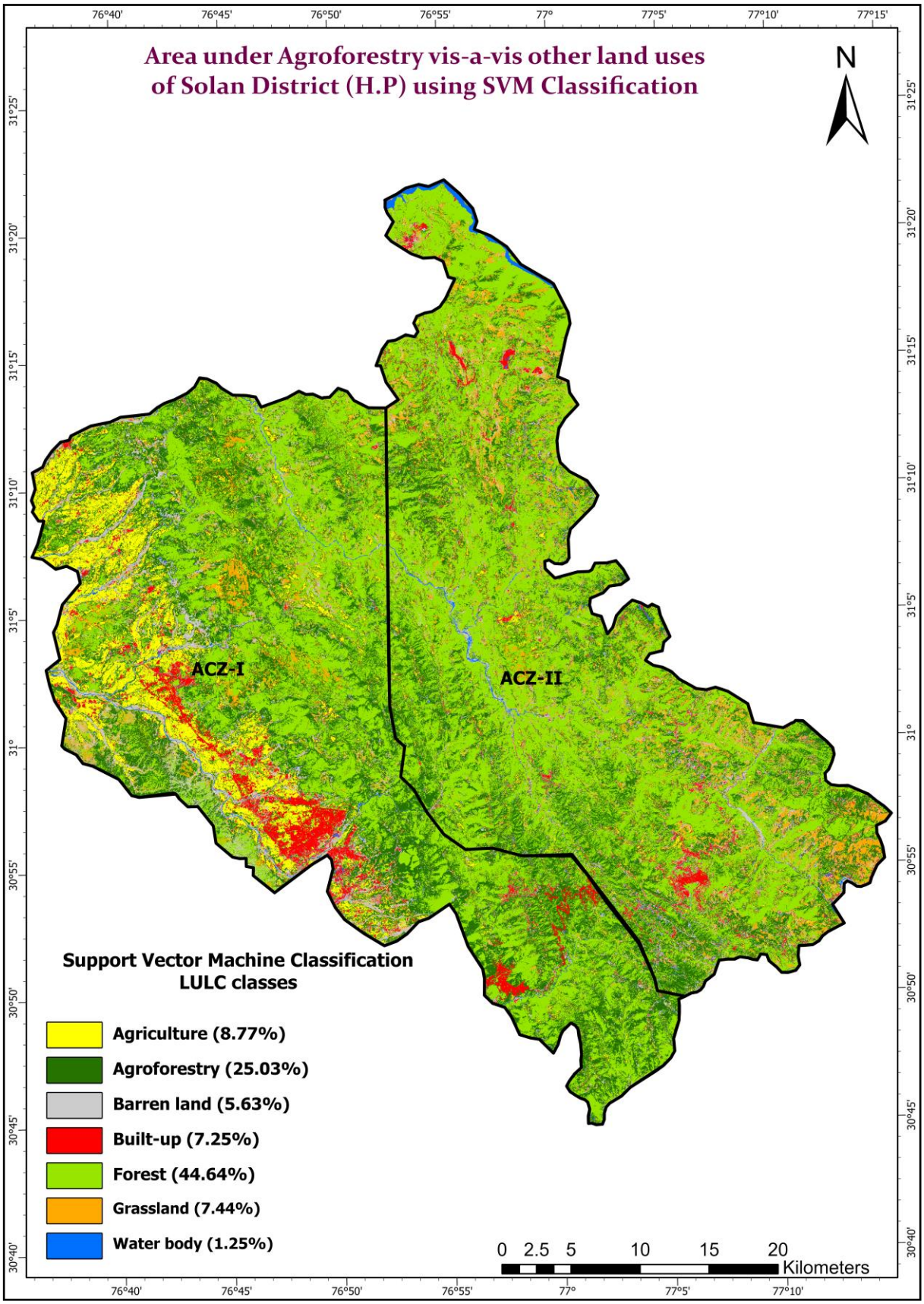

Figure 14. Map of the area (%) under major land-use classes using Support vector machine classification in Solan District (H.P)

The Solan district is divided into two agroclimatic zones, ACZ-I and ACZ-II, each with unique land-use patterns, as outlined in Table 17 and illustrated in Figure 15. The classification was done using a support vector machine. ACZ-I is dominated by expansive forested areas covering 355.50 sq. km (36.29%) of the total area. Agroforestry covers 286.48 sq. km (29.25%), highlighting the district's commitment to integrated land management practices. Agriculture is also a significant activity, covering 127.43 sq. km (13.01%), followed by built-up areas with 84.16 sq. km (8.59%), grassland with 57.48 sq. km (5.87%), barren land with 59.08 sq. km (6.03%) and water bodies with 9.37 sq. km (0.96%).

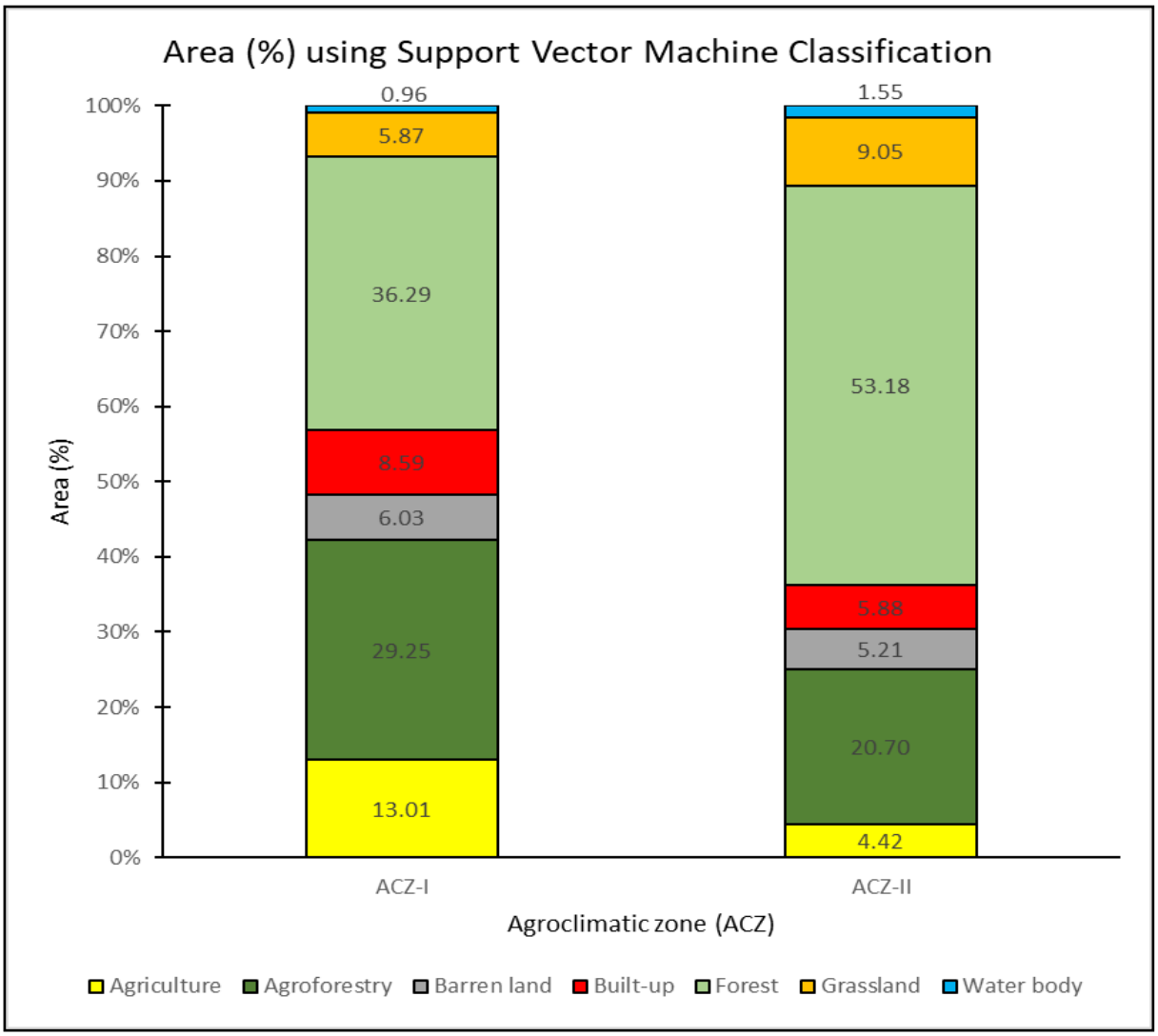

Figure 15. Area (%) under major land classes using Support vector machine classification in different agroclimatic zones of Solan District (H.P)

ACZ-II is a region where forested expanses are given high priority. They cover a substantial area of 508.68 sq. km (53.18%) of the total land. The region also demonstrates its commitment to sustainable land-use practices through agroforestry, which spans 198.04 sq.

km (20.70%). The landscape is diverse, with grassland, built-up areas and barren land covering 86.60 sq. km (9.05%), 56.21 sq. km (5.88%) and 49.88 sq. km (5.21%) respectively. The intricate interplay of natural and anthropogenic elements is highlighted by agriculture and water bodies occupying 42.29 sq. km (4.42%) and 14.80 sq. km (1.55%) respectively.

In the present study, the estimated area on percentage basis (23-26 %) under agroforestry in Solan district of Himachal Pradesh is found higher than previous reported values (up to 22.05%) by various scientists (Ahmad et al. 2016, Newaj et al. 2017, Rizvi et al. 2016a, 2016b, 2016c, 2020, 2021, 2019a, 2019b, Vikrant et al. 2018, Gupta et al. 2017 and Chavan et al. 2015) for other district of the country. As, per ISFR (2021) report under forest cover has been found to be 890.86 sq.km (46.02%) of the total geographic area of the district and 560.55 sq.km (28.95%) area comes under total cropped area for year 2021-2022 (DES 2022). In the present study, the 3 major land uses were agroforestry, agriculture and forest which accounts for 77-78 % of the total area and out of this 23-27 accounts for agroforestry. Therefore, estimation produced using the proposed techniques are consistent with those published statistics. In the present investigation the strip plantations along roads, railways and canals, linear array of trees on farm boundaries, man-made or naturally occurring tree clusters in the rural areas, patches of plantations on the community lands, farmlands, silvipastural system which generally found close to the forest area have also been considered for agroforestry area estimation. According to ISFR report (2021) the tree outside forest area of Himachal Pradesh was recorded as 5474 sq.km (9.84%) and usually *Pinus roxburghii, Cedrus deodara, Acacia catechu, Grewia oppositifolia, Quercus leucotrichophora, Mangifera indica, Morus spp*. tree species are usually found. According to Rizvi et al. (2021) other district of Himachal Pradesh *viz.*, Kangra, Kullu and Sirmour covers 13.39%, 9.89% and 9.50% agroforestry area respectively.

The current study also focused on Agro-Climatic Zones from which ACZ-I in the Solan district, has recorded slope ranging from less than 7 degrees to 7-16 degrees. This zone is known for its prevalent agriculture and agroforestry practices, with comparatively less forested area when compared to Agro-Climatic Zone II (ACZ-II). ACZ-I also has a greater extent of built-up areas, particularly in the Nalagarh/Buddi region, which is recognized as the industrial hub of the Solan district. On the other hand, ACZ-II, which is characterized by the presence of the Gambhar River and a smaller section of the Sutlej River, has a higher coverage of water bodies.

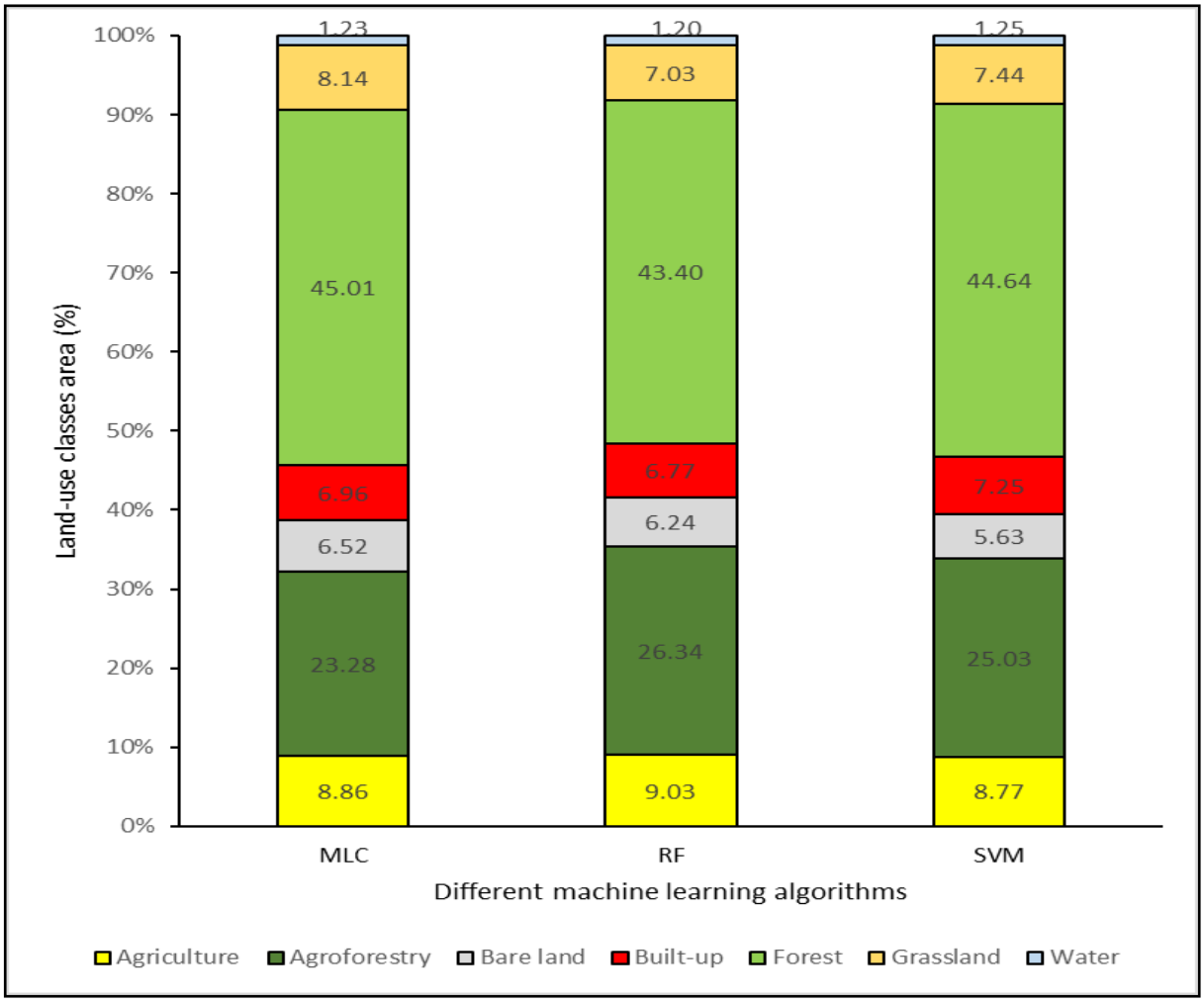

Figure 16. Area (%) of major land-use classes using different machine learning algorithms in Solan District (H.P)

4.1.2. Accuracy assessment

The accuracy assessment results of LULC classification have been achieved using error matrices. In the accuracy assessment, seven classified categories were considered: agriculture, agroforestry, barren land, built-up, forest, grassland and water body. Accuracy assessment was performed for MLC, RF and SVM classifiers to evaluate the prediction performance of the trained models using the multi-values to point feature (Figure 16 and Table 21, 22 and 23). The Random Forest (RF) classifier identified 9.03% of the total area as agricultural, achieving 90.82% user accuracy, as 7 pixels found as grassland class in actual and highest producer accuracy 93.68%, as 4 pixels were misclassified as grassland class. In comparison, the Support Vector Machine (SVM) classifier labelled 8.77% of the area as agricultural, demonstrating commendable 88.78% user accuracy as 8 classified pixels were found as grassland class and 91.58% producer accuracy as 6 pixels were misclassified as

grassland class. The Maximum Likelihood Classifier (MLC) marked 8.86% of the region as agricultural, with a user accuracy of 84.69% as 10 pixels were found as grassland in actual and a producer accuracy of 88.30% as 6 pixels were misclassified as grassland class.

The RF classifier effectively identified 26.34% of the overall area designated as agroforestry, showcasing a commendable user accuracy of 80.81% and 50 pixels were found as forest class and producer accuracy of 88.56% as 24 pixels were misclassified as forest class. The SVM classifier identified 25.03% of the area as agroforestry, achieving a user accuracy of 78.79% and 55 pixels were found as forest class in actual and a producer accuracy of 87.31%, as pixels (27) were misclassified as forest class. The MLC classifier recognized 23.28% of the area as agroforestry, with a user accuracy of 76.43%, as pixels (57) were found as forest class and a producer accuracy of 85.34%, as pixels (27) were misclassified as forest class. Notably, challenges arose due to primary confusion with the forest class, as the pixels of forest canopy less than 20% and agroforestry share similar characteristics. The significance of user accuracy and producer accuracy is highlighted, especially in scenarios where confusion between agroforestry and the forest class poses a significant challenge. These findings contribute valuable insights for decision-making in land use planning and resource management within the context of agroforestry.

In the categorization of barren land, the RF classifier identified 6.24% of the total area, achieving an 78.69% user accuracy, as pixels (4) were found as water body in actual and similar producer accuracy as pixels (5) were misclassified as built-up class. Meanwhile, the SVM classifier attributed 5.63% of the area to barren land, boasting an 73.77% user accuracy as pixels (4) were found as water body and 69.23% of producer accuracy as pixels (7) were misclassified as built-up class. The MLC classifier, attributing 6.52% of the land to barren status, exhibited a user accuracy of 70.49% as pixels (6) were found as water body and a producer accuracy of 63.32% as pixels (9) were misclassified as built-up class.

The RF classifier categorized 6.77% of the area as built-up with 86.27% user accuracy, as 5 pixels were found as barren land class and similar producer accuracy, as 4 pixels were misclassified as water body class. The SVM classifier identified 7.25% with 80.39% user accuracy, as pixels (7) were found as barren land class and 82% producer accuracy, as pixels (5) were misclassified as water body class. The MLC classifier classified built up area 6.96% with 72.55% user accuracy, as maximum pixels (9) were found as barren

land class and 71.15 % producer accuracy, as maximum pixels (6) were found in water body class. Notably, confusion between built-up, barren land and water body classes occurred due to minute colour differences in pixels (As-syakur et al. 2012).

The RF classifier identified 43.40% of the area as forest, achieving highest 91.75% of user accuracy, as 24 pixels were found as agroforestry class and 85% producer accuracy, as 50 pixels were misclassified in agroforestry class. Similarly, the SVM classifier categorized 44.64% as forest with 90.48% user accuracy, as 27 pixels were found as agroforestry class and 83.58% producer accuracy, as 55 pixels were misclassified as agroforestry class. The MLC classifier labelled 45.01% as forest, attaining 88.25% user accuracy, as 27 pixels were found as agroforestry class and 81.52% producer accuracy, as 57 pixels were misclassified as agroforestry class. The predominant challenge arises from the confusion of forest class pixels with agroforestry class pixels, primarily due to the shared colour characteristics and texture. The pixel colour similarity, especially in the forest canopy, extends up to 20%, contributing to the observed misclassification (Rizvi et al. 2020).

The RF classifier identified 7.03% of the area as grassland with 84.62% user accuracy, as 4 pixels were found as agriculture class and 74.58% producer accuracy, as 7 pixels were misclassified as agriculture class. Similarly, the SVM classifier categorized 7.44% as grassland with 78.85% user accuracy, as 6 pixels were found as agriculture class and 69.49% producer accuracy, as 8 pixels were misclassified as agriculture class. The MLC classifier labelled 8.14% as grassland, achieving 69.23% user accuracy, as maximum 7 pixels were found as agroforestry class and 64.29% producer accuracy, as 10 pixels were found in agriculture class. Notably, there were more instances of misclassification, particularly as agriculture class pixels.

The RF classifier identified 1.20% of the area as water body, achieving 69.23% user accuracy, as pixels (4) were found as barren land and built-up class and 78.26% producer accuracy, as pixels (4) were misclassified as barren land class. Similarly, the SVM classifier noted 1.25% as water body with 61.54% user accuracy, as pixels (5) were found as barren land and built-up class and 72.73% producer accuracy, as pixels (4) were misclassified as barren land class. The MLC classifier identified 1.23% as water body, attaining 57.69% user accuracy, as pixels (4) were found as barren land and built-up class and 68.18% producer

accuracy, as pixels (4) were misclassified as barren land class. Notably, there was increased confusion between barren land and built-up classes in the classification process.

Tables 21, 22 and 23, show detailed confusion matrices of classification accuracies for MLC, RF and SVM respectively. In the evaluation of three classification models—Random Forest (RF), Support Vector Machine (SVM) and Maximum Likelihood Classification (MLC), it is evident that the Random Forest classifier outperformed the others. Demonstrating the highest accuracy among the three, the RF classifier achieved an impressive 85.78%, accompanied by a robust Kappa Coefficient of 0.8092. Following closely, the SVM classifier exhibited an accuracy of 83.22% and a Kappa Coefficient of 0.775. The difference between RF And SVM is not statistically significant as the z-value is 1.8286 (p-value 0.17629**)** which is lower than 1.96 (Table. 18). On the other hand, MLC presented the lowest accuracy at 79.89%, with a corresponding kappa coefficient of 0.7305. The difference between MLC And SVM is statistically significant as the z-value is 3.82 (p-value 0.0485**)** which is more than 1.96 (Table. 19). Similarly, the difference between MLC and RF is also statistically significant as the z value is 4.32 (p-value 0.037514) (Table. 20).

These findings underscore the effectiveness of the Random Forest model in accurately classifying instances, showcasing its superior performance compared to SVM and MLC in this particular analysis. The RF classifier is known for its ability to handle high-dimensional and complex data, as well as its robustness to noise and outliers (Adam et al. 2014 and Belgiu and Dragut 2016, Kavzoglu et al. 2020 and Erdanaev et al. 2022). The SVM classifier is also a powerful technique that can handle nonlinear and non-separable data, but it may suffer from overfitting and high computational cost (Adam et al. 2014, Qian et al. 2015, Zhang et al. 2017, Kavzoglu et al. 2020, Sheykhmousa et al. 2020 and Erdanaev et al. 2022). The MLC classifier is a type of artificial neural network that can learn complex patterns and features from the data, but it may also be prone to overfitting and local minima (Basukala et al. 2017 and Erdanaev et al. 2022). Therefore, the choice of the best classifier depends on the characteristics of the data and the problem at hand. The similarity of performance of RF and SVM obtained in this study is consistent with Adam et al. (2014), Sheykhmousa et al. (2020) and Ashiagbor et al. (2023). As a result, the relatively high similar performance of SVM and RF in terms of classification accuracies makes them among the most popular machine learning classifiers within the RS community. Cengiz et al. (2023) also recorded RF algorithm yielded slightly better overall accuracies with higher Kappa Coefficient (92.5% and

0.90, respectively) as compared to the SVM algorithm where 91.7% overall accuracy and 0.89 Kappa Coefficient. The discovery that the Maximum Likelihood Classifier (MLC) demonstrated the lowest accuracy aligns with the findings of Erdanaev et al. (2022). In their research, SVM achieved an overall accuracy of 91.3% with a kappa coefficient of 0.90 and RF attained an overall accuracy of 90.5% with a Kappa Coefficient of 0.89. In contrast, MLC exhibited the lowest accuracy, with an overall accuracy of 85.5% and a kappa coefficient of 0.84. Similarly, Basheer et al. (2022) reported findings for Sentinel 2 A in the year 2021, where SVM demonstrated an overall accuracy of 86% with a kappa coefficient of 0.83, while MLC showed an overall accuracy of 83% with a Kappa Coefficient of 0.79. Both studies independently reported similar outcomes, further supporting the observation that MLC may have limitations or challenges in accurately classifying the data in the specific context or conditions studied.

Table 18. McNemar's test results for comparison of random forest (RF) and support vector machine (SVM) classifier

Classifier	**SVM**			
RF		**Correctly classified**	**Misclassified**	**Total**
	Correctly classified	736	22	758
	Misclassified	13	129	142
	Total	749	151	900
	Z-value	**1.8286**	**p-value**	**0.17629**

Table 19. McNemar's test results for comparison of and maximum likelihood classification (MLC) and Support vector machine (SVM) classifier

Classifier	**SVM**			
MLC		**Correctly classified**	**Misclassified**	**Total**
	Correctly classified	711	12	723
	Misclassified	25	152	177
	Total	736	164	900
	Z-value	**3.892**	**p-value**	**0.04852**

Table 20. McNemar's test results for comparison of and maximum likelihood classification (MLC) and random forest (RF) classifier

Classifier	**RF**			
MLC		**Correctly classified**	**Misclassified**	**Total**
	Correctly classified	736	18	754
	Misclassified	34	112	146
	Total	770	130	900
	Z-value	**4.327**	**p-value**	**0.037514**

Table 21. Confusion matrix of accuracy assessment of Agroforestry and other major land-use classes using Maximum Likelihood classification in Solan District of (H.P)

Class Value	Agriculture	Agroforestry	Barren land	Built-up	Forest	Grassland	Water body	Reference points	Commission error	User Accuracy (%)
Agriculture	**83**	2	2	0	1	10	0	98	0.15	**84.69**
Agroforestry	2	**227**	5	1	57	5	0	297	0.24	**76.43**
Barren land	1	2	**43**	5	2	2	6	61	0.30	**70.49**
Built-up	1	1	9	**37**	1	1	1	51	0.27	**72.55**
Forest	1	27	4	3	**278**	2	0	315	0.12	**88.25**
Grassland	6	7	1	0	2	**36**	0	52	0.31	**69.23**
Water body	0	0	5	6	0	0	**15**	26	0.42	**57.69**
Classified point	94	266	69	52	341	56	22	**900**		
Omission error	0.12	0.15	0.38	0.29	0.18	0.36	0.32			
Producer Accuracy (%)	**88.30**	**85.34**	**62.32**	**71.15**	**81.52**	**64.29**	**68.18**			
Overall Accuracy (%)	**79.89**									
Kappa Coefficient	**0.7305**									

Table 22. Confusion matrix of accuracy assessment of Agroforestry and other major land-use classes using Random Forest classification in Solan District of (H.P)

Class Value	Agriculture	Agroforestry	Barren land	Built-up	Forest	Grassland	Water body	Reference points	Commission error	User Accuracy (%)
Agriculture	**89**	2	0	0	0	7	0	98	0.09	**90.82**
Agroforestry	1	**240**	2	0	50	4	0	297	0.19	**80.81**
Barren land	1	2	**48**	3	1	2	4	61	0.21	**78.69**
Built-up	0	0	5	**44**	0	1	1	51	0.14	**86.27**
Forest	0	24	1	0	**289**	1	0	315	0.08	**91.75**
Grassland	4	3	1	0	0	**44**	0	52	0.15	**84.62**
Water body	0	0	4	4	0	0	**18**	26	0.31	**69.23**
Classified point	95	271	61	51	340	59	23	**900**		
Omission error	0.06	0.11	0.21	0.14	0.15	0.25	0.22			
Producer Accuracy (%)	**93.68**	**88.56**	**78.69**	**86.27**	**85.00**	**74.58**	**78.26**			
Overall Accuracy (%)	**85.78**									
Kappa Coefficient	**0.8092**									

Table 23. Confusion matrix of accuracy assessment of Agroforestry and other major land-use classes using Support Vector Machine classification in Solan District of (H.P)

Class Value	Agriculture	Agroforestry	Barren land	Built-up	Forest	Grassland	Water body	Reference points	Commission error	User Accuracy (%)
Agriculture	**87**	1	2	0	0	8	0	98	0.11	**88.78**
Agroforestry	1	**234**	2	0	55	5	0	297	0.21	**78.79**
Barren land	1	3	**45**	4	1	3	4	61	0.26	**73.77**
Built-up	0	0	7	**41**	0	1	2	51	0.20	**80.39**
Forest	0	27	2	0	**285**	1	0	315	0.10	**90.48**
Grassland	6	3	2	0	0	**41**	0	52	0.21	**78.85**
Water body	0	0	5	5	0	0	**16**	26	0.38	**61.54**
Classified point	95	268	65	50	341	59	22	**900**		
Omission error	0.08	0.13	0.31	0.18	0.16	0.31	0.27			
Producer Accuracy (%)	**91.58**	**87.31**	**69.23**	**82.00**	**83.58**	**69.49**	**72.73**			
Overall Accuracy (%)	**83.22**									
Kappa Coefficient	**0.7750**									

4.2 AGROFORESTRY SUITABILITY MAPPING

An assessment was conducted to determine the areas suitable for agroforestry based on 11 different criteria. These criteria included four topographical aspects: aspect, slope, elevation and hill shade, two vegetation parameters, land use land cover (LULC) and Normalized Difference Vegetation Index (NDVI), two climate variables, precipitation and temperature and one soil parameter: soil fertility. The assessment also considered two other parameters: distance from road and stream. The weights assigned to each criterion were derived using two different multi-criterion decision-making techniques: the analytical hierarchy process (AHP) and the fuzzy AHP technique. The various layers were overlaid using ArcMap 10.8.2. Soil fertility was determined by combining soil nutrients such as available nitrogen, phosphorus, potassium, boron and magnesium with soil characteristics such as soil texture, pH, organic matter, cation exchange capacity and bulk density.

4.2.1. Criterion

4.2.1.1. Land use and land cover

The data presented in Table 24 and Figure 17 show that forests are the most extensive land cover in the study area, covering 840.14 sq. km (43.40%) of the total area. Agroforestry comes in second place, occupying 509.88 sq. km (26.34%). Agriculture covers 174.87 sq. km (9.03%) of the total area, while grasslands cover 136.09 sq. km (7.03%). The built-up areas occupy 131.06 sq. km (6.77%), barren land covers 120.74 sq. km (6.24%) and water bodies constitute the smallest coverage at 23.22 sq. km (1.20%).

4.2.1.2. Normalized Difference Vegetation Index (NDVI)

The data in Table 24 and Figure 17 indicates that 4.68 per cent of the area (90.675 sq. km) has an NDVI value of less than 0, 17.16 per cent of the area (332.276 sq. km) has values ranging from 0 to 0.2, 29.79 per cent of the area (576.667 sq. km) has values ranging from 0.2 to 0.3, 32.66 per cent of the area (632.361 sq. km) has values ranging from 0.3 to 0.4 and 15.70 per cent of the area (304.021 sq. km) has an NDVI value between 0.4 and 0.5.

4.2.1.3. Rainfall

A clear representation of rainfall distribution across the study area emerges upon careful analysis of the data presented in Table 24 and Figure 17. It shows that approximately 388.35 sq.km (20.06%) of the area experiences rainfall between 1170-1240 mm, 560.83

sq.km (28.97%) receives rainfall between 1240-1300 mm, 452.38 sq.km (23.37%) receives rainfall between 1300-1370 mm, 247.43 sq.km (12.78%) receives rainfall between 1370-1440 mm and 287.01 sq.km (14.82%) receives rainfall between 1440-1510 mm.

4.2.1.4. Temperature

Upon analysing Table 24 and Figure 17, a clear depiction of the geographical temperature distribution in the study area can be observed. The data shows that out of the total area, approximately 159.70 sq. km (8.25%) experiences temperatures below 20°C, 194.21 sq. km (10.03%) falls within the range of 20-21 °C, 490.81 sq. km (25.35%) falls within the range of 21-22 °C, the most significant portion of 702.89 sq. km (36.31%) lies in the range of 22-23 °C and finally, 388.39 sq. km (20.06%) receives temperatures exceeding 23 °C.

4.2.1.5. Slope

Table 24 and Figure 18 show that the land area can be divided into different slope categories. Approximately 18.05 percent (349.54 sq. km) of the area has slopes that are less than 7 degrees. 22.07 per cent (427.33 sq. km) of the area has slopes ranging from 7 to 16 degrees. 28.89 per cent (559.37 sq. km) of the area has slopes ranging from 16 to 24 degrees. An area of 366.27 sq. km (18.92%) has slopes between 24 to 30 degrees, while an area of 233.51 sq. km (12.06%) has slopes greater than 30 degrees.

4.2.1.6. Elevation

After thoroughly examining the data presented in Table 24 and Figure 18, it is evident that the study region can be divided into five distinct elevation classes. These classes are as follows: less than 558 m, 558-893 m, 893-1178 m, 1178-1499 m and >1499 m. The areas covered by these elevation classes are 422.79 sq. km (21.84%), 382.46 sq. km (19.76%), 521.46 sq. km (26.93%), 435.14 sq. km (22.48%) and 197.25 sq. km (10.19%), respectively.

4.2.1.7. Aspect

A detailed review of the data presented in Table 24 and Figure 18, reveals the division of the study area into five distinct aspect classes. About 312.79 sq. km (16.16%) falls under the south-west and flat aspect, 586.99 sq. km (30.32%) are under south-east and south, 448.02 sq. km (23.14%) are under east and west, 482.07 sq. km (24.90%) are under north-west and north-east and 106.13 sq. km (5.48%) are under north aspect.

4.2.1.8. Hillshade

After conducting an extensive analysis of the data depicted in Table 24 and Figure 18, it is clear that the study area of about 1050.86 sq. km (54.28%) class receives less sunshine (<23) and are shadow areas, while 343.68 sq. km (17.752%) were the brightest area having hill shade value 151-180. Approximately 164.44 sq. km (8.49%), 173.77 sq. km (8.98%) and 203.26 sq. km (10.499%) area of Solan district was found to have hill shade values of 23-67, 67-110 and 110-151 respectively *i.e.*, medium sunshine.

4.2.1.9. Soil fertility

After a comprehensive analysis of the data presented in Table 24 and Figure 19, it becomes apparent that the study area is divided into five soil fertility classes: very low, low, medium, high and very high. Around 89.77 sq. km (4.64%) area had deficient soil fertility status, 246.12 sq. km (12.71%) area had low, 336.34 sq. km (17.37%) area had medium, 603.54 sq. km (31.17%) are high and 660.21 sq. km (34.10%) area had very high soil fertility status.

Table 24. List of criteria and sub-criteria along with area (ha) and percentage of area of Solan District (H.P)

Main criteria	Sub-criteria	Area (ha)	Area (%)
LULC	Agriculture	174.87	9.03
	Agroforestry	509.88	26.34
	Barren land	120.74	6.24
	Built-up area	131.06	6.77
	Forest	840.14	43.40
	Grassland	136.09	7.03
	Water	23.22	1.20
NDVI	<0	90.67	4.68
	0-0.2	332.28	17.16
	0.2-0.3	576.67	29.79
	0.3-0.4	632.36	32.66
	0.4-0.5	304.02	15.70
Slope (degree)	<7	349.54	18.05
	7.0-16.0	427.33	22.07
	16.0-24	559.37	28.89
	24-30	366.27	18.92
	>30	233.51	12.06
Aspect	SW, FLAT	312.79	16.16
	S, SE	586.99	30.32
	E, W	448.02	23.14
	NW, NE	482.07	24.90
	N	106.13	5.48

Main criteria	Sub-criteria	Area (ha)	Area (%)
Elevation (m)	<558	422.79	21.84
	558-893	382.46	19.76
	893-1178	521.46	26.93
	1178-1499	435.14	22.48
	>1499	197.25	10.19
Hillshade	<23	1050.86	54.280
	23-67	164.44	8.494
	67-110	173.77	8.976
	110-151	203.25	10.499
	151-180	343.68	17.752
Rainfall(mm)	1170-1240	388.35	20.06
	1240-1300	560.83	28.97
	1300-1370	452.38	23.37
	1370-1440	247.43	12.78
	1440-1510	287.01	14.82
Temperature (°C)	<20	159.70	8.25
	20-21	194.21	10.03
	21-22	490.81	25.35
	22-23	702.89	36.31
	>23	388.39	20.06
Soil fertility AHP	Very low	89.77	4.64
	Low	246.12	12.71
	Medium	336.34	17.37
	High	603.54	31.17
	Very high	660.21	34.10
Soil fertility FUZZY	Very low	191.97	9.92
	Low	255.06	13.17
	Medium	348.00	17.98
	High	413.54	21.36
	Very high	727.44	37.57
Distance from stream (km)	<0.92	705.13	36.42
	0.92-1.84	700.18	36.17
	1.84-2.76	257.09	13.28
	2.76-3.68	185.18	9.56
	>3.68	88.42	4.57
Distance from road (km)	<0.22	879.54	45.43
	0.22-0.59	561.23	28.99
	0.59-1.10	263.66	13.62
	1.10-1.85	119.13	6.15
	>1.85	112.45	5.81

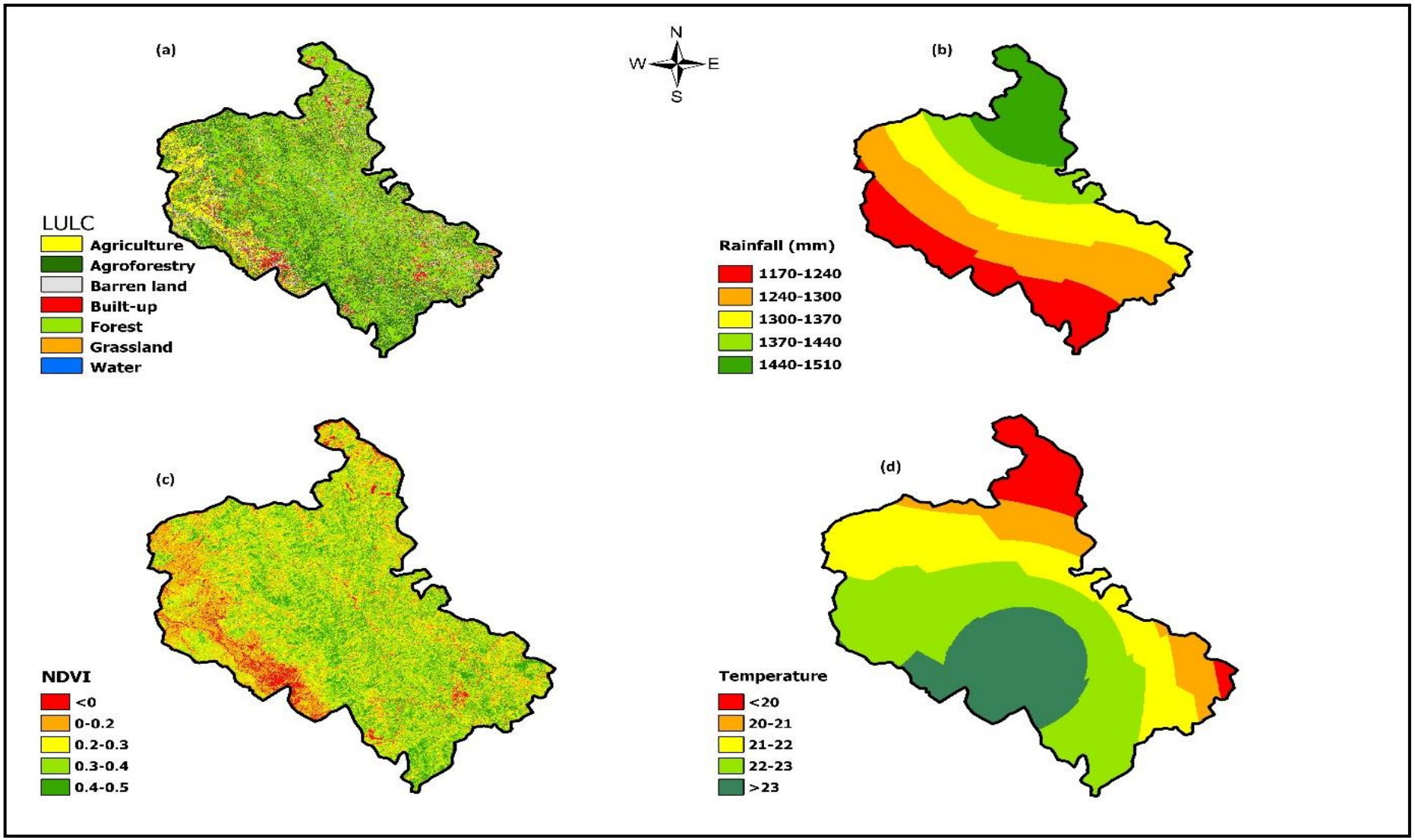

Figure 17. Climatic and ecological variables: (a) LULC, (b) rainfall (mm), (c) NDVI and (d) Temperature(°C)

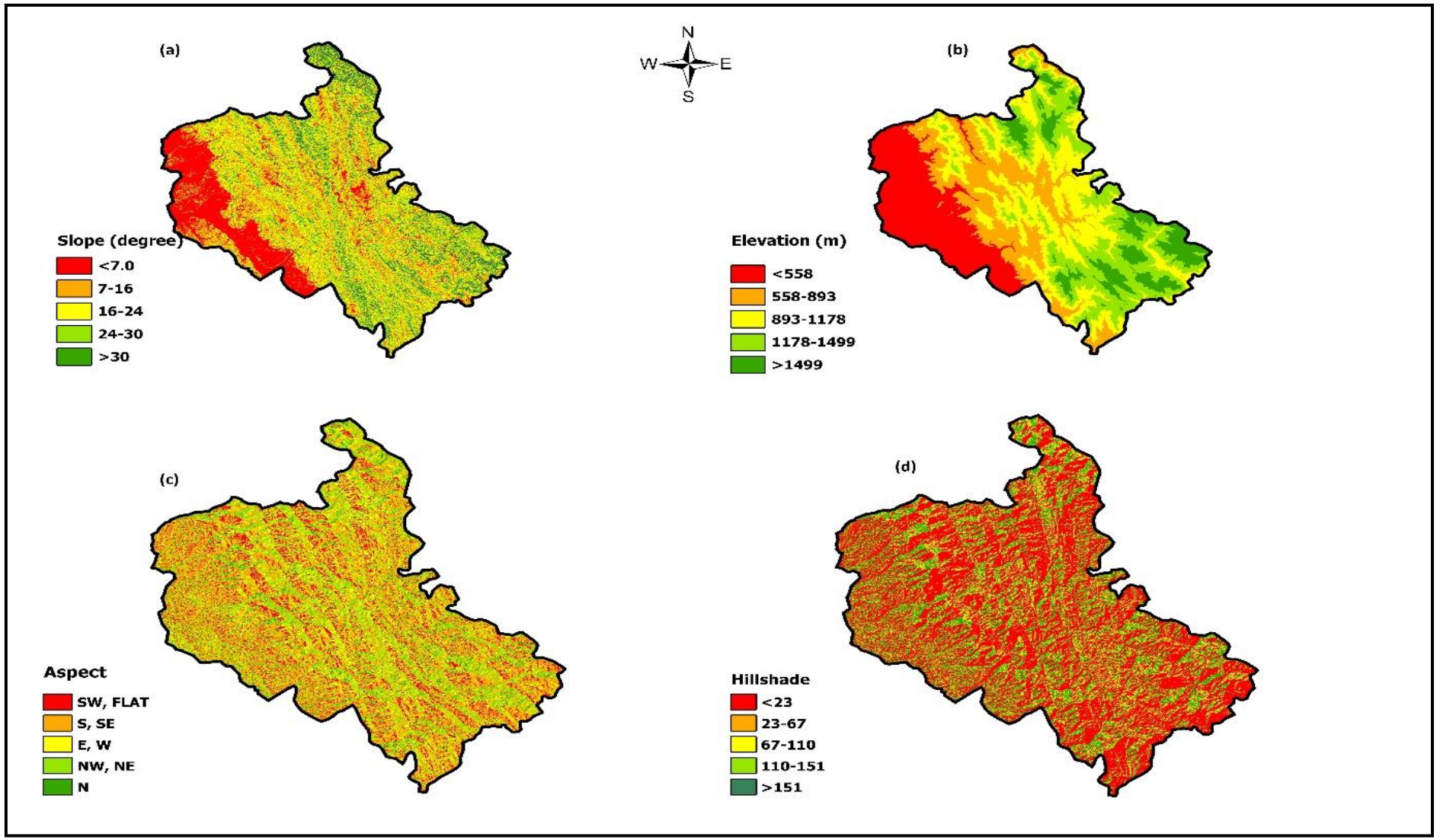

Figure 18. Topographical variables: (a) Slope(degree), (b) elevation (m), (c) aspect and (d) hillshade

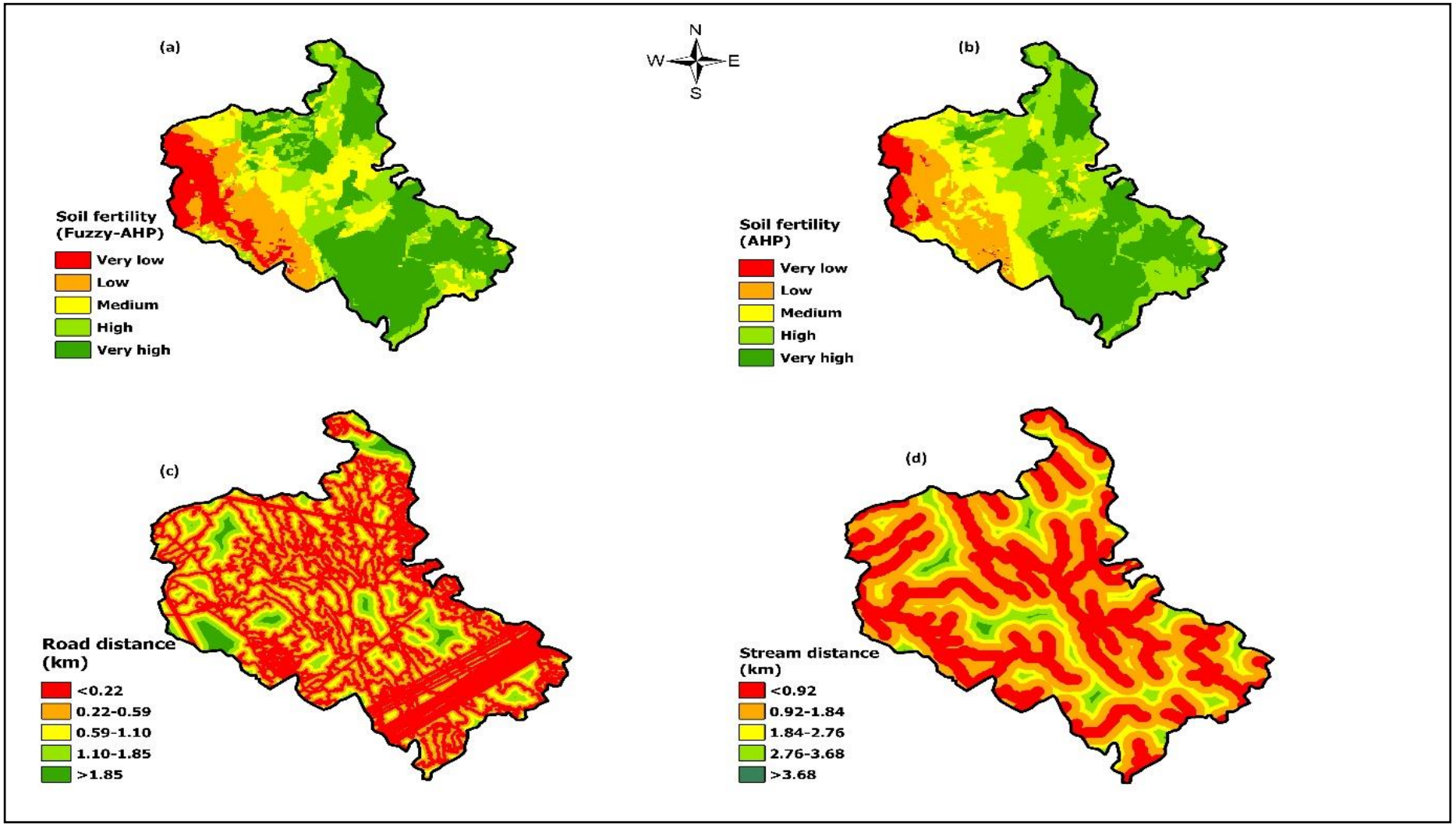

Figure 19. Soil and socioeconomic variables: (a) Soil fertility (Fuzzy-AHP), (b) soil fertility (AHP) (c) road distance (km) and (d) stream distance (km)

4.2.1.10. Distance from stream

According to the data presented in Table 24 and Figure 19, 36.42 per cent (705.13 sq. km) of the district's area, is located near rivers and streams (<0.92 km). Additionally, 36.17 per cent of the area (700.18 sq. km), is situated at a distance of 0.92-1.84 km from the rivers and streams. Furthermore, 13.28% of the area (257.09 sq. km), is located at a distance of 1.84-2.76 km from the rivers and streams. Also, 9.56% of the district's area (185.18 sq. km), is situated at a distance of 2.76-3.68 km from the rivers and streams. Finally, only 4.57% of the district's area (88.42 sq. km), is more than 3.68 km from the rivers or streams.

4.2.1.11. Distance from road

After analysing the data presented in Table 24 and Figure 19, it can be observed that out of the total area, 45.43 per cent (879.54 sq. km) is located within a distance of 0.22 km from the road. The second most significant area, 28.99 per cent (561.23 sq. km), is situated at a distance of 0.22-0.59 km from the road. The third most important area, 13.62 per cent (263.66 sq. km), is located at a distance of 0.59-1.10 km from the road. The fourth most considerable area of 6.15 per cent (119.13 sq. km) is situated at a distance of 1.10-1.85 km from the road. Finally, the fifth most important area, 5.81 per cent (112.45 sq. km), is more than 1.85 km from the road.

4.2.2 Multi-Criteria Decision-Making Process (MCDM)

In the present study, two Multi-Criteria Decision-Making (MCDM) methods, specifically the Analytic Hierarchy Process (AHP) and Fuzzy-AHP, were utilized to determine the relative importance of different criteria and sub-criteria.

4.2.2.1. Analytic Hierarchy Process (AHP)

The Analytical Hierarchy Process (AHP) involves the determination of weight for each individual criterion. This is accomplished by comparing factors in a pairwise manner to assess their relative preferences. The process identifies the eigenvalue linked to the primary eigenvector of the completed matrix and then normalizes the total factors to achieve a sum of one (Zhang et al. 2021, Sharma 2022 and Topuz and Deniz 2023).

4.2.2.1.1. Criterion weights (AHP approach)

The Table 25. below shows a pair comparison matrix based on the Saaty scale. The highest weight, 0.261, was given to land use land cover, followed by slope at 0.173, elevation

at 0.161, rainfall at 0.062, soil fertility at 0.091, NDVI at 0.118, aspect at 0.042, hillshade at 0.04, temperature at 0.024, stream distance at 0.015 and road distance at 0.012. The matrix has a consistency ratio of 0.085, which means that it is consistent. Using the weights derived from the AHP approach, the agroforestry suitability equation was developed:

Agroforestry suitability map=LULC × 0.261+ slope × 0.173 + elevation × 0.161+ rainfall × 0.062 + soil fertility × 0.091+ NDVI × 0.118+ aspect × 0.042+ hillshade × 0.04+ temperature × 0.024+ stream distance × 0.015+ road distance × 0.012.

4.2.2.1.2. Sub-Criterion weights (AHP approach)

The sub-criteria were assessed on a scale of 1 to 9, where a rating of 1 indicated the least suitability for agroforestry and a rating of 9 showed the highest suitability. These sub-criteria rankings were established by drawing insights from existing published literature in agroforestry, along with personal observations. The data presented in the Table 25 shows the suitability scores for various Land Use and Land Cover (LULC) categories. In this context, agroforestry received the highest score of 9, followed by agriculture and grassland, both scoring 7. Barren land received a score of 3. Forests, water bodies and built-up areas were not considered in the analysis, as they were deemed unsuitable for agroforestry at present.

The slope measures the rate of change of elevation of the land per unit distance. Steeper slopes allow water to move faster, while gentle slopes are suitable for plant growth as the water stays there for some time and provides adequate moisture to the soil. Therefore, gentle slopes are more ideal for agroforestry than steep slopes (Ahmad et al. 2017a and Ozkan et al. 2020). The measurement of the slope was obtained from SRTM DEM. Areas with a slope of less than 7 degrees were given the highest score of 9, followed by areas with slopes ranging from 7 to 16 degrees, which scored 7. The scores then decreased for areas with slopes of 16-24 degrees (5), 24-30 degrees (3) and slopes exceeding 30 degrees (1).

Elevation plays a significant role in the growth of plants. As the elevation increases, the vegetation decreases gradually, as per Ahmad et al. (2017a). The score for low-lying areas with elevations below 558 meters is the highest, receiving a score of 9, whereas measurements more than1499 meters receive the lowest score of 1.

Table 25. AHP pair comparison matrix for different data layers for multi-criteria weights

Criteria	LULC	SLOPE	ELEVATION	NDVI	SOIL FERTILITY	RAINFALL	ASPECT	HILLSHADE	TEMPERATURE	STREAM	ROAD	Weight
LULC	**1**	2	3	4	4	5	6	6	7	8	9	**0.261**
SLOPE	0.5	**1**	2	2	3	3	5	5	6	7	8	**0.173**
ELEVATION	0.33	0.5	**1**	2	3	4	5	6	7	8	8	**0.161**
NDVI	0.25	0.5	0.5	**1**	2	3	4	5	5	7	8	**0.118**
SOIL FERTILITY	0.25	0.33	0.33	0.5	**1**	2	3	4	6	7	8	**0.091**
RAINFALL	0.2	0.33	0.25	0.33	0.5	**1**	2	3	4	5	6	**0.062**
ASPECT	0.17	0.2	0.2	0.25	0.33	0.5	**1**	1	3	5	6	**0.042**
HILLSHADE	0.17	0.2	0.17	0.2	0.25	0.33	1	**1**	3	5	6	**0.040**
TEMPERATURE	0.14	0.17	0.14	0.2	0.17	0.25	0.33	0.33	**1**	3	4	**0.024**
STREAM	0.12	0.14	0.12	0.14	0.14	0.2	0.2	0.2	0.33	**1**	2	**0.015**
ROAD	0.11	0.12	0.12	0.12	0.12	0.17	0.17	0.17	0.25	0.5	**1**	**0.012**

These parameters indicate soil fertility and are essential for ensuring food security, as Ahmad et al. (2017a) and Subedi et al. (2022) mention. The different thematic maps were assigned weights and ranks based on sub-criteria for soil fertility, ranked in ascending order from 1 to 9, with a score of 1 representing the lowest fertility and 9 indicating the highest.

The strong relationship between NDVI (Normalized Difference Vegetation Index) values and vegetation density is well-established in remote sensing and monitoring. In general, higher NDVI values are associated with denser and healthier vegetation. This is because healthy vegetation reflects more near-infrared light and absorbs more red light. As a result, a higher NDVI indicates a more significant presence of chlorophyll and photosynthetically active vegetation (Gomes et al. 2017, Ahmad et al. 2019 and Subedi et al. 2022). A score of 1 corresponds to NDVI values below 0, a score of 3 was assigned to NDVI values ranging from 0 to 0.2, a score of 5 was designated for NDVI values between 0.2 and 0.3, a score of 7 was allocated to NDVI values falling within the range of 0.3 to 0.4 and a score of 9 was attributed to NDVI values spanning from 0.4 to 0.5.

Table 26. List of criteria along with weights and scores of the sub-criteria using AHP

Main criteria	Weight	Influence	Sub-criteria	Score
LULC	0.261	26.1	Agriculture	7
			Agroforestry	9
			Barren land	3
			Built-up area	Restricted
			Forest	Restricted
			Grassland	7
			Water	Restricted
Slope (degree)	0.173	17.3	<7	9
			7.0-16.0	7
			16.0-24	5
			24-30	3
			>30	1
Elevation (m)	0.161	16.1	<558	9
			558-893	7
			893-1178	5
			1178-1499	3
			>1499	1
NDVI	0.118	11.8	<0	1
			0-0.2	3
			0.2-0.3	5
			0.3-0.4	7
			0.4-0.5	9

Main criteria	Weight	Influence	Sub-criteria	Score
Soil fertility	0.091	9.1	Very low	1
			Low	3
			Medium	5
			High	7
			Very high	9
Rainfall (mm)	0.062	6.2	1170-1240	1
			1240-1300	3
			1300-1370	5
			1370-1440	7
			1440-1510	9
Aspect	0.042	4.2	SW, FLAT	9
			S, SE	7
			E, W	5
			NW, NE	3
			N	1
Hillshade	0.04	4	<23	1
			23-67	3
			67-110	5
			110-151	7
			151-180	9
Temperature	0.024	2.4	<20	9
			20-21	7
			21-22	5
			22-23	3
			>23	1
Distance from stream (km)	0.015	1.5	<0.92	9
			0.92-1.84	7
			1.84-2.76	5
			2.76-3.68	3
			>3.68	1
Distance from road(km)	0.012	1.2	<0.22	9
			0.22-0.59	7
			0.59-1.10	5
			1.10-1.85	3
			>1.85	1

As for aspects, the north aspect and hill shades in the 0-23 range were assigned a score of 1. The score increased to 3 for northwest and northeast aspects and hill shades between 23-67. A score of 5 was given to 67-110 hill shade values and east and west aspects. Furthermore, 110-151 hill shade values and south and south-eastern aspects received a score of 7, while a score of 9 was allocated to 151-180 hill shade values, south-western aspects and flat surface.

Locations closer to roads and streams, within 0.22 km and 0.92 km, respectively, have been assigned a higher score of 9. On the other hand, locations that are farther from streams (more than 3.68 km) and roads (more than 1.85 km) have received the lowest score of 1. The significance of distance to streets could indicate accessibility and connectivity. Most agroforestry interventions are carried out along the road or in proximity areas for better transportation of agroforestry products. The importance of distance to the settlement could be attributed to the farmers' preference for agroforestry interventions in and around their homes for easy access, regular monitoring and better management (Singh et al. 2022).

4.2.2.1.3. Agroforestry Suitability Map using Analytical Hierarchy process (AHP)

Upon careful examination of the data presented in the Table 27 and Figure 20, it becomes evident that the application of the Analytic Hierarchy Process (AHP) has resulted in the classification of land areas within Solan district according to their suitability for agroforestry practices. The analysis reveals that approximately 17.32% of the district's total area, equivalent to 335.32 sq. km, was classified as highly suitable for agroforestry, while 22.37% (433.07 sq. km) was considered moderately suitable. Moreover, 20.19% of the district's land area, totalling 390.97 sq. km, was classified as marginally suitable. A notable portion, accounting for 26.45% (512.04 sq. km), was currently not suitable for agroforestry and 13.67% (264.6 sq. km) was permanently unsuitable for such practices.

Table 27. Distribution of agroforestry suitability classes (AHP approach) in different agro-climatic zone of Solan District (H.P.)

Suitability Classes	ACZ-I (sq.km)	ACZ-II (sq.km)	Total (sq.km)	Area (%)
Highly Suitable	235.33	99.99	335.32	17.32
Moderately suitable	260.38	172.69	433.07	22.37
Marginal Suitable	168.67	222.3	390.97	20.19
Currently not Suitable	230.28	281.76	512.04	26.45
Permanently not suitable	84.84	179.76	264.6	13.67
Total area	979.5	956.5	1936	100.00

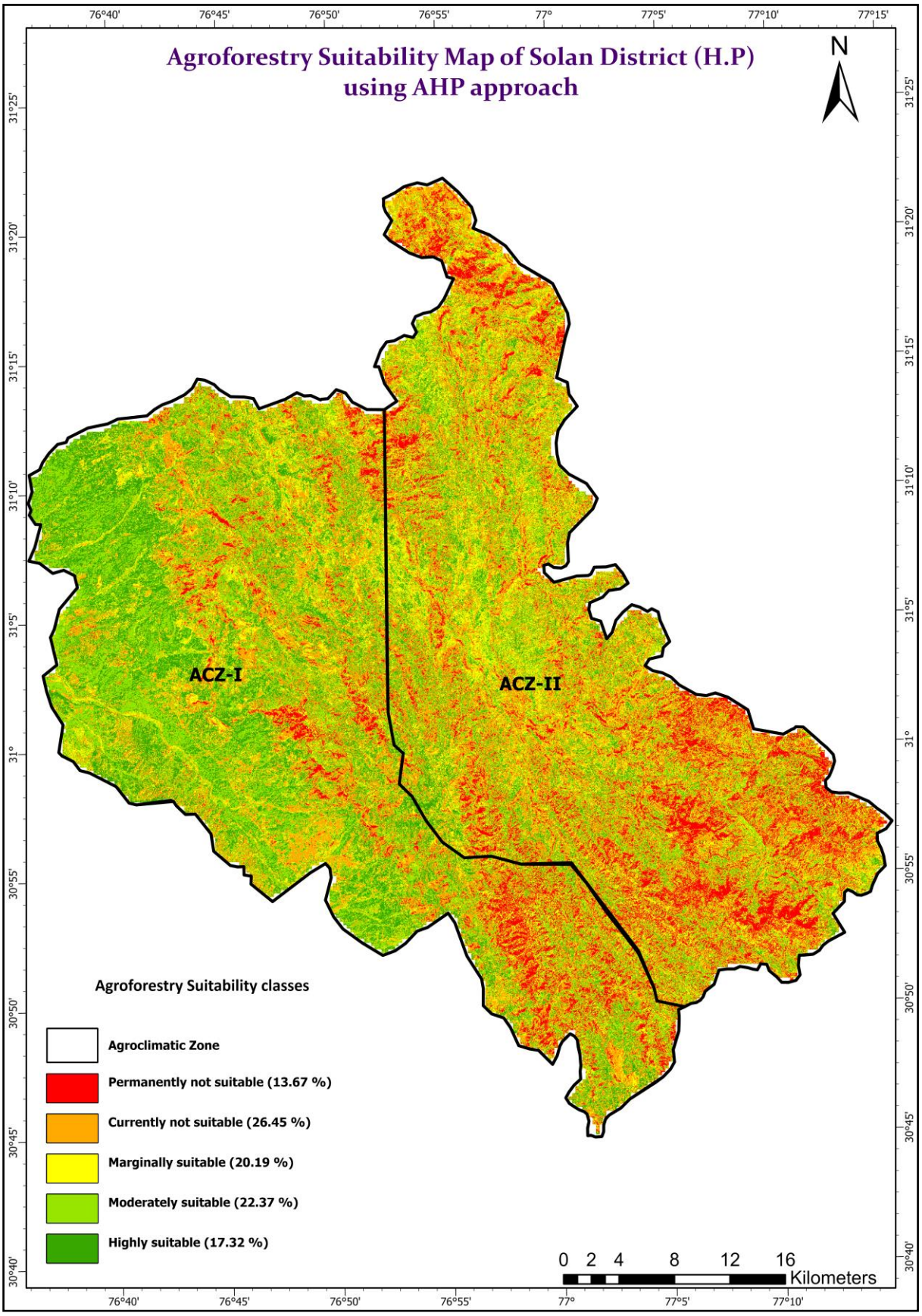

Figure 20. Agroforestry suitability map (using AHP approach) of Solan District (H.P)

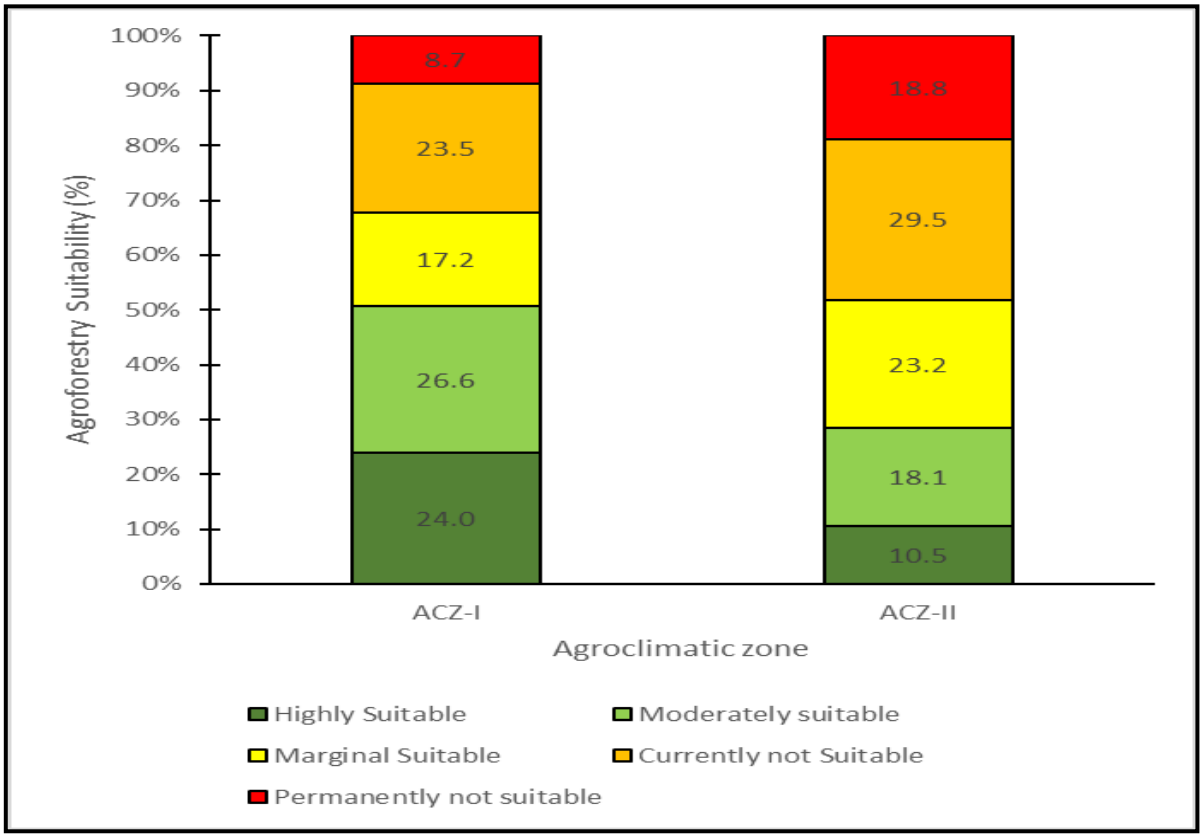

Figure 21. Distribution of agroforestry suitability classes (AHP approach) in different agroclimatic zone of Solan District (H.P.)

When focusing on agro-climatic zones (ACZ) (Table 27 and Figure 21), it was observed that ACZ-I encompasses 24% (235.33 sq. km) as highly suitable, 26.6% (260.38 sq. km) as moderately suitable, 17.2% (168.67 sq. km) as marginally suitable, 23.5% (230.28 sq. km) as currently not suitable and 8.7% (84.84 sq. km) as permanently not suitable for agroforestry. Meanwhile, in ACZ-II, 10.5% (99.99 sq. km) was categorized as highly suitable, 18.1% (172.69 sq. km) as moderately suitable, 23.2% (222.3 sq. km) as marginally suitable, 29.5% (281.76 sq. km) as currently not suitable and 18.8 % (179.76 sq. km) as permanently not suitable for agroforestry. These findings provide crucial insights into the suitability of various regions within Solan district for agroforestry practices, while also highlighting disparities between different agro-climatic zones.

The AFS suitability mapping methodology presents three key arguments. Firstly, there is a concern about potential bias due to the limited use of parameters, particularly in indigenous studies (Ahmad et al. 2018a, 2019b, 2020, 2021), where fewer than 12 parameters are often employed. Secondly, the absence of specific recommendations for AFS tree species in distinct regions is highlighted (Nath et al. 2021). Lastly, a common trend in AFS suitability

assessments is the focus on fertile lands, neglecting the potential of AFS to address the negative environmental impact of agriculture on nature and landscapes, as observed in studies of Amichev et al. (2020). It is emphasized that AFS, such as the silvipastural system, can be suitable for areas with slopes ranging from 18-50%, allowing farmers to cultivate poor soils or degraded land akin to arable land (Apan, 1996). Notably, the primary advantage of suitability mapping lies in its capacity to overlay data maps with ancillary information, facilitating the identification of potential sites where diversified and maximum benefits can be attained (Ahmad et al. 2019a). Despite the various methodologies available, the FAO methodology stands out as the most commonly employed approach in AFS suitability mapping, applied at district levels (Ahmad et al. 2018a, 2019a, Ahmad and Goparaju 2017a, 2017b), country levels (India and Nepal) (Ahmad et al. 2019b, 2021) and even across the South Asian region (Ahmad et al. 2020).

The results of present study showed that areas with high and moderate suitability were located in agricultural and agroforestry regions of southern aspects with flat surfaces and increased soil fertility. The crops grown in these areas include rice, maize, millet, wheat and pulses and can be supplemented with trees planted along the farmland boundaries. The Solan district was found to be marginally suitable due to its medium soil fertility, slopes and elevation. The study observed that areas with significantly high elevation (>1499) were not suitable for agroforestry due to extreme climate and biophysical environment, low temperatures and steep slopes. Additionally, forest areas, built-up areas and water bodies are unsuitable for agroforestry, as per the Indian Forest Act 1927, which prohibits the conversion of moderately dense and very dense forest areas into other land-use classes. Ahmad et al. (2020b) found that 51.6% of the geographical land area in South Asia is devoted to agriculture. Surprisingly, 76% of these areas exhibit high suitability (≥65%) for agroforestry, with coastal, northeast and Himalayan regions being particularly favourable. Conversely, the northwest regions, characterized by low soil fertility and arid conditions, show less than 25% agroforestry suitability. The study also provides a country-wise breakdown of agroforestry suitability in the supplementary section.

4.2.2.2. Fuzzy-AHP

Fuzzy-AHP is a method that combines traditional techniques with fuzzy logic to calculate the weights of criteria and sub-criteria. The concept of fuzzy set theory was first proposed by Zadeh (1965) and was later developed and applied by Kaufmann (1989) and

Sloan (1992). The model construction technology used a fuzzy set approach to transform all factor data to a range between 0 and 1 using a membership function. 0 represented unsuitable and 1 described 100% suitability.

4.2.2.2.1. Criterion weights (Fuzzy-AHP approach)

The following Table 28. presents the fuzzy pair comparison matrix obtained using the fuzzy triangular scale. Among the factors considered, the highest weight of 0.247 is assigned to land use and land cover, followed by the slope (0.186), elevation (0.160), rainfall (0.065), soil fertility (0.097), NDVI (0.117), aspect (0.039), hillshade (0.039), temperature (0.023), stream distance (0.014) and minimum distance from road (0.011). These weights are obtained using the Analytical Hierarchy Process (AHP) approach. Using the weights above, the agroforestry suitability equation is developed as follows:

Agroforestry suitability map = LULC × 0.247 + slope × 0. 186 + elevation × 0. 160 + rainfall × 0. 065 + soil fertility × 0. 097 + NDVI × 0. 117 + aspect × 0. 039 + temperature × 0. 023 + distance from stream × 0. 014 + distance from road × 0. 011.

4.2.2.2.2. Sub-Criterion weights (Fuzzy-AHP approach)

The study used a fuzzy pair comparison matrix based on the fuzzy triangular scale to evaluate each sub-criterion. As shown in Table 29 the highest weight of 0.586 was assigned to agroforestry, followed by agriculture with a weight of 0.264 and grassland with a weight of 0.109. The lowest weight of 0.0406 was given to barren land. Water, built-up and forest were excluded from consideration due to their unsuitability for agroforestry, following the same approach as the AHP.

In the assessment of different environmental factors, areas with the lowest slope (less than 7), lowest rainfall (between 1170-1240 mm), highest soil fertility and a southwestern aspect with a flat surface were given the highest value of 0.499. The areas with a slope of 7-16, rainfall between 1240-1300 mm, increased soil fertility and south or southeast aspect were assigned a weight of 0.262. Areas with a slope of 16-24, rainfall between 1300-1370 mm, medium soil fertility and east or west aspect were given a weight of 0.135. Furthermore, areas with a slope of 24-30, rainfall between 1370-1440 mm, low soil fertility and a north-west or north-east aspect received a weight of 0.068, while areas with a slope greater than 30, rainfall between 1440-1510 mm, very low soil fertility and a northern aspect were assigned a weight of 0.035.

Table 28. Fuzzy triangular pair comparison matrix for different data layers for multi-criteria weights

CRITERIA	LULC			SLOPE			ELEVATION			RAINFALL			SOIL FERTILITY			NDVI			ASPECT			HILLSHADE			TEMPERATURE			STREAM			ROAD			Weight
LULC	**1**	**1**	**1**	1	2	3	2	3	4	3	4	5	3	4	5	4	5	6	5	6	7	5	6	7	6	7	8	7	8	9	8	9	10	**0.247**
SLOPE	1/3	1/2	1	**1**	**1**	**1**	1	2	3	2	3	4	2	3	4	3	4	5	4	5	6	4	5	6	5	6	7	6	7	8	7	8	9	**0.186**
ELEVATION	1/4	1/3	1/2	1/3	1/2	1	**1**	**1**	**1**	2	3	4	2	3	4	3	4	5	4	5	6	4	5	6	5	6	7	6	7	8	7	8	9	**0.160**
RAINFALL	1/5	1/4	1/3	1/4	1/3	1/2	1/4	1/3	1/2	**1**	**1**	**1**	1	2	3	3	4	5	4	5	6	4	5	6	5	6	7	6	7	8	7	8	9	**0.117**
SOIL FERTILITY	1/5	1/4	1/3	1/4	1/3	1/2	1/4	1/3	1/2	1/3	1/2	1	**1**	**1**	**1**	2	3	4	3	4	5	3	4	5	4	5	6	6	7	8	7	8	9	**0.097**
NDVI	1/6	1/5	1/4	1/5	1/4	1/3	1/5	1/4	1/3	1/5	1/4	1/3	1/4	1/3	1/2	**1**	**1**	**1**	1	2	3	2	3	4	4	5	6	6	7	8	7	8	9	**0.065**
ASPECT	1/7	1/6	1/5	1/6	1/5	1/4	1/6	1/5	1/4	1/6	1/5	1/4	1/5	1/4	1/3	1/4	1/3	1/2	**1**	**1**	**1**	1	1	1	2	3	4	4	5	6	5	6	7	**0.039**
HILLSHADE	1/7	1/6	1/5	1/6	1/5	1/4	1/6	1/5	1/4	1/6	1/5	1/4	1/5	1/4	1/3	1/4	1/3	1/2	1	1	1	**1**	**1**	**1**	2	3	4	4	5	6	5	6	7	**0.039**
TEMPERATURE	1/8	1/7	1/6	1/7	1/6	1/5	1/7	1/6	1/5	1/7	1/6	1/5	1/6	1/5	1/4	1/6	1/5	1/4	1/4	1/3	1/2	1/4	1/3	1/2	**1**	**1**	**1**	2	3	4	3	4	5	**0.023**
STREAM	1/9	1/8	1/7	1/8	1/7	1/6	1/8	1/7	1/6	1/8	1/7	1/6	1/8	1/7	1/6	1/8	1/7	1/6	1/6	1/5	1/4	1/6	1/5	1/4	1/4	1/3	1/2	**1**	**1**	**1**	1	2	3	**0.014**
ROAD	1/10	1/9	1/8	1/9	1/8	1/7	1/9	1/8	1/7	1/9	1/8	1/7	1/8	1/7	1/6	1/8	1/7	1/6	1/7	1/6	1/5	1/7	1/6	1/5	1/5	1/4	1/3	1/3	1/2	1	**1**	**1**	**1**	**0.011**

Table 29. Weights of criteria and scores of the sub-criteria using Fuzzy-AHP

Main criteria	Weight	Sub-criteria	Sub-weight
LULC	**0.2472**	Agriculture	0.264
		Agroforestry	0.586
		Barren land	0.041
		Built-up area	Restricted
		Forest	Restricted
		Grassland	0.109
		Water	Restricted
Slope (degree)	**0.1863**	<7	0.500
		7.0-16.0	0.262
		16.0-24	0.135
		24-30	0.068
		>30	0.035
Elevation (m a.m.s.l)	**0.161**	<558	0.489
		558-893	0.247
		893-1178	0.148
		1178-1499	0.080
		>1499	0.036
Rainfall (mm)	**0.065**	1170-1240	0.500
		1240-1300	0.262
		1300-1370	0.135
		1370-1440	0.068
		1440-1510	0.035
Soil fertility	**0.098**	Very low	0.035
		Low	0.068
		Medium	0.135
		High	0.262
		Very high	0.500
NDVI	**0.117**	<0	0.034
		0-0.2	0.064
		0.2-0.3	0.134
		0.3-0.4	0.263
		0.4-0.5	0.504
Aspect	**0.039**	SW, flat	0.500
		S, SE	0.262
		E, W	0.135
		NW, NE	0.068
		N	0.035
Hillshade	**0.039**	<23	0.034
		23-67	0.065
		67-110	0.133
		110-151	0.263
		151-180	0.504
Temperature (°C)	**0.023**	<20	0.484
		20-21	0.267
		21-22	0.138
		22-23	0.072
		>23	0.037
Distance from stream (km)	**0.014**	<0.92	0.501
		0.92-1.84	0.262
		1.84-2.76	0.132
		2.76-3.68	0.063
		>3.68	0.043
Distance from road(km)	**0.011**	<0.22	0.501
		0.22-0.59	0.262
		0.59-1.10	0.132
		1.10-1.85	0.063
		>1.85	0.043

The topography variable (slope) was reclassified based on the fuzzy function "sigmoidal decreasing" which means a lower slope leads to the highest agroforestry suitability (Singh et al. 2022).

The altitude of a location is an essential factor, the lowest altitude, less than 558m, is given a weight of 0.489. The altitude range of 558-893m is given a weight of 0.247, while the range of 893-1178m is given a weight of 0.148. The altitude range of 1178-1499m is given a weight of 0.080 and the highest altitude range of >1499 m is given a weight of 0.036.

In terms of NDVI (Normalized Difference Vegetation Index) and hillshade, areas with the lowest score were assigned values of 0.034, given the lowest NDVI (<0) and hillshade (<23). Areas with an NDVI range of 0-0.2 and hillshade range of 23-67 were given a score of 0.065. Similarly, areas with an NDVI range of 0.2-0.3 and hillshade range of 67-110 receive a score of 0.133, while areas with an NDVI range of 0.3-0.4 and hillshade range of 110-151 were assigned a score of 0.263. The highest score was given to areas with an NDVI range of 0.4-0.5 and a hillshade range of 151-180.

For distance from roads and streams, the highest weight (0.501) was assigned to areas with distances less than 0.22 km from roads and less than 0.92 km from streams. This was followed by a weight of 0.262 for areas with distances ranging from 0.92 to 1.84 km from streams and from 0.22 to 0.59 km from roads. Additionally, areas with distances of 1.84 to 2.76 km from streams and 0.59-1.10 km from roads receive a weight of 0.132. Areas with distance 2.76-3.68 km from stream and distance 1.10-1.85 km from road receives weight 0.063. Lastly, areas with distances greater than 1.6 km from streams and greater than 2.8 km from roads were assigned the lowest weight of 0.043. Similarly, the socioeconomic variables were reclassified using the fuzzy function "Monotonically decreasing linear", which means a decreasing value leads to high importance in agroforestry suitability Singh et al. (2022). These assessments provide a comprehensive understanding of the factors influencing agroforestry suitability and their respective importance in the study's context.

4.2.2.2.3. Agroforestry Suitability Map using Fuzzy-AHP

Based on the data presented in Table 30 and Figure 22, it can be concluded that the Fuzzy-AHP approach was used to classify land in the Solan district according to its suitability for agroforestry. The study found that around 11.33 per cent of the district's total area,

equivalent to 219.34 sq. km, was highly suitable for agroforestry. Additionally, 24.76 per cent of the area, corresponding to 479.42 sq. km, was moderately appropriate, while 15.74 per cent (304.67 sq. km) was marginally suitable. A significant chunk of land, accounting for 26.30 per cent (509.14 sq. km) could have been better for agroforestry at present and 21.87 per cent (423.43 sq. km) was permanently unsuitable for such practices within the Solan district.

Table 30. Distribution of agroforestry suitability classes (FUZZY-AHP approach) in different agro-climatic zone of Solan District (H.P)

Suitability Classes	ACZ-I (sq.km)	ACZ-II (sq.km)	Total (sq.km)	Area (%)
Highly Suitable	148.18	71.16	219.34	11.33
Moderately suitable	302.63	176.79	479.42	24.76
Marginal Suitable	172.57	132.10	304.67	15.74
Currently not Suitable	200.51	308.63	509.14	26.30
Permanently not suitable	155.62	267.81	423.43	21.87
Total area	979.5	956.5	1936	100.00

The study examined the suitability and percentage of existing tree cover in various agro-climatic zones. After analysing the data (Table. 30 and Figure. 23), it was found that within ACZ-I, 148.18 sq. km (15.1%) of the land was highly suitable for agroforestry. Moderately suitable areas accounted for 302.63 sq. km (30.9%), marginally suitable areas accounted for 172.57 sq. km (17.6%), permanently not appropriate areas accounted for 200.51 sq. km (20.5%) and currently not suitable areas accounted for 155.62 sq. km (15.9%). In AGZ-II, the data showed that 71.16 sq. km (7.4%) of the land was highly suitable for agroforestry, while 176.79 sq. km (18.5%) was moderately suitable. The majority of the area, accounting for 304.67 sq. km (13.8%), was marginally suitable, with 509.14 sq. km (32.3%) considered currently not suitable and only 423.43 sq. km (28%) classified as permanently not suitable for agroforestry practices.

The Indian Forest Act of 1927 permanently deems the forest area unsuitable for any other land-use class. The study conducted by Singh et al. (2022) used the Fuzzy Analytic Hierarchy Process (Fuzzy-AHP) methodology to evaluate agroforestry suitability in the Bolangir district, Odisha state. The study considered various parameters such as soil depth, pH, texture, drainage, slope, temperature, rainfall and socioeconomic factors.

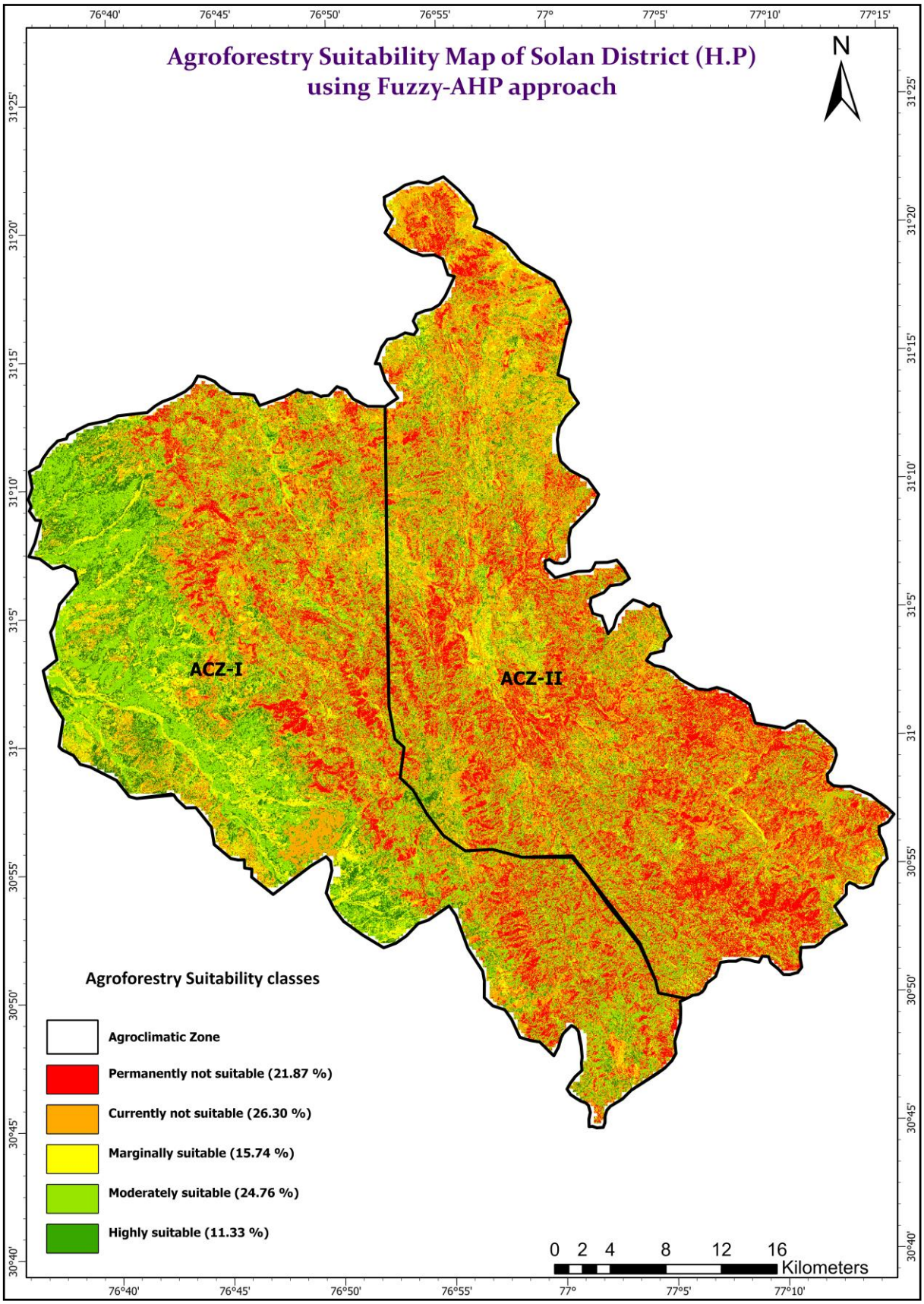

Figure 22. Agroforestry suitability map (using Fuzzy-AHP approach) of Solan District (H.P)

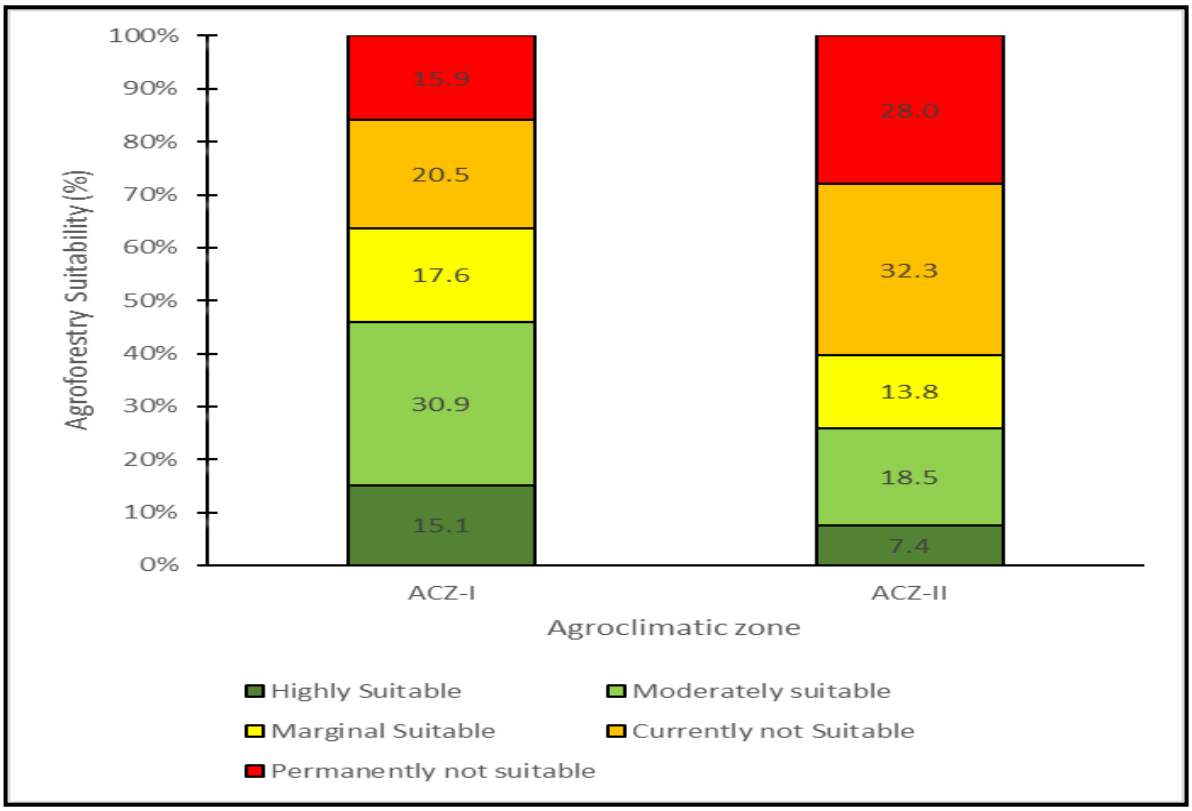

Figure 23. Distribution of agroforestry suitability classes (FUZZY-AHP approach) in different agroclimatic zone of Solan District (H.P)

Based on their findings, more than 90% (6602 ha) of the total area is highly suitable for double-cropping land. The predominant agricultural practice in the study site was single-crop paddy and a significant portion of the area was considered suitable for this cultivation. Additionally, the study identified a total area of 20,702.76 ha designated for bund and boundary plantation with conditional intercropping. Almost 92% of this area fell within the very high suitability category, indicating the immense potential for agroforestry practices as a viable and beneficial land-use strategy in the region. The results indicated high accuracy (average suitability >0.87 as indicated by the validation data) and highlighted the dominant influence of the socioeconomic variables compared to soil and climate variables. The results show that >90% of the agricultural land in the study area is suitable for various agroforestry interventions, such as bund plantation and intercropping, based on the cropping intensity. The Fuzzy-AHP method was also utilized by Zhang et al. (2021) and Ozkan et al. (2020) in their respective research for suitability.

4.2.2.2.4. Validation

Conducted a validation process to check the accuracy of the suitability map created using the AHP and Fuzzy-AHP methodologies. For this purpose, six different hotspot areas

within the Solan district, each representing varying suitability levels, namely high, moderate, marginal, currently not suitable and permanently not suitable were selected. To validate the map, we visually compared the selected areas with high-resolution Google Earth images.

Figure 24. Validation of the agroforestry suitability analysis (both AHP and Fuzzy AHP) using high-resolution Google Earth images

The visual validation results, as depicted in the provided Figure 24, clearly demonstrate a strong alignment between the characteristics observed in the Google Earth images and the outcomes derived from the AHP suitability and Fuzzy-AHP models, as well as the GIS-based modelling approach. The combined area under agroforestry and agriculture land, constituting 34-35% of Solan district, is categorized as highly and moderately suitable, with a combined percentage of 36.09% observed in the Fuzzy-AHP approach whereas, 39.69 % recorded using AHP approach. Notably, the Fuzzy-AHP approach identified the maximum forest area as permanently not suitable and the maximum built-up area as currently not suitable. This congruence reinforces the accuracy and reliability of our suitability mapping methods, with the Fuzzy-AHP approach standing out as the best method. The study conducted by Zhang et al. (2015) demonstrates that Fuzzy set provides an excellent mechanism to transform numerical data with various magnitudes into grades of membership functions in the range of 0–1 where 1 represents 100% suitable land. AHP is an effective and superior method to determine the weights of multiple factors in a systematic and logical way and its consistency may be measured and controlled in the presence of conflicting criteria

4.3 BIOMASS CARBON STOCK AND CARBON SEQUESTRATION POTENTIAL OF AGROFORESTRY SYSTEMS

4.3.1. Land use land cover mapping

4.3.1.1. Area assessment

The area assessment of land-use and land cover of year 2003, 2013 and 2023 was carried out using Landsat-07 ETM and Landsat-8 OLI/TIRS satellite data respectively and band combination *i.e.*, blue, green, red and NIR by applying random tree classifier in ArcGIS 10.8.2.

4.3.1.1.1. Area assessment of year 2003

In 2003, the study area had diverse land use patterns, illustrated in Table 31. and Figure 25. Agriculture covered 194.37 sq.km, which accounted for 10.04% of the total area, indicating a significant portion of land dedicated to farming activities. Agroforestry, occupying 414.47 sq.km (21.41%) of the land, highlighted a substantial commitment to sustainable land management practices. Barren land, which spanned 201.54 sq.km (10.41%), represented areas with limited or no vegetation cover. Built-up areas accounted for 80.15 sq.km (4.14%), indicating urban or developed regions. The study area also featured extensive

open forests covering 459.03 sq.km (23.71%), moderate forests covering 293.52 sq.km (15.16%) and dense forests covering 47.21 sq.km (2.44%). This underscores the richness of the study area's forested landscape. According to the ISFR state forest report (2003), the open forests were 466 sq.km, moderate forest were 314 sq.km and dense forests were 39 sq. km in 2003. Additionally, grasslands covered 216.67 sq.km (11.19%), reflecting open areas with grass vegetation. Water bodies comprised 29.04 sq.km (1.50%) and comprised lakes, rivers and other aquatic features.

Table 31. Area (sq. km) and Area (%) under major land-use and land cover classes of Solan District (H.P) in 2003

Classes	Area (sq.km)	Area (%)
Agriculture	194.37	10.04
Agroforestry	414.47	21.41
Barren land	201.54	10.41
Built-up	80.15	4.14
Open forest	459.03	23.71
Moderate forest	293.52	15.16
Dense forest	47.21	2.44
Grassland	216.67	11.19
Waterbody	29.04	1.50
Total area	1936	100

4.3.1.1.2. Area assessment of year 2013

In 2013, the land use distribution within the study area, as illustrated in Table 32. and Figure 25, exhibited a diverse landscape. Agricultural land occupied 185.12 sq. km, constituting 9.56% of the total area, highlighting a continued presence of farmlands. Agroforestry was prevalent, covering 462.32 sq. km (23.88%) of the region, emphasizing a substantial commitment to sustainable land management practices. Barren land, accounting for 128.16 sq. km (6.62%), represented areas with minimal or no vegetative cover. Built-up areas, encompassing 106.44 sq.km (5.50%), signified urban or developed zones. Open forests extended over 404.43 sq.km (20.89%), while moderate forests covered 380.04 sq.km (19.63%) and dense forests were observed on 55.95 sq.km (2.89%) of the land, underscoring the rich forested diversity. The ISFR state forest report (2013) reported 55 sq.km under dense forest, 404 sq.km under moderate forest and 391 sq.km under open forest. Furthermore, grassland spanned 186.63 sq.km (9.64%), denoting open areas with grassy vegetation, while water bodies, spanning 26.92 sq.km (1.39%), represented aquatic features such as lakes and rivers.

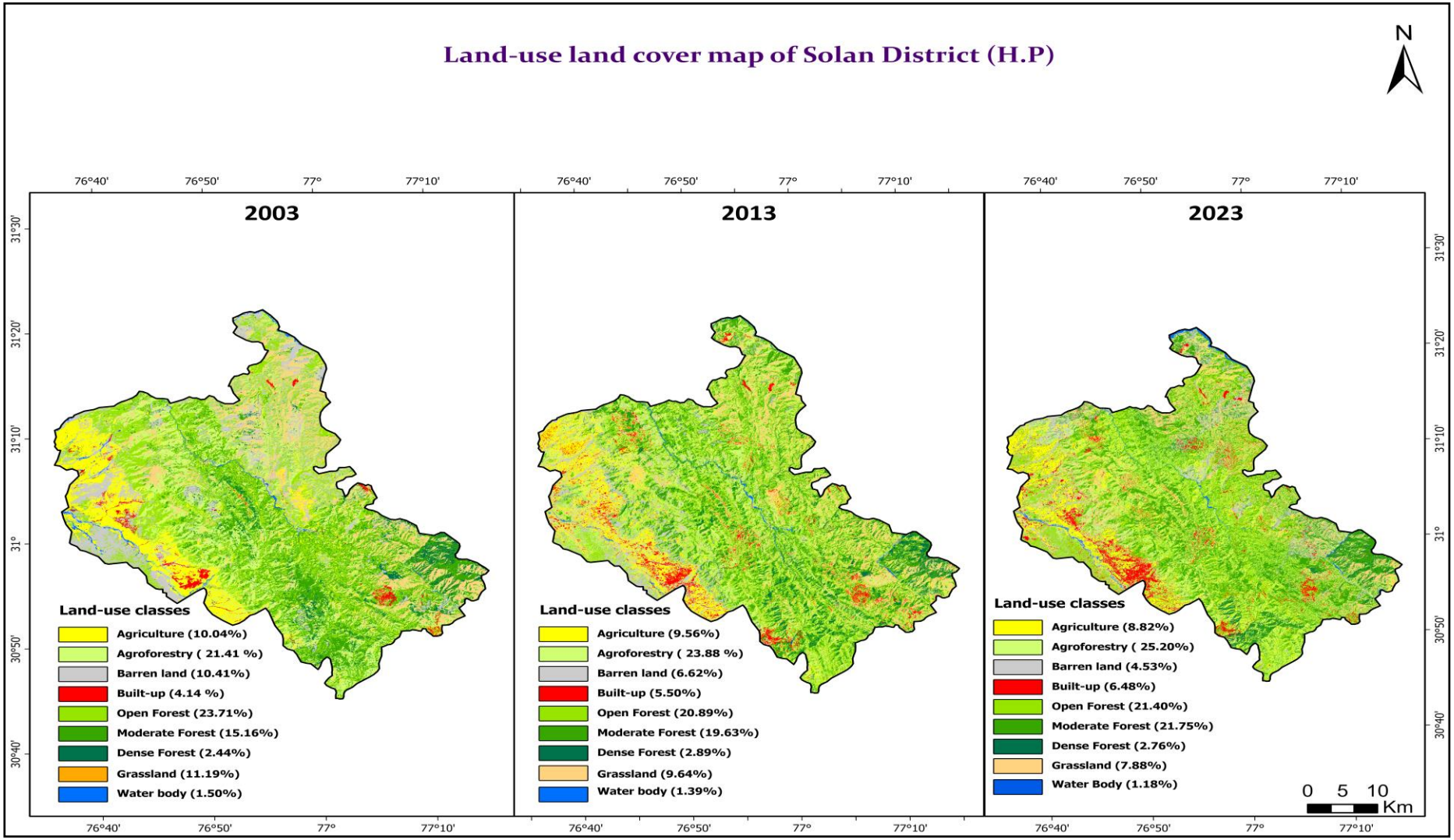

Figure 25. Land use and land cover map of Solan District (H.P) at different period of time 2003,2013 and 2023

Table 32. Area (sq. km) and Area (%) under major land-use and land cover classes of Solan District (H.P) in 2013

Classes	Area (sq.km)	Area (%)
Agriculture	185.12	9.56
Agroforestry	462.32	23.88
Barre land	128.16	6.62
Built-up	106.44	5.50
Open forest	404.43	20.89
Moderate forest	380.04	19.63
Dense forest	55.95	2.89
Grassland	186.63	9.64
Waterbody	26.92	1.39
Total area	1936.00	100.00

4.3.1.1.3. Area assessment of year 2023

In 2023, an examination of the data in Table 33. and Figure 25. reveals a varied land use distribution within the study area. Agricultural land covered 170.77 sq. km, accounting for 8.82% of the total area, underscoring the presence of farming activities. Agroforestry was prominently established, occupying 487.93 sq. km (25.20%) of the landscape, emphasizing a substantial commitment to sustainable land management practices. Barren land comprising 87.70 sq. km (4.53%), denoted areas with limited vegetative cover or non-vegetated conditions. Built-up areas encompassed 125.45 sq. km (6.48%) representing urban or developed regions. The region also featured expansive open forests, spanning 414.30 sq. km (21.40%). In comparison, moderate forests covered 421.08 sq. km (21.75%) and dense forests were identified on 53.43 sq. km (2.76%) of the land, showcasing a diverse forested landscape. The ISFR state forest report (2021) reported 43.78 sq. km under dense forest, 443.56 sq. km under moderate forest and 403.52 sq. km under open forest. Additionally, grassland extended over 152.50 sq. km (7.88%) reflecting open areas with grassy vegetation and water bodies, covering 22.84 sq. km (1.18%) constituted features like lakes and rivers.

Table 33. Area (sq. km) and Area (%) under major land-use and land cover classes of Solan District (H.P) in 2023

Classes	Area (sq.km)	Area (%)
Agriculture	170.77	8.82
Agroforestry	487.93	25.20
Barren land	87.70	4.53
Built-up	125.45	6.48
Open forest	414.30	21.40
Moderate forest	421.08	21.75
Dense forest	53.43	2.76
Grassland	152.50	7.88
Waterbody	22.84	1.18
Total area	1936	100.00

4.3.1.1.4. Accuracy assessment

4.3.1.1.4.1 Accuracy assessment of year 2003

The accuracy assessment for land use and land cover (LULC) in 2003 utilized a Random Forest classifier. As shown in Table 34, the overall accuracy achieved was 76.75%, with a Kappa Coefficient of 0.7314. The dense forest class showed the highest user accuracy at 83.96%, as 5 pixels were found as moderate forest in actual. On the other hand, the producer accuracy peaked at 83.96%, as 6 pixels were misclassified as agroforestry class.

The agriculture class recorded the second-highest user accuracy at 80.41%, but the most significant misclassification of pixels (9) needed to be correctly identified as grassland. The highest producer accuracy, reaching 87.64%, was associated with agroforestry, with the pixels (3) misclassified as grassland. For the moderate forest class, a user accuracy of 80% was recorded, misclassifying the maximum number of pixels (6) as open forest. The producer accuracy was 70.33%, with the highest pixel count 8 misclassified as agroforestry and open forest classes. In the built-up class, a user accuracy of 78.26% was achieved, with the maximum misclassification (4) identified as barren land. The producer accuracy, also at 78.26%, as pixels (4) were misclassified as barren land class. Open forest exhibited a user accuracy of 76.99%, as the maximum number of pixels (12) were found as agroforestry in actual. The producer accuracy reached 69.05%, as 21 pixels were misclassified as agroforestry class.

A user accuracy of 75.68% was observed for the grassland class, with the maximum misclassified pixels (5) identified as moderate forest in actual. The producer accuracy reached 76.71%, with the maximum pixels (9) misclassified as grassland. In the agroforestry class, a user accuracy of 73.26% was recorded as the maximum number of pixels (8) were observed as moderate forest in actual. The producer accuracy, at 83.03%, was linked to the maximum pixel count (12) misclassified as open forest. Barren land exhibited a user accuracy of 71.23%, with the maximum misclassified pixel (6) identified as a water body in real. The producer accuracy, at 68.42%, was associated with the maximum pixel (7) found in the agroforestry class. Finally, the water body achieved a user accuracy of 62.50%, with the maximum misclassified pixels (3) each identified as built-up and dense forest in real. The producer accuracy, at 53.57%, was linked to the maximum pixel count (6) misclassified barren land.

4.3.1.1.4.2 Accuracy assessment of year 2013

The accuracy assessment for land use and land cover (LULC) 2013 was conducted using a Random Forest classifier and the results are presented in Table 35. The overall accuracy was 77.75%, with a Kappa Coefficient of 0.7446. The dense forest class had the highest user accuracy of 87.38%, with a maximum of 6 pixels were found as a moderate forest. On the other hand, the producer accuracy peaked at 85.71%, with the maximum pixels (3) each misclassified as agroforestry, built-up, open forest and water body class. The built-up class had the second-highest user accuracy, 81.82%, but had the most significant misclassified pixels (3), erroneously identified as barren land, dense forest and water body class. In contrast, the highest producer accuracy of 88.52% was observed in the barren land class, with the maximum pixels (4) found in that class.

The agriculture class had a user accuracy of 80.72%, but it misclassified the maximum number of pixels (7) and were found as grassland class in actual. The producer accuracy was 81.71%, with the highest misclassified pixel count (4) as the moderate forest and grassland classes. The grassland class had a user accuracy of 80.36%, with the maximum misclassified pixels (4) identified as agriculture class in actual. The producer accuracy reached 71.43%, with the maximum pixels (7) misclassified as the agriculture class. Open forest exhibited a user accuracy of 76.19%, but maximum number of pixels (10) were found agroforestry. The producer accuracy reached 68.38%, with the highest pixel count (17) misclassified as agroforestry class.

Table 34. Confusion matrix of accuracy assessment of major land-use and land cover classes of 2003 using Random Forest classification in Solan District of (H.P)

Class Value	Agriculture	Agroforestry	Barren land	Built up	Open Forest	Moderate Forest	Dense Forest	Grassland	Water body	Reference points	Commission error	User Accuracy (%)
Agriculture	**78**	3	4	1	2	0	0	9	0	97	0.20	**80.41**
Agroforestry	3	**137**	7	1	21	8	6	3	1	187	0.27	**73.26**
Barren land	2	2	**52**	4	4	1	0	2	6	73	0.29	**71.23**
Built up	1	1	4	**36**	0	0	1	0	3	46	0.22	**78.26**
Open forest	1	12	3	0	**87**	8	2	0	0	113	0.23	**76.99**
Moderate forest	1	4	1	0	6	**64**	3	1	0	80	0.20	**80.00**
Dense forest	0	3	1	1	4	5	**89**	1	2	106	0.16	**83.96**
Grassland	3	3	2	0	2	5	2	**56**	1	74	0.24	**75.68**
Water body	0	0	2	3	0	0	3	1	**15**	24	0.38	**62.50**
Classified point	89	165	76	46	126	91	106	73	28	**800**		
Omission error	0.12	0.17	0.32	0.22	0.31	0.30	0.16	0.23	0.46			
Producer Accuracy (%)	**87.64**	**83.03**	**68.42**	**78.26**	**69.05**	**70.33**	**83.96**	**76.71**	**53.57**			
Overall Accuracy (%)	**76.75**											
Kappa Coefficient	**0.7314**											

Table 35. Confusion matrix of accuracy assessment of major land-use classes of 2013 using Random Forest classification in Solan District of (H.P)

Class Value	Agriculture	Agroforestry	Barren land	Built up	Open Forest	Moderate Forest	Dense Forest	Grassland	Water body	Reference points	Commission error	User Accuracy (%)
Agriculture	**67**	2	4	1	2	0	0	7	0	83	0.19	**80.72**
Agroforestry	2	**130**	5	0	17	9	3	5	1	172	0.24	**75.58**
Barren land	2	3	**65**	4	5	2	0	3	6	90	0.28	**72.22**
Built up	2	1	3	**54**	0	0	3	0	3	66	0.18	**81.82**
Open forest	1	10	5	0	**80**	6	3	0	0	105	0.24	**76.19**
Moderate forest	4	7	2	0	8	**72**	2	2	0	97	0.26	**74.23**
Dense forest	0	1	0	1	3	6	**90**	0	2	103	0.13	**87.38**
Grassland	4	1	1	0	2	1	1	**45**	1	56	0.20	**80.36**
Water body	0	0	4	1	0	0	3	1	**19**	28	0.32	**67.86**
Classified point	82	155	89	61	117	96	105	63	32	**800**		**80.72**
Omission error	0.18	0.16	0.27	0.11	0.32	0.25	0.14	0.29	0.41			
Producer Accuracy (%)	**81.71**	**83.87**	**73.03**	**88.52**	**68.38**	**75.00**	**85.71**	**71.43**	**59.38**			
Overall Accuracy (%)	**77.75**											
Kappa Coefficient	**0.7446**											

Table 36. Confusion matrix of accuracy assessment of major land-use classes of 2023 using Random Forest classification in Solan District of (H.P)

Class Value	Agriculture	Agroforestry	Barren land	Built up	Open Forest	Moderate Forest	Dense Forest	Grassland	Water body	Reference points	Commission error	User Accuracy (%)
Agriculture	**83**	2	2	1	3	1	0	4	0	96	0.14	**86.46**
Agroforestry	3	**129**	7	0	18	6	7	1	1	172	0.25	**75.00**
Barren land	1	4	**69**	2	5	2	1	2	4	90	0.23	**76.67**
Built up	0	0	6	**47**	0	0	2	1	5	61	0.23	**77.05**
Open forest	4	14	4	0	**78**	5	1	0	0	106	0.26	**73.58**
Moderate forest	2	5	2	0	5	**68**	2	0	0	84	0.19	**80.95**
Dense forest	0	1	3	1	4	4	**86**	0	2	101	0.15	**85.15**
Grassland	1	2	4	0	4	1	1	**49**	1	63	0.22	**77.78**
Water body	0	0	2	4	0	0	3	1	**17**	27	0.37	**62.96**
Classified point	94	157	99	55	117	87	103	58	30	**800**		
Omission error	0.12	0.18	0.30	0.15	0.33	0.22	0.17	0.16	0.43			
Producer Accuracy (%)	**88.30**	**82.17**	**69.70**	**85.45**	**66.67**	**78.16**	**83.50**	**84.48**	**56.67**			
Overall Accuracy (%)	**78.25**											
Kappa Coefficient	**0.7501**											

In the agroforestry class, a user accuracy of 75.58% was recorded, as maximum number of pixels (17) were found as open forest. The producer accuracy, at 83.87%, was linked to the maximum pixel count (10) misclassified as open forest. For the moderate forest, the maximum 8 pixels found as open forest, while the highest producer accuracy of 75% was for the maximum pixels (9) misclassified as agroforestry class. Barren land had a user accuracy of 72.22%, with the maximum pixel (6) identified as a water body. The producer accuracy, at 68.42%, was associated with the maximum pixel (7) found in agroforestry class. Finally, the water body achieved a user accuracy of 67.86%, but it misclassified the maximum pixel (4) identified as barren land in actual. The producer accuracy, at 59.38%, was linked to the maximum pixel count (6) misclassified as barren land.

4.3.1.1.4.3 Accuracy assessment of year 2023

According to Table 36, the accuracy assessment for land use and land cover (LULC) in 2023 utilized a Random Forest classifier. The overall accuracy achieved was 78.25%, with a Kappa Coefficient of 0.7501. The agriculture class had the highest user accuracy at 86.46%, but 4 pixels found as grassland. On the other hand, the producer accuracy peaked at 88.30%, as pixels (4) were misclassified as open forest. The dense forest class had the second-highest user accuracy at 85.15%, but the most significant misclassified pixels (4) were each identified as open forest and moderate forest class. Conversely, the producer accuracy reached 83.50%, with the pixels (7) misclassified as the agroforestry class. For the moderate forest, 80.95% user accuracy and identified each 5 pixels as agroforestry and open forest and 78.16% producer accuracy, as 6 pixels were misclassified as the agroforestry class. A user accuracy of 77.78% was observed for the grassland class, with the misclassified pixels (4) each identified as barren land and open forest class. The producer accuracy reached 84.48%, as 4 pixels were misclassified as the agriculture class.

For the built-up class, a user accuracy of 77.05% was seen, with the misclassified (6) pixels found as barren land and 85.45% producer accuracy was the pixel (4) misclassified as water body class. Barren land exhibited a user accuracy of 76.67%, with the misclassified pixels (5) identified as open forest. The producer accuracy, at 69.70%, was associated with the pixels (7) misclassified as agroforestry class. In the agroforestry class, a user accuracy of 75% was recorded, with the number of pixels (18) actually identified as open forest.

Table 37. Land use and land cover change statistics from 2003,2013 and 2023 of Solan District (H.P)

Land use classes	Land use and land cover statistics of 2003,2013 and 2023.						Change (2003-2013)		Change (2013-2023)		Total Change (2003-2023)	
	2003		2013		2023							
	Area (sq.km)	Area (%)	Area (sq.km)	Area (%)	Area (sq.km)	Area (%)	Area (sq.km)	Area (%)	Area (sq.km)	Area (%)	Area (sq.km)	Area (%)
Agriculture	194.37	10.04	185.12	9.56	170.77	8.82	-9.3	-0.48	-14.4	-0.74	-23.6	-1.22
Agroforestry	414.47	21.41	462.32	23.88	487.93	25.20	47.8	2.47	25.6	1.32	73.5	3.79
Barren land	201.54	10.41	128.16	6.62	87.7	4.53	-73.4	-3.79	-40.5	-2.09	-113.8	-5.88
Built up	80.15	4.14	106.44	5.50	125.45	6.48	26.3	1.36	19.0	0.98	45.3	2.34
Open Forest	459.03	23.71	404.43	20.89	414.3	21.40	-54.6	-2.82	9.9	0.51	-44.7	-2.31
Moderate forest	293.52	15.16	380.04	19.63	421.08	21.75	86.5	4.47	41.0	2.12	127.6	6.59
Dense forest	47.21	2.44	55.95	2.89	53.43	2.76	8.7	0.45	-2.5	-0.13	6.2	0.32
Grassland	216.67	11.19	186.63	9.64	152.5	7.88	-30.0	-1.55	-34.1	-1.76	-64.2	-3.31
Water body	29.04	1.50	26.92	1.39	22.84	1.18	-2.1	-0.11	-4.1	-0.21	-6.2	-0.32
Total Area (sq.km)	1936	100	1936	100	1936	100						

The producer accuracy, 82.17% was linked to the pixel count (14) misclassified as open forest. Open forest exhibited a user accuracy of 73.58%, misclassifying the number of pixels (14) were observed as agroforestry in actual. The producer accuracy reached 66.67%, as highest pixel count (18) was misclassified as agroforestry class. Finally, the water body achieved a user accuracy of 62.96%, with the misclassified pixel (4) identified as built-up. The producer accuracy, at 56.67% was linked to the pixel count (5) misclassified as built-up class.

4.3.2. Land use land cover change detection

4.3.2.1. Land use land cover change statistics from 2003-2023

Table 37. shows significant changes in land use dynamics in the study area from 2003 to 2023. The agricultural landscape saw a decrease of 9.3 sq. km (0.48%) from 2003 to 2013, going from 194.37 sq. km (10.04%) to 185.12 sq. km (9.56%). This was followed by a further decline of 14.4 sq. km (0.74%) from 2013 to 2023, resulting in a total area of 170.77 sq. km (8.82%) in 2023. Overall, there was a decrease of 23.6 sq. km (1.22%) in the agricultural landscape from 2003 to 2023. Barren land also experienced a significant decrease of 73.4 sq. km (3.79%) from 2003 to 2013, from 201.54 sq. km (10.41%) to 128.16 sq. km (6.62%). Later, there was a decline of 40.5 sq. km (2.09%) from 2013 to 2023, resulting in a total area of 87.70 sq. km (4.53%) in 2023. Overall, declined of 113.8 sq. km (5.88%) from 2003 to 2023 in barren land.

From 2003 to 2013, the grassland area experienced a transformation, decreasing from 216.67 sq. km (11.19%) to 186.63 sq. km (9.64%), reflecting a decline of 30 sq. km (1.55%). The overall decline in the grassland area from 2003 to 2023 amounted to 64.2 sq. km (3.31%), therefore observed 152.50 sq.km (7.88%) area in 2023. In contrast, agroforestry and the built-up regions experienced expansion during this period. Agroforestry, comprising 414.47 sq. km (21.41%) of the landscape in 2003, witnessed growth to 487.93 sq. km (25.20%) in 2023, reflecting an increase of 73.2 sq. km (3.79%). Extensive tree plantations on non-forest lands were raised by the State Forest Departments under social forestry schemes. Along with this many people particularly farmers took up agro forestry and farm forestry on their lands in several regions of the country for higher economic returns from their agricultural lands (FSI Technical Information Series 2020). Built-up areas experienced growth from 80.15 sq. km (4.14%) in 2003 to 125.45 sq. km (6.48%) in 2023, indicating an increase of 45.3 sq. km (2.34%). Finally, the area covered by water bodies decreased from 29.04 sq. km (1.50%) to 26.92 sq. km (1.39%) from 2003 to 2013, followed by a decline of

4.1 sq. km (0.21%) from 2013 to 2023, resulting in a total of 22.84 sq. km (1.18%) in 2023. The overall change in the water body area from 2003 to 2023 decreased by 6.2 sq. km (0.32%).

Over the years, the dynamics of forested areas have undergone notable shifts. The open forest area reduced from 459.03 sq. km (23.71%) in 2003 to 404.43 sq. km (20.89%) in 2013, resulting in a 54.6 sq. km (2.82%) decrease in forest cover. However, in the following decade (2013 to 2023), there was a modest increase of 9.9 sq. km (0.51%) in open forest area, rising from 404.43 sq. km (20.89%) to 414.30 sq. km (21.40%). Overall, from 2003 to 2023, there was a net decline of 44.7 sq. km (2.31%) in open forest area. Moderate forest area, on the other hand, exhibited a substantial increase, expanding from 293.52 sq. km (15.16%) in 2003 to 380.04 sq. km (19.63%) in 2013, reflecting a significant increment of 86.5 sq. km (4.47%). This positive trend continued into 2023, with moderate forest area reaching 421.08 sq. km (21.75%), accounting for a further increase of 41 sq. km (2.12%). Overall, the increment from 2003 to 2023 in moderate forest areas was 127.6 sq. km (6.59%). There was an increase in dense forest area, from 47.21 sq. km (2.44%) in 2003 to 55.95 sq. km (2.89%) in 2013, accounting for 8.7 sq. km (0.45%) increase in the forested region. Then decline was recorded in 2023, with dense forest area from 55.95 sq. km (2.89) to 53.43 sq. km (2.76%). The overall increment in dense forest area from 2003 to 2023 was observed as 6.2 sq. km (0.32%).

The ISFR reports of 2003, 2013 and 2021 also noted the decline in open forest from 2003 to 2013 and an increase in area from 2013 to 2023, in moderate forest an increment from 2003 to 2023 and in dense forest initially an increment in area was noted from 2003 to 2013 and decline from 2013 to 2023. This alignment between the data presented and the findings in the ISFR reports underscores the reliability and continuity of these trends over the specified timeframe. Shifts in land use and land cover dynamics have been observed from 2003 to 2023, indicating changes in different land cover categories. Study conducted by Kumar et al. (2021) thoroughly analysed Land Use and Land Cover (LULC) in the Parasai-Sindh watershed in Jhansi, covering the years 2008, 2011 and 2016. The study highlighted an increase in the proportion of land designated for agroforestry, which rose from 3.63% in 2008 to 5.08% in 2016. This shift signifies an evolving trend in land use practices. Specifically, the area designated for agroforestry/plantation expanded from 45.27 ha in 2008 to 63.29 ha in 2016. The analysis also revealed an increase in the area dedicated to crop cultivation, escalating from 797.76 ha in 2008 to 946.87 ha in 2016. Additionally, there was a marginal

increase in the built-up area, rising from 1.83% in 2008 to 2.38% in 2016. The LULC analysis underscores the dynamic shifts in land use practices over the examined period, highlighting the increased emphasis on agroforestry, crop cultivation and built-up areas in the Parasai-Sindh watershed. Studies conducted by Kafy et al. (2021), Abebe et al. (2022), (Houssoukpèvi et al. (2023), Islam et al. (2022), Xu et al. (2023) and Zheng and Zheng (2023) have contributed to our understanding of the evolving landscape and provided valuable insights into the changes in land cover over time. These findings are significant for informing environmental management strategies and sustainable development practices.

4.3.2.2. Land use land cover change matrix

Table 38 shows the changes in land use from 2003 to 2023, as represented by the chord diagram (Figure 26). The chart visually illustrates the dynamic shifts in land use over the years. Initially, the agriculture area covered 194.37 sq. km (10.04%). Over the years, 81.91 sq. km remained in agriculture, while 47.63 sq. km transitioned from agroforestry, 2.29 sq. km from barren land, 11.52 sq. km from built-up areas, 8.82 sq. km from open forest, 2.01 sq. km from moderate forest, 3 sq. km from dense forest, 12.75 sq. km from grassland and0.84 sq. km from water bodies. As of 2023, 170.77 sq. km (8.82%) remains designated as agricultural land.

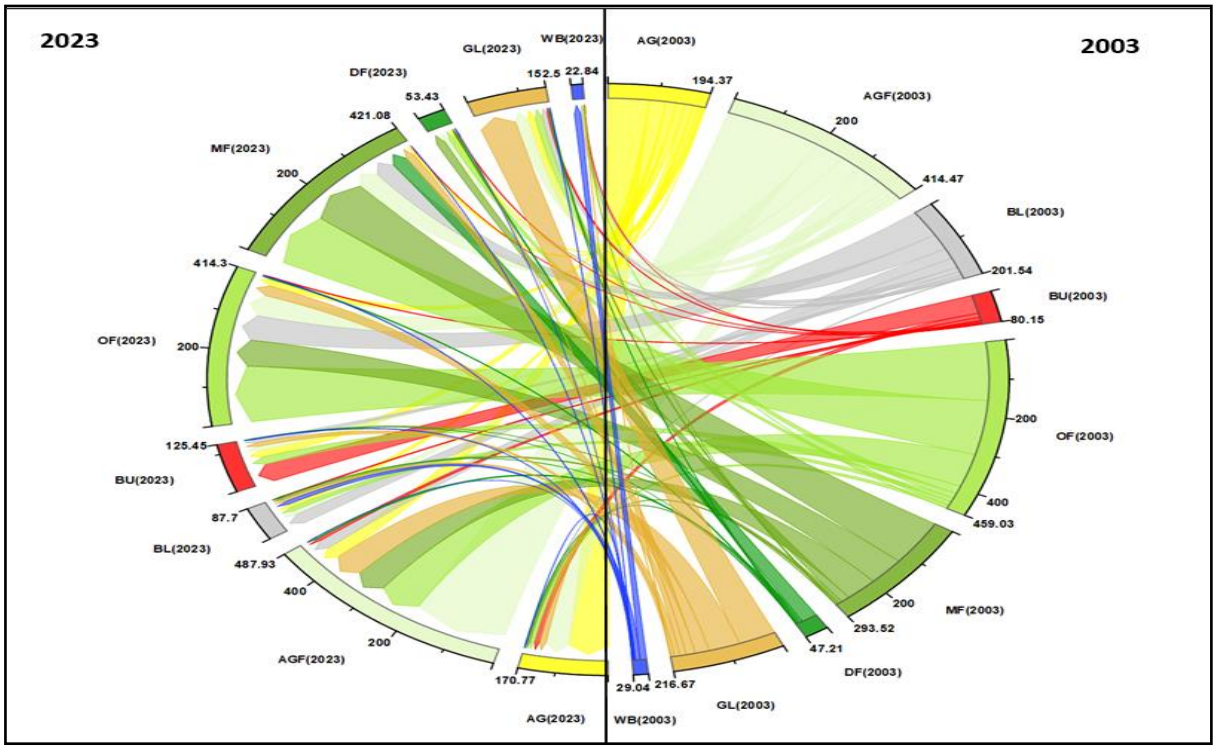

Figure.26 Chord diagram showing the conversion of land area in terms of land use over the period of 2003 to 2023

Table 38. Land use and land cover change matrix for the period of 2003-2023 in Solan District (H.P)

LULC Class		2003										
		Agriculture	**Agroforestry**	**Barren land**	**Built up**	**Open Forest**	**Moderate Forest**	**Dense Forest**	**Grassland**	**Water body**	**Area (sq.km)**	**Area (%)**
2023	**Agriculture**	81.91	47.63	2.29	11.52	8.82	4.01	1	12.75	0.84	170.77	**8.82**
	Agroforestry	32.98	197.73	26.26	8.03	89.45	65.01	5.07	63.3	0.1	487.93	**25.20**
	Barren land	10.69	11.74	28.72	3.15	10.72	6.12	0.11	6.86	9.59	87.70	**4.53**
	Built up	20.05	11.72	9.85	49.47	20.93	1.04	0.02	10.65	1.72	125.45	**6.48**
	Open Forest	18.18	59.25	70.58	1.98	157.78	73.34	2.89	28.31	1.99	414.30	**21.40**
	Moderate Forest	7.27	48.67	42.68	1.05	146.48	122.88	33.12	18.09	0.84	421.08	**21.75**
	Dense Forest	5.79	11.47	2.46	1.2	9.63	18	4	0.84	0.04	53.43	**2.76**
	Grassland	16.76	26.19	12.31	3.12	14.12	3.1	1	74.89	1.01	152.50	**7.88**
	Water body	0.74	0.07	6.39	0.63	1.1	0.02	0	0.98	12.91	22.84	**1.18**
	Area (sq.km)	194.37	414.47	201.54	80.15	459.03	293.52	47.21	216.67	29.04	1936.00	**100.00**
	Area (%)	**10.04**	**21.41**	**10.41**	**4.14**	**23.71**	**15.16**	**2.44**	**11.19**	**1.50**	**100.00**	

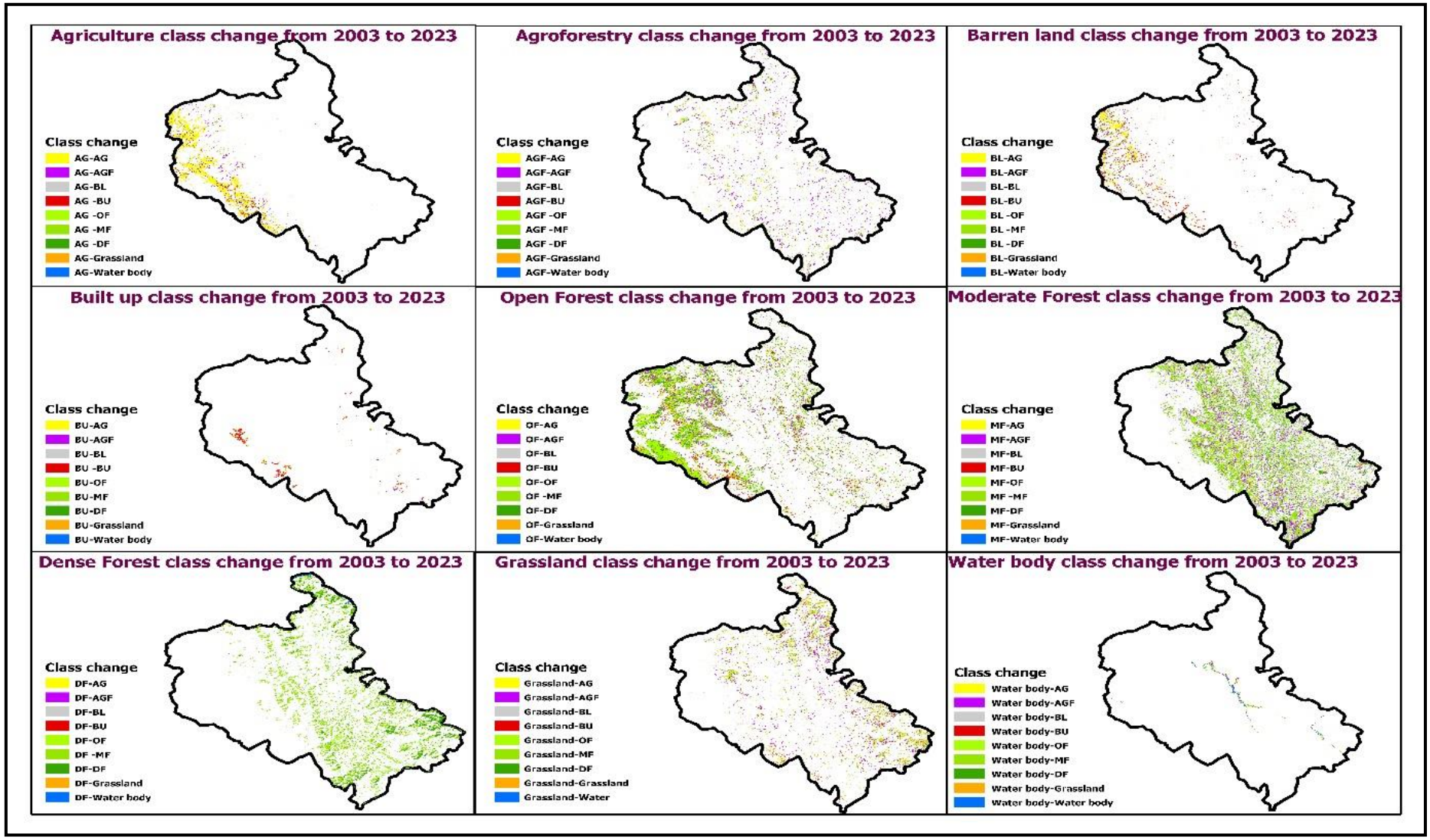

Figure 27. Land use and land cover change map for the period of 2003-2023 in Solan District (H.P)

In 2003, agroforestry spanned 414.47 sq. km (21.41%). Through conversions, including 32.98 sq. km from agriculture, 197.73 sq. km from agroforestry, 26.26 sq. km from barren land, 8.03 sq. km from built-up areas, 89.45 sq. km from open forest, 65.01 sq. km from the moderate forest, 5.07 sq. km from dense forest, 63.3 sq. km from grassland and 0.1 sq. km from water bodies, agroforestry totalled 487.93 sq. km (25.20%) in 2023. Barren land, initially 201.54 sq. km (10.41%) in 2003, saw conversions, including 10.69 sq. km from agriculture, 11.74 sq. km from agroforestry, 28.72 sq. km from barren land, 3.15 sq. km from built-up areas, 10.72 sq. km from open forest, 6.12 sq. km from moderate forest, 0.11 sq. km from dense forest, 6.86 sq. km from grassland and9.59 sq. km from water bodies, resulting in a total of 87.70 sq. km (4.53%) in 2023. Built-up areas, starting at 80.15 sq. km (4.14%) in 2003, underwent conversions, including 20.05 sq. km from agriculture, 11.72 sq. km from agroforestry, 9.85 sq. km from barren land, 49.47 sq. km from built-up areas, 20.93 sq. km from open forest, 1.04 sq. km from moderate forest, 0.02 sq. km from dense forest, 10.65 sq. km from grassland and1.72 sq. km from water bodies, leading to a total of 125.45 sq. km (6.48%) in 2023.

Over the two-decade span from 2003 to 2023, there have been notable alterations in the expanse of forested areas. The area covered by open forest was initially 459.03 sq. km (23.71%) in 2003, but it has undergone various conversions over the years. These include 18.18 sq. km from agriculture, 59.25 sq. km from agroforestry, 70.58 sq. km from barren land, 1.98 sq. km from built-up areas, 157.78 sq. km from open forest, 63.27 sq. km from moderate forest, 12.96 sq. km from dense forest, 28.31 sq. km from grassland and1.99 sq. km from water bodies. As a result, the open forest area has decreased to 414.30 sq. km (21.40%) in 2023. Moderate forest, which was initially at 236.57 sq. km (12.22%) in 2003, has also undergone conversions. These include 7.27 sq. km from agriculture, 48.67 sq. km from agroforestry area, 42.68 sq. km from barren land, 1.05 sq. km from built-up areas, 146.48 sq. km from open forest, 122.88 sq. km from moderate forest, 33.12 sq.km from dense forest, 18.09 sq. km from grassland and0.84 sq. km from water bodies. This has led to a total of 421.08 sq. km (21.75%) in 2023.

The dense forest area initially covered 47.21 sq. km (2.44%) in 2003. However, by 2023, it had increased to 53.43 sq. km (2.76%). The changes included 5.79 sq. km from agriculture, 11.47 sq. km from agroforestry, 2.46 sq. km from barren land, 1.2 sq. km from built-up areas, 9.63 sq. km from open forest, 18 sq. km from moderate forest, 4 sq. km from

dense forest, 0.84 sq. km from grassland and 0.04 from water body. In 2003, the expanses of grassland encompassed 216.67 sq. km (11.19%) of the total landscape. By 2023, this area has experienced a notable reduction, shrinking to 152.50 sq. km (7.88%) of the overall coverage. The changes included 16.76 sq. km from agriculture, 26.19 sq. km from agroforestry, 12.31 sq. km from barren land, 3.12 sq. km from built-up areas, 14.12 sq. km from open forest, 3.1 sq. km from moderate forest, 1 sq. km from dense forest, 74.89 sq. km from grassland and1.01 sq. km from water bodies. The water body area initially covered 29.04 sq. km (1.50%) in 2003. Subsequently, by 2023, it has decreased to 22.84 sq. km (1.18%). The changes included 0.74 sq. km from agriculture, 0.07 sq. km from agroforestry, 6.39 sq. km from barren land, 0.63 sq. km from built-up areas, 1.1 sq. km from open forest, 0.02 sq. km from moderate forest, 0.98 sq. km from grassland and12.91 sq. km from water bodies.

Research conducted between 2003 and 2023 has explored the dynamics of land changes, revealing a complex pattern of ups and downs in different land cover types. This investigation collectively sheds light on how the landscape evolves, highlighting noticeable increases and decreases in various land cover categories. Croplands transformed into built-up areas, surpassing forests and crop-plantation zones. Study conducted by Houssoukpèvi et al. (2023) on the Allada Plateau, in the Atlantic Department of southern Benin, crop-plantation areas changed into adult palm groves and croplands. Forests diminished, making way for adult palm groves, croplands and crop-plantation areas. Tree plantations expanded mainly through cropland and crop-plantation conversions from 2000 to 2018. Minor built-up areas transformed into tree plantations, adult palm groves and croplands, potentially due to classification errors. These shifts underscore dynamic changes in land use patterns, highlighting the complex interplay of agriculture, urbanization and forestry. Similar studies have been conducted by Rawat et al. (2013), Taloor et al. (2020), Kogo et al. (2021), Xu et al. (2023) and Zheng and Zheng (2023).

4.3.2. InVest model outcomes

4.3.2.1. The carbon value (Mg/900 sq.m) in 2003,2013 and 2023.

In 2003, the region was classified into five zones based on the carbon values per 900 square meters of land (Table 39. And Figure. 28). The first zone covered an area of 36.43 sq.km, accounting for 1.88% of the total region, with carbon values ranging from 0 to 3.17 Mg/900 sq.m. The second zone, which covered 667.56 sq.km or 34.38% of the region, had

low carbon values ranging from 3.17 to 6.8 Mg/900 sq.m. The third zone, covering 412.82 sq.km or 21.32% of the region, had medium carbon values ranging from 6.8 to 10.95 Mg/900 sq.m. The fourth zone, with high carbon values ranging from 10.95 to 15.71 Mg/900 sq.m, covered an area of 477.29 sq.km or 24.65% of the total region. Lastly, the fifth zone, with exceptionally high carbon values ranging from 15.71 to 21.15 Mg/900 sq.m, covered 341.90 sq.km or 17.66% of the region.

Table 39. Area (sq.km) and Area (%) under different category of Carbon value in Solan District (H.P) in 2003

Carbon value (Mg/900 sq. m)	Area (sq.km)	Area (%)
Very Low (0 - 3.17)	36.43	1.88
Low (3.17 - 6.8)	667.56	34.48
Medium (6.8 - 10.95)	412.82	21.32
High (10.95 - 15.71)	477.29	24.65
Very High (15.71- 21.15)	341.90	17.66
Total Area (sq.km)	1936	100.00

In 2013 (Table 40 and Figure 28), the region was divided into different carbon value zones. The largest zone, covering an area of 73.44 sq. km or 3.79% of the total area, had shallow carbon values ranging from 0 to 3.17 Mg/900 sq.m. Another zone, covering an area of 553.52 sq. km or 28.59% of the region, had low carbon values ranging from 3.17 to 6.8 Mg/900 sq.m. The third zone, covering an area of 457.08 sq. km or 23.61% of the region, had medium carbon values ranging from 6.8 to 10.95 Mg/900 sq.m. The fourth zone, covering an area of 418.31 sq. km or 21.61% of the region, had high carbon values ranging from 10.95 to 15.71 Mg/900 sq.m. Finally, the region had a zone with very high carbon values ranging from 15.71 to 21.15 Mg/900 sq.m, covering an area of 433.66 sq. km or 22.40% of the region.

Table 40. Area (sq.km) and Area (%) under different category of Carbon value in Solan District (H.P) in 2013

Carbon value (Mg/900 sq. m)	Area (sq.km)	Area (%)
Very Low (0 - 3.17)	73.44	3.79
Low (3.17 - 6.8)	553.52	28.59
Medium (6.8 - 10.95)	457.08	23.61
High (10.95 - 15.71)	418.31	21.61
Very High (15.71- 21.15)	433.66	22.40
Total Area (sq.km)	1936	100.00

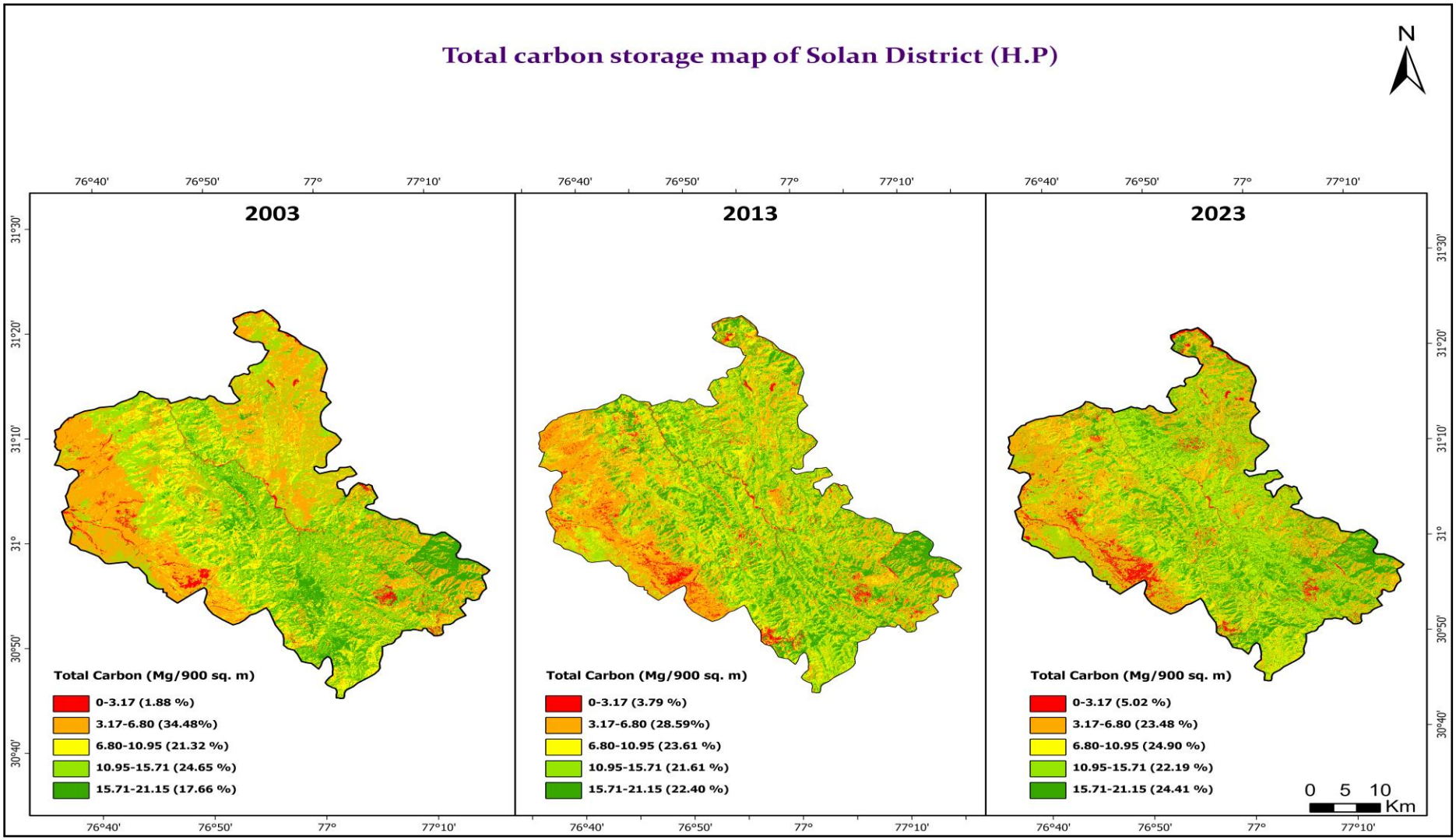

Figure 28. Total carbon storage map of Solan District (H.P) of different year 2003, 2013 and 2023

In 2023, the region displayed distinct carbon value zones, as shown in Table 41. and Figure 28. A total of 97.12 sq. km, which accounts for 5.02% of the region, had extremely low carbon values ranging from 0 to 3.17 Mg/900 sq.m. Low carbon values, ranging from 3.17 to 6.8 Mg/900 sq.m, covered an area of 454.62 sq. km, representing 23.48% of the region. Additionally, 482.09 sq. km of the area, which is 24.90% of the total, displayed medium carbon values ranging from 6.8 to 10.95 Mg/900 sq.m. The zone characterized by high carbon values, extending from 10.95 to 15.71 Mg/900 sq.m, encompassed 429.59 sq. km, accounting for 22.19% of the total. Finally, an area of 472.58 sq. km, constituting 24.41% of the region, exhibited very high carbon values ranging from 15.71 to 21.15 Mg/900 sq.m.

Table 41. Area (sq.km) and Area (%) under different category of Carbon value in Solan District (H.P) in 2023

Carbon value (Mg/900 sq. m)	Area (sq.km)	Area (%)
Very Low (0 - 3.17)	97.12	5.02
Low (3.17 - 6.8)	454.62	23.48
Medium (6.8 - 10.95)	482.09	24.90
High (10.95 - 15.71)	429.59	22.19
Very High (15.71- 21.15)	472.58	24.41
Total Area (sq.km)	1936	100.00

Table 42. Area (sq. km) under different category of Carbon value (Mg/900 sq. m) in Solan District (H.P) during 2003, 2013 and 2023

Carbon value (Mg/900 sq. m)	Area (sq.km)		
Very Low (0 - 3.17)	**2003**	**2013**	**2023**
Low (3.17 - 6.8)	36.43	73.44	97.12
Medium (6.8 - 10.95)	667.56	553.52	454.62
High (10.95 - 15.71)	412.82	457.08	482.09
Very High (15.71- 21.15)	477.29	418.31	429.59
Total Area (sq.km)	341.90	433.66	472.58

According to Table 42. and Figure 29, the area with very low carbon values (ranging from 0 to 3.17 Mg/900 sq.m) increased from 36.43 sq. km in 2003 to 73.44 sq. km in 2013 and reached 97.12 sq. km in 2023. Similarly, areas with medium carbon values (6.8 - 10.95 Mg/900 sq.m) and very high carbon values (15.71 - 21.15 Mg/900 sq.m) also expanded from

412.82 sq. km in 2003 to 457.08 sq. km in 2013. Further, they increased to 482.09 sq. km in 2023 and from 341.90 sq. km in 2003 to 433.66 sq. km in 2013 before reaching 472.58 sq. km in 2023, respectively. However, the area designated as having low carbon values (ranging from 3.17 to 6.8 Mg/900 sq.m) decreased from 667.56 sq. km in 2003 to 553.52 sq. km in 2013 and continued to decrease to 454.62 sq. km in 2023. In contrast, areas with high carbon values (10.95 - 15.71 Mg/900 sq.m) decreased from 477.29 sq. km in 2003 to 418.31 sq. km in, but slightly increased to 429.59 sq. km in 2023.

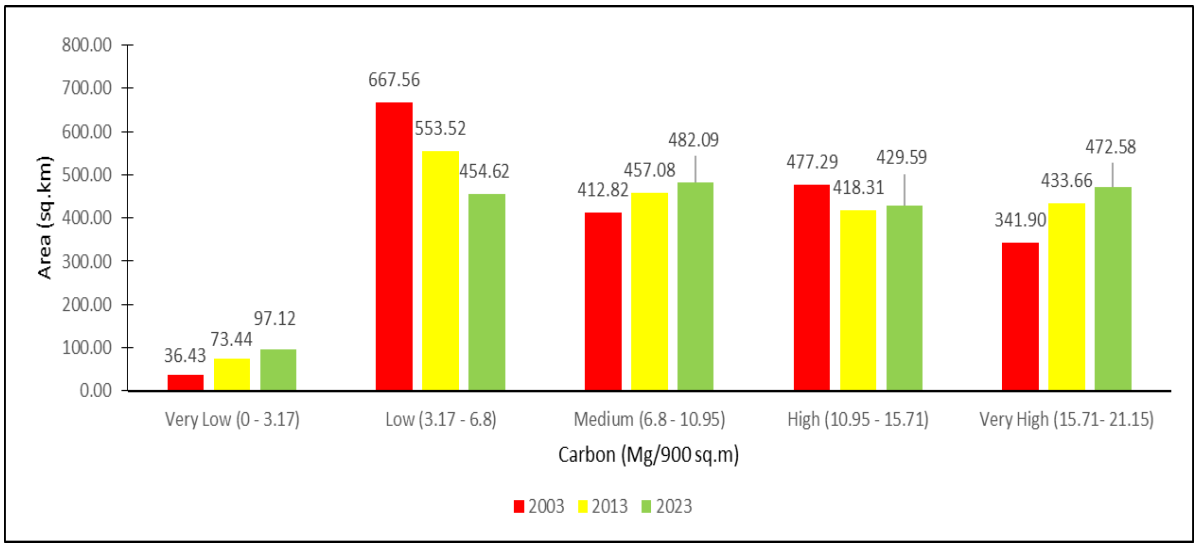

Figure 29. Area under different category of carbon value (Mg/900 sq. m) in Solan District (H.P) during 2003, 2013 and 2023

4.3.2.2. The conversion of carbon density (Mg) over the period of 2003 – 2023

As depicted in the Table 43 and illustrated by a chord diagram (Figure 30), there has been a significant transformation in all carbon classes from 2003 to 2023. Notably, the area classified as very low carbon value, which measured 36.44 sq.km in 2003, has experienced substantial growth, reaching 97.12 sq.km in 2023. This change was attributed to the shifts from various carbon classes, including 17.94 sq.km from very low carbon value, 48.94 sq.km from low carbon value, 12.06 sq.km from medium carbon value, 14.36 sq.km from high carbon value and 3.82 sq.km from very high carbon value. Similarly, there was an upward trend both medium and very high carbon values**.** A total of 2.08 sq.km from very low carbon, 116.44 sq.km from low carbon, 194.2 sq.km from medium carbon, 100.44 sq.km from high carbon and 68.93 sq.km from very high carbon underwent a transformation, contributing to the increase in the medium carbon value range (6.8-10.95 Mg/900 sq.m). Furthermore, 1.09 sq.km converted from very low carbon, 92.08 sq.km converted from low carbon, 60.98 sq.km

converted from medium carbon, 138.47 sq.km converted from high carbon and 179.96 sq.km converted from very high carbon collectively formed an area measuring 472.58 sq.km designated as very high carbon value (15.71-21.15 Mg/900 sq.m) in 2023.

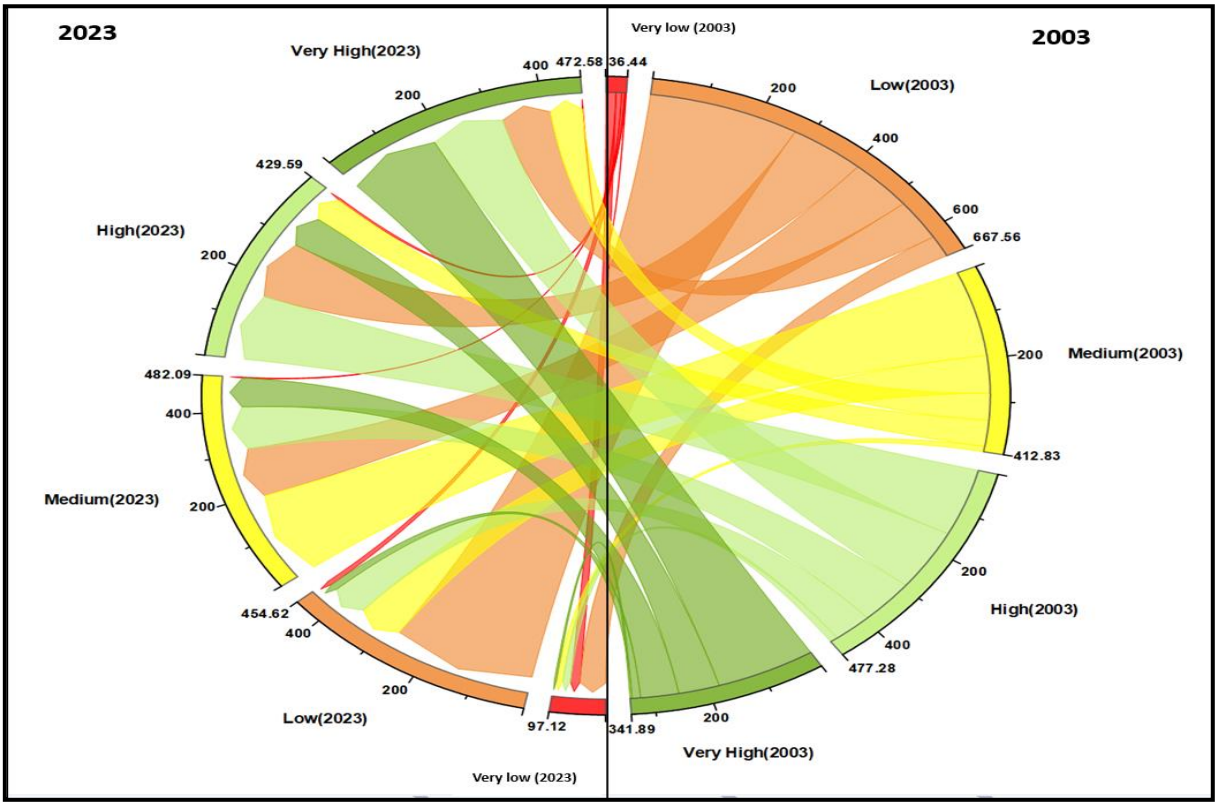

Figure 30. Chord diagram showing the conversion of carbon density (Mg C) over the period of 2003 - 2023 in Solan District (H.P)

In 2023, an area measuring 429.59 sq.km, characterized by high carbon values falling within the range of 10.95 to 15.71 Mg/900 sq.m carbon value, was composed of 5.2 sq.km converted from very low carbon, 136.87 sq.km converted from low carbon. 59.76 sq.km converted from medium carbon, 153.59 sq.km converted from high carbon and 74.17 sq.km converted from very high carbon value. A discernible downward trend in low carbon values (3.17 to 6.8 Mg/900 sq.m) has been observed. In 2023, 10.13 sq.km converted from very low carbon, 273.23 sq.km from low carbon, 85.83 sq.km from medium carbon, 70.42 sq.km from high carbon and 15.01 sq.km from very high carbon. Collectively, these converted areas now constitute a total of 454.62 sq.km.

These transformations indicate a significant shift in the distribution and composition of carbon values, which reflects changes in the environmental landscape. The 97.12 sq.km area and the 454.62 sq.km observed under very low and low carbon levels need to be

safeguarded and conserved. This can be achieved by raising awareness about the importance of carbon storage and the role of trees in mitigating climate change. Involving local communities in tree planting and conservation efforts fosters a sense of ownership, leading to long-term commitment and sustainable practices. Additionally, exploring carbon farming techniques, such as cover cropping, rotational grazing and other regenerative agricultural practices, can contribute to soil carbon sequestration and overall carbon storage. Further evidence supporting this claim has been found in similar studies conducted by Jiang et al. (2017) and Babbar et al. (2021). Contradicting the majority of studies that suggest different urban expansion policies can reduce the landscape's ability to capture and store carbon, this study demonstrates that any decision made regarding land use can significantly impact the carbon sequestration function of the landscape.

Table 43. Area (sq. km) matrix across different Carbon classes of Solan District (H.P) from 2003 to 2023

Carbon value		2003					
		Very Low (0 - 3.17	**Low (3.17 -6.8)**	**Medium (6.8 - 10.95)**	**High (10.95 - 15.71)**	**Very High (15.71- 21.15)**	**Total area (sq. km)**
2023	**Very Low (0 - 3.17)**	17.94	48.94	12.06	14.36	3.82	**97.12**
	Low (3.17 - 6.8)	10.13	273.23	85.83	70.42	15.01	**454.62**
	Medium (6.8 - 10.95)	2.08	116.44	194.2	100.44	68.93	**482.09**
	High (10.95 - 15.71)	5.2	136.87	59.76	153.59	74.17	**429.59**
	Very High (15.71- 21.15)	1.09	92.08	60.98	138.47	179.96	**472.58**
	Total area (sq. km)	**36.44**	**667.56**	**412.83**	**477.28**	**341.89**	**1936**

4.3.2.3. Evolution of the C stocks distribution among the different C pools

According to Table 44, the distribution of C stocks in different pools shows that aboveground and soil (0-30 cm) were the most critical C pools were. These pools were observed to have significant carbon storage compared to other carbon pools. In 2003, under the open forest ecosystem, the maximum carbon storage of 4.084 Tg C was observed in aboveground biomass, while the minimum carbon storage of 0.142 Tg C was recorded in dead carbon. Additionally, 0.896 Tg C was stored belowground, emphasizing the importance of roots and subterranean structures in carbon sequestration and 2.761 Tg C was present in the soil, illustrating the significance of soil as a reservoir for carbon. Furthermore, moderate

forest had a maximum aboveground 2.872 Tg C, highlighting the importance of trees and vegetation in carbon storage, conversely, the minimum in dead carbon was 0.167 Tg C, representing organic matter in a state of decomposition. Belowground components stored 0.660 Tg C and the soil, extending to a depth of 0-30 cm, harboured a substantial carbon stock of 2.214 Tg C.

Within the agroforestry context, the distribution of carbon storage among various pools was noteworthy. In this ecosystem, the maximum carbon storage, totalling 1.641 Tg C, was observed in the soil and the minimum was under dead carbon at 0.156 Tg C. Aboveground stored a substantial amount of carbon, with 1.182 Tg C highlighting the importance of trees and vegetation in carbon storage within the agroforestry system. Additionally, belowground components, including roots and subterranean structures, contributed 0.306 Tg C to the overall carbon storage. This nuanced distribution among different carbon pools provides insights into the carbon dynamics within the agroforestry ecosystem. It has implications for understanding its role in carbon sequestration and overall environmental health. In the dense forest ecosystem, there are different carbon storage pools. The aboveground is the largest carbon reservoir, storing 0.685 Tg C. The soil (0-30 cm) is another major carbon reservoir, storing 0.469 Tg C. Belowground components, such as roots and subterranean structures, contributed 0.160 Tg C to the overall carbon storage. Dead carbon stored a smaller but significant amount, totalling 0.050 Tg C.

This nuanced distribution of carbon among different pools in the dense forest ecosystem provides insights into their diverse roles in carbon sequestration in this specific ecological setting. Significant carbon storage was observed in barren land, with 0.520 Tg C stored in the soil, 0.266 Tg C in aboveground biomass, 0.142 Tg C in belowground components and 0.033 Tg C in dead organic matter. This breakdown highlights the importance of soil as a significant carbon reservoir in barren land. In grassland, the maximum carbon storage was found in the soil, amounting to 0.736 Tg C, followed by 0.083 Tg C in aboveground biomass, 0.040 Tg C in belowground components and the least stored in dead organic matter at 0.022 Tg C. Agricultural areas exhibit varying carbon storage, with the maximum stored in the soil at 0.540 Tg C, followed by 0.110 Tg C in aboveground and relatively similar amounts in belowground components (0.0233 Tg C) and dead litter (0.0235 Tg C). In contrast, the built-up area stored the least carbon in 2003, with 0.030 Tg C in the soil, 0.006 Tg C in aboveground biomass, 0.005 Tg C in dead carbon and the least, 0.003 Tg C in belowground components.

Table 44. Distribution of stock of carbon (tera-gram C) in various pools combined according to the land use of Solan District (H.P) for the years 2003, 2013 and 2023

Land-use classes	2003					2013					2023				
	Above ground	Below ground	Soil carbon	Dead Carbon	Total	Above ground	Below ground	Soil carbon	Dead Carbon	Total	Above ground	Below ground	Soil carbon	Dead Carbon	Total
Agriculture	0.110	0.0233	0.540	0.0235	**0.698**	0.107	0.022	0.521	0.023	**0.673**	0.094	0.0198	0.459	0.0200	**0.593**
Agroforestry	1.182	0.306	1.641	0.156	**3.285**	1.306	0.338	1.814	0.173	**3.631**	1.381	0.357	1.918	0.183	**3.839**
Barren land	0.266	0.142	0.520	0.033	**0.961**	0.188	0.100	0.367	0.023	**0.679**	0.129	0.069	0.251	0.016	**0.464**
Built-up	0.006	0.003	0.030	0.005	**0.045**	0.017	0.008	0.083	0.013	**0.122**	0.022	0.011	0.105	0.017	**0.154**
Open	4.084	0.896	2.761	0.142	**7.882**	3.628	0.796	2.452	0.126	**7.002**	3.674	0.806	2.484	0.127	**7.091**
Moderate Forest	2.872	0.660	2.214	0.167	**5.913**	3.730	0.856	2.874	0.217	**7.677**	4.168	0.957	3.212	0.242	**8.579**
Dense Forest	0.685	0.160	0.469	0.050	**1.364**	0.746	0.218	0.493	0.059	**1.515**	0.711	0.192	0.475	0.047	**1.425**
Grassland	0.083	0.040	0.736	0.022	**0.881**	0.069	0.033	0.613	0.018	**0.734**	0.063	0.030	0.553	0.017	**0.662**
Total C	**9.289**	**2.229**	**8.911**	**0.598**	**21.027**	**9.791**	**2.372**	**9.218**	**0.652**	**22.032**	**10.241**	**2.441**	**9.457**	**0.669**	**22.807**

In 2003, the total carbon distribution among different pools indicates that the highest amount was in aboveground biomass, totalling 9.289 Tg C. Following closely, soil carbon represented a significant reservoir, amounting to 8.911 Tg C. Belowground components contributed 2.229 Tg C to the overall carbon storage. The least amount of carbon was stored in the dead litter, totalling 0.598 Tg C. These figures provide insights into the relative contributions of different carbon pools to the total carbon stock in 2003, illustrating the importance of aboveground and soil.

In 2013, the moderate-density forests exhibited the highest carbon storage, with 3.730 Tg C stored aboveground, 2.874 Tg C in soil, 0.856 Tg C belowground and 0.217 Tg C in dead litter. The open-density forests ranked second in carbon storage, registering 3.628 Tg C aboveground, 2.452 Tg C in soil, 0.796 Tg C belowground and 0.126 Tg C in dead litter. Agroforestry demonstrated considerable carbon storage with 1.306 Tg C aboveground, 1.814 Tg C in soil, 0.338 Tg C belowground and 0.173 Tg C in dead litter. In dense forests, most of the carbon resided aboveground, accounting for 0.746 Tg C, with additional substantial contributions from soil (0.493 Tg C), belowground (0.218 Tg C) and dead litter (0.059 Tg C). In grasslands, carbon storage was predominantly in the soil, amounting to 0.613 Tg C, while aboveground vegetation contributed 0.069 Tg C, belowground storage accounted for 0.033 Tg C and dead litter contained 0.018 Tg C. Barren lands exhibited a distinctive carbon storage profile, with 0.367 Tg C stored in the soil, followed by 0.188 Tg C aboveground, 0.100 Tg C belowground and 0.023 Tg C in dead litter. Agriculture displayed noteworthy carbon storage, particularly in the soil where a maximum of 0.521 Tg C was sequestered, while aboveground vegetation stored 0.107 Tg C, dead litter contained 0.023 Tg C and belowground storage amounted to 0.022 Tg C. Conversely, the built-up area demonstrated minimal carbon storage, with the highest proportion, 0.083 Tg C, found in the soil. Aboveground structures stored 0.017 Tg C, dead litter contained 0.013 Tg C and the least amount, 0.008 Tg C, was stored belowground. In 2003, the total carbon distribution among different pools indicates that the highest amount was in aboveground biomass, totalling 9.791 Tg C. Following closely, soil carbon represented a significant reservoir, amounting to 9.218 Tg C. Belowground components contributed 2.372 Tg C to the overall carbon storage. The least amount of carbon was stored in the dead litter, totalling 0.652 Tg C. These figures provide insights into the relative contributions of different carbon pools to the total carbon stock in 2013, illustrating the importance of aboveground and soil.

In 2023, it was discovered that the primary carbon reservoir was located in moderate forests, with a total of 8.579 Tg C stored. Most of this carbon storage, at 4.168 Tg C, was found aboveground, followed by 3.212 Tg C in soil, 0.957 Tg C belowground and the least amount, 0.242 Tg C, in dead litter. The second-highest carbon storage was observed in open forests at 7.091 Tg C. This includes 3.674 Tg C aboveground, 2.484 Tg C in soil, 0.806 Tg C belowground and 0.127 Tg C in dead litter. Agroforestry exhibits a carbon storage distribution of 1.918 Tg C in soil, 1.381 Tg C aboveground, 0.357 Tg C belowground and 0.183 Tg C in dead litter. In dense forests, the maximum carbon storage was 0.711 Tg C aboveground, 0.475 Tg C in soil, 0.192 Tg C belowground and 0.047 Tg C in dead litter. Grasslands store 0.553 Tg C in soil, 0.063 Tg C aboveground, 0.030 Tg C belowground and 0.017 Tg C in dead litter. Agriculture predominantly stores carbon in the soil, with 0.459 Tg C, followed by 0.094 Tg C aboveground, 0.020 Tg C in the dead litter and nearly equivalent amounts of 0.198 Tg C belowground. Barren lands contain 0.251 Tg C in soil, 0.129 Tg C aboveground, 0.069 Tg C belowground and 0.016 Tg C in dead litter. The least carbon storage was observed in built-up areas, with 0.105 Tg C in soil, 0.022 Tg C aboveground, 0.017 Tg C in dead litter and 0.011 Tg C belowground. In 2023, the total carbon distribution among different pools indicates that the highest amount was in aboveground biomass, totalling 10.241 Tg C. Following closely, soil carbon represented a significant reservoir, amounting to 9.457 Tg C. Belowground components contributed 2.441 Tg C to the overall carbon storage. The least amount of carbon was stored in the dead litter, totalling 0.669 Tg C. These figures provide insights into the relative contributions of different carbon pools to the total carbon stock in 2003, illustrating the importance of aboveground and soil.

This passage discusses the varying carbon sequestration processes across different land use categories. It highlights the importance of understanding these variations in the context of broader ecological and climate change perspectives. Notably, K.V.G and Barik (2018), Islam et al. (2022) and He et al. (2023) have contributed to this field of knowledge. Houssoukpèvi et al. (2022) conducted a study that estimated the distribution of carbon stocks in different pools between 2000 and 2018 in the Allada Plateau, in the Atlantic Department of southern Benin. The study found that the most significant carbon pools were the aboveground and the soil (0-30 cm). These two pools accounted for 45% and 39% of the total carbon stock in the considered area in 2000 and 45% and 37% in 2018, respectively.

Table 45. Change in dynamics of C (Tg-tera gram) in Solan District (H.P)

Land use classes	2003	2013	2023	Change in C			Rate of change in C		
	Total C	Total C	Total C	2003-2013	2013-2023	2003-2023	2003-2013	2013-2023	2003-2023
Agriculture	0.698	0.673	0.593	-0.025	-0.080	-0.105	-0.002	-0.008	-0.005
Agroforestry	3.285	3.631	3.839	0.346	0.209	0.555	0.035	0.021	0.028
Barren land	0.961	0.679	0.464	-0.282	-0.214	-0.496	-0.028	-0.021	-0.025
Built-up	0.045	0.122	0.154	0.077	0.032	0.109	0.008	0.003	0.005
Open forest	7.882	7.002	7.091	-0.880	0.089	-0.791	-0.088	0.009	-0.040
Moderate Forest	5.913	7.677	8.579	1.765	0.902	2.666	0.176	0.090	0.133
Dense Forest	1.364	1.515	1.425	0.152	-0.090	0.061	0.015	-0.009	0.003
Grassland	0.881	0.734	0.662	-0.148	-0.072	-0.220	-0.015	-0.007	-0.011
Total C	**21.027**	**22.032**	**22.807**	**1.005**	**0.775**	**1.780**	**0.101**	**0.077**	**0.089**

4.3.2.4. Evolution of the C stocks distribution among the land uses

The total carbon stock map, shown in Table 45, provides a comprehensive assessment of the changes in carbon storage across various land cover types from 2003 to 2023. The open forest had the highest carbon storage in 2003, with 7.882 Tg C. However, over the following decade, the carbon stock decreased to 7.002 Tg C in 2013. But, by 2023, it rebounded to 7.091 Tg C. Conversely the Dense forests stored 1.364 Tg C in 2003 which increased to 1.515 Tg C in 2013 and then decreased to 1.425 Tg C in 2023. These fluctuations indicate the dynamic nature of carbon storage in open and dense forests, which are influenced by environmental factors and land use changes over time. Agriculture, barren land and grassland experienced a decline in total carbon stock as their respective areas decreased from 2003 to 2023. Agriculture had 0.698 Tg C in 2003, which fell to 0.673 Tg C in 2013 and 0.593 Tg C in 2023. Barren land had 0.961 Tg C in 2003, 0.679 Tg C in 2013 and 0.464 Tg C in 2023. Grassland had 0.881 Tg C in 2003, 0.734 Tg C in 2013 and 0.662 Tg C in 2023.

On the other hand, agroforestry, built-up areas and moderate forests showed an increasing trend of carbon stock, as their areas also increased over the years. Agroforestry had 3.285 Tg C in 2003, which increased to 3.631 Tg C in 2013 and 3.839 Tg C in 2023. Built-up areas had the lowest carbon stock in 2003, with 0.045 Tg C. However, it increased to 0.122 Tg C in 2013 and is expected to rise to 0.154 Tg C by 2023, indicating a growing carbon presence in urban and developed areas. Moderate forests had a substantial carbon stock of 5.913 Tg C in 2003, ranking second-highest after the open forest. Over the subsequent decade, there was a significant increase, reaching 7.677 Tg C in 2013. By 2023, the carbon stock in the moderate forest surged even further, reaching its peak at 8.579 Tg C, surpassing the carbon stocks of all other land cover types.

The dynamics between land cover changes and carbon stock variations are complex and interrelated. Li et al. (2022) researched Huining County within China's Loess Plateau region, revealing significant insights into carbon storage dynamics. The study found an annual net increase of approximately 59.82 Gg in forest carbon storage. Additionally, the conversion to grassland positively contributed to carbon storage, with a net gain of 38.01 Gg per year. However, the transformation of farmland to alternative land types resulted in a cumulative net rise of 1,820.72 Gg over the past 17 years, indicating a substantial impact on carbon storage. The augmentation of carbon storage in both forests and grasslands was primarily attributed to the conversion of farmland. However, the study identified a net carbon

loss of 842.85 Gg in the first stage and 741.19 Gg in the second stage when forests, grasslands and farmlands were converted to unused land. The total carbon loss over the entire study period amounted to 1,584.04 Gg.

These findings underscore the nuanced relationship between land use changes and carbon dynamics, emphasizing the importance of understanding and managing these transitions for effective carbon storage management. Similar studies have been conducted by various researchers, including Zhao et al. (2019), Houssoukpèvi et al. (2023), Islam et al. (2022) and Xu et al. (2023). These studies likely contribute valuable insights and comparisons to assessing carbon storage dynamics in different regions or ecosystems.

4.3.2.5. Rate of change in dynamics of C (tera-gram) in different land-uses from 2003-2023

According to Table 45, the carbon storage across various land-use categories has fluctuated significantly over a period of 20 years from 2003 to 2023. The changes were attributed to variations in land cover dynamics during this time. In 2003, open forests had the highest carbon storage at of the total 7.882 Tg C. However, by 2013, there was a reduction to 7.002 Tg C of the total carbon, a decrease of 0.880 Tg C. Interestingly, in 2023, there was a slight rebound with the increasing to 7.091 Tg C, representing a modest increment of 0.089 Tg C. Overall, there was a total reduction of 0.791 Tg C in carbon storage from 2003-2023. The rate of change observed was -0.088 from 2003-2013, 0.009 from 2013-2023 and -0.040 in total from 2003-2023.

In 2003, moderate forests had the second-highest carbon storage at 5.913 Tg C. Over the following decade, there was a significant increase of 1.765 Tg C, resulting in a total storage of 7.677 Tg C in 2013. Remarkably, by 2023, moderate forests surpassed all other categories to become the highest carbon storage, with an additional increase of 0.902 Tg C totalling 8.579 Tg C. Throughout the 20-year span from 2003 to 2023, moderate forests had a cumulative increase of 2.666 Tg C. The rate of change observed during this period was 0.176 in 2003, 0.090 in 2013 and 0.133 in 2023, indicating dynamic shifts in carbon sequestration patterns over the two-decade timeframe. In 2003, agroforestry stored 3.285 Tg C. From 2003 to 2013, there was an increase of 0.346 Tg C, with a rate of change of 0.035. Subsequently, from 2013 to 2023, there was a further increase of 0.209 Tg C and the rate of change during this period was 0.021. By 2023, the total carbon storage in agroforestry reached 3.839 Tg C, reflecting a cumulative increase of 0.555 Tg C from 2003 to 2023, with a rate of change of

0.028. In the case of dense forests, 1.364 Tg C was initially stored. It experienced an increment of 0.152 Tg C from 2003 to 2013 with a rate of change of 0.015. A decrease of 0.090 Tg C occurred from 2013 to 2023 with a rate of change of -0.009. In 2023, 1.425 Tg C was stored, resulting in a total increment of 0.061 Tg C from 2003 to 2023 with a rate of change of 0.003. In barren lands, 0.961 Tg C was initially stored. It experienced a reduction of 0.282 Tg C from 2003 to 2013 with a rate of change of -0.028. A further decrease of 0.214 Tg C occurred from 2013 to 2023 with a rate of change of -0.021. In 2023, 0.464 Tg C was stored, resulting in a total reduction of 0.496 Tg C from 2003 to 2023 with a rate of change of -0.025.

In grasslands, 0.881 Tg C was initially stored. It experienced a reduction of 0.148 Tg C from 2003 to 2013 with a rate of change of -0.015. A further decrease of 0.072 Tg C occurred from 2013 to 2023 with a rate of change of -0.007. In 2023, 0.662 Tg C was stored resulting in a total reduction of 0.220 Tg C from 2003 to 2023 with a rate of change of -0.011. In agriculture, 0.698 Tg C was initially stored. It experienced a reduction of 0.025 Tg C from 2003 to 2013 with a rate of change of -0.002. A further decrease of 0.080 Tg C occurred from 2013 to 2023, with a rate of change of -0.008. In 2023, 0.593 Tg C was stored, resulting in a total reduction of 0.105 Tg C from 2003 to 2023 with a rate of change of -0.005. In built-up areas, 0.045 Tg C was initially stored. It experienced an increase of 0.077 Tg C from 2003 to 2013 with a rate of change of 0.008. A further rise of 0.032 Tg C occurred from 2013 to 2023 with a rate of change of 0.003. In 2023, 0.154 Tg C was stored resulting in a total increase of 0.109 Tg C from 2003 to 2023 with a rate of change of 0.005.

In the baseline year of 2003, the cumulative carbon storage measured 21.027 Tg C. Advancing into subsequent years, this metric exhibited an upward trajectory, registering at 22.032 Tg C in 2013 by increase of 1.005 Tg C, with rate of change of 0.101 and culminating in 22.807 Tg C by the terminal year of 2023 with increase of 0.775 Tg C and rate of change of 0.077. Overall change of carbon storage from 2003 to 2023 recorded as 1.780 Tg C with rate of change of 0.089. The dynamic interaction between land use and the environment highlights the importance of adopting sustainable land-use practices in regions undergoing rapid changes to promote carbon storage and enhance environmental benefits. In a comprehensive study spanning three decades (1988-2018), Islam et al. (2022) analyzed the impact of land-use changes on carbon dynamics in the Eastern Coastal Zone of Bangladesh.

The study revealed that Tree Outside Forests (TOF) played a crucial role in carbon sequestration consistently outperforming other land-use types during the study period. Specifically, TOF contributed to the sequestration of 9.0 Tg C, while losses resulting from changes in agriculture and hill vegetation amounted to 3.09 Tg C and 5.16 Tg C respectively. Conversion of agricultural and hill vegetation land to other uses led to a net reduction of 7.98 Tg C underscoring the complex relationship between land-use changes and carbon storage in the region. Zhao et al. (2019), Houssoukpèvi et al. (2023), Li et al. (2022) and Xu et al. (2023) also conducted similar research.

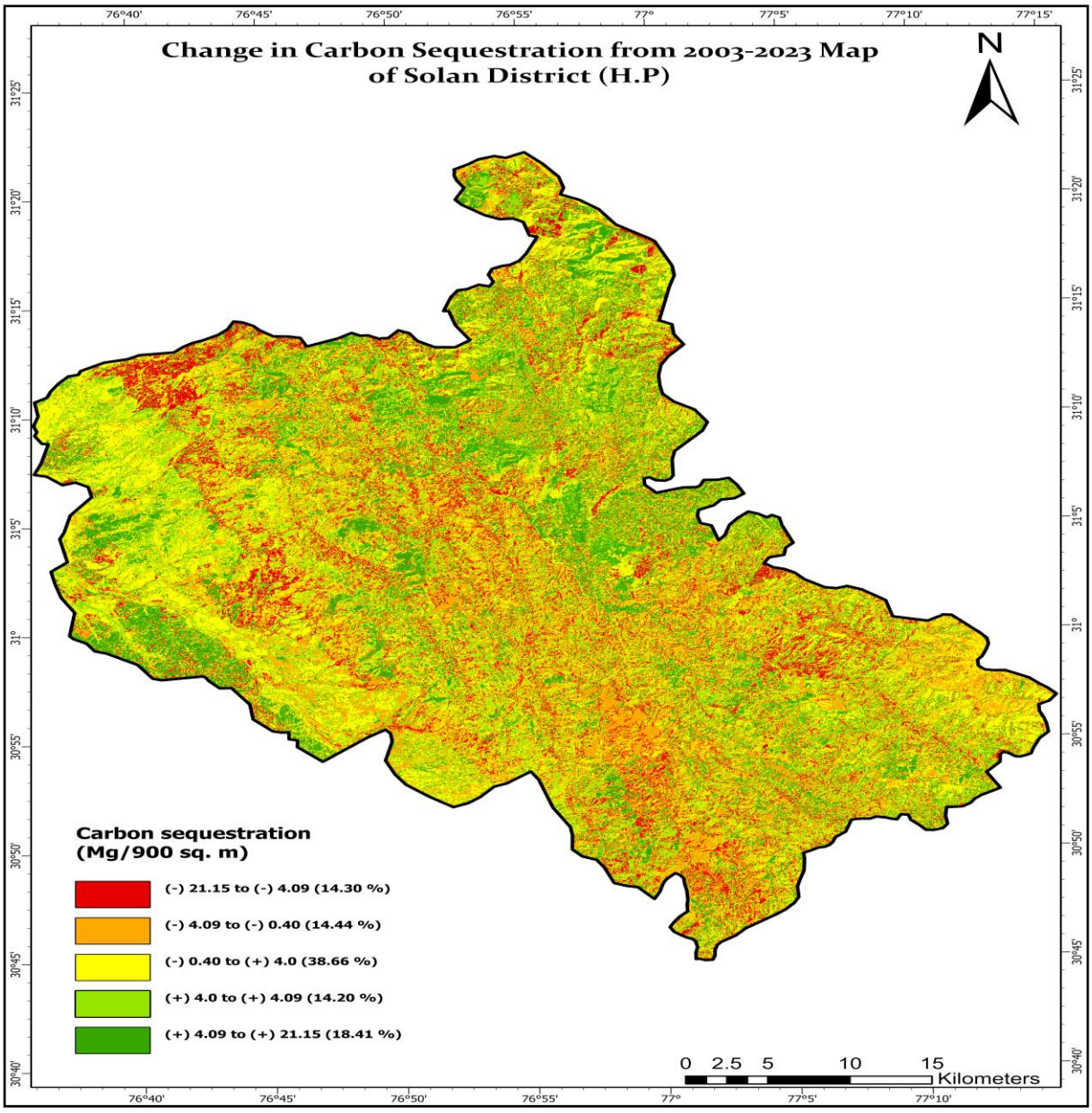

Figure 31. Change in Carbon Sequestration value in different Carbon density classes from 2003 to 2023 in Solan District (H.P)

4.3.2.6. Change in carbon sequestration and Net present value of carbon sequestration ($) from 2003-2023

Table 46. and Figure 31 present the changes in carbon sequestration in the Solan district between 2003 and 2023. The data suggests that there were five categories of carbon sequestration changes in the district. The first category recorded carbon sequestration changes ranging from (-)21.15 to (-)4.1 Mg/900 sq.m, covering an area of 14.30% (276.83 sq. km). The second category saw changes from (-)4.09 to (-)0.40 Mg/900 sq.m, covering 14.44% (279.49 sq. km). The third and most significant transformation occurred from (-)0.4 to (+)0.4 Mg/900 sq.m, covering a maximum area of 38.66% (748.36 sq. km). The fourth category witnessed carbon sequestration changes from (+)0.40 to (+)4.1 Mg/900 sq.m, covering 14.20% (274.94 sq. km) of the district. Finally, there was a range of (+)4.1 to (+)21.15 Mg/900 sq.m, which saw carbon sequestration changes and comprised 18.41% (356.39 sq. km) of the district.

Table 46. Area under categories of change Carbon sequestration classes from 2003-2023 in Solan District (H.P)

Carbon sequestration (Mg/900 sq. m)	Area (sq. km)	Area (%)
(-)21.15 to (-)4.1	276.82	14.30
(-)4.09 to (-)0.40	279.49	14.44
(-)0.40 to (+) 0.40	748.36	38.66
(+)0.4 to (+)4.1	274.94	14.20
(+)4.1 to (+)21.15	356.39	18.41
Total area (sq. km)	1936	100

In the study, the Net Present Value (NPV) of carbon sequestration was computed and results are presented in Figure 32 and Table 47. The NPV ($) values were calculated for different ranges of carbon sequestration changes, ranging from (-)21.15 to (+)21.15 Mg/900 sq.m, over a 20-year period. For the range of (-)21.15 to (-)4.1 Mg/900 sq.m, the NPV ($) ranges from (-)376.67 to (-)72.96. In the (-)4.09 to (-)0.40 Mg/900 sq.m range, the NPV ($) varies from (-)72.96 to (-)7.13. Within the range of (-)0.40 to (+)0.40 Mg/900 sq.m, the NPV ($) records a range of (-)7.13 to (+)7.13. Moving to the (+)0.40 to (+)4.1 Mg/900 sq.m range, the NPV ($) varies from (+)7.13 to (+)72.96. Finally, in the (+)4.1 to (+)21.15 Mg/900 sq.m range, the NPV ($) ranges from (+)72.96 to (+)376.67. These NPV values provide insights into the economic implications associated with different levels of carbon sequestration changes observed over the specified ranges during the 20-year period.

Table 47. Net present value ($) of Carbon sequestration from 2003-2023 in Solan District (H.P)

Carbon sequestration (Mg/900 sq. m)	Net present value of carbon sequestration ($)
(-)21.15 to (-)4.1	(-)376.67 to (-)72.96
(-)4.09 to (-)0.40	(-)72.96 to (-)7.13
(-)0.40 to (+) 0.40	(-)7.13 to 7.13
(+)0.4 to (+)4.1	(+)7.13 to (+)72.96
(+)4.1 to (+)21.15	(+)72.96 to (+)376.67

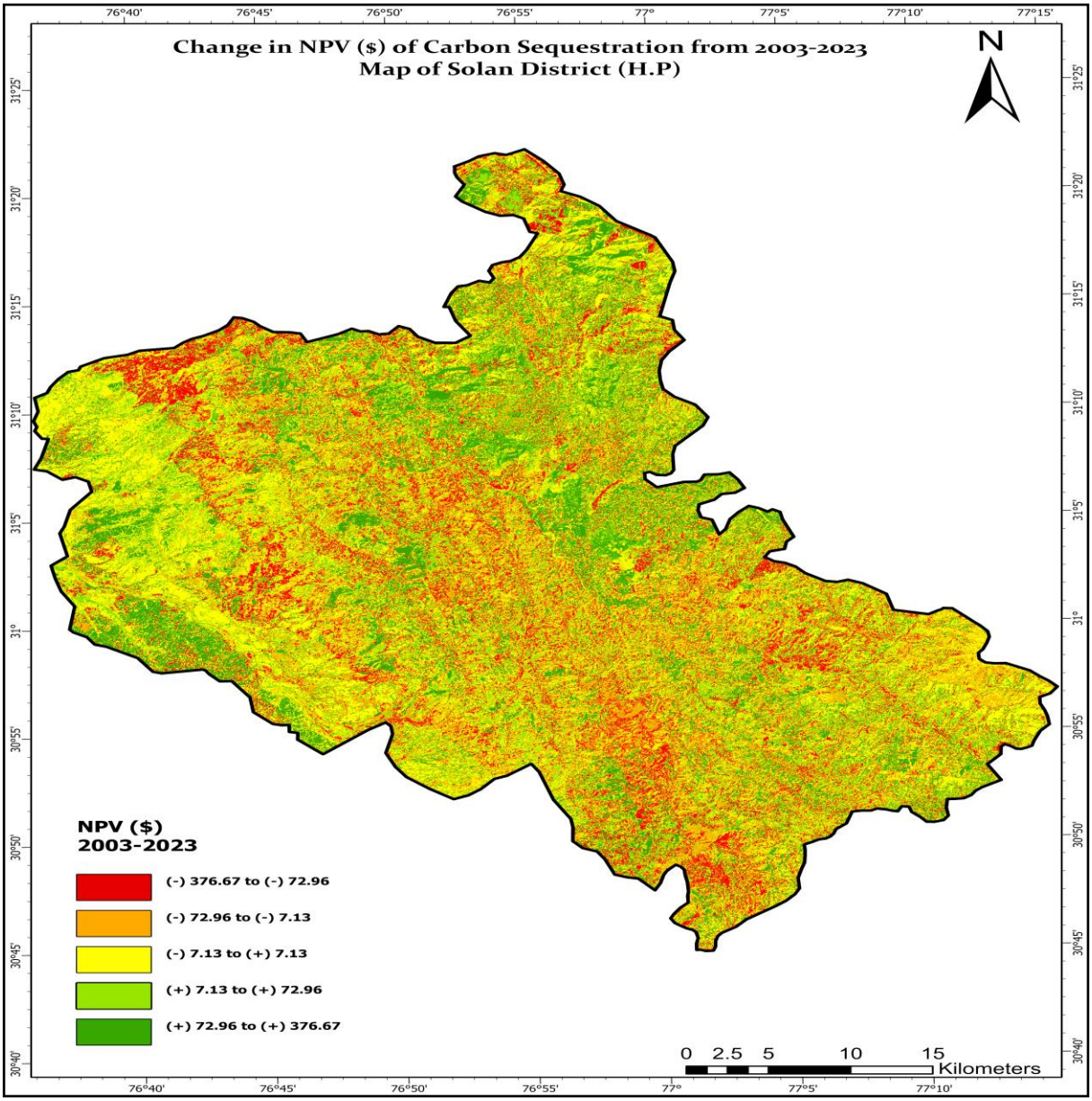

Figure 32. Map of change in Net Present Value ($) of Carbon Sequestration from 2003 to 2023 in Solan District (H.P)

Table 48. displays that the total carbon content in 2003 was 21.027 Tg C. This increased to 22.807 Tg C by 2023, indicating a rise in carbon sequestration of 1.780 Tg C over a period of 20 years (2003-2023). The Net Present Value (NPV) of carbon sequestration between 2003 and 2023 amounts to $27.037 million. These figures demonstrate the changes in carbon dynamics and sequestration within the given timeframe, which reflects both the accumulations and fluctuations in carbon storage. This increase in carbon storage contributes positively to climate change mitigation efforts. In the context of environmental sustainability, the larger carbon storage implies a greater capacity to sequester carbon dioxide from the atmosphere, thereby helping to reduce greenhouse gas concentrations and mitigate the impacts of climate change. This contribution is significant for addressing the challenges associated with global warming and underscores the importance of the studied agroforestry implementation in the Solan District of India. Study conducted by Babbar et al. (2021) in Sariska Tiger Reserve Alwar district of Rajasthan observed that 1.351 Tg carbon has already been lost from 2000 to 2018 in the forest area of Sariska Tiger Reserve and another 0.107 Tg of carbon is expected to be lost in the predicted future, when compared the land use land cover of the year 2035 with the present scenario. The study shows that the economic value of carbon lost from 2000 to 2018 is $ 214.57 million and the economic value of the predicted year 2035, carbon sequestration is worth $ 17.19 million.

Table 48. Cumulative value of Total Carbon sequestration and Net Present Value ($) in Solan District (H.P)

Sr. No	Total Carbon (Tg C)	Value
1	Total Carbon in the year 2003	21.027
2	Total Carbon in the year 2023	22.807
3	Carbon sequestration (Tg C) over a period of 20 year (2003-2023)	1.780
4	NPV of Carbon sequestration from (2003-2023) ($)	27.037 million

Chapter-5

SUMMARY AND CONCLUSION

The present investigations entitled **"Remote sensing approach for estimating agroforestry area, suitability mapping and carbon sequestration potential of agroforestry systems in Solan district of Himachal Pradesh"** were carried out during the year of 2022-2023. The study was aimed at delineating the area under the agroforestry practices, assessment of land suitability to agroforestry in the Solan district and estimation of carbon sequestration potential and using the remote sensing and GIS. For mapping the area under the agroforestry practices vis- à-vis other land use systems, different machine learning algorithms were applied *i.e.*, Maximum Likelihood, Random Forest and Support vector machine.

The Solan district was also assessed for the land suitability to agroforestry practices using two different Multi-Criteria Decision-Making Approaches *i.e.*, Analytic Hierarchy Process (AHP) and Fuzzy-AHP to calculate weight for each criterion and sub-criterions. The 11 criterions including, four topographical parameters (aspect, slope, elevation and hill-shade), two vegetation parameters [land use land cover (LULC) and Normalized Difference Vegetation Index (NDVI), two climate variables (precipitation and temperature) and one soil parameter (soil fertility), two other parameters (distance from road and stream) were considered and weighted overlay to generate the agroforestry suitability map.

The carbon stock and carbon sequestration potential of different land-use land cover classes were estimated by using InVEST (Integrated Valuation of Ecosystem Services and Trade-offs) model. Input parameters that encompass land use maps for the years 2003, 2013, and 2023. For each specific land use category, data on carbon stocks within the four carbon pools, namely living aboveground, belowground, litter and deadwood, and soil organic carbon within the 0-40 cm soil depth range were considered.

A brief summary of the outcomes from current investigations presented as below:

5.1 AGROFORESTRY VIS-À-VIS OTHER LAND USE SYSTEM MAPPING

- According to the maximum likelihood classifier, agroforestry accounts for 450.62 sq. km (23.28%), forests span 871.41 sq. km (45.01%), agriculture covers 171.62 sq. km (8.86%), grassland covers 157.66 sq. km (8.14%), barren land spans 126.14 sq. km (6.52%), built-up areas encompass 134.71 sq. km (6.96%), and water bodies account for 23.85 sq. km (1.23%). In ACZ-I, the forest covers an area of 358.58 sq. km (36.61%), with agroforestry occupying 259.33 sq. km (26.48%), agriculture covers 124.43 sq. km (12.70%), built-up areas span 85.24 sq. km (8.68%), barren land comprises 85.01 sq. km (8.70%), and grassland and water bodies cover 57.47 sq. km (5.87%) and 9.44 sq. km (0.96%), respectively. In the ACZ-II region, the forest covers 512.83 sq. km (53.62%), agroforestry covers 191.29 sq. km (20%), grassland 100.19 sq. km (10.47%), built-up areas 49.70 sq. km (5.20%), and agriculture occupy 47.18 sq. km (4.93%), barren land covers 40.90 sq. km (4.28%), and water bodies comprise 14.41 sq. km (1.51%). The overall accuracy of the MLC recorded as 79.89%, with a corresponding Kappa Coefficient of 0.7305. The agroforestry class exhibits producer accuracy and user accuracy of 85.34% and 76.43%, respectively.
- According to the Random Forest classifier, forest covers 840.14 sq. km (43.40%), agroforestry occupying 509.88 sq. km (26.34%), agricultural 174.87 sq. km (9.03%), grassland 136.09 sq. km (7.03%), built-up areas 131.06 sq. km (6.77%), barren land covers 120.74 sq. km (6.24%), water bodies 23.22 sq. km (1.20%). ACZ-I is mainly covered by forests 350.26 sq. km (35.76%), agroforestry covers 301.79 sq. km (30.81%), agriculture 121.07 sq. km (12.36%), followed by built-up areas (77.48 sq. km or 7.91%), grassland (62.12 sq. km or 6.34%), barren land 57.90 sq. km (5.91%), and water bodies (8.88 sq. km or 0.91%). In ACZ-II, forest covers 489.88 sq. km (51.22%), agroforestry 208.09 sq. km (21.76%), grassland (73.97 sq. km or 7.73%), barren land (62.84 sq. km or 6.57%), built-up areas (53.58 sq. km or 5.60%), agriculture 53.80 sq. km (5.62%) and water bodies 14.34 sq. km (1.50%). RF classifier achieved an overall accuracy of 85.78%, and Kappa Coefficient of 0.8092. The agroforestry class exhibits producer accuracy and user accuracy of 88.56% and 80.81%, respectively.
- According to the Support Vector Machine classifier, forest covers 864.18 sq. km (44.64%) followed by agroforestry 484.52 sq. km (25.03%), 169.72 sq. km (8.77%) agriculture, 144.08 sq. km (7.44%) of grassland, 140.37 sq. km (7.25%) built-up

areas, 108.96 sq. km (5.63%) of barren land and 24.17 sq. km (1.25%) occupied by water bodies. ACZ-I is dominated by expansive forested areas covering 355.5 sq. km (36.29%) of the total area followed by agroforestry 286.48 sq. km (29.25%), agriculture 127.43 sq. km (13.01%), built-up areas with 84.16 sq. km (8.59%), grassland with 57.48 sq. km (5.87%), barren land with 59.08 sq. km (6.03%), and water bodies with 9.37 sq. km (0.96%). In ACZ-II forest covers 508.68 sq. km (53.18%) of the total land followed by agroforestry 198.04 sq. km (20.70%), grassland 86.60 sq. km (9.05%), built-up areas 56.21 sq. km (5.88%), and barren land 49.88 sq. km (5.21%), agriculture 42.29 sq. km (4.42%) and water bodies occupying 14.80 sq. km (1.55%). SVM classifier exhibited an accuracy of 83.22% and a Kappa Coefficient of 0.775. The agroforestry class exhibits producer accuracy and user accuracy of 87.31% and 78.79%, respectively.

- McNemar's test result showed the difference between RF And SVM is not statistically significant as the z-value is 1.8286 (p-value 0.17629**)** which is lower than 1.96. The difference between MLC And SVM is statistically significant as the z-value is 3.82 (p-value 0.0485**)** which is more than 1.96. Similarly, the difference between MLC and RF is also statistically significant as the z value is 4.32 (p-value 0.037514).

5.2 AGROFORESTRY SUITABILITY ASSESSMENT

- The maximum weight in both AHP and Fuzzy AHP was found to be given to LULC criterion (0.261) and followed the trend: LULC> slope > elevation > rainfall > soil fertility> NDVI > aspect hill shade > temperature > stream distance > road distance. The minimum weight (0.012) was found for the distance from road criterion.
- Using AHP approach, about 17.32 per cent area district is categorized as highly suitable for the agroforestry, 22.37 per cent as moderately suitable, 20.19 per cent as marginal suitable, 26.45 per cent as currently not suitable and 13.67 per cent as permanently not suitable. In the ACZ-I, highly suitable areas for agroforestry accounts for 24 per cent, the moderate suitable area 26.6 per cent, marginal suitable accounts 17.2 percent, currently not suitable 23.5 per cent, and permanently not suitable 8.7 per cent. In the ACZ-II, highly suitable areas for agroforestry accounts for 10.5 per cent, the moderate suitable area 18.1 per cent, marginal suitable accounts 23.2 percent, currently not suitable 29.5 per cent, and permanently not suitable 18.8 per cent.

- Using FUZZY-AHP approach, about 11.33 per cent area district is categorized as highly suitable for the agroforestry, 24.76 per cent as moderately suitable, 15.74 per cent as marginal suitable, 26.30 per cent as currently not suitable and 21.87 per cent as permanently not suitable. In the ACZ-I, highly suitable areas for agroforestry accounts for 15.1 per cent, the moderate suitable area 30.9 per cent, marginal suitable accounts 17.6 percent, currently not suitable 20.6 per cent, and permanently not suitable 15.9 per cent. In the ACZ-II, highly suitable areas for agroforestry accounts for 7.4 per cent, the moderate suitable area 18.5 per cent, marginal suitable accounts 13.8 percent, currently not suitable 32.3 per cent, and permanently not suitable 28 per cent.

5.3 Carbon storage and sequestration potential quantification

- In 2003, agriculture area was found to be 194.37 sq.km (10.04%), agroforestry 414.47 sq.km (21.41%), barren land 201.54 sq.km (10.41%), built-up areas 80.15 sq.km (4.14%), open forests 459.03 sq.km (23.71%), moderate forests 293.52 sq.km (15.16%), and dense forests 47.21 sq.km (2.44%), grasslands 216.67 sq.km (11.19%), and water bodies 29.04 sq.km (1.50%). The overall accuracy achieved was 76.75%, with a Kappa Coefficient of 0.7314.
- In 2013, agriculture area was found to be 185.12 sq.km (9.56%), agroforestry 462.32 sq.km (23.88%), barren land 128.16 sq.km (6.62%), built-up areas 106.44 sq.km (5.50%), open forests 404.43 sq.km (20.89%), moderate forests 380.04 sq.km (19.63%), and dense forests 55.95 sq.km (2.89%), grasslands 186.63 sq.km (9.64%), and water bodies 26.92 sq.km (1.39%). The overall accuracy was 77.75%, with a Kappa Coefficient of 0.7446.
- In 2023, agriculture area was found to be 170.77 sq.km (8.82%), agroforestry 487.93 sq.km (25.20%), barren land 87.70 sq.km (4.53%), built-up areas 125.45 sq.km (6.48%), open forests 414.30 sq.km (21.40%), moderate forests 421.08 sq.km (21.75%), and dense forests 53.43 sq.km (2.76%), grasslands 152.50 sq.km (7.88%), and water bodies 22.84 sq.km (2.18%). The overall accuracy achieved was 78.25%, with a Kappa Coefficient of 0.7501.
- In the agricultural landscape from 2003 to 2023, overall decrease of 23.6 sq. km (1.22%) to be found. Agroforestry increased by 73.5 sq. km (3.79%). Barren land representing a decrease of 113.8 sq. km (5.88%). Built-up areas experienced growth

of 45.3 sq. km (2.34%). Overall, there was a net decline of 44.7 sq. km (2.31%) in open forest area from 2003 to 2023. There was an increment of 127.6 sq. km (6.59%) in moderate forest areas from 2003 to 2023. An increment of 6.2 sq. km (0.32%) occurred in dense forest area from 2003 to 2023. The overall decline in the grassland area from 2003 to 2023 amounted to 64.2 sq. km (3.31%). The overall change in the water body area from 2003 to 2023 decreased by 6.2 sq. km (0.32%).

- In 2013, the largest zone, covering an area of 73.44 sq. km (3.79%), carbon values ranging from 0 to 3.17 Mg/900 sq.m, second zone, covering an area of 553.52 sq. km (28.59%) had low carbon values ranging from 3.17 to 6.8 Mg/900 sq.m. The third zone, covering an area of 457.08 sq. km (23.61%), had medium carbon values ranging from 6.8 to 10.95 Mg/900 sq.m. The fourth zone, covering an area of 418.31 sq. km (21.61%) had high carbon values ranging from 10.95 to 15.71 Mg/900 sq.m. Finally, the region had a zone with very high carbon values ranging from 15.71 to 21.15 Mg/900 sq.m, covering an area of 433.66 sq. km (22.40%) of the region.
- In 2023, a total of 97.12 sq. km (5.02%) of the region, had extremely low carbon values ranging from 0 to 3.17 Mg/900 sq.m. Carbon values, ranging from 3.17 to 6.8 Mg/900 sq.m, covered an area of 454.62 sq. km (23.48%). 482.09 sq. km of the area, (24.90%) displayed medium carbon values ranging from 6.8 to 10.95 Mg/900 sq.m. High carbon values, extending from 10.95 to 15.71 Mg/900 sq.m, encompassed 429.59 sq. km (22.19%). An area of 472.58 sq. km (24.41%) of the region, exhibited very high carbon values ranging from 15.71 to 21.15 Mg/900 sq.m.
- In 2003, the open forest ecosystem showcased maximum carbon storage in aboveground carbon (4.084 Tg C) and least in dead litter (0.142 Tg C), followed by moderate forests with aboveground carbon storage at 2.872 Tg C, and dense forests with aboveground carbon storage at 0.685 Tg C. In agroforestry, carbon storage was observed to be maximum in the soil at 1.641 Tg C, followed by barren land with soil carbon storage of 0.520 Tg C, grassland with carbon storage in the soil at 0.736 Tg C, agricultural areas with soil carbon storage of 0.540 Tg C, and the built-up area exhibiting carbon storage of 0.030 Tg C in the soil. The least carbon was stored in built-up belowground 0.003 Tg C.
- In 2013, moderate forests showed the highest carbon storage in aboveground (3.730 Tg C) and least in dead litter 0.217 Tg C, followed by open forests aboveground carbon 3.628 Tg C, dense forests aboveground carbon storage 0.746 Tg C.

Agroforestry displayed maximum carbon storage soil (1.814 Tg C) followed by grassland soil carbon 0.613 Tg C, barren lands soil carbon 0.367 Tg C, agriculture carbon storage in the soil 0.521 Tg C, and the built-up area exhibiting carbon storage of 0.083 Tg C in the soil. The least carbon was stored in built-up belowground 0.008 Tg C.

- In 2023, moderate forests showed the highest carbon in aboveground (4.168 Tg C) and soil (3.212 Tg C) and least in dead litter (0.242 Tg C), followed by open forests aboveground carbon 3.674 Tg C, dense forests aboveground carbon 0.711 Tg C. Agroforestry highest carbon storage in soil 1.918 Tg C, followed by grasslands 0.553 Tg C and agricultural areas soil carbon 0.459 Tg C, barren lands soil carbon reservoir 0.251 Tg, built-up area exhibiting carbon storage of 0.105 Tg C in the soil. The least carbon was stored in built-up belowground 0.011 Tg C.
- In 2003, the carbon storage trend in different land uses found to be: open forest (7.882 Tg C) > moderate forest (5.913 Tg c) > agroforestry (3.285 Tg C)> dense forest (1.364 Tg C)> grassland (0.881 Tg C)> barren land (0.961 Tg C)> agriculture (0.698 Tg C) > built-up (0.045 Tg C). 21.027 Tg C was recorded as total carbon storage for the year.
- In 2013, the carbon storage trend in different land uses found to be: moderate forest (7.677 Tg c) > open forest (7.002 Tg C) >agroforestry (3.631 Tg C)> dense forest (1.515 Tg C)> grassland (0.734 Tg C)> barren land (0.679 Tg C)> agriculture (0.673 Tg C) > built-up (0.122 Tg C). 22.032 Tg C was recorded as total carbon storage for the year.
- In 2023, the carbon storage trend in different land uses found to be: moderate forest (8.579 Tg c) > open forest (7.091 Tg C) >agroforestry (3.839 Tg C)> dense forest (1.425 Tg C)> grassland (0.662 Tg C)> barren land (0.464 Tg C)> agriculture (0.593 Tg C) > built-up (0.154 Tg C). 22.807 Tg C was recorded as total carbon storage for the year.
- Total rate of change in carbon storage from 2003-2023 was found to be -0.005 for agriculture, 0.028 for agroforestry, -0.025 for barren land, 0.005 for built-up, -0.040 for open forest, 0.133 for moderate forest, 0.003 for dense forest and -0.011 for grassland. Overall rate of change was recorded as 0.089 from 2003 to 2023.
- There were five categories of carbon sequestration changes in the district. The first category recorded carbon sequestration (-)21.15 to (-)4.09) Mg/900 sq.m, covering an

area 14.30 per cent, second category (-)4.09 to (-)0.40) Mg/900 sq.m, covering 14.44 per cent. The third (-)0.4 to 0.4 Mg/900 sq.m, covering a maximum area of 38.66 per cent. The fourth category witnessed carbon sequestration 0.40 to 4.1 Mg/900 sq.m, covering 14.20 per cent and carbon sequestration 4.1 to 21.15 Mg/900 sq.m covered 18.41 percent of the district. Total carbon sequestration over a period of 20 years observed was 1.780 Tg C.

- The Net Present Value (NPV) of carbon sequestration (-)21.15 to (-)4.09 Mg/900 sq.m, ranges from (-)376.67 to (-)72.96. In the (-)4.09 to (-)0.40 Mg/900 sq.m range, the NPV ($) varies from (-)72.96 to (-)7.13. Within the range of (-)0.40 to 4.0 Mg/900 sq.m, the NPV ($) records a range of (-)7.13 to 7.13. Moving to the 4.0 to 4.1 Mg/900 sq.m range, the NPV ($) varies from 7.13 to 72.96. Finally, in the 4.1 to 21.15 Mg/900 sq.m range, the NPV ($) ranges from 72.96 to 376.67. The Net Present Value (NPV) of carbon sequestration between 2003 and 2023 amounts to $27.037 million.

CONCLUSION

The findings from our current investigation lead to the conclusion that among the three machine learning classifiers, the random forest classifier demonstrated superior performance in estimating the area under agroforestry practice in Solan district. It achieved an impressive overall accuracy of 85.78%, coupled with a Kappa Coefficient of 0.8092. The analysis revealed that 11-17% of the district is highly suitable for agroforestry, while 22-24% is moderately suitable, and 15-20% falls within the marginally suitable category.

Looking ahead to 2023, the total carbon storage was projected to be 22.807 Tg C, indicating a substantial increase of 1.780 Tg C over the 20-year period from 2003 to 2023. The Net Present Value (NPV) of carbon sequestration was estimated at $27.037 million. The outcomes of this research hold significant implications for decision-makers, scientists, and planners, offering crucial insights for the development and execution of agroforestry policies in Solan District, located in the northwestern Himalayas. This study serves as an indispensable resource, providing essential support for the improvement of rural livelihoods and the strengthening of resilience to climate change impacts. The wealth of information presented is pivotal for making informed decisions and crafting sustainable strategies tailored to the unique needs of the region, promoting its overall development.

LITERATURE CITED

Abebe G, Getachew D and Ewunetu A. 2022. Analysing land use/land cover changes and its dynamics using remote sensing and GIS in Gubalafito district, Northeastern Ethiopia. *SN Applied Sciences*. 4(1):30.

Adam E, Mutanga O, Odindi J, Abdel-Rahman EM. 2014. Land-use/cover classification in a heterogeneous coastal landscape using RapidEye imagery: evaluating the performance of random forest and support vector machines classifiers. *International Journal of Remote Sensing*. 35(10):3440-58.

Ahmad F and Goparaju L. 2016. Geospatial technology in urban forest suitability analysis for Ranchi, Jharkhand, India. *Ecological Questions.* 24:45-57.

Ahmad F and Goparaju L. 2017a. Land evaluation in terms of agroforestry suitability an approach to improve livelihood and reduce poverty a FAO based methodology by geospatial solution a case study of Palamu district, Jharkhand, India. *Ecological Questions* 2:67-84.

Ahmad F and Goparaju L. 2017b. Geospatial approach for Agroforestry Suitability mapping to Enhance Livelihood and Reduce Poverty FAO based documented procedure-case study of Dumka district, Jharkhand, India. *Biosciences Biotechnology Research Asia*. 14(2):651-665.

Ahmad F and Goparaju L. 2017c. Soil and water conservation prioritization using geospatial technology–a case study of part of Subarnarekha Basin, Jharkhand, India. *AIMS Geosciences.* 3:375-395.

Ahmad F, Goparaju L and Qayum A. 2017. Agroforestry suitability analysis based upon nutrient availability mapping a GIS based suitability mapping. *AIMS Agriculture and Food.* 2(2):201- 220.

Ahmad F, Goparaju L and Qayum A. 2019b. FAO guidelines and geospatial application for agroforestry suitability mapping case study of Ranchi, Jharkhand, India. *Agroforestry Systems*. 93(2):531-544.

Ahmad F, Malik MS, Perween S, Akhtar N, Talukdar NR, Dash PC and Kumar SP. 2020a. Land Potentiality Investigation for Agroforestry Purpose using Remote Sensing and GIS. *International Journal of Current Microbiology and Applied Sciences*. 9(11):1683-1691.

Ahmad F, Uddin MM and Goparaju L. 2018a. Assessment of remote sensing and GIS application in identification of land suitability for agroforestry A case study of Samastipur, Bihar India. *Contemporary Trends in Geoscience.* 7:214-228.

Ahmad F, Uddin MM and Goparaju L. 2018b.Geospatial application for agroforestry suitability mapping based on FAO guideline case study of Lohardaga, Jharkhand, India. *Spatial Information Research.* 26:517-526.

Ahmad F, Uddin MM, and Goparaju L. 2019a. Agroforestry suitability mapping of India Geospatial approach based on FAO guidelines. *Agroforestry Systems*. 93:1319-1336.

Ahmad F, Uddin MM, Goparaju L, Dhyani SK, Oli BN and Rizvi J.2021. Tree suitability modeling and mapping in Nepal: A geospatial approach to scaling agroforestry. *Modeling Earth Systems and Environment*. 7:169-179.

Ahmad F, Uddin MM, Goparaju L, Rizvi J and Biradar C. 2020b. Quantification of the land potential for scaling agroforestry in South Asia. *KN-Journal of Cartography and Geographic Information*. 70(2):71-89.

Ahmad T, Sahoo PM and Jally SK. 2016. Estimation of area under agroforestry using high resolution satellite data. *Agroforestry systems*. 90(2):289-303.

Albrecht A and Kandji ST. 2003. Carbon sequestration in tropical agroforestry systems. *Agriculture Ecosystems and Environment*. 99(1-3):115–27.

Ashiagbor G, Asare-Ansah AO, Amoah EB, Asante WA, Mensah YA. 2023. Assessment of machine learning classifiers in mapping the cocoa-forest mosaic landscape of Ghana. *Scientific African*. 20:e01718.

As-Syakur AR, Adnyana IW, Arthana IW, Nuarsa IW. 2012. Enhanced built-up and bareness index (EBBI) for mapping built-up and bare land in an urban area. *Remote sensing*. 4(10):2957-70.

Awad M and Khanna R. 2015. Support vector machines for classification. p 39-66. In: Efficient Learning Machines (eds): Theories, Concepts, and Applications for Engineers and System Designers. Apress Press. Berkeley, California, US.

Ayehu GT and Besufekad SA. 2015. Land Suitability Analysis for Rice Production A GIS Based Multi-Criteria Decision Approach. *American Journal of Geographic Information System*. 4(3):95-104.

Babbar D, Areendran G, Sahana M, Sarma K, Raj K and Sivadas A. 2021. Assessment and prediction of carbon sequestration using Markov chain and InVEST model in Sariska Tiger Reserve, India. *Journal of Cleaner Production*. 278:123333.

Babu BH, Kumar KE, Arya S, Kumari B and Nanda K. 2022. Monitoring and identification of potential agroforestry sites in Panchkula district of Haryana state India using geospatial techniques. *The Pharma Innovation Journal*. 11(5):26-30.

Balaguru B, Britto SJ, Nagamurugan N, Natarajan D, Soosairaj S, Ravipaul S, Arockiasamy DI. 2003. Vegetation mapping and slope characteristics in Shervaryan Hills, Eastern Ghats using remote sensing and GIS. *Current Science*. 10:645-53.

Basheer S, Wang X, Farooque AA, Nawaz RA, Liu K, Adekanmbi T, Liu S. 2022. Comparison of land use land cover classifiers using different satellite imagery and machine learning techniques. *Remote Sensing*. 14(19):4978.

Basukala AK, Oldenburg C, Schellberg J, Sultanov M, Dubovyk O. 2017. Towards improved land use mapping of irrigated croplands: Performance assessment of different image classification algorithms and approaches. *European Journal of Remote Sensing*. 50(1):187-201.

Belgiu M and Dragut L. Random forest in remote sensing: A review of applications and future directions. *ISPRS J Photogrammetry Remote Sensing*. 114:24–31.

Bhardwaj DR, Banday M, Pala NA and Rajput BS. 2016. Variation of biomass and carbon pool with NDVI and altitude in sub-tropical forests of northwestern Himalaya. *Environmental monitoring and assessment*.188:1-13.

Bishaw B, Soolanayakanahally R, Karki U and Hagan E. 2022. Agroforestry for sustainable production and resilient landscapes. *Agroforestry Systems*, 96(3):447-451.

Buckley JJ. 1985. Fuzzy hierarchical analysis. *Fuzzy Sets and Systems*. 17(3).

Cengiz AV, Budak M, Yağmur N, Balçik F. 2023. Comparison between random forest and support vector machine algorithms for LULC classification. *International Journal of Engineering and Geosciences*. 8(1):1-10.

Chavan SB, Keerthika A, Dhyani SK, Handa AK, Newaj R and Rajarajan K. 2015. National Agroforestry Policy in India: a low hanging fruit. *Current Science*. 108:1826-1834.

Cheng J, Cao S and Xu X. 2020. Agroforestry Classification Using Sentinel-2 Imagery and Deep Learning. *Remote Sensing*. 12(4):637.

Chhabra SS .2004. Modelling the effects of scale on mapping trees outside forests. *ITC*

Chu X, Zhan J, Li Z, Zhang F and Qi W. 2019. Assessment on forest carbon sequestration in the Three-North Shelterbelt Program region China. *Journal of Cleaner Production.* 215:382-389

Chuma GB, Cirezi NC, Mondo JM, Mugumaarhahama Y, Ganza DM, Katcho K, Mushagalusa GN and Schmitz S. 2021. Suitability for agroforestry implementation around Itombwe Natural Reserve (RNI), eastern DR Congo: Application of the Analytical Hierarchy Process (AHP) approach in geographic information system tool. *Trees, Forests and People*. 6:100125.

Das T and Das AK. 2014. Mapping and identification of home gardens as a component of the trees outside forests using remote sensing and geographic information system. *Journal of the Indian Society of Remote Sensing.* 42:233-242.

Den Herder M, Moreno G, Mosquera-Losada RM, Palma JH, Sidiropoulou A, Freijanes JJS, Crous-Duran J, Paulo JA, Tomé M, Pantera A and Papanastasis VP. 2017. Current extent and stratification of agroforestry in the European Union. *Agriculture Ecosystems and Environment.* 241:121-132.

DES. 2022. Statistical abstract of Himachal Pradesh 2022-23. Department of Economic and Statistics, Government of Himachal Pradesh, Shimla. 149 p.

Dhyani SK, Handa AK, Prasad R, Alam B, Rizvi RH, Gupta G and Jain A. 2013. Modeling analysis of potential carbon sequestration under existing agroforestry systems in three districts of Indo-Gangetic plains in India. *Agroforestry systems.* 87:1129-1146.

Ekadinata A and Vincent G. 2011. Rubber agroforests in a changing landscape: analysis of land use/cover trajectories in Bungo district, Indonesia. *Forests Trees and Livelihoods*. 20(1):3-14.

Ellis EA, Nair PK, Linehan PE, Beck HW and Blanche CA. 2000. A GIS-based database management application for agroforestry planning and tree selection. *Computers and Electronics in Agriculture.* 27:41-55.

Erdanaev E, Kappas M and Wyss D. 2022. The Identification of Irrigated Crop Types Using Support Vector Machine Random Forest and Maximum Likelihood Classification Methods with Sentinel-2 Data in 2018: Tashkent Province Uzbekistan. *International Journal of Geoinformatics*. 18(2).

FAO. 2015. Mapping tree cover and loss using satellite data: A primer Food and Agriculture Organization of the United Nations.

FAO. 2020. Terms and Definitions Forest Resource Assessment: Forest Resources Assessment Working Paper 188; Food and Agriculture Organisation of United Nations: Rome Italy.

Feliciano D, Ledo A, Hillier J and Nayak DR. 2018. Which agroforestry options give the greatest soil and above ground carbon benefits in different world regions? *Agriculture Ecosystems and Environment.* 254:117–129.

Foody GM. 2004. Thematic Map Comparison: Evaluating the Statistical Significance of Differences in Classification Accuracy. *Photogrammetric Engineering and Remote Sensing.* 70(5): 627–633.

FSI. 2020. Trees Outside Forest Resources in India. FSI Technical Information Series. Ministry of Environment, Forest and Climate Change, Dehradun, Uttarakhand, India. 2(1). 30 p.

Ganz S, Adler P and Kändler G. 2020. Forest cover mapping based on a combination of aerial images and Sentinel-2 satellite data compared to National Forest Inventory data. *Forests*. 11(12):1322.

Gomes AC, Bernardo N and Alcântara E. 2017. Accessing the southeastern Brazil 2014 drought severity on the vegetation health by satellite image. *Natural Hazards*. 89:1401-1420.

Gumus AT. 2009. Evaluation of hazardous waste transportation firms by using a two-step fuzzy-AHP and TOPSIS methodology. *Expert systems with applications*, *36*(2):4067-4074.

Gungor E and Sevinc AY. 2020. Prioritization of Criteria and Tree Species in Agroforestry. *Bartın Orman Fakültesi Dergisi*. 22(1):185-198.

Gupta S, Nainwal A, Anand S and Singh S. 2017. Valuation of carbon sequestration in Bidhalna micro watershed Uttarakhand India using InVEST model. *International Journal of Advancement in Earth Environment Sciences.* 5:10-15.

Handa AK, Dhyani SK, Bhat GM, Malik AR, Dutt V, Masoodi TH, Jain U and Jain A. 2017.Quantification of carbon stocks and sequestration potential through existing 25 agroforestry systems in the hilly Kupwara district of Kashmir valley in India Current science 113:782-785.

Hassanin MOHD, Kanga SHRUTI, Farooq MAJID, and Singh SK. 2020. Mapping of Trees outside Forest (ToF) from Sentinel-2 MSI satellite data using object-based image analysis. *Gujarat Agricultural Universities Research Journal*. 207:204-213.

He Y, Kuang Y, Zhao Y and Ruan Z. 2021. Spatial correlation between ecosystem services and human disturbances: A case study of the Guangdong–Hong Kong–Macao Greater Bay Area China. *Remote Sensing*. 13(6):1174.

He Y, Ma J, Zhang C and Yang H. 2023. Spatio-Temporal Evolution and Prediction of Carbon Storage in Guilin Based on FLUS and InVEST Models. *Remote Sensing*. 15(5):1445.

Hein L, Van Koppen K, De Groot RS, Van Ierland EC. 2006. Spatial scales stakeholders and the valuation of ecosystem services. *Ecological Economics*. 57(2):209-228.

Hopkins LD. 1977. Methods for generating land suitability maps: a comparative evaluation. *Journal of the American institute of planners.* 43(4):386-400.

Houghton RA. 2003. Why are estimates of the terrestrial carbon balance so different? *Global change biology.* 9(4):500-509.

Houssoukpèvi IA, Le Maire G, Aholoukpè HNS, Fassinou DJM, Amadji G L, Chapuis-Lardy L and Chevallier T. 2023. Effect of land use change on carbon stocks in an agricultural region of southern Benin. *Land Degradation and Development.* 34(5):1447-1463.

Imran M and Din NU. 2021. Geospatially mapping carbon stock for mountainous forest classes using InVEST model and Sentinel-2 data: a case of Bagrote valley in the Karakoram range. *Arabian Journal of Geosciences*. 14(9):756.

IPCC. 2014. Mitigation of climate change. Contribution of Working Group III to the Fifth Assessment Report of the Intergovernmental Panel on Climate Change. Cambridge University Press, Cambridge, United Kingdom and New York, USA. 1435 p.

IPCC. 2022. Impacts, Adaptation and Vulnerability. Contribution of Working Group II to the Sixth Assessment Report of the Intergovernmental Panel on Climate Change. Cambridge University Press. Cambridge University Press, Cambridge, UK and New York, USA. 3056 p.

ISFR. 2003. Forest Survey of India. Ministry of Environment, Forest and Climate Change, Dehradun, Uttarakhand, India.

ISFR. 2013. Forest Survey of India. Ministry of Environment, Forest and Climate Change, Dehradun, Uttarakhand, India.

ISFR. 2021. Forest Survey of India. Ministry of Environment, Forest and Climate Change, Dehradun, Uttarakhand, India.

Islam I, Cui S, Hoque MZ, Abdullah HM, Tonny KF, Ahmed M, Ferdush J, Xu L and Ding S. 2022.Dynamics of tree outside forest land cover development and ecosystem carbon storage change in eastern coastal zone Bangladesh. *Land*. 11(1):76.

Jahan H, Rahman MW, Islam MS, Rezwan-Al-Ramim A, Tuhin MMUJ and Hossain ME. 2022. Adoption of agroforestry practices in Bangladesh as a climate change mitigation option: Investment drivers and SWOT analysis perspectives. *Environmental Challenges.* 7:100509.

Kafy AA, Naim MNH, Subramanyam G, Ahmed NU, Al-Rakib A, Kona MA and Sattar GS. 2021. Cellular Automata approach in dynamic modelling of land cover changes using Rapid Eye images in Dhaka, Bangladesh. *Environmental Challenges*. 4. 100084 p.

Kafy AA, Saha M, Fattah MA, Rahman MT, Duti BM, Rahaman ZA, Bakshi A, Kalaivani S, Rahaman SN and Sattar GS. 2023. Integrating forest cover change and carbon storage dynamics: Leveraging Google Earth Engine and InVEST model to inform conservation in hilly regions. *Ecological Indicators*. 152 :110374.

Kahsay A, Haile M, Gebresamuel G and Mohammed M. 2018. Land suitability analysis for sorghum crop production in northern semi-arid Ethiopia: Application of GIS-based fuzzy AHP approach. *Cogent food and agriculture*. 4(1):1507184.

Karlen DL, Stott DE, Cambardella CA, Kremer RJ, King KW and McCarty GW. 2014. Surface soil quality in five midwestern cropland conservation Effects Assessment Project watersheds. Journal of Soil and Water Conservation. 69: 393-401.S

Kaufmann A and Gupta MM. 1988. Fuzzy mathematical models in engineering and management science.

Kaul M, Mohran GMJ and Dadhwal VK. 2010. Carbon storage and sequestration potential of selected tree species in India. *Mitigation and Adaptation Strategies for Global Change.* 15:489-510

Kaur S, Babbar D, Sarif O, Ghatak A and Jaafari A. 2022. Assessment of Carbon Sequestration Using InVEST Model in Delhi, India. *Conservation, Management and Monitoring of Forest Resources in India.* 33-56 p.

Kavzoglu T, Bilucan F and Teke A. 2020. Comparison of support vector machines random forest and decision tree methods for classification of sentinel-2A image using different band combinations. In:*41st Asian Conference on Remote Sensing, ACRS*. 41:1-8.

Kogo BK, Kumar L and Koech R. 2021. Analysis of spatio-temporal dynamics of land use and cover changes in Western Kenya. *Geocarto International*. 36(4):376-91.

Kumar D, Rizvi RH, Bhatt S, Singh R and Chaturvedi OP. 2021. Land use/land cover change and soil fertility mapping using GIS and remote sensing: A case study of Parasai-Sindh watershed in Bundelkhand region of central India. *Range Management and Agroforestry*. 42(1):15-21.

Kumar M, Kumar R, Bishnoi P, Sihag V, Bishnoi R, Rani S, Sindhu P, Budhwar S, Kumar P, Sharma S, Sharma P, Sharma R, Pandey V, Dahhiya M, Arya VS, Singh TP and Kumar V. 2021. A geo-spatial approach to assess Trees outside Forest (ToF) in Haryana State, India. *Land Degradation and Development*. 32(13): 3588-3597.

Kumar P, Kaur P, Chakraborty M and Shukla Y. 2019. Estimation of Agroforestry Plantation Area Using High-Resolution Satellite Imagery and GIS. *Journal of the Indian Society of Remote Sensing*. 47(5):787-796.

Kumar S, Kumar S, Kumar KM and Hooda RS. 2014. Mapping of Tree Outside Forest in Kalesar Block Yamunanagar District, Haryana using Geo-Informatics Techniques. *International Journal of Science Environment and Technology.* 3(5):1835-1842.

KVG RK and Barik DK. 2018. Assessment of carbon storage and erosion using invest model in Visakhapatnam district Andhra Pradesh. *Journal of Rural Development.* 207-220 p.

Lahiji RN, Dinan NM, Liaghati H, Ghaffarzadeh H, Vafaeinejad A. 2020. Scenario-based estimation of catchment carbon storage: Linking multi-objective land allocation with InVEST model in a mixed agriculture-forest landscape. *Frontiers of Earth Science*. 14:637-46.

Leeuw JD, Jia H, Yang L, Liu X, Schmidt K and Skidmore AK. 2006. Comparing Accuracy Assessments to Infer Superiority of Image Classification Methods. *International Journal of Remote Sensing*. 27(1): 223–232.

Li K, Cao J, Adamowski JF, Biswas A, Zhou J, Liu Y, Zhang Y, Liu C, Dong X and Qin Y. 2021. Assessing the effects of ecological engineering on spatiotemporal dynamics of carbon storage from 2000 to 2016 in the Loess Plateau area using the InVEST model: A case study in Huining County, China. *Environmental Development.* 39:100641.

Li Y, Liu Z, Li S and Li X. 2022. Multi-scenario simulation analysis of land use and carbon storage changes in Changchun city based on FLUS and InVEST model. *Land*. *11*(5):647.

Liang Y, Liu L and Huang J. 2017. Integrating the SD-CLUE-S and InVEST models into assessment of oasis carbon storage in northwestern, China. *PLoS One*. 12(2): e0172494.

Liu S, Brandt M, Nord-Larsen T, Chave J, Reiner F, Lang N and Fensholt R. 2023. The overlooked contribution of trees outside forests to tree cover and woody biomass across Europe. *Science Advances.* 9(37): 4097.

Longley PA, Goodchild MF, Maguire DJ and Rhind DW. 2005. Geographic information systems and science (1st ed). Wiley Publisher. 517 p.

Luedeling E, Sileshi G, Beedy T and Dietz J. 2011. Carbon Sequestration Potential of Agroforestry Systems in Africa. *Carbon sequestration potential of agroforestry systems: Opportunities and challenges.* 8: 61–83.

Mahato S, Dasgupta S, Todaria NP and Singh VP. 2016. Agroforestry mapping and characterization in four districts of Garhwal Himalaya. *Energy, Ecology and Environment*. 1: 86-97.

Mahato S, Dasgupta S, Todaria NP and Singh VP. Agroforestry mapping and characterization in four districts of Garhwal Himalaya. *Energy, Ecology and Environment*. 1:86-97.

Malkoc E Rüetschi M Ginzler C and Waser L T2021Countrywide mapping of trees outside forests based on remote sensing data in Switzerland. *International Journal of Applied Earth Observation and Geoinformation.* 100:102336.

Meneguzzo DM, Liknes GC and Nelson MD. 2013. Mapping trees outside forests using high-resolution aerial imagery: a comparison of pixel-and object-based classification approaches. *Environmental monitoring and assessment*. 185:6261-6275.

Mengist W, Soromessa T and Feyisa GL. 2023. Responses of carbon sequestration service for landscape dynamics in the Kaffa biosphere reserve southwest Ethiopia. *Environmental Impact Assessment Review*. 98:106960.

Mushtaq R, Yadav RK, Fayaz FA, Ahmed P and Singh H. 2023. Multi-criteria land suitability assessment for mulberry-based agroforestry using AHP and GIS approach in Anantnag district of the Kashmir valley India to achieve sustainable agriculture. *Environment Development and Sustainability.* 1-23 p.

Nair PKR, Kumar BM and Nair VD. 2009. Agroforestry as a strategy for carbon sequestration. *Journal of plant nutrition and soil science.* 172:10–23.

Nair PR, Kumar BM, Nair VD, Nair PR, Kumar BM and Nair VD. 2021. Historical Developments: The Coming of Age of Agroforestry. *An Introduction to Agroforestry: Four Decades of Scientific Developments*. 3-20 p.

Nandasena WDKV, Brabyn L, and Serrao-Neumann S. 2022. Using Google Earth Engine to classify unique forest and agroforest classes using a mix of Sentinel 2a spectral data and topographical features: a Sri Lanka case study. *Geocarto International*. 37(25):9544-9559.

Nath AJ, Kumar R, Devi NB, Rocky P, Giri K, Sahoo UK and Pandey R. 2021. Agroforestry land suitability analysis in the Eastern Indian Himalayan region. *Environmental Challenges*. 4:100199.

Newaj R, Rizvi RH, Chaturvedi OP, Alam B, Prasad R, Kumar D and Handa AK. 2017. A Country Level Assessment of Area under Agroforestry and its Carbon Sequestration Potential. *Technical bulletin*. 48 p.

Ngwijabagabo H, Niyonzima T, Nyandwi E, Hirwa H, Nishyirimbere A, Mwizerwa F, Hategekimana G, Barifashe T, Uwera D. 2021. Spatial suitability analysis and mapping of Agroforestry areas. Case study of Musanze District in Northern Province of Rwanda. *Rwanda Journal of Engineering, Science, Technology and Environment*. 4(1).

Olofsson P, Herold M, Stehman SV, Woodcock CE and Wulder MA. 2014. Good practices for estimating area and assessing accuracy of land change. *Remote Sensing of Environment*. 148:42-57.

Ottosen TB, Petch G, Hanson M and Skjoth CA. 2020. Tree cover mapping based on Sentinel-2 images demonstrate high thematic accuracy in Europe. *International Journal Appiled Earth Observation and Geoinformatics*. 84:0101947.

Ozkan B, Dengiz O and Turan İD. 2020. Site suitability analysis for potential agricultural land with spatial fuzzy multi-criteria decision analysis in regional scale under semi-arid terrestrial ecosystem. *Scientific reports*.10(1):22074.

Panwar P, Mahalingappa DG, Kaushal R, Bhardwaj DR, Chakravarty S, Shukla G, Thakur NS, Chavan SB, Pal S, Nayak BG and Srinivasaiah HT. 2022. Biomass production and carbon sequestration potential of different agroforestry systems in India: A critical review. *Forests.* 13(8):1274.

Paquit J. 2017. Modeling the spatial pattern of carbon stock in Central Mindanao University using inVEST tool. *Journal of Biodiversity and Environmental Sciences*. 10(4):103-113.

Pechanec V, Purkyt J, Benc A, Nwaogu C, Sterbova L and Cudlín P. 2018. Modelling of the carbon sequestration and its prediction under climate change. *Ecological Informatics.* 47:50-54.

Pujar GS, Dadhwal VK, Murthy MSR, Trivedi S, Reddy PM, Swapna D and Jha CS. 2016. Geospatial approach for national level TOF assessment using IRS high resolution IMAGINE early results. *Journal of the Indian Society of Remote Sensing*. 44:321-333.

Qian Y, Zhou W, Yan J, Li W, Han L. 2014. Comparing machine learning classifiers for object-based land cover classification using very high-resolution imagery. *Remote Sensing*. 7(1):153-68.

Rahman A, Kumar S, Fazal S, Siddiqui MA. 2012. Assessment of land use/land cover change in the North-West District of Delhi using remote sensing and GIS techniques. *Journal of the Indian Society of Remote Sensing*. 40:689-97.

Rahmawaty R, Batubara R, Rauf A and Frastika S. 2020a. Mapping of land suitability for rambutan (Nephelium lappaceum) in community agroforestry land at Gunung Ambat Village and Simpang Kuta Buluh Village. *Journal of Tropical Soils*. 25(2):107-117.

Rahmawaty R, Frastika S, Rauf A, Batubara R and Harahap FS. 2020b. Land suitability assessment for Lansium domesticum cultivation on agroforestry land using matching method and geographic information system. *Biodiversitas Journal of Biological Diversity*. 21(8).

Rawat JK, Dasgupta S, Kumar R, Kumar A and Chauhan KVS. 2003. Training manual on inventory of trees outside forests (TOF).

Rawat JS, Biswas V and Kumar M. 2013. Changes in land use/cover using geospatial techniques: A case study of Ramnagar town area, district Nainital, Uttarakhand, India. *The Egyptian Journal of Remote Sensing and Space Science*. 16(1):111-7.

Reppin S, Kuyah S, Neergaard A, Oelofse M and Rosenstock TS. 2020. Contribution of agroforestry to climate change mitigation and livelihoods in Western Kenya. *Agroforestry Systems*. 94:203-220.

Ritung S, Wahyunto FA and Hidayat H. 2007. Land Suitability Evaluation with a case map of Aceh Barat District, Indonesian Soil Research Institute and World Agro Centre Bogor Indonesia.

Rizvi RH, Dhyani SK, Newaj R, Karmakar PS and Saxena A. 2014. Mapping agroforestry area in India through remote sensing and preliminary estimates. *Indian Farming*. 63:62–64.

Rizvi RH, Dhyani SK, Newaj R, Saxena A and Karmakar PS. 2013. Mapping extent of agroforestry area through remote sensing issues estimates and methodology. *Indian Journal of Agroforestry*. 15(2):26-30.

Rizvi RH, Handa AK, Alam B, Chavan SB, and Prasad R. 2020a. Mapping of tree species and assessment of area under agroforestry systems in Karnataka, India. *Indian Journal of Agroforestry*. 22:16-20.

Rizvi RH, Handa AK, Sridhar KB, Kumar A, Bhaskar S and Chaudhari SK. 2020b. Mapping agroforestry and trees outside forest. ICAR, Central Agroforestry Research Institute, (CAFRI), Jhansi and World Agroforestry ICRAF South Asia Regional Programme, New Delhi.

Rizvi RH, Newaj R, Chaturvedi OP, Prasad R, Alam B, Handa AK, Karmakar PS, Saxena A, Singh A, Singh K and Chaturvedi M .2017a. Mitigating climate vagaries through adoption of agroforestry land use in Maharashtra, India. *Indian Journal of Agricultural Sciences* 87:1524– 1527.

Rizvi RH, Newaj R, Chaturvedi OP, Prasad R, Handa AK and Alam B. 2019d. Carbon sequestration and CO_2 absorption by agroforestry systems: An assessment for Central Plateau and Hill region of India. *Journal of Earth System Science*. 128:1-9 27.

Rizvi RH, Newaj R, Dhyani SK, Karmakar PS, Saxena A and Airon B. 2015. Role of Geospatial Technologies to Estimate Extent of Agroforestry Area in India: An Initiative. Biotech Books, New Delhi.

Rizvi RH, Newaj R, Handa AK, Sridhar KB and Kumar A. 2019b. Agroforestry mapping in India through geospatial technologies present status and way forward. *Technical Bulletin.* 1:1-35.

Rizvi RH, Newaj R, Handa AK, Sridhar KB and Kumar A. 2019c. Agroforestry mapping in India through geospatial technologies Present status and way forward. *Technical Bulletin.* 1:1- 35.

Rizvi RH, Newaj R, Karmakar PS, Saxena A and Dhyani SK. 2016a. Remote sensing analysis of agroforestry in Bathinda and Patiala districts of Punjab using sub-pixel method and medium resolution data. *Journal of the Indian Society of Remote Sensing*. 44(4):657-664.

Rizvi RH, Newaj R, Karmakar PS, Saxena A, Maurya A and Jain A. 2017b. Agroforestry and grassland mapping in two districts of Uttarakhand through geospatial technology. *Range Management and Agroforestry*. 38:254-258.

Rizvi RH, Newaj R, Prasad R, Handa AK, Alam B, Chavan SB, Saxena A, Karmakar PS, Jain A, Chaturvedi M. 2016b. Assessment of carbon storage potential and area under agroforestry systems in Gujarat Plains by CO2FIX model and remote sensing techniques. *Current science*. 25:2005-11.

Rizvi RH, Newaj R, Srivastava S and Yadav M. 2019a. Mapping Trees on Farmlands Using OBIA Method and High-Resolution Satellite Data: A Case Study of Koraput District, Odisha. *The International Archives of the Photogrammetry, Remote Sensing and Spatial Information Sciences*. 42:617-621.

Rizvi RH, Vishnu R, Handa AK, Ramanan S, Yadav M, Mehdi A and Qaisar N. 2021. Mapping of agroforestry systems and Salix species in Western Himalaya agroclimatic zone of India. *Current science (00113891121)*. 121(10):1347-1351.

Rizvi RH, Yadav RS, Singh R, Datt K, Khan IA and Dhyani SK. 2009. Spectral analysis of remote sensing image for assessment of agroforestry areas in Yamunanagar district, of Haryana. National Symposium on Advances in Geo-spatial Technologies with Special Emphasis on Sustainable Rainfed Agriculture, RRSSC Nagpur. 7.

Rodcha R, Tripathi NK, Prasad Shrestha R. 2019. Comparison of cash crop suitability assessment using parametric, AHP, and FAHP methods. *Land*. 8(5):79.

Rosenstock TS, Dawson IK, Aynekulu E, Chomba S, Degrande A, Fornace K, Jamnadass R, Kimaro A, Kindt R, Lamanna C, Malesu M, Mausch K, McMullin S, Murage P, Namoi N, Njenga M, Nyoka I, Valencia AM, Sola P, Shepherd K, Steward P.2019. A planetary health perspective on agroforestry in Sub-Saharan Africa. *One Earth.* 1(3):330–344.

Rwanga SS and Ndambuki JM.2017. Accuracy assessment of land use/land cover classification using remote sensing and GIS. *International Journal of Geosciences.* 8(04):611.

Saaty TL. 1977. A scaling method for priorities in hierarchical structures. *Journal of mathematical psychology.* 15(3):234-81.

Saaty TL. 1980. The analytic hierarchy process McGraw hill, New York. *Agricultural Economics Review.* 70(804):10-21236.

Sanneh A. 2007. Status of carbon stock under different land use systems in wet temperate North Western Himalaya. M.Sc.Thesis. Dr Y.S. Parmar University of Horticulture and Forestry, Nauni, Solan, (H.P.), India. 81 p.

Sarathchandra C, Alemu AY, Worthy FR, Lakmali WI, Ma H, Yingfeng B, Jiayu G, Chen H, Yan Q, Geng Y and Weragoda DS. 2021. Impact of land use and land cover changes on carbon storage in rubber dominated tropical Xishuangbanna South West China. *Ecosystem Health and Sustainability.* 7(1): 1915183.

Sarti M, Ciolfi M, Lauteri M, Paris P and Chiocchini F. 2021. Trees outside forest in Italian agroforestry landscapes detection and mapping using sentinel-2 imagery. *European Journal of Remote Sensing*. 54: 609-623.

Shalaby A and Tateishi R. 2007. Remote sensing and GIS for mapping and monitoring land cover and land-use changes in the Northwestern coastal zone of Egypt. *Applied geography*. 27(1):28-41.

Sharma P. 2022. Geospatial estimation of agroforestry area, suitability mapping and carbon sequestration potential of Agroforestry systems in Kangra district of Himachal Pradesh. (Ph.D. Thesis) Dr. YS Parmar University of Horticulture and Forestry, Nauni, Solan, Himachal Pradesh, India. 132 p.

Sheykhmousa M, Mahdianpari M, Ghanbari H, Mohammadimanesh F, Ghamisi P and Homayouni S. 2020. Support vector machine versus random forest for remote sensing image classification: A meta-analysis and systematic review. *IEEE Journal of Selected Topics in Applied Earth Observations and Remote Sensing*. 13:6308-6325.

Singh M, Gupta B, Sarvade S and Awasthe RK. 2015. Biomass and carbon sequestration potential in different agroforestry systems in Giri catchment of North Western Indian Himalaya. *Indian Journal of Agroforestry*. *17*(2):42-48.

Singh RK, Behera MD, Das P, Rizvi J, Dhyani SK, Biradar CM. 2022. Agroforestry suitability for planning site-specific interventions using machine learning approaches. *Sustainability*. 14(9):5189.

Singha C and Swain KC. 2016. Land suitability evaluation criteria for agricultural crop selection: A review. *Agricultural reviews*. 37(2):125-32.

Sisodia PS, Tiwari V and Kumar A. 2014. Analysis of supervised maximum likelihood classification for remote sensing image, p 1-4. In: International conference on recent advances and innovations in engineering (ICRAIE-2014).

Sloan DS. 1992. A Review of: Fuzzy set theory and its applications Second Edition. *International Journal Of General System*. 21(1):117–119.

Taloor AK, Kumar V, Singh VK, Singh AK, Kale RV, Sharma R, Khajuria V, Raina G, Kouser B and Chowdhary NH. 2020. Land use land cover dynamics using remote sensing and GIS Techniques in Western Doon Valley, Uttarakhand, India. p 37-51. In: Sahdev S, Singh R, Kumar M. (eds). Geoecology of Landscape Dynamics: Advances in Geographical and Environmental Sciences. Springer Publication. Singapore.

Talukdar S, Singha P, Mahato S, Pal S, Liou YA and Rahman A. 2020. Land-use land cover classification by machine learning classifiers for satellite observations-A review. *Remote Sensing.* 12(7):1135.

Tao Y, Tian L, Wang C and Dai W. 2023. Dynamic simulation of land use and land cover and its effect on carbon storage in the Nanjing metropolitan circle under different development scenarios. *Frontiers in Ecology and Evolution.* 11:1102015.

Tassew T. 2017. Assessing and mapping ecosystem services of trees outside forest. *Journal of Ecology and the Natural Environment.* 9(9):151-164.

Tauqeer A, Sahoo PM and Jally SK. 2016. Estimation of area under agroforestry using high resolution satellite data. *Agroforestry Systems*. 90:289-303.

Topuz M and Deniz M. 2023. Application of GIS and AHP for land use suitability analysis: case of Demirci district, Turkey. *Humanities and Social Sciences Communications.* 10(1)1-15.

Torralba M, Fagerholm N, Burgess PJ, Moreno G, Plieninger T. 2016. Do European agroforestry systems enhance biodiversity and ecosystem services? A meta-analysis. *Agriculture, ecosystems and environment*. 230:150–161.

Toyi MS, Barima S, Mama A, Andre M, Bastin JF, De Cannière C, Sinsin B and Bogaert J. 2013. Tree plantation will not compensate natural woody vegetation cover loss in the Atlantic Department of Southern Benin. *Tropicultura*. 31(1).

Vaidya P, Bhardwaj SK and Sood S. 2017. Regional land Use/Land cover change dynamics and drivers for mid-hills of Solan district, Himachal Pradesh Indian. *Journal of Ecology*. 44:914- 918.

Vens C and Costa F. 2011. Random forest-based feature induction. p 744-753. In:2011 IEEE 11th International conference on data mining.

Vikrant KK, Chauhan DS, Rizvi RH and Maurya A. 2018. Mapping the extent of agroforestry area in different altitudes of Tehri District, North Western Himalaya, India through GIS and remote sensing data. *Journal of the Indian Society of Remote Sensing*. 46:1471-1480.

Wani AA, Joshi PK, and Singh O. 2014. Mapping agroforestry cover and trend in the southern region of Kashmir Himalayas using remote sensing and GIS (abstr). Agricultural Science Congress, Organic Agriculture Prospects in Jammu and Kashmir. 68

World Bank. 2004. Sustaining forests: a development strategy. The World Bank, Washington DC, US.

Xu L, Fang K, Huang Y and Xu S. 2023. Demand Priority of Green Space from the Perspective of Carbon Emissions and Storage. *Sustainability*. 15(14):11199.

Yadav Y, Chhetri BBK, Raymajhi S, Tiwari K and Sitaula B. 2019. Dynamics of land use land cover change and mapping of tree outside forest (TOF) in Terai Nepal. *International Journal of Environmental Science and Technology*. 19(1):4-9.

Yohe G, Lasco R, Ahmad QK, UK NA, Cohen S, Janetos T, Perez R, Ebi K, Lankao PR, Malone E, Malone T. 2006. Perspectives on climate change and sustainability 3. *Change*. 15(39):40.

Zahoor S, Wani AA, Masoodi TH, Islam MA, Gatoo AA and Gangoo SA. 2020. Land Use Land Cover Classification and Mapping using Geospatial Techniques in Ganderbal District, J and K. *International Journal of Current Microbiology and Applied Sciences*. 9(11):3838-3847.

Zhang F, Xu N, Wang C, Wu F and Chu X. 2020. Effects of land use and land cover change on carbon sequestration and adaptive management in Shanghai China. *Physics and Chemistry of the Earth Parts A/B/C*. 120:102948.

Zhang J, Su Y, Wu J and Liang H. 2015. GIS based land suitability assessment for tobacco production using AHP and fuzzy set in Shandong province of China. *Computers and Electronics in Agriculture.*114: 202-211.

Zhang S, Liu X, Wang X, Gao Y and Yang Q. 2021. Evaluation of coffee ecological adaptability using Fuzzy AHP and GIS in Yunnan Province, China. *Arabian Journal of Geosciences*. 14: 1-18.

Zhang Y, Xin Y, Li Q, Ma J, Li S, Lv X, Lv W. 2017. Empirical study of seven data mining algorithms on different characteristics of datasets for biomedical classification applications. *Biomedical engineering online*. 16(1):1-5.

Zhao M, He Z, Du J, Chen L, Lin P and Fang S. 2019. Assessing the effects of ecological engineering on carbon storage by linking the CA-Markov and InVEST models. *Ecological Indicators*. 98:29-38.

Zheng H and Zheng H. 2023. Assessment and prediction of carbon storage based on land use/land cover dynamics in the coastal area of Shandong Province. *Ecological Indicators.* 153:110474.

Zomer RJ, Bossio DA, Trabucco A, Yuanjie L, Gupta DC and Singh VP. 2007. Trees and water Smallholder agroforestry on irrigated lands in Northern India Colombo, Sri Lanka. International Water Management Institute. 47 p.

APPENDIX-I

Land use patterns of Solan district (Statistical outline of Himachal Pradesh 2022-23)

Land-use pattern	Geographical area	Net sown area	Forest area	Land under non-agricultural uses	Permanent pastures and other grazing land	Cultural waste	Land under misc. tree	Barren and unculturable land	Current fallow	Other fallows	Total cropped area
Hectare	193600	31532	21233	15821	74818	14244	492	10276	9293	3326	56055

(State of Forest Report -2003)-Himachal Pradesh District-Solan

Land-use pattern	Geographical area	Very Dense Forest	Moderately Dense Forest	Open Forest	Proportion of Forest Cover to District Geographic Cover to Area (%)
Km^2	1936	39	314	466	42.03

(State of Forest Report -2013)-Himachal Pradesh District-Solan

Land-use pattern	Geographical area	Very Dense Forest	Moderately Dense Forest	Open Forest	Proportion of Forest Cover to District Geographic Cover to Area (%)	Scrub
Km^2	1936	55	404	391	43.90	38

(State of Forest Report -2021)-Himachal Pradesh District-Solan

Land-use pattern	Geographical area	Very Dense Forest	Moderately Dense Forest	Open Forest	Proportion of Forest Cover to District Geographic Cover to Area (%)	Scrub
Km^2	1936	43.78	443.56	403.52	46.02	52.33

APPENDIX-II

Pairwise comparison matric for different soil nutrient data layers for multi-criteria including weights, maximum eigen value (λmax) and consistency ratio (CR)

Criteria	N	P	K	B	Mg	Weights
N	1	1	1	9	9	**0.310**
P	1	1	1	9	9	**0.310**
K	1	1	1	9	9	**0.310**
B	1/9	1/9	1/9	1	1	**0.035**
Mg	1/9	1/9	1/9	1	1	**0.035**

Λmax=5.37654, CR=0.083709

Pairwise comparison matric for different soil characteristics data layers for multi-criteria including weights, maximum eigen value (λmax) and consistency ratio (CR)

Criteria	Soil particle	OC	CEC	BD	pH	Weight
Soil particle	1	3	4	5	7	**0.447**
OC	1/3	1	3	4	6	**0.255**
CEC	1/4	1/3	1	3	5	**0.150**
pH	1/5	1/4	1/3	1	3	**0.099**
BD	1/7	1/6	1/5	1	1	**0.049**

Λmax= 5.380401, CR=0.084567

Area and percentile distributions of the soil nutrient, soil characteristics and soil fertility's main and sub-criteria parameters in the study area.

Main criteria	Sub-criteria	Area (sq.km)	Area (%)
Soil nutrient			
Available N	Low (<280 kg/ha)	1056.28	54.56
	Medium (280-500	879.72	45.44
Available P	Medium (10-25 kg/ha)	260.39	13.45
	High (>25kg/ha)	1675.61	86.55
Available K	Medium (118-280	613.13	31.67
	High (>280 kg/ha)	1322.87	68.33
Available Mg	Sufficient (>1.0 c	1071.38	55.34
	Deficient (<1.0 c	864.62	44.66
Available B	Deficient (<0.5ppm)	51.69	2.67
	Sufficient (>0.5ppm)	1884.31	97.33
Soil characteristics			
Soil texture	Loam	1462.84	75.56
	sandy loam	438.31	22.64
	Clay loam	34.85	1.8
OC	Medium (5-10 g/kg)	1170.96	60.48
	High (>10 g/kg)	765.04	39.52
CEC (c mol/kg)	0-9	15.49	0.8
	9-14.2	181.98	9.4
	14.2-17.5	958.32	49.5
	17.5-19.2	685.34	35.4
	19.2-22.2	94.86	4.9
pH	Acidic (<6.5)	745.36	38.5
	Neutral (6.5-7.5)	1190.64	61.5
Bulk Density (kg/dm^3)	0.00	22.84	1.18
	0-1.21	421.27	21.76
	1.21-1.26	601.52	31.07
	1.26-1.32	562.21	29.04
	1.32-1.41	328.15	16.95
Soil fertility			
Soil nutrient (AHP)	very low	94.67	4.89
	low	423.23	21.86
	medium	268.65	13.88
	high	361.23	18.66
	very high	788.22	40.71
Soil nutrient (Fuzzy-AHP)	very low	37.89	1.96
	low	476.23	24.60
	medium	278.45	14.38
	high	446.11	23.04
	very high	697.32	36.02
Soil characteristic (AHP)	very low	45.89	2.37
	low	369.22	19.07
	medium	297.13	15.35
	high	1123.45	58.03
	very high	100.31	5.18
Soil characteristic (Fuzzy-AHP)	very low	366.33	18.92
	low	404.45	20.89
	medium	464.53	23.99
	high	325.47	16.81
	very high	375.22	19.38

Weight of soil nutrient, soil characteristics and soil fertility criteria and scores of the sub-criteria using AHP

Main criteria	Weight	Influence	Sub-criteria	Score
Soil nutrient				
Available N	0.3103	31.04	Low (<280 kg/ha)	3
			Medium (280-500 kg/ha)	6
Available P	0.3103	31.03	Medium (10-25 kg/ha)	6
			High (>25kg/ha)	9
Available K	0.3103	31.03	Medium (118-280 kg/ha)	6
			High (>280 kg/ha)	9
Available Mg	0.0345	3.45	Sufficient (>1.0 c mol(p+)/kg)	6
			Deficient (<1.0 c mol(p+)/kg)	3
Available B	0.0345	3.45	Sufficient (>0.5ppm)	6
			Deficient (<0.5ppm)	3
Total		100		
Soil characteristics				
Soil texture	0.446933	44.69	Loam	9
			sandy loam	3
			Clay loam	7
OC	0.254707	25.5	Medium (5-10 g/kg)	3
			High (>10 g/kg)	6
CEC	0.150406	15.04	0-9	1
			9-14.2	3
			14.2-17.5	5
			17.5-19.2	7
			19.2-22.2	9
pH	0.098709	9.87	Acidic (<6.5)	3
			Neutral (6.5-7.5)	7
BD	0.049246	4.9	0	9
			0-1.21	7
			1.21-1.26	5
			1.26-1.32	3
			1.32-1.41	1
Total		100		
Soil fertility				
Soil nutrient	0.5	50	very low	1
			low	3
			medium	5
			high	7
			very high	9
soil characteristics	0.5	50	very low	1
			low	3
			medium	5
			high	7
			very high	9
Total		100		

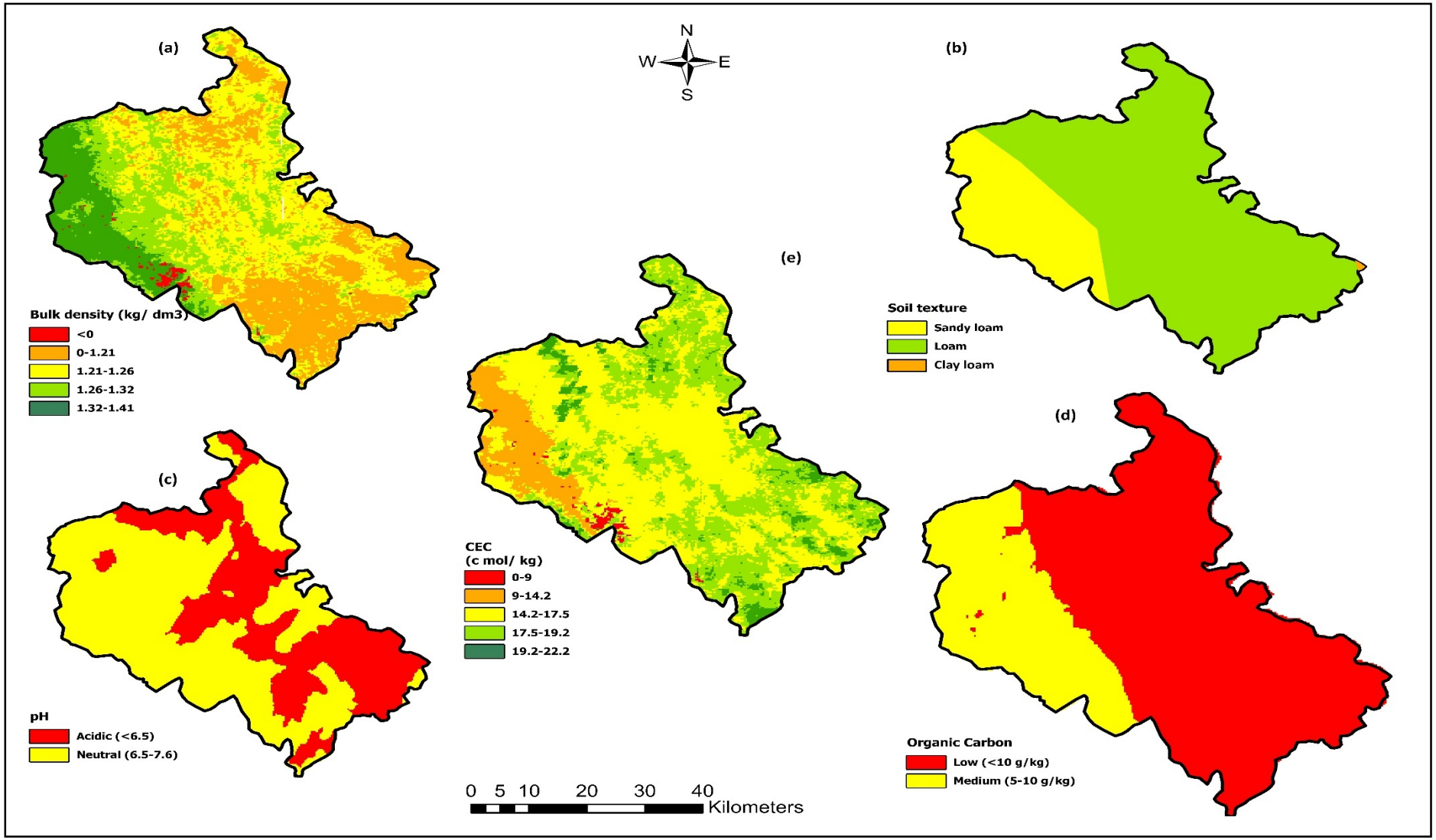

Soil characteristics: (a) bulk density (kg/dm^3); (b) soil texture; (c) pH; (d) Organic carbon and (e) Cation exchange capacity (CEC) (c mol/kg).

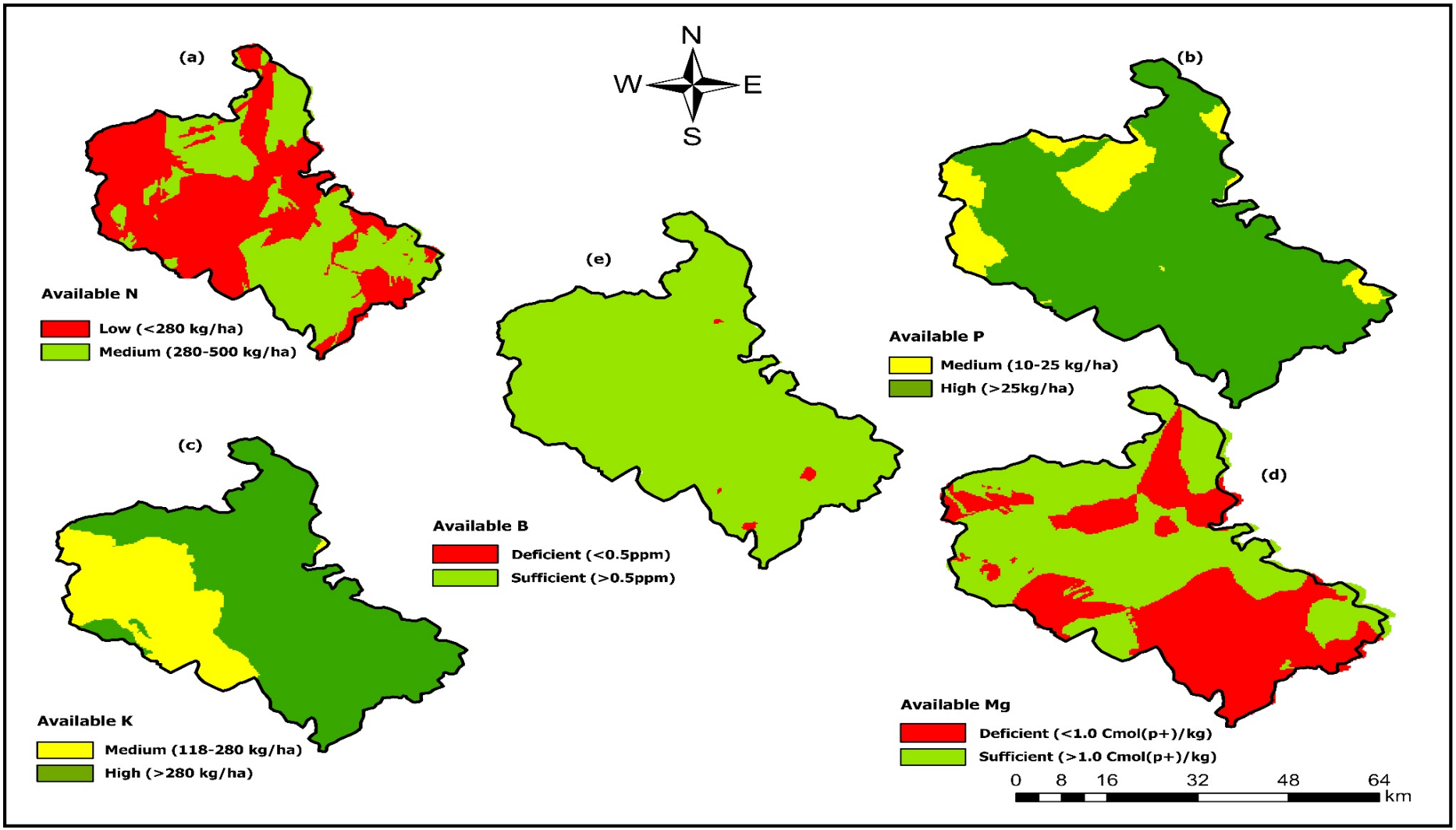

Soil nutrients: (a) Available N; (b) available P; available K; (d) available Mg and (e) available B

Table 15. Fuzzy triangular pair comparison matrix for Nitrogen sub-criteria

N	Medium			Low			Weight
Medium	**1**	**1**	**1**	3	4	5	**0.794**
Low	1/5	1/4	1/3	**1**	**1**	**1**	**0.206**

Fuzzy triangular pair comparison matrix for Phosphorus and Potassium sub-criteria

P and K	High			Medium			Weight
High	1	1	1	4	5	6	**0.830**
Medium	1/6	1/5	1/4	1	1	1	**0.170**

Fuzzy triangular pair comparison matrix for pH sub-criteria

pH	Neutral			Acidic			Weight
Neutral	1	1	1	4	5	6	**0.830**
Acidic	1/6	1/5	1/4	1	1	1	**0.170**

Fuzzy triangular pair comparison matrix for organic carbon sub-criteria

OC	High			Medium			Weight
High	1	1	1	4	5	6	**0.830**
Medium	1/6	1/5	1/4	1	1	1	**0.170**

Fuzzy triangular pair comparison matrix for Boron and Magnesium sub-criteria

B	Sufficient			Deficient			Weight
Sufficient	1	1	1	2	3	4	**0.739**
Deficient	1/4	1/3	1/2	1	1	1	**0.261**

Fuzzy triangular pair comparison matrix for soil texture sub-criteria

Soil texture	Loam			Sandy loam			Clay loam			Weight
loam	1	1	1	3	4	5	6	7	8	**0.688**
Sandy loam	1/5	1/4	1/3	1	1	1	4	5	6	**0.239**
Clay loam	1/8	1/7	1/6	1/8	1/7	1/6	1	1	1	**0.073**

Fuzzy triangular pair comparison matrix for bulk density sub-criteria

BD	0			0-1.21			1.21-1.26			1.26-1.32			1.32-1.41			Weight
0	1	1	1	2	3	4	4	5	6	6	7	8	8	9	10	**0.500**
0-1.21	1/4	1/3	1/2	1	1	1	2	3	4	4	5	6	6	7	8	**0.262**
1.21-1.26	1/6	1/5	1/4	1/4	1/3	1/2	1	1	1	2	3	4	4	5	6	**0.135**
1.26-1.32	1/8	1/7	1/6	1/6	1/5	1/4	1/4	1/3	1/2	1	1	1	2	3	4	**0.068**
1.32-1.41	1/10	1/9	1/8	1/8	1/7	1/6	1/6	1/5	1/4	1/4	1/3	1/2	1	1	1	**0.035**

Fuzzy triangular pair comparison matrix for LULC

LULC	Agriculture			Agroforestry			Grassland			Barren land			Weight
Agroforestry	1	1	1	3	4	5	6	7	8	8	9	10	**0.586**
Agriculture	1/5	1/4	1/3	1	1	1	4	5	6	6	7	8	**0.264**
Grassland	1/8	1/7	1/5	1/6	1/5	1/4	1	1	1	4	5	6	**0.109**
Barren land	1/10	1/9	1/8	1/8	1/7	1/6	1/6	1/5	1/4	1	1	1	**0.041**

Fuzzy triangular pair comparison matrix for cation exchange capacity sub-criteria

CEC	19.2-22.2			17.5-19.2			14.2-17.5			9-14.2			0-9			Weight
19.2-22.2	1	1	1	2	3	4	4	5	6	6	7	8	8	9	10	**0.500**
17.5-19.2	1/4	1/3	1/2	1	1	1	2	3	4	4	5	6	6	7	8	**0.262**
14.2-17.5	1/6	1/5	1/4	1/4	1/3	1/2	1	1	1	2	3	4	4	5	6	**0.135**
9-14.2	1/8	1/7	1/6	1/6	1/5	1/4	1/4	1/3	1/2	1	1	1	2	3	4	**0.068**
0-9	1/10	1/9	1/8	1/8	1/7	1/6	1/6	1/5	1/4	1/4	1/3	1/2	1	1	1	**0.035**

Fuzzy triangular pair comparison matrix for slope sub-criteria

Slope (degree)	<7.0			7-16			16-24			24-30			>30			Weight
<7.0	1	1	1	2	3	4	4	5	6	6	7	8	8	9	10	**0.500**
7-16	1/4	1/3	1/2	1	1	1	2	3	4	4	5	6	6	7	8	**0.262**
16-24	1/6	1/5	1/4	1/4	1/3	1/2	1	1	1	2	3	4	4	5	6	**0.135**
24-30	1/8	1/7	1/6	1/6	1/5	1/4	1/4	1/3	1/2	1	1	1	2	3	4	**0.068**
>30	1/10	1/9	1/8	1/8	1/7	1/6	1/6	1/5	1/4	1/4	1/3	1/2	1	1	1	**0.035**

Fuzzy triangular pair comparison matrix for elevation sub-criteria

Elevation a.m.s.l l	<558			558-893			893-1178			1178-1499			>1499			Weight
<558	**1**	**1**	**1**	2	3	4	4	5	6	5	6	7	7	8	9	**0.489**
558-893	1/4	1/3	1/2	**1**	**1**	**1**	1	2	3	4	5	6	6	7	8	**0.247**
893-1178	1/6	1/5	1/4	1/3	1/2	1/1	**1**	**1**	**1**	2	3	4	4	5	6	**0.148**
1178-1499	1/7	1/6	1/5	1/6	1/5	1/4	1/4	1/3	1/2	**1**	**1**	**1**	3	4	5	**0.080**
>1499	1/9	1/8	1/7	1/8	1/7	1/6	1/6	1/5	1/4	1/5	1/4	1/3	**1**	**1**	**1**	**0.036**

Fuzzy triangular pair comparison matrix for rainfall sub-criteria

Rainfall (mm)	1170-1240			1240-1300			1300-1370			1370-1440			1440-1510			Weight
1170-1240	1	1	1	2	3	4	4	5	6	6	7	8	8	9	10	**0.500**
1240-1300	1/4	1/3	1/2	1	1	1	2	3	4	4	5	6	6	7	8	**0.262**
1300-1370	1/6	1/5	1/4	1/4	1/3	1/2	1	1	1	2	3	4	4	5	6	**0.135**
1370-1440	1/8	1/7	1/6	1/6	1/5	1/4	1/4	1/3	1/2	1	1	1	2	3	4	**0.068**
1440-1510	1/10	1/9	1/8	1/8	1/7	1/6	1/6	1/5	1/4	1/4	1/3	1/2	1	1	1	**0.035**

Fuzzy triangular pair comparison matrix for soil fertility sub-criteria

Soil fertility	Very High			High			Medium			Low			Very low			Weight
Very high	1	1	1	2	3	4	4	5	6	6	7	8	8	9	10	**0.500**
High	1/4	1/3	1/2	1	1	1	2	3	4	4	5	6	6	7	8	**0.262**
Medium	1/6	1/5	1/4	1/4	1/3	1/2	1	1	1	2	3	4	4	5	6	**0.135**
Low	1/8	1/7	1/6	1/6	1/5	1/4	1/4	1/3	1/2	1	1	1	2	3	4	**0.068**
Very low	1/10	1/9	1/8	1/8	1/7	1/6	1/6	1/5	1/4	1/4	1/3	1/2	1	1	1	**0.035**

Fuzzy triangular pair comparison matrix for NDVI sub-criteria

NDVI	0.4-0.5			0.3-0.4			0.2-0.3			0-0.2			<0			Weight
0.4-0.5	1	1	1	2	3	4	5	6	7	6	7	8	8	9	10	**0.504**
0.3-0.4	1/4	1/3	1/2	1	1	1	2	3	4	5	6	7	6	7	8	**0.263**
0.2-0.3	1/7	1/6	1/5	1/4	1/3	1/2	1	1	1	2	3	4	5	6	7	**0.134**
0-0.2	1/8	1/7	1/6	1/7	1/6	1/5	1/4	1/3	1/2	1	1	1	2	3	4	**0.065**
<0	1/10	1/9	1/8	1/8	1/7	1/6	1/7	1/6	1/5	1/7	1/6	1/5	1	1	1	**0.034**

Fuzzy triangular pair comparison matrix for aspect sub-criteria

Aspect	SW, FLAT			S, SE			E, W			NW, NE			N			Weight
SW, FLAT	1	1	1	2	3	4	4	5	6	6	7	8	8	9	10	**0.500**
S, SE	1/4	1/3	1/2	1	1	1	2	3	4	4	5	6	6	7	8	**0.262**
E, W	1/6	1/5	1/4	1/4	1/3	1/2	1	1	1	2	3	4	4	5	6	**0.135**
NW, NE	1/8	1/7	1/6	1/6	1/5	1/4	1/4	1/3	1/2	1	1	1	2	3	4	**0.068**
N	1/10	1/9	1/8	1/8	1/7	1/6	1/6	1/5	1/4	1/4	1/3	1/2	1	1	1	**0.035**

Fuzzy triangular pair comparison matrix for hillshade sub-criteria

Hillshade	151-180			110-151			67-10			23-67			<23			Weight
151-180	1	1	1	2	3	4	5	6	7	6	7	8	8	9	10	**0.504**
110-151	1/4	1/3	1/2	1	1	1	2	3	4	5	6	7	6	7	8	**0.263**
67-10	1/7	1/6	1/5	1/4	1/3	1/2	1	1	1	2	3	4	5	6	7	**0.134**
23-67	1/8	1/7	1/6	1/7	1/6	1/5	1/4	1/3	1/2	1	1	1	2	3	4	**0.065**
<23	1/10	1/9	1/8	1/8	1/7	1/6	1/7	1/6	1/5	1/7	1/6	1/5	1	1	1	**0.034**

Fuzzy triangular pair comparison matrix for temperature sub-criteria

Temperature (°C)	<20			20-21			21-22			22-23			>23			Weight
<20	**1**	**1**	**1**	2	3	4	4	5	6	5	6	7	7	8	9	**0.489**
20-21	1/4	1/3	1/2	**1**	**1**	**1**	1	2	3	4	5	6	6	7	8	**0.247**
21-22	1/6	1/5	1/4	1/3	1/2	1/1	**1**	**1**	**1**	2	3	4	4	5	6	**0.148**
22-23	1/7	1/6	1/5	1/6	1/5	1/4	1/4	1/3	1/2	**1**	**1**	**1**	3	4	5	**0.080**
>23	1/9	1/8	1/7	1/8	1/7	1/6	1/6	1/5	1/4	1/5	1/4	1/3	**1**	**1**	**1**	**0.036**

Fuzzy triangular pair comparison matrix for road distance sub-criteria

Road Distance (km)	<0.22			0.22-0.59			0.59-1.10			1.10-1.85			>1.85			Weight
<0.22	1	1	1	2	3	4	4	5	6	6	7	8	7	8	9	**0.501**
0.22-0.59	1/4	1/3	1/2	1	1	1	2	3	4	4	5	6	5	6	7	**0.262**
0.59-1.10	1/6	1/5	1/4	1/4	1/3	1/2	1	1	1	2	3	4	3	4	5	**0.132**
1.10-1.85	1/8	1/7	1/6	1/6	1/5	1/4	1/4	1/3	1/2	1	1	1	1	2	3	**0.063**
>1.85	1/9	1/8	1/7	1/7	1/6	1/5	1/5	1/4	/3	1/3	1/2	1/1	1	1	1	**0.043**

Fuzzy triangular pair comparison matrix for stream distance sub-criteria

Stream Distance (km)	<0.92			0.92-1.84			1.84-2.76			2.76-3.68			>3.68			Weight
<0.92	1	1	1	2	3	4	4	5	6	6	7	8	7	8	9	**0.501**
0.92-1.84	1/4	1/3	1/2	1	1	1	2	3	4	4	5	6	5	6	7	**0.262**
1.84-2.76	1/6	1/5	1/4	1/4	1/3	1/2	1	1	1	2	3	4	3	4	5	**0.132**
2.76-3.68	1/8	1/7	1/6	1/6	1/5	1/4	1/4	1/3	1/2	1	1	1	1	2	3	**0.063**
>3.68	1/9	1/8	1/7	1/7	1/6	1/5	1/5	1/4	/3	1/3	1/2	1/1	1	1	1	**0.043**

Weights of soil nutrients, soil characteristics and soil fertility criteria and scores of the sub-criteria using Fuzzy-AHP.

Main criteria	Weight	Sub-criteria	Sub-weight
Soil nutrient			
Available N	**0.319**	Low (<280 kg/ha)	0.206
		Medium (280-500 kg/ha)	0.794
Available P	**0.293**	Medium (10-25 kg/ha)	0.170
		High (>25kg/ha)	0.830
Available K	**0.276**	Medium (118-280 kg/ha)	0.170
		High (>280 kg/ha)	0.830
Available Mg	**0.077**	Sufficient (>1.0 c mol(p+)/kg)	0.739
		Deficient (<1.0 c mol(p+)/kg)	0.261
Available B	**0.035**	Sufficient (>0.5ppm)	0.739
		Deficient (<0.5ppm)	0.261
Soil characteristics			
Soil texture	**0.314**	Loam	0.688
		sandy loam	0.239
		Clay loam	0.073
OC	**0.295**	Medium (5-10 g/kg)	0.170
		High (>10 g/kg)	0.830
CEC	**0.275**	0-9	0.035
		9-14.2	0.068
		14.2-17.5	0.135
		17.5-19.2	0.262
		19.2-22.2	0.500
pH	**0.084**	Acidic (<6.5)	0.1698
		Neutral (6.5-7.5)	0.8301
BD	**0.032**	0	0.500
		0-1.21	0.262
		1.21-1.26	0.135
		1.26-1.32	0.068
		1.32-1.41	0.035
Soil fertility			
Soil nutrient	**0.5**	Very high	0.500
		High	0.262
		Medium	0.135
		Low	0.068
		Very low	0.035
soil characteristics	**0.5**	Very high	0.500
		High	0.262
		Medium	0.135
		Low	0.068
		Very low	0.035

Dr. Y.S. Parmar University of Horticulture and Forestry
Nauni, Solan-173230 (H.P.)
Department of Silviculture and Agroforestry

Title of the thesis	:	**"Remote sensing approach for estimating agroforestry area, suitability mapping and carbon sequestration potential of agroforestry systems in Solan district of Himachal Pradesh"**
Name of the student	:	Divya Khatri
Admission Number	:	F-2020-09-D
Major Advisor	:	Dr. D. R. Bhardwaj
Major Field	:	Forestry
Major Field(s)	:	Agroforestry
Degree Awarded	:	Ph.D. (Agroforestry)
Year of Award of degree	:	2024
No. of pages in Thesis	:	165+x
No. of words in Abstract	:	340

ABSTRACT

The present investigation entitled " Remote sensing approach for estimating agroforestry area, suitability mapping and carbon sequestration potential of agroforestry systems in Solan district of Himachal Pradesh " was carried out in Solan district of the Himachal Pradesh during the year 2021-2023 for delineation of area under agroforestry practices, assessment of land suitability to agroforestry and estimation of carbon stock and carbon sequestration potential. The study demonstrates the superior performance of the random forest classification in land use mapping, particularly in Solan district. The district's land cover distribution, as determined by the random forest classifier, reveals that agroforestry constitutes 26.34 percent, making it the second-largest land cover. Forested areas encompass 43.40 percent, while agriculture occupies 9.03 percent. Grasslands and built-up areas contribute 7.03 percent and 6.77 percent, respectively. Barren land makes up 6.24 percent, and water bodies account for 1.20 percent of the district's total land cover. The overall accuracy of the classification is commendable at 85.78%, accompanied by a robust Kappa Coefficient of 0.8092. Notably, agroforestry class exhibits high accuracy, with producer and user accuracies reaching 88.56% and 80.81%, respectively. Utilizing the analytic hierarchy process (AHP), the study categorizes 17.32 per cent of the district as highly suitable for agroforestry, 22.37 per cent as moderately suitable, 20.19 per cent as marginally suitable, 26.45 per cent as currently not suitable, and 13.67% as permanently not suitable. Employing the Fuzzy-AHP technique, the results indicate 11.33 per cent highly suitable, 24.76 per cent moderately suitable, 15.74 per cent marginally suitable, 26.30 per cent currently not suitable, and 21.87 per cent permanently not suitable for agroforestry in Solan district. In terms of environmental impact, the projected carbon storage of 22.807 Tg C shows a substantial increase of 1.780 Tg C over 20 years, contributing to climate change mitigation. The Net Present Value of carbon sequestration is estimated at $27.037 million. Overall, the findings provide valuable insights for policymakers, facilitating informed decision-making and intervention strategies for the adoption, development, and management of agroforestry in Solan District, to address the challenges posed by climate change.

Signature of Major Advisor **Signature of Student**

Countersigned

Professor and Head
Department of Silviculture and Agroforestry
Dr. Y.S. Parmar University of Horticulture and Forestry
Nauni, Solan-173230 (H.P.)

BRIEF BIO-DATA

Name	**:**	**Divya Khatri**
Father's Name	**:**	Sh. Virendra Singh Khatri
Date of Birth	**:**	19-03-1997
Sex	**:**	Female
Marital Status	**:**	Unmarried
Nationality	**:**	Indian

Educational qualifications:

Certificate/Degree	Class/Grade	Board/University	Year
Matriculation	First	CBSE	2012
10+2	First	CBSE	2014
BSc. Forestry	First	VCSG Uttarakhand University of Horticulture and Forestry, Ranichauri, Tehri Garhwal	2018
M.Sc. Agroforestry	First	Banaras Hindu University	2020

Scholarship/ Stipend/ Fellowship any other financial assistance received during the study period **: No**

Publications **2 submitted**

Abstract **: 5**

(Divya Khatri)